Platinum(II) Aminophosphine Anticancer Complexes and their Interactions with Nucleotides

A Thesis

Submitted for the Degree of

Doctor of Philosophy

by

Elaine Beth Watchman, *B.Sc.*

Department of Chemistry

Faculty of Science and Engineering

University of Edinburgh

January 2002

Abstract

A series of platinum(II) aminophosphine complexes has been prepared and their interactions with nucleotides studied. Such complexes are potential anticancer agents combining cytotoxic phosphines with features of platinum am(m)ine drugs. Ligands of the form $Ph_2P(CH_2)_3NRR'$ have been prepared, where R and R' are alkyl groups of varying steric bulk. On complexation with platinum the ligands form six-membered chelate rings bound via P and N and the extent of chelation has been shown to be controlled by the bulk of the substituents. Chelate formation is also pH dependent with low pH favouring a ring-opened structure due to protonation of the amine group. All the complexes formed were fully characterised by the use of ^{31}P NMR and X-ray crystallography.

Nucleotides are ideal model compounds for studying the interactions of platinum complexes with DNA, the target for platinum drugs *in vivo*. The aminophosphine complexes prepared were reacted with four different nucleotides and their binding analysed by ^{1}H NMR. Binding was most prominent to the nucleotides guanosine and thymidine. The complexes can bind two guanosine per Pt to form bifunctional adducts but with the other nucleotides only monofunctional binding was observed. The formation of these bound adducts was confirmed by electrospray ionisation mass spectrometry. The pH dependence of thymidine binding was investigated since binding occurs through the endocyclic N3 site which has a high pK_a of ca. 10. Although the extent of binding of the complexes decreased at low pH, the thymidine remained fully bound over an unusually wide pH range, 4-12. For the less sterically hindered complexes binding also decreased at low pH due to competition from chelate ring-closing reactions Competition reactions were carried out with the complexes and all four nucleotides together to determine the selectivity of binding by capillary electrophoresis. Surprisingly thymidine binding was as prevalent as guanosine. This is in contrast to Pt-am(m)ine anticancer complexes which have a much higher affinity for the purine bases than pyrimidines.

The binding of the complex $[Pt\{Ph_2P(CH_2)_3NMe_2\text{-}P\}_2Cl_2]$ to calf thymus DNA and synthetic polynucleotides was also investigated. The selectivity for thymine seen with individual nucleotides was not evident in polymeric DNA structures. The binding profile was however distinctly different to Pt(amine) complexes, in particular the rate of binding increased greatly. This is due to electrostatic interactions between the protonated amines of the ligands in the complex and the phosphate groups on DNA.

In addition, the binding of the complexes to AZT (3'-azido, 3'-deoxy thymidine) was investigated. AZT is an anti-HIV drug and it is predicted that Pt-AZT complexes could act as multifunctional antiviral agents incorporating the cytotoxic properties of the platinum complex. The binding profiles observed were similar to those for binding thymidine, with a pH dependence due to protonation of the N3 binding site. The adducts produced were monofunctional and existed as a mixture of diastereomers.

To my husband, without his love and support this thesis would certainly have never been written

Acknowledgements

I would like to thank my supervisor, Professor Peter J. Sadler for his advice and encouragement throughout my years of PhD study. I am very grateful to him for everything I have learned and achieved in my time in Edinburgh.

Special thanks must go to several members of the PJS group for their help in different areas of expertise – Dr. Abraha Habtemariam for helping me to tackle synthetic chemistry, Dr. John A. Parkinson for patiently explaining NMR, Dr Socorro Murdoch for making HPLC more interesting, and Dr. Zijian Guo for being an expert in just about everything. I would also particularly like to thank Mark Harrison for his contributions to this work and for giving me a timely boost in motivation. I am indebted to these and all other PJS group members, past and present, for taking the time to help whenever it was needed and making the chemistry department an enjoyable place to be.

I would also like to acknowledge the help of the following people in the Chemistry Department at Edinburgh: Dr. Simon Parsons, Dr. Robert Coxall, and Andrew Parkin for X-ray crystallography and John Miller for NMR.

I would like to thank Dr. Viktor Brabec and his group, at the Academy of Sciences of the Czech Republic in Brno, especially Kamila Neplechová for making me feel welcome during my visit and for teaching me new experimental techniques.

I am very grateful to Dr. P. Langridge-Smith for allowing me to use his CE equipment and to David Simpson for helping to get it running.

I must also acknowledge the help and support (including financial) of my parents and sister, in helping me to survive through my years of student life.

Finally, I would like to thank all my family and friends who have helped to keep me vaguely sane over the last four years, in particular while I have been struggling to write this thesis. It is thanks to your motivation and constant nagging that I have finally made it.

Declaration

I hereby declare that except where specific reference is made to other sources, the work contained in this thesis is the original work of my own research since registration for the PhD degree in October 1997, and any collaboration has been indicated clearly. This thesis has been composed by myself and has not been submitted, in whole or in part, for any other degree, diploma, or other qualification.

Beth Watchman

January 2002

Contents

Chapter 2 Materials and Methods

Abbreviations

AMP	5'-adenine monophosphate
AZT	3'-azido, 3'-deoxy thymidine
BDPPA	*N*-tertiary-butyl, diphenyl-phosphino, propyl amine
B.p.	boiling point
bp	base pair
CE	capillary electrophoresis
COD	cyclooctadiene
CMP	5'-cytosine monophosphate
CT	calf thymus
DMDPPA	*N,N*-dimethyl, diphenyl-phosphino, propyl amine
DNA	deoxyribonucleic acid
DPP	differential pulse polarography
DPPA	diphenyl-phosphino, propyl amine
ds	double-stranded
dTMP	5'-deoxythymine monophosphate
ESI-MS	electrospray ionisation mass spectrometry
FAB	fast atom bombardment
GMP	5'-guanine monophosphate
HPLC	high performance liquid chromatography
MDPPA	*N*-methyl, diphenyl-phosphino, propyl amine
NMR	nuclear magnetic resonance spectroscopy
r_b	ratio of bound Pt to nucleotides
RNA	ribonucleic acid
ss	single-stranded
T_{50}	time taken to bind 50% of nucleotide/Pt present
TBAHS	tetrabutyl ammonium hydrogen sulphate

Chapter One

Introduction

1.1 Platinum

1.1.1 Discovery and Extraction

Platinum (atomic number 78, mass number 195.08) is in Group 10 of the periodic table. Platinum-containing objects date back as early as 700 BC although Pt was not formally discovered until 1735 by the Spanish astronomer A. de Ulloa, in deposits from the Pinto River in Colombia, and brought to Europe. Platinum is typically metallic, a face-centred cubic structure with a silver-white appearance, and it is both malleable and ductile. Due to its inertness and high melting point (2045 K), platinum required complex aqueous chemical processing for isolation and identification. Thus few developments were made in its chemistry until the 19^{th} century, when powder metallurgical techniques were developed by Frenchman P. F. Chabeneau and later W. H. Wollaston in London.[1]

The abundance of platinum in the earth's crust is approximately 10^{-6}% by weight. Virtually all platinum comes from nickel or copper sulfide ores and must be selectively extracted from other Platinum Group metals (ruthenium, rhodium, palladium, osmium, and iridium). The world's major deposits of platinum are in Bushfeld-South Africa, Sudbury-Canada, and Norilsk-Talnakah-Russia. These deposits are exploited by underground mining and the sulfide ores concentrated by flotation separation. Copper and nickel sulfides are then leached out leaving a residue that is 15-20% platinum metals. This concentrate is dissolved in aqua regia dissolving only platinum and palladium. Platinum is then precipitated from the solution with ammonium chloride. The resulting salt is heated to give a crude metallic product which is purified by redissolving in aqua regia, reprecipitating with ammonium chloride and heating. The world production of platinum is currently about 90 tonnes per year.

1.1.2 Uses

Platinum has widespread uses due to its various properties. Its lusterous appearance has lead to its use in jewellery for many centuries. It is usually alloyed with palladium or ruthenium for extra strength. More recently the most notable use is in catalysis, where about 42% of the platinum in the western world is employed.[2] Uses include cracking oil to form hydrocarbons, and as catalytic converters in the automotive industry. Here the platinum promotes the conversion of unburned hydrocarbons, carbon monoxide and nitric oxides to water, carbon dioxide and nitrogen. Due to its inertness, platinum also has widespread uses as electrodes, thermocouple elements, electrical contacts, wire and crucibles for laboratory use, dentistry, and coating for jet engine fuel nozzles.

1.1.3 Chemistry

Platinum has 6 isotopes: ^{190}Pt and ^{192}Pt account for less than 0.8% and are unstable α-emitters. ^{194}Pt (32.9%), ^{195}Pt (33.8%), ^{196}Pt (25.3%) and ^{198}Pt (7.2%) are stable isotopes. All the isotopes have nuclear spin quantum number of 0, except for ^{195}Pt which has I=1/2 making it useful for NMR observation. The electronic configuration of platinum is [Xe] $4f^{14}$ $5d^9$ $6s^1$, and it has an electronegativity of 2.28.

The principal oxidation states of platinum are +2 and +4, although +1 and +3 are known in which M-M bonds are often present.[3]

Platinum(IV) complexes are octahedral and diamagnetic with t_{2g}^6 electronic configuration. They are thermodynamically stable and kinetically inert. Complexes with halide, pseudo-halide and N-donor ligands are especially numerous. K_2PtCl_6 is the most common commercially available form, and is useful as a route into Pt(II) chemistry, by reduction with sulphur dioxide to K_2PtCl_4.[4]

Platinum(II) complexes are d^8 and also diamagnetic. They are principally square-planar as the splitting of the d-orbitals in this geometry provides the opportunity to

place all 8 d electrons in four lower orbitals leaving the uppermost ($d_{x^2-y^2}$) orbital empty. For a 3rd row transition metal, the d-orbital splitting is sufficient to offset the energy required to pair-up two electrons favouring a square-planar geometry (Figure 1.1).

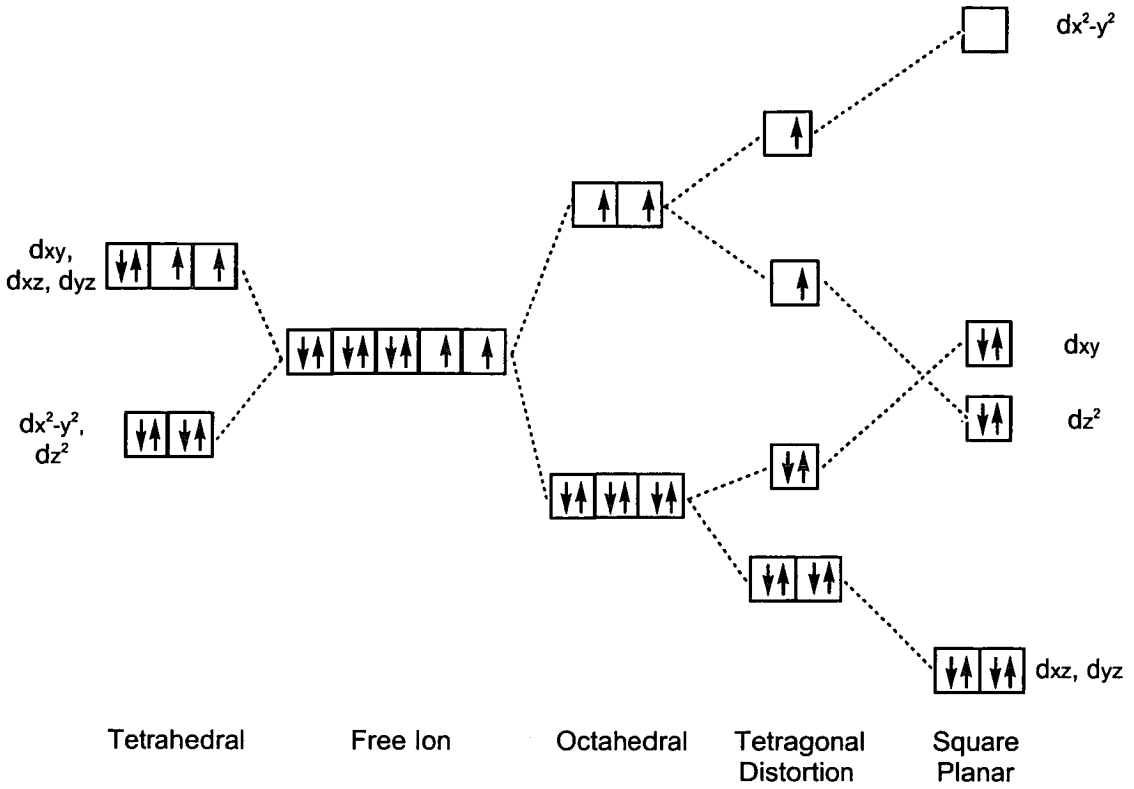

Figure 1.1 Effect of complexation on d-orbital splitting for Pt(II)

Platinum(II) shows a low affinity for O-donor and F^- ligands preferring heavier halogens and π-bonding ligands. Platinum(II) complexes have played an important role in the development of various aspects of coordination chemistry, such as geometric isomerism and reaction mechanisms due to their conveniently slow rates of reaction.

An important phenomenon of reactions of square planar complexes is the ***trans effect*** – the effect of a ligand on the rate of substitution of a ligand *trans* to it. Ligand displacement on Pt(II) occurs almost entirely by an associative pathway, via a 5-coordinate intermediate. Generally the stereochemistry of the complex is retained but if the intermediate is sufficiently long-lived it can undergo pseudorotation leading to the opposite isomer (Figure 1.2).

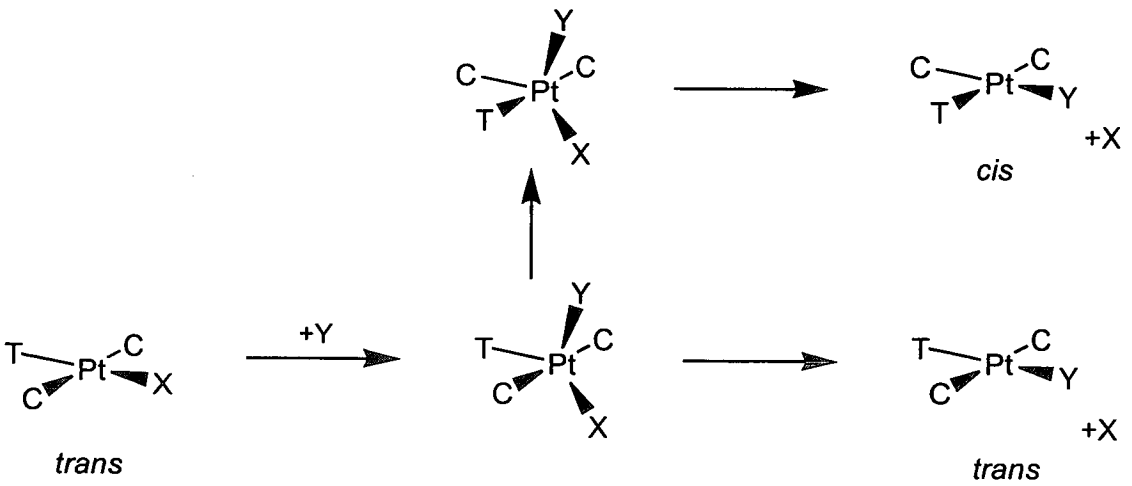

Figure 1.2 Associative mechanism of ligand substitution in Pt(II) square-planar complexes

The trans effect series in order of decreasing rate of displacement at *trans* position is[5]:

$CO, CN^-, C_2H_4 > PR_3, H^- > CH_3^- > C_6H_5^-, NO_2^-, I^-, SCN^- > Br^-, Cl^- > py, NH_3, OH^-, H_2O$

The ligands exerting the strongest *trans effect* are those for which the bonding to Pt(II) is thought to have the most π-acceptor character. This removes electron density from the metal and the reduced density on the opposite side means that nucleophilic attack is more likely to take place. The *trans effect* is a kinetic

phenomenon affecting the rates of reaction and isomer formation. This series is useful in rationalising known synthetic procedures and devising new ones.

A related property of ligands in square planar complexes is the ***trans influence***. This is a thermodynamic effect of one ligand on the strength of the bond to the ligand *trans* to it. The series of ligands with decreasing *trans influence* is[5]:

$$H^- > PR_3 > SCN^- > I^-, CH_3^-, CO, CN^- > Br^- > Cl^- > NH_3 > OH^-$$

This effect is greatest for ligands which are strong σ-donors producing an axial polarisation of the platinum, the lone pair inducing a positive charge on the nearside of the metal and a concomitant negative charge on the far side. This will weaken the *trans* bond. The *trans influence* is apparent in ground state properties such as bond lengths, vibrational frequencies and NMR coupling constants.

1.2 Cancer

Cancer is a group of related diseases characterised by uncontrolled multiplication and disorganised growth of the affected cells.[6] Normal mammalian cells divide only 20-50 times before dying whereas cancer cells are said to be "immortal", they can go on dividing indefinitely if they have a continual supply of nutrients. Potential problems arise when a normal cell is *transfomed* into a cancer cell. If this cell evades the body's immune system it may proliferate to form a tumour, a mass of cancer cells within an otherwise normal tissue. If these cells remain at the original site, the tumour is said to be *benign*, such tumours can usually be removed by surgery and do not cause serious problems. If however, the tumour becomes invasive enough to impair the functions of one or more organs it becomes *malignant*. Invasiveness usually implies an ability to break loose, enter the blood stream or lymphatic vessels and form secondary tumours (*metastases*) at other sites in the body. The more widely a cancer metastasises, the harder it becomes to eradicate.

It is now known that cancer can be caused by a number of factors[7] including a wide variety of chemical substances, various types of ionising radiation, and various classes of viruses. Cancer is a genetic disease; either defective genes are passed from parent to child, or a mutation occurs by activation of DNA tumour viruses forming an *onocogene.* These genetic mutations can lead to malfunctioning proteins that interfere with the cell cycle machinery. For example, the proteins necessary for cell division may be activated at the wrong time causing uncontrollable growth, or the proteins that halt cell growth may be inactivated or lost. As understanding of the causes of cancer increases, better methods of treatment can be developed.

Cancers are classified according to the tissue and cell type from which they arise.[7] *Carcinomas* derive from epithelial cells which comprise skin and the covering and lining of the organs and internal passageways. Examples include lung, breast, testicular and ovarian cancers. *Sarcomas* derive from connective or muscle tissue such as blood, bone, and cartilage. Other cancers do not fit in either of these broad catagories including leukemias, derived from hemopoietic cells in the bone marrow and lymph systems.

1.2.1 Treatment of Cancer

Successful treatment of cancer requires the complete removal or destruction of all cancerous tissue or the disease can recur. Three main types of treatment exist[7].

1. *Surgery* is the most effective form of treatment, although it is limited in that it must be performed before the cancer has spread into organs and tissues that cannot safely be removed. Surgery is often used in conjunction with another kind of treatment in order to help prevent remission.

2. *Radiation therapy* makes use of ionising radiations – X-rays, electrons, neutrons and gamma rays. These generate reactive oxygen species in the body which lead to to DNA strand breaks, resulting in cell death. Precautions must be taken to shield and protect normal cells, which can also be killed. Some cancers however are not responsive to radiation, cells of differing origin have varying sensitivities. In addition to this individual cells within the same tumour may also have widely

differing susceptibility to irradiation. Radio sensitisers are used to increase the damage to localised areas without having to increase the radiation dose.

3. *Chemotherapy* uses synthetic chemicals and antibiotics that can differentiate to some extent between normal tissue cells and cancer cells. These agents are used to interfere at various points in the cell division process of cancer cells, preventing them from multiplying. Most drugs are limited in their usefulness by three factors. Firstly, most cancer drugs can only destroy the certain proportion of the cell population undergoing division at any one time, making it difficult to completely destroy a tumour. Another problem is that cancer drugs damage normal, as well as cancer, cells and tissues. Since the drugs target rapidly dividing cells (like cancers), healthy rapidly dividing cells such as hair follicles, the gastrointestinal lining, and bone marrow cells, are also open to attack. This results in the typical side-effects experienced with chemotherapy: hair loss, nausea and poor immuno-response. In addition, some cancer cells eventually become resistant to drugs. In order to overcome these three difficulties, combinations of chemotherapeutic agents that act on cells in different ways have been used in treatment programs simultaneously or in sequence.

1.3 Platinum Anticancer Agents

1.3.1 Discovery of Cisplatin

Cis-diamminedichloroplatinum(II), cisplatin, is one of the most widely utilized antitumour drugs in the world and currently has annual sales of approximately $500 million (U.S.).[8,9] Although the compound was first synthesised in 1845[10] and known as *Peyrone's Chloride*, its cytotoxic activity was a serendipitous discovery in the 1960's by Barnett Rosenberg at Michigan State University. Whilst investigating the effect of electric field on the growth of *E. coli* bacteria, Rosenberg noticed strong filamentous growth but no cell division.[11] After further investigation, the cause of this phenomenon was determined to be the presence of small amounts of certain

platinum compounds formed by slow dissolution of the "inert" platinum electrodes used.

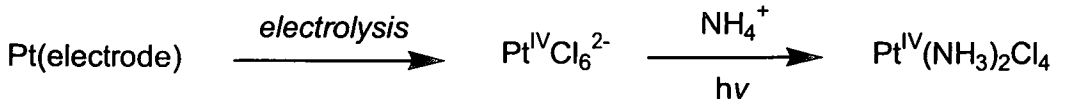

By synthesising and testing various complexes, $Pt(NH_3)_2Cl_4$ was found to be the active species. Other similar complexes were synthesised and tested and only complexes with a *cis*-geometry showed filamentous growth (Figure 1.3).[12] The Pt (II) analogue *cis*-$[Pt(NH_3)_2Cl_2]$, now known as cisplatin, exhibited the greatest effect.

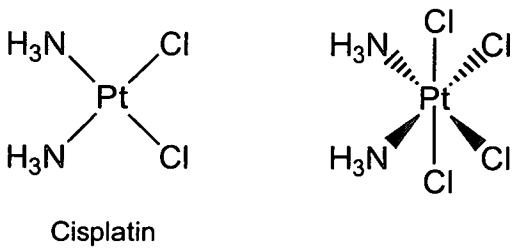

Cisplatin

Figure 1.3 Platinum compounds identified as having antitumour activity

Further investigations were carried out to test the postulate that if these complexes could stop cell division in bacteria at concentrations without marked toxicity, then perhaps they would stop cell division in rapidly growing tumours without unacceptable toxicity to the host animal. Rosenberg and his co-workers performed initial antitumour experiments on mice bearing Sarcoma 180 solid tumours and Leukaemia L1210. These demonstrated the potency of these complexes in the treatment of tumours.[13,14] In addition the drugs showed the ability to totally regress large Sarcoma-180 tumours, a result not seen for any other anticancer agent at the time.

In 1971 the first clinical trials of cisplatin were initiated.[15] Approval of cisplatin for the treatment of testicular and ovarian cancer was given in 1978. Today it is routinely used in the clinic and is most effective against testicular and ovarian cancers.[16] Until the 1970's, testicular cancer was usually a fatal diagnosis, and fewer than 10% of patients enjoyed long-term survival. With the advent of aggressive chemotherapy, over 90% of patients can now expect to be cured. The most important contribution to this success is the development of cisplatin and its use in combination treatments for the disease. The response rates of other solid malignancies, such as head, neck, lung and bone tumours can also be improved with cisplatin treatment.[17] In combination with other antitumour drugs, such as 5′-Fluorouracil, synergistic effects have been achieved.[18] 5′-Fluorouracil interferes with excision repair and is thought to reduce the repair of cisplatin-induced DNA damage, thereby enhancing the cytotoxicity of cisplatin.

A severe limitation of the clinical use of cisplatin has been its toxicity. Platinum compounds accumulate in the kidney and tubular damage is the major origin of cisplatin induced nephrotoxicity.[19] Saline hydration and diuresis is used to reduce this nephrotoxicity, although this makes outpatient treatment impossible.[20] Other toxic side-effects, because of the high doses required, are bone marrow suppression, neurotoxicity, loss of high frequency hearing and gastrointestinal toxicity (nausea, vomiting, and diarrhoea). It is these side-effects which limit the dose of cisplatin which can be given to patients; typical doses are 100 mg/day for up to five consecutive days.[21] Resistance to cisplatin treatment also significantly limits cure rates. Some tumours have natural resistance to cisplatin whilst others develop acquired resistance after initial treatment. Several mechanisms for this resistance have been proposed and are discussed in detail in Section 1.3.2.4.

These drawbacks associated with an otherwise highly successful drug have provided the impetus for the development of an improved platinum anticancer agent. Since the introduction of cisplatin, thousands of Pt compounds have been synthesised and their cytotoxicity evaluated.

1.3.2 Mechanism of Action

It is generally accepted that it is the interaction of cisplatin with DNA that is responsible for its antitumour activity. This was suspected after Rosenberg's early experiments, since *E. coli* cell division was stopped suggesting inhibition of DNA replication. Later biochemical studies measuring the uptake of radiolabelled precursors for proteins and nucleic acids confirmed this, showing only inhibition of DNA synthesis and not RNA or protein synthesis on administration of cisplatin.[22]
It is still unclear how cisplatin can cross the cell membrane to reach the target DNA.

1.3.2.1 Hydrolysis

In considering the *in vivo* interactions of cisplatin, it was first necessary to consider the effect of the biological environment on its structure. Since the dichloro form of cisplatin is relatively unreactive, it was soon realised that the hydrolysis of the complex to the more reactive aqua forms could be an important step in the action of the drug. Furthermore deprotonation of the aqua ligands is also then possible. Several studies have been carried out to determine the rate constants for the two-step aquation process and the pK_a values for the acid-base equilibria of each aqua species. A summary of all these reactions is given in Figure 1.4 and the experimentally determined values in Table 1.1 (aquation rates)[23] and Table 1.2 (pK_a values).[24,25,26]

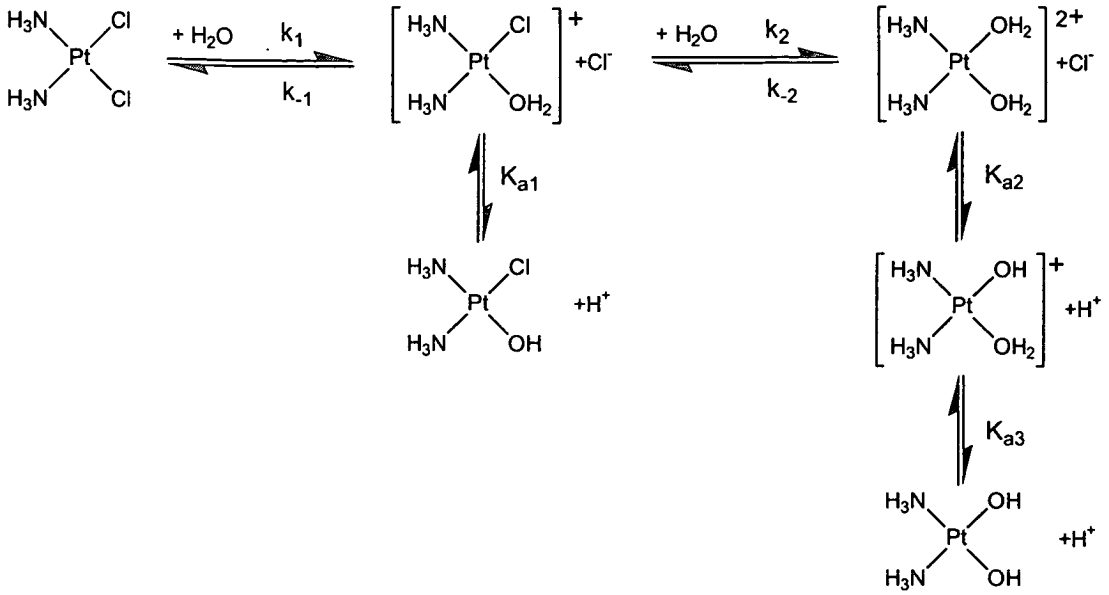

Figure 1.4 Aquation-anation, and acid-base equilibia of cisplatin

Rate/Equilibrium Constants	
k_1 [s^{-1}]	$(1.9 \pm 0.2) \times 10^{-4}$
k_{-1} [$M^{-1}s^{-1}$]	$(6.0 \pm 1.5) \times 10^{-2}$
K_1 [M]	3.2×10^{-3}
k_2 [s^{-1}]	$(2.3 \pm 0.3) \times 10^{-4}$
k_{-2} [$M^{-1}s^{-1}$]	$(9.8 \pm 1.4) \times 10^{-1}$
K_2 [M]	2.3×10^{-4}

Table 1.1 Aquation rate constants (k) and equilibrium constants (K) for cisplatin[23] (see Figure 1.4)

Ref.	*24*	*25*	*26*
pK_{a1}	6.85 ± 0.1	6.41 ± 0.02	
pK_{a2}	5.93 ± 0.1	5.37 ± 0.09	5.24 ± 0.05
pK_{a3}	7.9 ± 0.1	7.21 ± 0.09	7.42 ± 0.10

Table 1.2 pK_a values for acid-base equilibria of aquation products of cisplatin[24, 25, 26] (see Figure 1.4)

The discrepancies between the pK_a values determined by various groups are due to differences in experimental conditions such as temperature and ionic strength. For this reason a set of "concensus" values can be drawn up for room temperature and physiological conditions. These values (pK_{a1} = 6.6, pK_{a2} = 5.5, pK_{a3} = 7.3) and the rate constants quoted have been used to determine the proportions of each species which are present *in vivo*.[27] (Table 1.3) Two environments must be considered: the blood plasma since the drug is administered intavenously, and the cell where the drug reaches its target, DNA. The widely differing chloride concentrations in these two areas (plasma 104 mM, cell 4 mM) must also be taken into account.

Ligands	Plasma (104 mM Cl^-)	Cell (4 mM Cl^-)
Cl^-, Cl^-	0.67	0.03
Cl^-, H_2O	0.04	0.05
Cl^-, OH^-	0.26	0.30
H_2O, H_2O	1 x 10^{-4}	0.003
OH^-, H_2O	0.009	0.28
OH^-, OH^-	0.012	0.35

Table 1.3 Mole fractions of $(NH_3)_2Pt(II)$ species at pH 7.4, at plasma and intracellular chloride ion concentrations

The major species present in the cell are the chloro-hydroxo, aqua-hydroxo and dihydroxo complexes. These then are the most likely species that go on to interact with DNA.

1.3.2.2 Platination of DNA

As previously stated, the major target of cisplatin in the cell is DNA. Since platinum(II) behaves as a "class b" metal ion, it is expected to bind preferentially with the nitrogen atoms of the nucleobases.[28] Figure 1.5 shows a schematic structure of a single-stranded fragment of DNA containing the four common nucleobases with indications of their preferred metal binding sites.[21] After hydrolysis, binding of cisplatin occurs mainly at the N7 position of guanine bases, followed by adenine-N7, adenine-N1, and cytosine-N3, although the latter two are not usually accessible in double-stranded DNA as they are involved in base pairing to the complementary strand. Calculations of electrostatic potentials indicate that the guanine carbonyl group enhances the basicity of N7, while the amino group in adenine reduces the relative basicity. Also in double-stranded DNA, N7 of guanine is exposed on the surface of the major groove making it accessible for platinum binding.

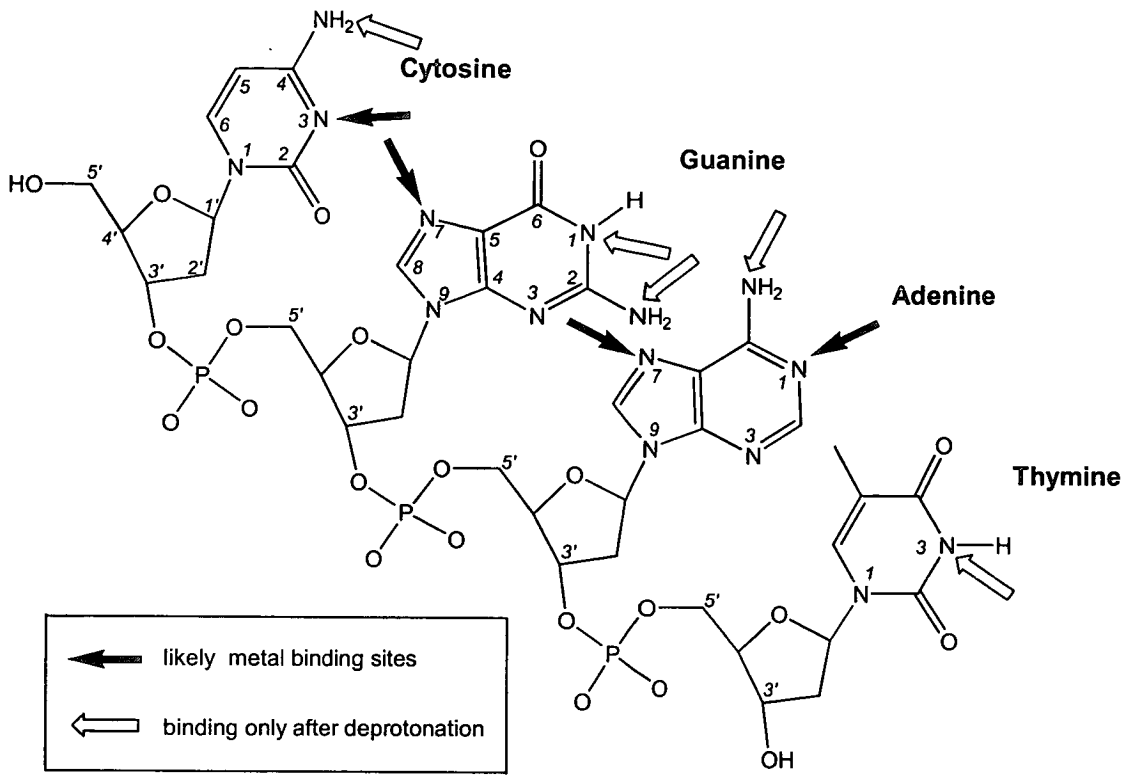

Figure 1.5 Schematic structure of 5'-CGAT DNA fragment showing ring numbering and metal binding sites (adapted from J. Reedijk, ref. 21)

Several modes of binding of cisplatin to DNA are possible since the drug has two potential binding sites, with labile hydroxo ligands. These include *intra*strand crosslinks, where the platinum binds to two bases on the same strand of the DNA, and *inter*strand crosslinks where the platinum binds to two bases on opposite strands of the DNA. Monofunctional adducts are also possible where binding to only one base occurs and the presence of S-donor ligands in the cell also gives the possibility of protein-DNA crosslinks. These binding modes are all represented in Figure 1.6.

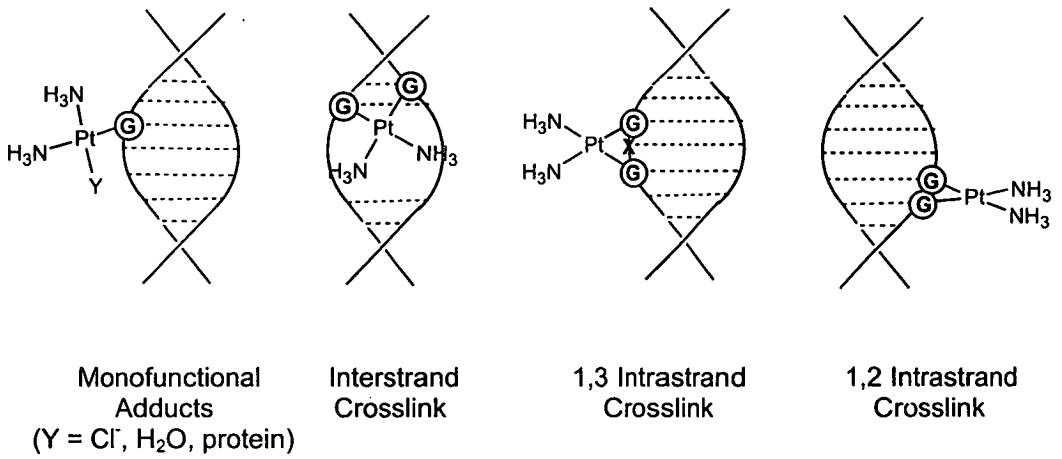

Figure 1.6 Some possible DNA-cisplatin adducts

In order to determine which adducts of cisplatin are formed on DNA, experiments have been carried out using cisplatin-treated salmon sperm DNA.[29] Pt binding was studied by enzymatic digestion, chromatographic separation of products, and NMR analysis. The major products were 1,2 intrastrand crosslinks between adjacent bases (GpG or ApG), and other adducts formed were 1,3 intrastrand crosslinks/interstrand crosslinks (not distinguishable by method employed) and monofunctional adducts. The proportions of adducts observed are detailed in Table 1.4.

Adducts	%
cis-[Pt(NH$_3$)$_2${dGpG}]	60-65
cis-[Pt(NH$_3$)$_2${dApG}]	20-25
cis-[Pt(NH$_3$)$_2${dGpNpG}] *or cis*-[Pt(NH$_3$)$_2${dG}{dG}]	4-8
cis-[Pt(NH$_3$)$_2${dG}Y] (Y = Cl⁻, H$_2$O, OH⁻, protein)	2-3

Table 1.4 Platinum-DNA adducts formed on treatment of salmon sperm DNA with cisplatin[29]

It is notable that although both d(GpG) and d(ApG) 1,2 intrastrand crosslinks are observed, there are no occurrences of d(GpA) crosslinks. Studies using *cis*-$[Pt(NH_3)_2(H_2O)_2]^{2+}$ on various oligonucleotides have shown the following[30]: the rate constants for platination of A are much lower than for G (this is due to the fact that G has the highest electron density on DNA[31]) 3′-monoadducts chelate up to 10 times faster than 5′ monoadducts (this could be due to the rigidity of the DNA and the relative distances to adjacent bases). These factors mean that in the GA case the rate of closure for the less nucleophilic A in the geometrically unfavoured 3′ position to the Pt would be expected to be very low. This could account for the absence of the GA adduct.

The mechanism of reaction of cisplatin has been investigated using ^{195}Pt NMR spectroscopy.[32-33] The hydrolysis reaction is the rate limiting step for DNA binding, the half-life being ~ 2h. Aquated cisplatin subsequently binds to an N7 atom of a guanine base in DNA, which displaces the water molecule in a relatively fast reaction step (half-life ~ 0.1 h), forming a monofunctional adduct. Closure of the monofunctional adduct to form a bifunctional adduct involves hydrolysis of the second chloride ligand with a half-life of ~ 2 h.

By labelling cisplatin with $^{15}NH_3$ ligands, the DNA adducts and intermediates can be characterised by NMR.[34] In the formation of the GG interstrand crosslink, the diaqua complex shows little selectivity for 5′G or 3′G in the initial platination step whereas the chloro-complex preferentially platinates the 3′G. However replacement of T by C at the 3′ side of the GG site increases the selectivity of the diaqua by a factor of 6. Unexpectedly, the 5′G monoadduct is much longer lived ($t_{1/2}$ ~ 4 h – aqua, $t_{1/2}$ ~ 80 h – chloro) than the 3′G monoadduct ($t_{1/2} \leq 45$ min – aqua, $t_{1/2}$ ~ 6 h – chloro) on a double stranded oligonucleotide, but the lifetimes of the two monofunctional adducts are the same on the GG single strand.[34] This suggests the three-dimensional structure of DNA plays a role in stabilising the 5′-G adduct either by shielding the Cl ligand from hydrolysis or, or by constraining the position of the incoming 3′-G N7 ligand.

Since the most prevalent adduct formed on treatment of DNA with cisplatin is the 1,2-intrastrand crosslink it was suggested that these may be important for anticancer activity. Many structural studies have since been carried out to determine the nature of this cisplatin adduct on double and single-stranded DNA fragments, these have recently been reviewed.[35]

The first X-ray crystal structures determined of *cis*-GG crosslinks were for the dinucleotide d(pGpG)[36] and the trinucleotide d(CpGpG).[37] The structures are shown in Figure 1.7, (A) and (B) respectively. The dinucleotide structure has the two guanine rings in a "head-to-head" configuration, with the two O6 atoms on the same side of the platinum coordination plane. The bases are forced to destack with an average dihedral angle of 81.1°. A hydrogen bond is also present between one of the platinum ammine ligands and an oxygen atom on the 5′-phosphate group.

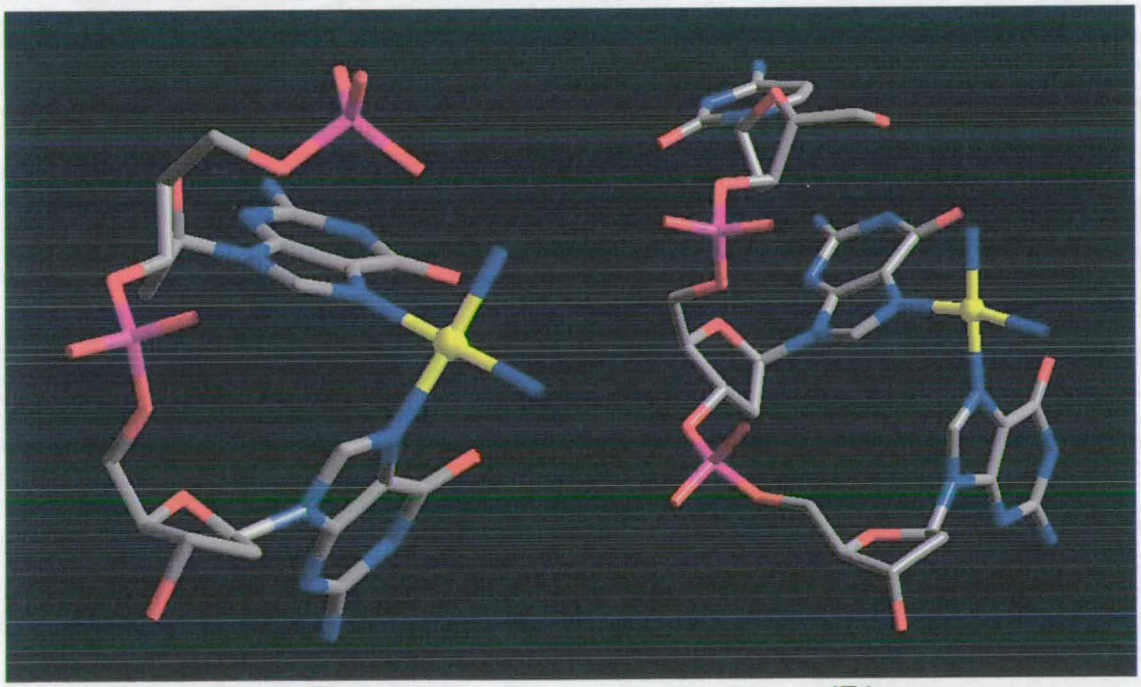

Figure 1.7 (A) – X-ray crystal structure of d(pGpG) containing a *cis*-GG Pt adduct[36]
(B) – X-ray crystal structure of d(CpGpG) containing a *cis*-GG Pt adduct[37]

To obtain structural information on the cisplatin adduct in longer oligonucleotide structures, gel electrophoresis studies were initially employed.[38] These indicated a bending and unwinding of the DNA duplex structure. This was then followed by several high-resolution X-ray and NMR structural studies. Figure 1.8 shows a 2.6 Å resolution X-ray structure of a DNA dodecamer duplex containing a 1,2-intrastrand crosslink.[39-40] The structure contained two molecules in the asymmetric unit with very similar structures. The two duplexes show a significant bend towards the major groove (39° and 55°). The dihedral angle between the guanine bases is 30°, considerably less than that seen in the d(pGpG) structure. However, the ammine-phosphate hydrogen bond is conserved. The base pairs at the platination site are propeller-twisted, but retain their hydrogen bonds. The platinum is displaced from the planes of the guanine rings by ~ 1 Å resulting in a strained square-planar environment for Pt(II). The conformation of the DNA alters at the site of platination. In the 5′ direction it adopts the A-form with the sugar rings in a C3′ endo configuration, while in the 3′ direction it is B-form with a C2′ endo sugar pucker. An overall consequence of the platinum binding is a widened shallow minor groove, a feature that may be important for protein recognition and anticancer activity.

An NMR structure of the same platinated dodecamer duplex has been determined allowing comparison of solid and solution phase structures. This structure (Figure 1.9)[41] shows an overall helix bend of 78° and the dihedral angle between adjacent guanines was 47°. These values are larger than those observed for the crystal structure reflecting the influence of crystal packing. The base pairing is also more distorted in the solution structure. The platinum still shows distorted geometry and the overall helix structure is similar with a wide flat minor groove. Other NMR duplex structures have been determined for a platinated octamer[42] and a palindromic dodecamer.[43] The major features of all these structures are compared in Table 1.5.[35]

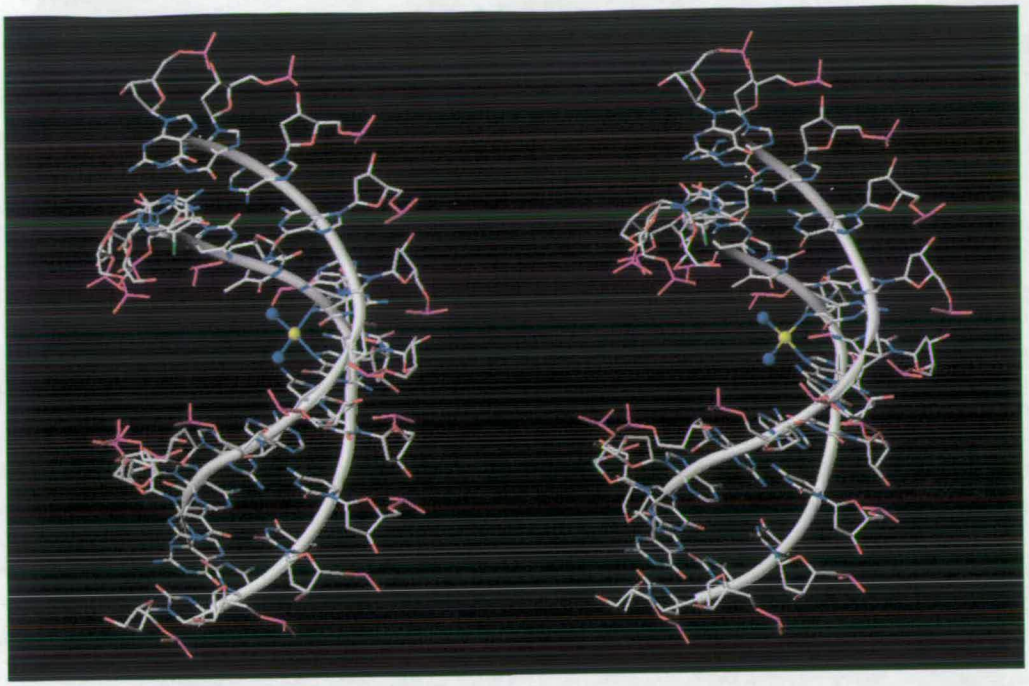

Figure 1.8 X-ray crystal structure of $\{Pt(NH_3)_2\}^{-}$ d(CCTCTG*G*TCTCC)·d(GGAGACCAGAGG), containing a *cis*-GG adduct where G* represents platination site (PDBID 1GPG)[39-40]

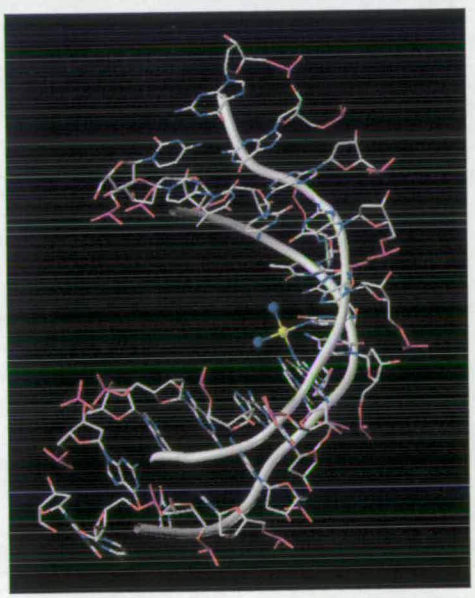

Figure 1.9 NMR solution structure of $\{Pt(NH_3)_2\}^{-}$ d(CCTCTG*G*TCTCC)·d(GGAGACCAGAGG), containing a *cis*-GG adduct where G* represents platination site (PDBID 1A84)[41]

Structure reference	*39, 40*	*41*	*42*	*43*
Sequence	d(CCTCTGGTCTCC) d(GGAGACCAGAGG)	d(CCTCTGGTCTCC) d(GGAGACCAGAGG)	d(CCTGGTCC) d(GGACCAGG)	d(CTCTCGGTCTC) d(GAGAGCCAGAG)
Method	X-ray	NMR	NMR	NMR
DNA form	A/B junction	primarily B	primarily B	primarily B
Minor groove width/depth (Å)	9.5-11.0 / 3.0	9.4-12.5 / 1.4	4.5-7.8 / 3.2	9.0-12 / 2.1
Average P-P distance (Å)	5.5	6.9	6.8	6.8
Roll at platinated bases (°)	26	49	42	59
Pt atom displacement from	1.3 - 5′	0.8 - 5′	1.0 - 5′	0.5 - 5′
guanine ring planes (Å)	0.8 - 3′	0.8 - 3′	0.8 - 3′	0.65 - 3′
Average helical twist (°)	32	25	25	26
DNA bend (°)	39, 55	78	58	~81

Table 1.5 Selected structural parameters of GG cisplatin-DNA adducts

The octamer structure shows an interesting rearrangement from the 1,2 intrastrand crosslink to a more stable interstrand crosslink promoted by the presence of a nucleophilic chloride ion.[42] Structures of some minor cisplatin-DNA adducts have also been determined including an interstrand crosslink[44] and a 1,3 intrastrand crosslink.[45]

In conclusion these high resolution studies all indicate that the major 1,2 intrastrand crosslink of cisplatin affords a bent and unwound duplex with a wide, shallow minor groove, unlike any other cisplatin adducts. This specific feature could be significant in cisplatin's anticancer activity.

1.3.2.3 Recognition of Cisplatin-DNA Adducts

A number of proteins has been identified which show affinity towards cisplatin modified DNA and have recently been reviewed.[46] A large family of related proteins with the ability to bind to cisplatin adducts is the HMG (High Mobility Group)

proteins. The binding ability was discovered 10 years ago during initial screening experiments. Two species were identified, of molecular mass ~100 kDa and 28 kDa, which bind to double-stranded DNA modified with cisplatin. In the same study two cDNA clones were isolated from a human B-cell cDNA library which encoded portions of a protein that bind specifically to the cisplatin adduct. This ultimately led to the isolation and characterisation of a full-length human cDNA clone that coded for a structure-specific recognition protein (SSRP). This protein contained a number of highly-charged domains, including the 75 amino acid DNA binding region known as the HMG domain. Although these domains had been shown to bind specific DNA sequences; this work demonstrated that such a domain could also recognise specifically DNA having altered structures. These initial experiments suggested that HMG-domain proteins were strong candidates for binding preferentially to cisplatin-modified DNA and perhaps affecting its biological properties.

Proteins in the family can contain multiple HMG domains. They bind in the minor groove of DNA and bend DNA on binding. HMG1 is a chromosomal protein containing two prototypical HMG domains, A and B, both have three α-helices forming an L shape with ~80° between the arms. The NMR solution structure of domain A is shown in Figure 1.10(A).[47] This L-shape seems to be common amongst HMG domains and may be necessary for positioning on the DNA. The binding affinity of HMG1 towards a series of cisplatin-modified 15-mer DNA duplexes d(CCTCTCN1G*G*N2TCTTC)·d(GAAGAN3CCN4GAGAGG) has been investigated and shown to be highly dependent on the bases adjacent to the Pt-lesion.[48] The affinity for HMG domain A decreases by over two orders of magnitude in the order N2 = dA > T > dC. When N1 = N2 = dA, Pt DNA binds 100-fold stronger to HMG1 domain A then to domain B. Several studies show that binding of HMG full-length protein or individual domains can further bend the kinked DNA structure by up to 90°. A recent X-ray crystal structure has been determined of the HMG1 domain A bound to a 16-bp DNA probe, containing a *cis*-GG adduct.[49] (Figure 1.10 (B)) This structure shows that the protein binds through its concave surface and bends the DNA by ~61° The protein bend is offset from the platination site, by 2-bp to the 3′ side. The protein intercalates a Phe side chain into the DNA, in

a hydrophobic section in the minor groove opposite the platinum adduct. The geometry of the platinum site is less constrained than in either the X-ray or NMR structures of the cisplatin-modified duplex.

Several mechanisms have been considered for how HMG-domain proteins might modulate the sensitivity of cells to cisplatin. Two of the more prominent hypotheses are as follows.

1. The cisplatin-DNA adducts hijack proteins away from their normal binding sites, thereby disrupting cellular function. Since many HMG-domain proteins function as transcription factors, their removal from promoter or suppresser sequences by binding to cisplatin-DNA adducts could severely alter tumour cell biology.
2. HMG-domain proteins block cisplatin-DNA adducts from damage recognition needed for repair. This would result in diminished repair of the adducts, and persistence of platinum on the DNA would lead to cell death.

The hypotheses are not mutually exclusive and could both contribute to cisplatin cytotoxicity. Although it remains to be proved that HMG proteins are important mediators in cisplatin activity, a large body of experimental evidence points to their likely importance.[46] Recently S. J. Lippard's group have described work[50] in which human cancer cells with steroid hormone receptors, have been treated with the appropriate hormone estrogen and/or progesterone. The potency of cisplatin and carboplatin to these cells is then increased by causing overexpression of the HMG1 protein. This could have major implications in the treatment of ovarian and breast tumours which carry the hormone receptors.

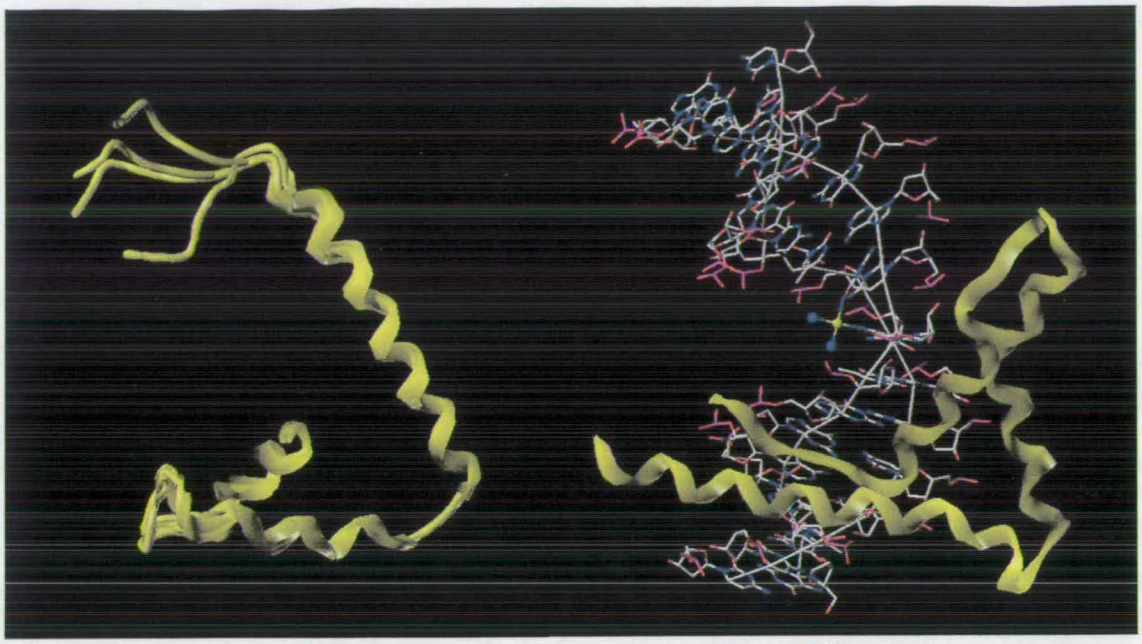

Figure 1.10 (A) The NMR refined structure of HMG1 protein domain A (PDBID-1AAB)[47] **(B)** The X-ray crystal structure of HMG1 domain A bound to a 16-mer containing a *cis*-GG adduct (PDBID-1CKT)[49]

In over 35 years of research since the discovery of cisplatin, much has been elucidated about the anticancer activity of the complex. Although this research is far from complete, the information gathered so far is useful for the design of new more powerful drugs with the aims of reducing toxic side-effects, improving the spectrum of activity and overcoming resistance.

1.3.2.4 Resistance to Cisplatin Treatment

Resistance to cisplatin can be both natural and acquired. Some tissues are inherently resistant to cisplatin and do not respond to treatment, whilst other types, such as ovarian cancer may respond initially to treatment but acquire resistance over time.

Cisplatin-resistant cells can be made through repeated exposure to the drug. Comparison between parental and resistant cell lines then provides an insight into the mechanism. Three main processes have been proposed for cellular resistance and it is likely that a combination of these factors plays a role. These processes have been comprehensively reviewed[51] and are discussed below.

1. *Changes in intracellular accumulation of the drug* - A number of studies on ovarian cell lines have shown significantly reduced accumulation of platinum inside resistant cells by up to 50%. This is due to either reduced intake or enhanced efflux of cisplatin. This feature is not consistent in all resistant cell lines however and cannot be the sole cause of resistance. A P-glycoprotein, found in multi-drug resistant cell lines, has been found to act as a pump, which prevents the accumulation of drugs in the cell.
2. *Increased production of intracellular thiols* - The affinity of platinum ions for S-donor ligands suggests that cisplatin may bind to intracellular peptides such as glutathione (GSH) and metallothionein (MT), thus preventing or reducing binding to DNA. Elevated levels of GSH or MT have been observed in some cisplatin-resistant cells. The role of S-peptides in transport of platinum drugs can not be ruled out as it has been shown that sulphur-containing ligands (kinetically preferred) can be displaced by nucleotide/DNA binding (thermodynamically more favoured) in platinum (II) complexes.[52]
3. *Increased capability of cells to repair cisplatin-DNA damage* – Numerous experiments have revealed enhanced DNA repair in cisplatin-resistant lines, however increased repair does not always correlate with the level of cisplatin resistance.

From the experimental results reported so far, the mechanism of cisplatin resistance appears to be to be complex and multifactorial. More work must be done to solve this important problem if the goal of overcoming cisplatin-resistance is to be realised.

1.3.3 Development of New Platinum Drugs

Since the introduction of cisplatin there have been many attempts to design improved platinum anticancer agents. This is because the applicability of cisplatin is still limited to a relatively narrow range of tumours, resistance is a major problem and the major toxic side-effects are dose limiting. Cisplatin also has limited solubility in water and must be administered intravenously making it inconvenient for outpatient oral treatment. Although many compounds have been made and their antitumour activity tested, very few make it into clinical trials.

1.3.3.1 Classical Structure-Activity Rules

The initial criteria deemed necessary for activity of platinum complexes were derived from early systematic studies. Various factors must be considered in the structure of an active compound. Firstly the geometry of the complex. This was thought to be limited to *cis*-compounds by Rosenberg's initial results. Secondly, the nature of the leaving groups determines the reactivity of the complex. If they are too labile (for example nitrate ligands) the complex is too toxic, binding to other biomolecules *in vivo* before reaching the active site. However, if the leaving ligands are too strongly coordinating (e.g. iodide), the complex will not bind to DNA and will be inactive. The non-leaving groups (amines) also have a large effect in activity as they can exert steric hindrance on the platinum centre controlling the rate of substitution. The H-bonding ability of the amines can also be important as well as their *trans* effects, in controlling the binding properties of the complexes. The oxidation state of the platinum is also a factor since platinum(IV) compounds are far more inert *in vivo* than their platinum(II) counterparts.

The requirements for an active complex were determined to be:[53]

1. A *cis*-complex of the form $PtX_2(amine)_2$ for Pt(II), and $PtX_2(amine)_2Y_2$ for Pt(IV), (with Y ligands *trans*)

2. The X ligand (leaving group) should be an anion with intermediate binding strength such as Cl^-, citrate, oxalate, and other carboxylic acid residues. The Y ligands can be Cl^-, OH^-, or $^-O(CO)C_nH_{2n+1}$
3. The complex should be uncharged, as it is believed they are taken into the cell by passive transport through the lipophilic cell wall, a pathway less available to charged compounds.
4. The amine should possess at least one NH moiety, necessary for H-bonding interactions with DNA. These H-bonds (to O6 of guanine or the 5′-phosphate group) are important thermodynamically to stabilise the DNA adduct, and kinetically, directing the platinum to the N7 position.

1.3.3.2 Second Generation Platinum Anticancer Agents

Although over 28 complexes have entered human trials the only one to have received worldwide approval and achieved routine clinical use apart from cisplatin is Carboplatin, [diammine(cyclo-butanedicarboxylato-O,O′)platinum(II)], (Figure 1.11, complex **1**). The greater chemical stability of this complex, compared to cisplatin,[54] results in slower hydrolysis reactions.[55] It therefore shows a lower reactivity towards biomolecules leading to reduced side-effects *in vivo*. This means higher doses of up to 2000 mg/dose can be administered.[21] Other clinically approved compounds are a glycolato complex, nedaplatin and an oxalato complex, oxaliplatin (Figure 1.11, complexes **2** and **3**). These have been approved for clinical use in Japan and France, respectively, and are particularly effective in combination chemotherapy for advanced lung, colorectal and ovarian cancers.[56] These classical compounds show no major advantages over cisplatin and so the search continues for new active agents. One approach is to develop sterically hindered complexes, an example being *cis*-amminedichloro(2-methylpyridine)platinum(II) (ZD0473, Figure 1.11, complex **4**). This was rationally designed to circumvent resistance by hindering substitution by GSH and other cellular thiols while retaining the ability to form cytotoxic lesions with DNA. The crystal structure of the complex shows the pyridine ring to be tilted out of the platinum plane by 102.7° placing the methyl group directly over the square plane.[57] This reduces the rate of hydrolysis reactions as it is blocking axial access to

the platinum, inhibiting the formation of the five-coordinate intermediate. In vitro studies of ZD0473 showed it to be active in cisplatin-resistant cell lines. The compound entered clinical trials in 1997 and has also been shown to be orally active.

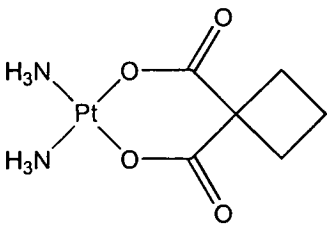

(1) Carboplatin

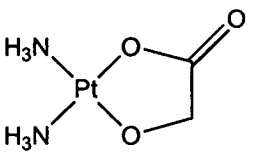

(2) Nedaplatin

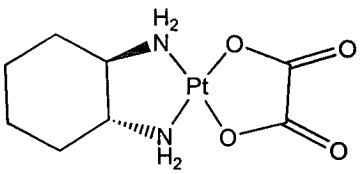

(3) Oxaliplatin

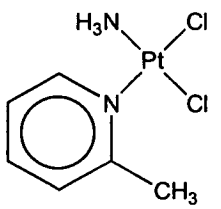

(4) ZD0473

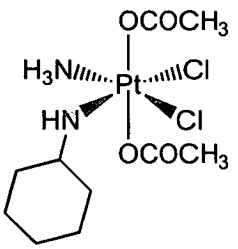

(5) JM216

Figure 1.11 New platinum anticancer agents, clinically approved or in human trials

The desire to develop an orally active Pt drug has reinitiated the interest in Pt(IV) compounds. The complex JM216 (Figure 1.11, complex **5**), in currently in phase II clinical trials and shows increased *in vitro* and *in vivo* activity against human cervical, small cell lung, and ovarian carcinoma cell lines.[56] Since Pt(IV) compounds are much more inert to ligand substitution than Pt(II), it is generally believed that they are reduced to Pt(II) by extracellular and intracellular agents prior

to reaction with DNA. The electron-withdrawing ability and steric hindrance of the axial and carrier ligands have a large influence on the redox process and biological activity of these complexes.

1.3.3.3 New Rule-Breaking Platinum Compounds

More recently a number of complexes which do not adhere to the classical structure-activity relationships, has been shown to exhibit antitumour activity.[56]
Since the *in vivo* behaviour and mechanism of actions of these complexes is expected to be completely different from those for cisplatin or carboplatin, it is hoped that they could overcome platinum resistance in tumours and be applicable to a broader range of cancers.

Most of the previous work on the design of platinum complexes has concentrated on *cis* complexes since the early discovery, by Rosenberg, that *trans*-$[Pt(NH_3)_2Cl_2]$ was inactive. However, since the report that *trans*-$[Pt(pyridine)_2Cl_2]$ is potently cytotoxic,[58] there has been renewed interest in the *trans* geometry. It is now believed that the higher kinetic reactivity of transplatin compared to cisplatin leads to its deactivation by reactions with biomolecules *in vivo*. It is then possible to design complexes using sterically hindered ligands to reduce the reactivity of the Pt. The *trans* complexes are not capable, sterically, of forming the cisplatin-like 1,2-intrastrand crosslinks, they form mainly interstrand crosslinks. In this way *trans* complexes could overcome cisplatin resistance. Several groups have persued this concept of activating the *trans* geometry.

Farrell and colleagues have compared the cytotoxicities of three series of *trans* complexes with the general formula $[PtCl_2(L)(L')]$ where: (i) L = L′ = pyridine, N-methylimidazole, thiazole, (ii) L = quinoline, and L′ = RR′SO (R = methyl, and R′ = methyl, phenyl, benzyl), (iii) L = quinoline and L′ = NH_3.[59] Examples are shown in Figure 1.12, complexes **6**, **7** and **8** respectively. The Pt compounds in these three series showed comparable activity to cisplatin in sensitive cell lines and also activity in cisplatin-resistant cell lines.[59] Interestingly they also showed higher activity than their *cis* counterparts. In particular the complexes showed activity in cisplatin

resistant cell lines where the mechanism of resistance was known to be due to reduced Pt accumulation and enhanced removal of and/or increased tolerance to Pt-DNA adducts. Kelland *et al.*[60] have shown that a series of Pt(II) and Pt(IV) complexes of the type *trans*-$[Pt(NH_3)(RNH_2)Cl_2]$ and *trans, trans, trans*-$[Pt(NH_3)(RNH_2)(OH)_2Cl_2]$ are highly active *in vitro*, where R = cyclohexyl (JM335) activity is comparable to cisplatin (Figure 1.12, complex **9**). Coluccia *et al.* have also demonstrated the activity of the *trans* geometry with a series of Pt(II) complexes with iminoether ligands.[61] For example, *trans*-$[Pt\{E\text{-}HN{=}C(OMe)Me\}_2Cl_2$ (Figure 1.12, complex **10**) has much higher antitumour activity than its *cis*-analogue . The mechanism of action appears to different to that of cisplatin and may be related to the properties of the imino ether ligands.[62] Although these *trans* complexes react with DNA more slowly than cisplatin, they achieve the same level of DNA binding after 24h. The *trans E,E* complex is the most effective in inhibiting DNA synthesis and cell proliferation, but does not induce large local DNA conformational changes.[63]

Another approach to the design of complexes that form radically different Pt-DNA adducts is the use of multinuclear complexes with bridging linkers.[53, 56] Farrell and colleagues have been most active in this area investigating complexes of the form $[\{PtCl_m(NH_3)_{3-m}\}\mu\text{-}H_2N\text{-}R\text{-}NH_2\text{-}\{PtCl_n(NH_3)_{3-n}\}]^{[(2-m)+(2-n)]+}$ (m or n = 0-3, and R is a linear or substituted aliphatic linker). The most successful of these complexes is BBR3464.[64] (Figure 1.12, complex **11**) The central Pt moiety has no leaving groups and is capable only of forming hydrogen bonds with DNA. The high charge greatly enhances DNA affinity, with the major adduct formation being long-range interstrand crosslinks up to 6 base-pairs apart with significant unwinding and efficient, irreversible B- to Z-DNA conversion. These adducts terminate DNA synthesis *in vitro*. In preclinical trials this compound has exhibited a complete lack of cross-resistance to cisplatin-resistant cell lines. It is also significantly more potent than cisplatin in some carcinomas.

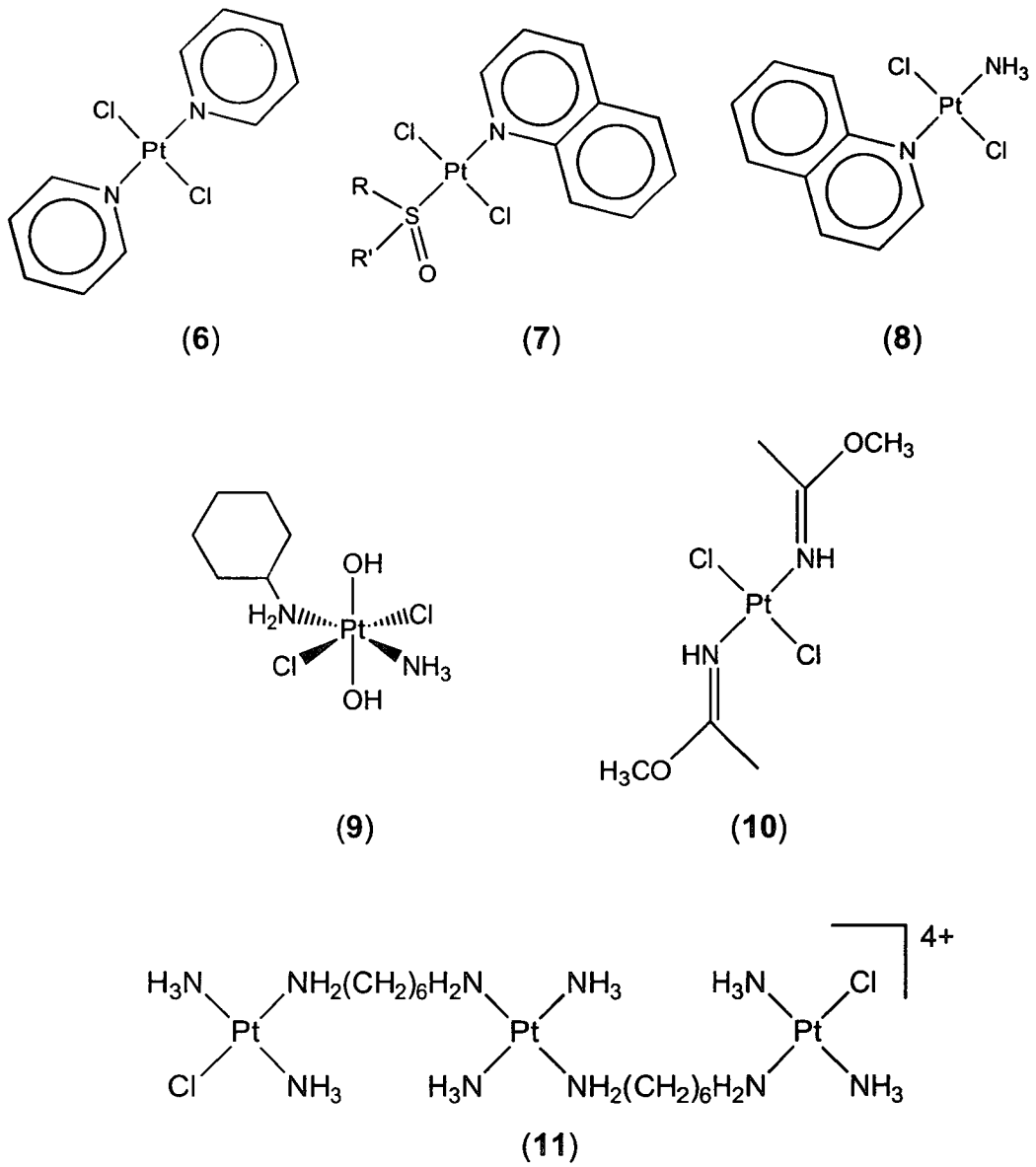

Figure 1.12 Antitumour-active platinum compounds, not adhering to classical structure-activity relationships

There is good hope that these new classes of compounds may help to expand the realm of platinum chemotherapy treatment.

1.4 Phosphines in Medicine

1.4.1 Chemistry of Phosphines

In mammalian systems, the chemistry of phosphorus is entirely that of the P(V) oxidation state and the whole of biology revolves around phosphate and its derivatives. The term "phosphine" describes both PH_3 and its substituted derivatives PH_2R, PHR_2, and PR_3. The most dominant characteristic of all phosphine compounds is the presence of the lone pair of electrons on P. These compounds can therefore act as both nucleophiles and bases. The P atom is larger and less electronegative than N and therefore has higher nucleophilic reactivity than the analogous nitrogen compounds. This high nucleophilicity and formation of strong bonds to C, N, O, or S, have made them one of the most widely used class of regents in organic synthesis. In addition, phosphorus has the ability to expand its valence shell to ten electrons and thus trivalent phosphorus compounds can also behave as electrophiles. This is generally only seen for PR_3 compounds containing electron-withdrawing substituents (e.g. Cl, F). One of the most common features of tertiary phosphines is the formation of very strong P=O (phosphoryl) bonds, with energies lying in the range 534 to 582 $kJmol^{-1}$.[65] This bond formation can act as the driving force for many phosphine reactions.

Complexes of phosphines with virtually every transition metal have be shown to form, making them one of the most versatile and commonly encountered ligands available.[66] The electronic versatility of phosphines, mentioned above, makes it possible to bind to metals in both very high and low oxidation states (+IV to –I). The biological activity of phosphines may be related to their ability to coordinate to metals in critical sites, but whilst the chemistry of phosphines and metal phosphine complexes has been well studied their biological properties have not.

1.4.2 Gold Antiarthritic Drugs

The chemistry of gold drugs has recently been comprehensively reviewed.[67] Gold has been used in the field of medicine from as early as 2500 BC in Chinese and

Arabic traditions as a "cure-all" treatment. In 1929, Forestier discovered that gold was effective for the treatment of rheumatoid arthritis[68], but it was not until 1960 that controlled clinical trials were able to prove the efficacy of gold therapy.[67] A number of injectable gold thiolate compounds are now in clinical use for very difficult arthritis cases. (Examples are shown in Figure 1.13, structures **12** and **13**). These complexes are now known to be polymeric in the solid state and solution, forming ring or chain structures.[69, 70] The drugs have some side effects associated with their use, the most severe being exfoliative dermatitis, bone marrow suppression, and nephrosis.[67] In the mid 1960's a search was undertaken by the Smith Kline and French company to find an orally active drug to overcome these problems and those associated with painful intramuscular injections of the thiolate compounds. It was hoped this would allow blood levels of gold to be maintained with a low daily dose, preventing the accumulation of gold in tissues following the large injected doses. Several gold(I) phosphines were found to have oral activity in animal models, including Et_3PAuCl and $(Et_3P)_2AuCl$, but these had severe side effects.[71] Eventually a tetraacetylthioglucose derivative, auranofin (Figure 1.13, structure **14**) was approved for use in 1985 under the trâdename "Ridaura".

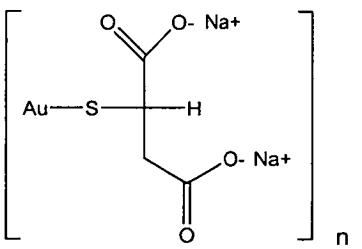

(12) aurothiomalate
(Myocrysin)

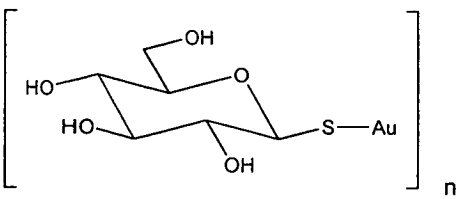

(13) aurothioglucose
(Solganol)

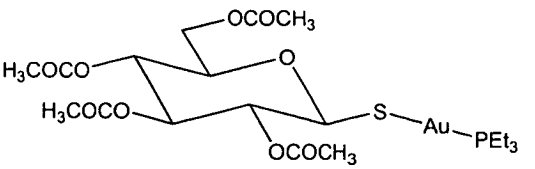

(14) auranofin (Ridaura)

Figure 1.13 Clinically approved gold antiarthritic drugs (Tradename)

Ligand-exchange reactions of linear gold(I) complexes are facile, via an associative mechanism with a 3-coordinate intermediate. The Au-P bond is strong but the thiol ligand can easily be displaced *in vivo* by sulfur containing serum proteins. Over 80% of gold in circulation in the body after administration can be found bound to albumin at Cys-34[72] (the only one of the 35 Cys residues not oxidised in a disulfide bond). The high affinity of Cys-34 for Au(I) is consistent with its reported low pK_{SH} (ca. 5.5). Once the gold is bound to the albumin, the phosphine can be displaced by another ligand such as CN^- (this may affect the rate of gold metabolism in smokers). The free phosphine can then reduce a disulfide bridge in the albumin to free thiols which are then available to bind more drug.[73] This results in a series of gold-albumin complexes with variation in the position of gold binding determined by which of the disulfide bridges is oxidised. This illustrates the *trans effect* resulting in labilisation of the phosphine. After loss of the phosphine, the products from metabolism of auranofin could be similar to the products from gold(I) thiolate drugs. The phosphine ligand therefore may influence the distribution of gold *in vivo* without necessarily contributing to the antiarthritic activity of the complex.

1.4.3 Cytotoxicity of Gold-Phosphine Complexes

1.4.3.1 Auranofin and its Analogues

Lorber and co-workers first demonstrated that auranofin exhibited cytotoxic activity to human cell lines in culture and increased the survival time of mice with P388 leukaemia.[74] Further studies showed that while it has potent cytotoxicity against a variety of cell lines *in vitro*, it is active only against the P388 tumour model *in vivo*.[75] It is therefore not useful as an anticancer agent, and a large number of other gold(I) phosphine complexes of the form R_3PAuX have had their cytotoxicity evaluated.[76] These all exhibited potent cytotoxicity *in vitro*. *In vivo* the activity was related to the leaving group, X, being lowest when X was a good leaving group (e.g. Cl^- or NO_3^-). These complexes are very reactive to thiols and it is likely the *trans* ligand will be rapidly displaced by –SH groups *in vivo* so that R_3PAu- will bind to proteins and be prevented from reaching intracellular targets. Indeed, the cytotoxic potency of

auranofin to cultured tumour cells *in vitro* has been shown to be reduced ten-fold when the culture medium contains serum proteins, suggesting gold-protein binding can be correlated with loss of activity.[75]

It appears that the phosphine is responsible for the anticancer activity of these complexes since replacement of the phosphine with another thiolate group gives complexes with at best marginal activity *in vivo*. Over 150 free tertiary phosphines have been tested for anticancer activity but again none showed more than marginal activity.[77] It is likely that phosphines will be rapidly oxidised *in vivo,* since they are very good reducing agents, and this could inactivate them. It is possible that coordination to gold(I) may protect the phosphine from unfavourable oxidation allowing it to be carried to the target site.

1.4.3.2 Diphosphine Chelated Gold Complexes

In order to design gold(I) phosphine complexes with increased activity, it was therefore necessary to design complexes with increased stability, less reactive to ligand exchange reactions. In this way binding to serum proteins can be prevented allowing the active component to reach its target. This has been achieved through the use of tetrahedral gold(I) complexes. In contrast to linear Au(I) complexes these do not undergo ligand exchange via an associative mechanism but by a dissociative mechanism, since no 5-coordinate intermediate is observed. The use of a diphosphine chelating ligand introduces further stability to the complexes because ligand exchange will also require a ring-opening mechanism. ^{31}P NMR studies showed the existence of such a four-coordinate gold complex, $[Au(dppe)_2]Cl$, (dppe = 1,2-bis(diphenylphosphino)ethane), along with free dppe in a solution of the bridged compound $ClAu(Ph_2P(CH_2)_2PPh_2)AuCl$.[78] Furthermore this complex appeared to have high kinetic stability and was stable at room temperature. Since this discovery, both five- and six-membered rings have been shown to form readily on Au(I) with phenyl-substituted diphosphines[79] whilst bisphosphines with longer

chain length prefer to form annular 3-coordinate gold dimers or bridged digold species with trigonal and linear coordination geometries respectively. (Figure 1.14)

$[Au(dppe)_2]Cl$ is much less reactive to ligand exchange than auranofin and consequently exhibits a wider spectrum of anticancer activity, including activity in a cisplatin resistant cell line. Moreover, $[Au(dppe)_2]Cl$ and cisplatin can be administered concurrently at their respective maximum tolerated doses to tumour bearing mice with no lethality. This combination of treatment is more effective against moderately advanced P388 leukaemia than cisplatin alone,[80] indicating that a different mechanism or site of action is involved.

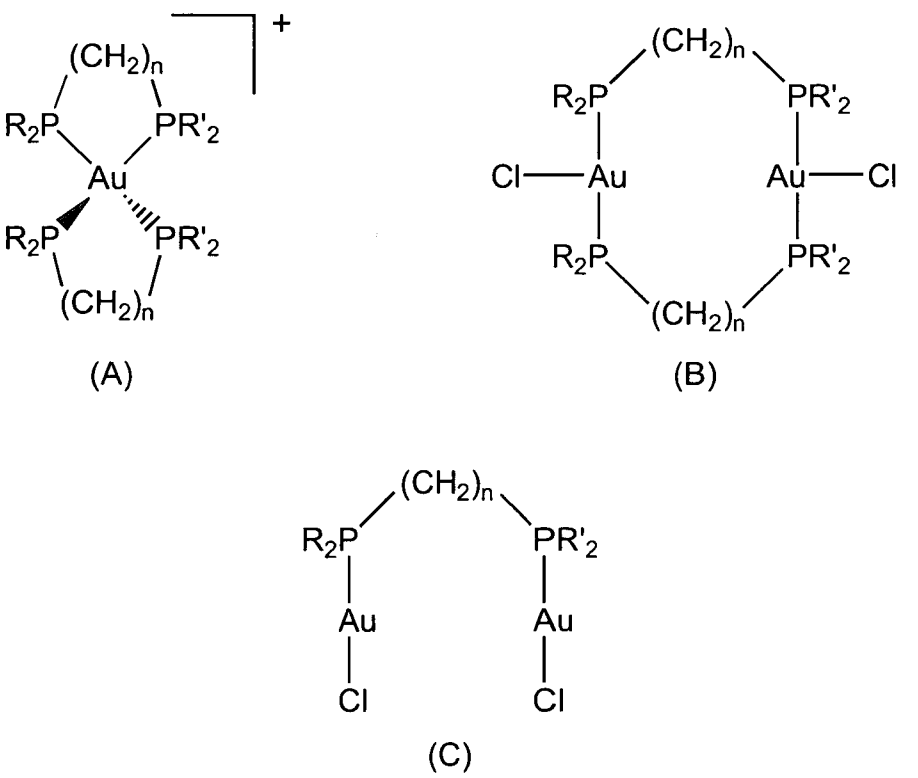

Figure 1.14 Structures of cytotoxic Au(I) diphosphine complexes: (A) tetrahedral gold bisdiphosphine, (B) annular digold bisdiphosphine, (C) bridged linear digold diphosphine

The series of free ligands, $Ph_2P(CH_2)_nPPh_2$, and dppe-bridged digold complexes of diphosphine ligands exhibit a pattern of activity towards P388 leukaemia similar to that of $[Au(dppe)_2]Cl$, although the complexes are much more potent (lower doses for same activity) than the free ligands.[81] Again this can be attributed to oxidation of the free phosphines, reducing their activity. The cytotoxicities of all the Au-phosphine complexes studied have been compiled and reviewed in references 67 and 77. In general the most active complexes seem to be those where the phosphines contain 2 or 3 carbon atoms in the bridge or where the bridge is *cis*-ethylene. These ligands are all capable of forming 5- or 6-membered chelate rings suggesting the mechanism of action may involve chelation of metal ions *in vivo*. Activity is lost if the phenyl groups on the phosphines are replaced by ethyl groups, but is retained if the gold(I) is replaced by silver(I) or copper (I). $[Au(dppe)_2]Cl$ was the most potent diphosphine compound of those tested.

1.4.3.3 Mechanism of Action

$[Au(dppe)_2]Cl$ shows very different cytotoxic effects to auranofin indicating a different mechanism of action. The complex is known to induce DNA-protein crosslinks and DNA single strand breaks when incubated with L 1210 cells.[80] The strand breaks are only significant at lethal concentrations but the crosslinks occur within the cytotoxic concentration range of the complex. The mechanism of action for these complexes is still not well understood but many have been postulated. The high kinetic and thermodynamic stability of these complexes along with their high lipophilicity is likely to mean that they can penetrate cells intact. It is still believed that the phosphine is the active component in the compound so the Au-P bond must be sufficiently labile to allow release of the phosphine at the target site. Since chelation of metals also appears to be involved in the mechanism of action, binding to copper may have an important role. Indeed, the cytotoxic potency of $[Au(dppe)_2]Cl$ is significantly increased in the presence of Cu-salts whereas Mg(II), Fe(II), Co(II) and Cd(II) have no effect.[82] Since phosphines readily reduce Cu(II) salts to Cu(I), chelation of copper could have major implications in Cu metabolism in the cell. Copper has previously been implicated in the anticancer activity of several

other chelating agents. Since Au is a soft metal, it has a high affinity for sulfur-containing ligands so many proteins could be bound *in vivo*. It is notable that many nucleic-binding and gene-regulatory proteins contain sites with multiple Cys residues, these could receive Au(I) or Cu(I) ions with functional consequences to the cell. It is possible that diphosphines could even remove metal ions from metalloproteins and metalloenzymes or act as inhibitors by binding to metal ions in active sites.

1.4.3.4 Development of New Phosphine Drugs

In preclinical trials $[Au(dppe)_2]Cl$ exhibited cardiac, hepatic and vascular toxicity.[83] For this reason no diphosphine gold(I) complex has entered full clinical trials as yet. These side effects have been attributed to the ability of the complex to uncouple oxidative phosphorylation in mitochondria and rapidly destroy the electrochemical potentials across the inner mitochondria membrane.[84] This has the effect of increasing the permeability of the mitochondrial membrane to cations (e.g. Ca^{2+}, K^{+}) disrupting the function of the mitochondria.

This toxicity towards mitochondria can be utilised in the design of new anticancer agents. Gold-diphenylphosphine complexes are extremely lipophilic and so non-selectively target mitochondria in all cells leading to the unwanted side effects described above. Recent work has been undertaken with the aim of modifying the ligands in metal complexes related to $[Au(dppe)_2]Cl$, in order to vary the hydrophilic character of the complex and achieve greater selectivity for tumour cells versus normal cells. Such lipophilic cations still target mitochondria but exhibit preferential cytotoxicity in carcinoma cells with hyperpolarised membranes. Recent results with $[Au(dppe)_2]Cl$ analogues, in which some or all the aromatic groups have been replaced by hydrophobic pyridyl groups, have shown that the position of the N atom in the pyridyl ring finely modulates this lipophilic-hydrophilic balance and greatly affects the cytotoxicity of the complex.[85]

1.5 Aminophosphine Complexes of Platinum (II)

Aminophosphine complexes of platinum(II) combine two important characteristics – platinum bound amino groups of classical am(m)ine anticancer agents, and aryl phosphines as in the previously described cytotoxic gold complexes. In this manner it is possible to envisage complexes of this kind acting as multifunctional drugs which can exhibit antitumour activity via two different mechanisms.

1.5.2 Chemistry of Aminophosphine Complexes

Aminophosphines are mixed donor ligands containing a soft phosphorus donor and a hard nitrogen donor. They can therefore be chelating ligands conferring high stability to a metal complex. In complexes with platinum(II), a soft metal, the nitrogen atom binds more weakly than the phosphorus especially when the N is in a *trans* position to a P, which exerts a high *trans influence*.[86] Furthermore the strength of the M-N bond is affected much more by steric factors than that of the corresponding M-P bond.[87] Variation of the chain length in the ligand (and hence size of chelate ring) along with the substituents on the nitrogen can lead to displacement of the amino group from the metal to form ring-opened complexes with ligands bound only through phosphorus. This leaves a potential binding site on the metal, thereby increasing its inherent biological or catalytic activity. It is possible to form a series of complexes varying from bis-chelate to non-chelate by changing the ligand and the solution conditions. There have been many previous reports relating the potential use of aminophosphine complexes in catalysis including asymmetric hydroformylation of olefins or acetylenes.[88,89] The utility of these ligands in homogeneous catalysis lies in the susceptibility of the weak donor N to displacement by a substrate molecule, whereas the chelate effect confers additional stability on the catalyst precursor in the absence of the substrate. Another potential catalytic use is carbonylation, for example in hydroformylation, alkoxylation and polyketone production.[90,91] In contrast very few studies have explored the potential biological activity of these complexes.[92]

1.5.2 Biological Activity of Aminophosphine Platinum(II) Complexes

Recent studies involving complexes with ligands of the type:

$$R_2N(CH_2)_2PPh_2$$

(R = H, Me) have established that chelate ring-opening can be controlled under biologically relevant conditions of pH and chloride concentration.[93] The primary-amino ligand $H_2N(CH_2)_2PPh_2$ formed a bis-chelated structure (Figure 1.15, complex **15**), in the solid state and solution, due to the lack of steric bulk on the N substituents. However when the tertiary-amino ligand $Me_2N(CH_2)_2PPh_2$ was used, a mono-chelate product (Figure 1.15, complex **16b**) was formed. On dissolution in D_2O, ^{31}P NMR showed evidence of both this product and the bis-chelate, fully ring-closed form (Figure 1.15, complex **16a**). The equilibrium between the two was shown to be pH^* dependent, with the ring-opened species being favoured at low pH^*, and reversible. The p*K* value for this ring-opening reaction was determined to be 6.9. The equilibrium is also dependent on chloride concentration as would be expected. When all the Cl^- was removed by precipitation with $AgNO_3$, it was much harder to ring-open the chelate and a pH* of *ca.* 2 was required. Conversely when excess Cl^- was added it was possible to maintain the ring-opened form even at high pH* (>9).

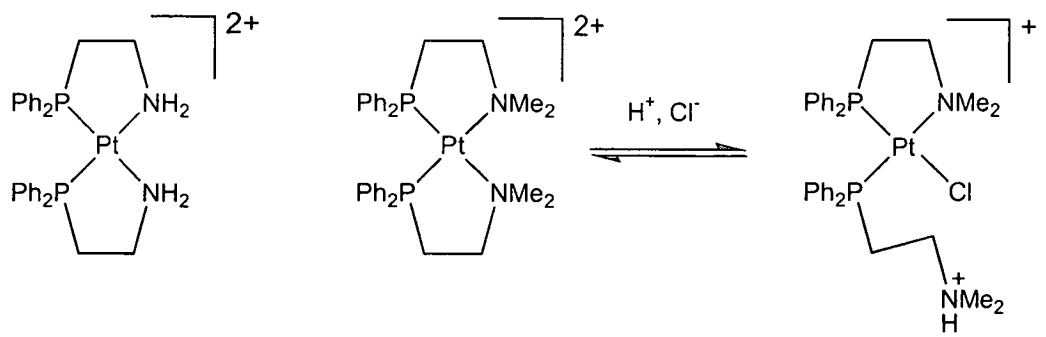

(15) **(16a)** **(16b)**

Figure 1.15 Aminophosphine platinum(II) complexes: (**15**) bis-chelate, (**16**) ring-opening equilibrium controllable by pH and [Cl^-]

The binding of these complexes to 5′-guanosine monophosphate (GMP) was investigated as a model nucleotide since the DNA base guanine is the most prominent binding site for platinum drugs in cells. The bis chelate complex **15** does not undergo facile reactions with 5′-GMP. Complex **16** reacts rapidly with 5′-GMP, (minutes) forming two isomers of the product *cis*-[Pt{$Me_2(CH_2)_2PPh_2$-*N,P*}-{$Me_2(CH_2)_2PPh_2$-*P*}(5′-GMP-N^7)]$^{2+}$ identified by ^{31}P and ^{1}H NMR. The bound 5′-GMP can easily be displaced by chloride which appears to be unprecedented. Surprisingly no reaction was observed between this complex and 5′-adenosine monophosphate (AMP) the second most prevalent base for platinum binding on DNA (see Section 1.3.2.2).

The bis-chelated and ring-opened complexes exhibit contrasting cytotoxicities towards cancer cell lines. The ring-closed complex **15** is relatively non-cytotoxic to LXFL non-small cell lung carcinoma and OVXF ovarian adenocarcinoma cells in culture whereas the ring-opened complex **16b** is only slightly less potent than cisplatin. In contrast both **15** and **16b** are active against A2780 cells and are as potent as cisplatin. However complex **16b** has a much lower resistance factor against an A2780 cell line which has acquired resistance to cisplatin, than either complex **15** or cisplatin itself. Therefore it seems likely that ring-opened and ring-closed aminophosphine complexes can act via different mechanisms in different types of cells. This could involve attack on DNA by platinum (like cisplatin-type complexes, section 1.3.2), interference with mitochondrial membrane potentials (since they are lipophilic cations like cytotoxic gold complexes, section 1.4.3.3) and/or redox reactions of the phosphine ligand (section 1.4.3.3).

Further investigation into reactions of complex **16b** with nucleotides showed an unexpected ability to bind strongly and reversibly to thymine and uracil under physiological conditions.[94] The N3 atom of thymine should provide a strong binding site for platinum[95] but has a high pK_a value (*ca.* 10)[96] and is usually inaccessible in double-stranded DNA due to involvement in A·T base pairs. Complex **16b** reacts with the nucleotide deoxythymine 5′-monophosphate (5′-dTMP) rapidly, within minutes, to form two diastereomers of the product *cis*-[Pt{$Me_2(CH_2)_2PPh_2$-*N,P*}-

$\{Me_2(CH_2)_2PPh_2\text{-}P\}(5'\text{-dTMP-}N^3)]^{2+}$. (Figure 1.16, complex **17**) These differ by 180° rotation around the Pt-N3 bond giving head and tail conformations of coordinated 5′-dTMP. Formation of this product may be influenced by the ability of the non-coordinated "dangling arm" amino group to accept a proton, aiding the deprotonation of the N3 site. Interactions of this dangling arm and the dTMP may help to stabilise these isomers. Reaction with the RNA nucleotide 5′-UMP was shown to follow a similar course. The pH-dependent stability of the 5′-dTMP complex was investigated and it was shown to exist over a wide range (pH* 3-8) with a p*K* of 5.1. The binding of 5′dTMP although strong is also reversible in the presence of chloride ions.

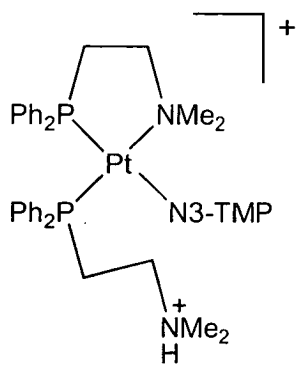

(17)

Figure 1.16 Binding of deoxythymine 5′-monophosphate to complex **16**

Following these discoveries, the binding of the complex to thymine in double stranded DNA was investigated using the self-complementary octamer oligonucleotide d(TTGGCCAA) which has previously been used to study the mechanism of formation of intrastrand crosslinks by cisplatin[97] but no thymine binding was reported to occur. The appearance of new singlet ^{1}H NMR peaks for thymine CH_3 groups shifted to high field, suggested direct binding of platinum to the N3 site as with 5′-dTMP. Some binding to N7 of guanine was also indicated

although the spectrum was too complex to assign fully. This is because binding to G and T on both strands is possible giving a large number of possible products.

The unusual binding of Pt to thymine is most likely to be due to a combination of the strong *trans* influence of the P and the role of the dangling arm amino group. This specificity of attack on DNA and control of chelate ring-opening could prove to be useful in the design of new anticancer platinum complexes with improved therapeutic properties, in particular overcoming factors which limit the use of current drugs: narrow spectrum of activity, resistance and toxic side effects.

1.6 Platinum(II) Complexes Containing Antiviral Nucleoside Analogues

1.6.1 Nucleoside Analogues as Antiviral Agents

Although there has always been much scepticism in the pharmaceutical industry about the development of nucleosides as antiviral agents, the majority of the drugs currently licensed in this field are nucleoside analogues. Nucleosides containing a free primary hydroxyl group or a phosphonate function in the sugar moiety are always good candidates for enzymatic phosphorylation potentially leading to incorporation of the modified nucleotide into the DNA. This incorporation may lead to mutagenesis subsequently followed by cell proliferation. This is a danger for host cells as well as viruses.

The enzymes used by virus and host to activate nucleosides and incorporate them in DNA are very similar. A nucleoside accepted as a substrate for a viral enzyme is therefore also a potential substrate for host enzymes. Moreover, the enzymatic machinery used to activate the nucleoside so that it becomes an antiviral agent and/or a toxic compound is often the same. In order to achieve an active antiviral agent a selectivity between virus and host must be achieved.

The range of nucleotide analogue classes having therapeutic potential has increased significantly in recent years.[98] In addition to modifications of conventional nucleosides, acyclic nucleosides have received a lot of attention and the success of acyclovir (Figure 1.17, complex **18**) has been a major influence in promoting this area. Other areas of interest are in carbocyclic nucleoside analogues, 4′-thionucleosides and L-nucleosides.

1.6.1.1 Acyclovir

The leading antiviral nucleoside agent to date is acyclovir which was discovered in 1974 (Zovirax - Figure 1.17, complex **18**). The antiviral activity, pharmacokinetic properties and therapeutic efficacy of acyclovir have recently been reviewed.[99] It was first launched for treatment of the herpes simplex virus (HSV), but its effectiveness and clinical safety profile have made it the drug of choice for a wide range of viral infections including varicella zoster virus (VZV) in both the primary infection (chicken pox) and recurrent infections (shingles). More than 30 million people have taken oral acyclovir and no serious side-effect has yet been identified. This is particularly due to the fact that acyclovir is taken up into virally-infected cells much more efficiently than into normal cells and is selectively monophosphorylated by the virally-encoded thymidine kinase. It is however a very poor substrate for the cellular enzyme. After further phosphorylation by host enzymes the resultant triphosphate is a substrate for and selective inhibitor of viral DNA polymerase. Incorporation of acyclovir into the growing DNA strand blocks elongation and prevents viral replication.

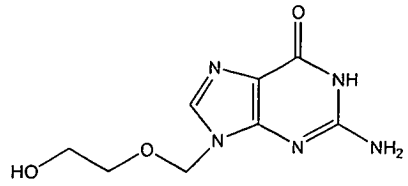

(18) Acyclovir

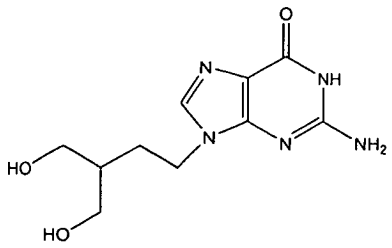

(19) Pencyclovir

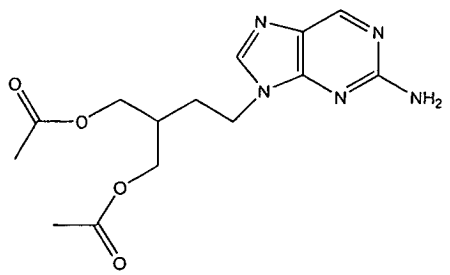

(20) Famcyclovir

Figure 1.17 Acyclovir, a potent antiviral guanosine analogue, and analogues

There are only two significant disadvantages associated with acyclovir. The drug is only approximately 20% bioavailable after oral administration and is absorbed through the gastrointestinal tract. Acyclovir-resistant strains of both HSV and VZV have been found and whilst resistance to acyclovir is not a problem for immunocompetent people, it may be for immunocompromised individuals who are prone to recurrent disease. As a result there has been a search for further acyclic analogues resulting in new compounds such as pencyclovir and famcyclovir[98] (Figure 1.17, complexes **19** and **20**). The antiviral activity of pencyclovir is similar to that of acyclovir but has a number of advantages such as faster onset, increased potency and longer duration of action, attributed to the increased half-life of its triphosphate relative to acyclovir. Famcyclovir is a prodrug for pencyclovir and has improved oral absorption.

1.6.1.2 AZT – an anti HIV agent

The emergence of the human immunodeficiancy virus (HIV) which is the causative agent of AIDS, further intensified efforts to identify active antiviral agents and 2′,3′-dideoxy analogues of conventional β-D nucleosides have featured prominently. 3′-Azido-3′-deoxythymine (AZT, zidovudine - Figure 1.18, complex **21**) was the first agent approved for use against HIV. HIV is a retrovirus, containing an RNA-directed DNA polymerase (reverse transcriptase) which catalyses the synthesis of a double-stranded DNA copy of the viral RNA, the first step in viral replication. The pharmacodymanic and pharmacokinetic properties, and therapeutic efficacy of AZT have been comprehensively reviewed.[100] AZT is taken up by T lymphocytes, immune system cells that are particularly vulnerable to HIV infection, and converted to AZT triphosphate (AZTTP) by thymidine kinase (the triphosphate cannot be administered directly as it cannot cross the plasma membrane). The HIV reverse transcriptase has a higher affinity for AZT triphosphate than deoxythymidine triphosphate (dTTP)[101] so the AZT acts as an inhibitor of dTTP binding. AZTTP can then be added to the 3′ end of the growing RNA/DNA chain, but because it contains no 3′ hydroxyl the RNA/DNA synthesis is terminated. The compound is not toxic to the T lymphocytes themselves as the cellular DNA polymerases have a low affinity for AZTTP compared to dTTP. Unfortunately the drug appears to be toxic to the bone marrow cells that are the progenitors of erythrocytes, and patients often develop anaemia. AZT can increase the survival time of patients with advanced AIDS by about a year and has also been shown to delay the onset of AIDS in individuals in the early stages of HIV infection.

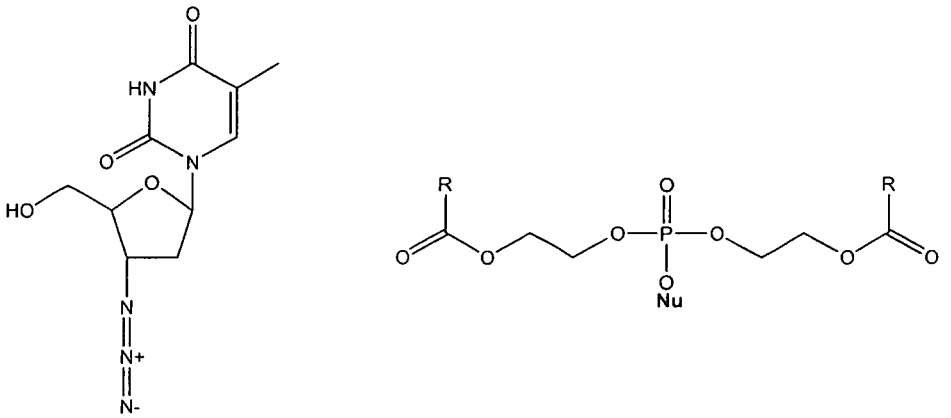

(21) AZT **(22)** Nu = AZT^-

Figure 1.18 Anti-HIV agent, AZT and a prodrug derivative

Chronic administration of AZT is associated with haematological toxicity and the emergence of resistant strains of the virus.[102] A number of strategies are being employed to overcome these problems. Clear advantages have been demonstrated in the clinic by using the approach of combination therapy with other nucleoside analogues and other agents. Another novel strategy is to devise a prodrug allowing intracellular delivery of AZT monophosphate to overcome the first highly demanding phosphorylation step. For example a phosphotriester derivative[103] (Figure 1.18, complex **22**) has been shown to undergo sequential intracellular carboxyesterase-mediated decomposition processes leading to the parent nucleotide.

1.6.2 Platinum Nucleoside Complexes

Cisplatin is known to be effective against virally-induced cancer. This coupled to the fact that it has a high affinity for guanine have lead to the rationale that cisplatin and related platinum antitumour agents may by effective in treating herpes simplex virus (HSV) infections. HSV viral DNA has a much higher GC (guanine-cytosine) content (66-70%) than normal human DNA (GC~40%). It was hypothesised that the viral DNA might be more susceptible to binding of cisplatin because of this and hence cisplatin might inhibit viral-DNA replication. Initially the *in vitro* activity of

cisplatin and several related species was evaluated against HSV-1 and HSV-2 viruses.[104] Cisplatin was the most active of the complexes tested with an activity comparable to that of acyclovir. The *in vivo* activity of cisplatin was then evaluated in an HSV-2 genital mouse model. The drug was found to have some effect when applied topically to the site of infection and no abnormal side effects were observed.

Following these promising results on the antiherpes activity of platinum drugs, a broad-based research project was initiated to investigate the antiviral activities of other inorganic and organometallic complexes.[105] Studies have initially been confined to complexes with known carcinostatic properties. Organotin complexes of the form $R_2SnX_2L_2$ (where R = CH_3, C_2H_5, C_6H_5; X = Cl^-, Br^-, L_2 = phenanthroline, or 1-(2-pyridyl)benzimidazole), were tested but showed only weak activity at most towards a range of DNA and RNA viruses and were non-inhibitory towards HIV-1. A range of metallocene and metallocenium complexes showed more promising results, $[(C_2H_5)_2Ti(bipy)][CF_3SO_3]_2$ having distinct activity against selected strains of the DNA virus herpes simplex.

A new strategy that emerged was the discovery that a number of platinum(II) square planar complexes containing selected antiviral nucleosides as part of the coordination sphere were, in many instances, less toxic to normal cells than either component and had similar or enhanced antiviral activities.[105] This strategy is based on the idea of combination treatment commonly used in cancer chemotherapy. Synergistic interactions between agents with different mechanisms of action can occur and the development of resistant cell lines is prevented. This has spawned the idea of *multifunctional drugs*,[106] i.e. combining two different cytotoxic moieties in the same drug. In contrast, investigation into antiviral drug combinations is relatively non-existent.

The complexes initially studied were $(NH_3)_2PtNu_2$ and $(dach)PtNu_2$ with the antiviral nucleosides acyclovir, DHPG (9-{1,3-dihydroxy-1-propoxy-methyl}-guanine), and DHBG (9-{3,4-dihydroxybutylguanine}). All the complexes were active against

HSV-1 and HSV-2 and showed a dramatic decrease in toxicity compared to the platinum precursor complexes for reasons not yet understood.

More recently, the complex $[PtCl(NH_3)_2(acyclovir)]NO_3$ has been synthesised and tested for antiviral and anticancer activity.[107] The multifunctional compound maintained the antiviral activity of the parent drug acyclovir, *in vitro* against HSV-1. Although, as an anticancer agent, it was markedly less potent than cisplatin on a mole-equivalent basis, it was as effective as cisplatin when administered in equitoxic doses *in vivo* to P388 leukaemia bearing mice. The complex was also active against a cisplatin-resistant subline of the P388 leukaemia suggesting that it acts via a different mechanism of action. The DNA binding properties of the complex have been investigated in more detail[108] and the major DNA adduct was identified as a monofunctional adduct of $\{Pt(NH_3)_2(acyclovir)\}^+$ with a guanine residue. In contrast to DNA adducts of other monodentate and clinically inactive platinum(II) compounds, the adducts terminated *in vitro* DNA and RNA synthesis. The lack of bifunctional adducts confirms the difference in mechanism of action from cisplatin.

On the basis of these studies, multifunctional complexes consisting of platinum(II) complexes coupled with antiviral nucleosides present a novel strategy for attacking viral diseases.

1.7 Nucleotides

Nucleotides are the monomer building blocks of DNA and RNA and as such are ideal models for investigating interactions of platinum and its biological target. DNA comprises four different heterocyclic bases: the bi-cyclic purines guanine (G) and adenine (A), and the mono-cyclic pyrimidines cytosine (C) and thymine (T). These bases are connected to a pentose sugar ring, D-ribose for RNA and 2-deoxy-D-ribose for DNA, by a bond from the C-1' of the sugar to the N-1 of C or T and N-9 of A or G. In the polymeric structure of DNA these nucleoside units are linked together

via a phospo-diester linkage from the 5' site on one nucleoside to the 3' site on the next. This forms a chain-like structure which can bind a complementary strand via hydrogen bonds between the bases. The usual Watson –Crick base pairs are G≡C and A=T, as shown in Figure 1.19.

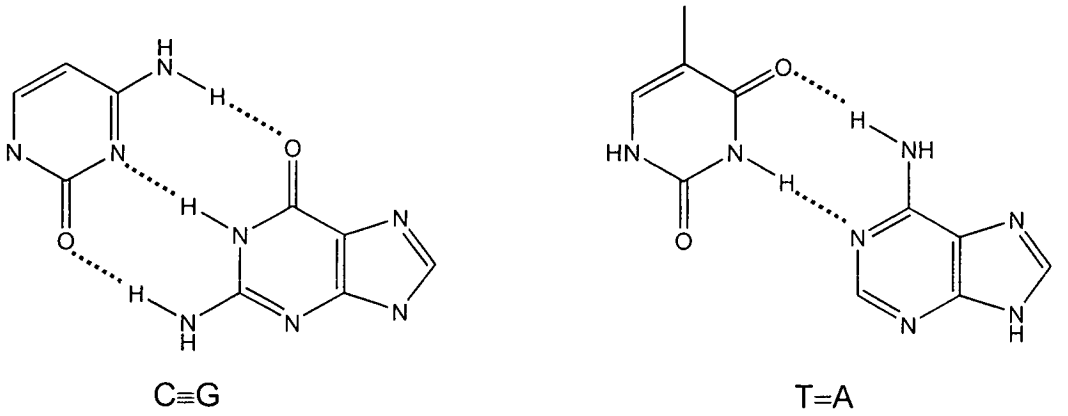

Figure 1.19 Watson-Crick hydrogen bonding between DNA bases

A nucleotide is the phosphate ester of a nucleoside and so consists of three components: a nucleobase (G,C,A,T), a pentose ring, and a phosphate group (mono-, di- or tri-) at the 3' or 5' site. For the purpose of this thesis the nucleotides used have been monophosphates and have all been *ribo*nucleotides (5'-GMP, 5'-AMP, 5'-CMP) with the exception of the thymine monophosphate which was in the *2-deoxyribose* form (5'-dTMP) since T does not occur in RNA. The structures with full numbering schemes are shown in Figure 1.20.

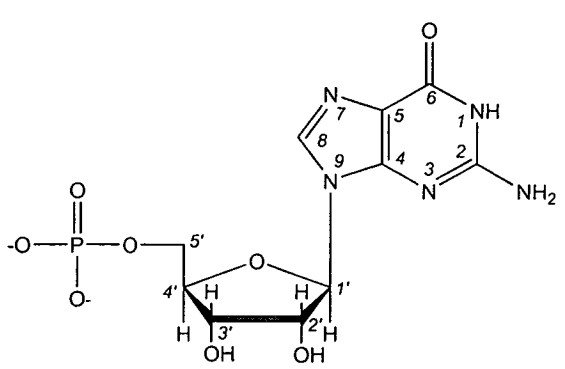

5'-guanosine monophosphate

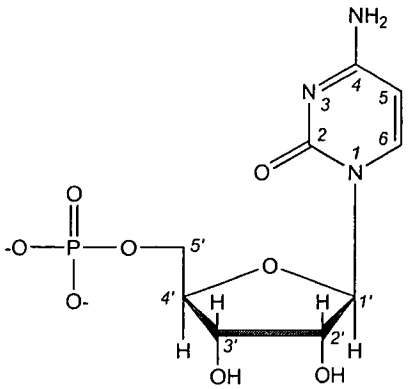

5'-cytidine monophosphate

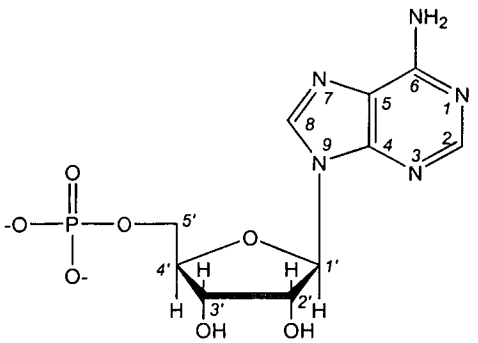

5'-adenosine monophosphate

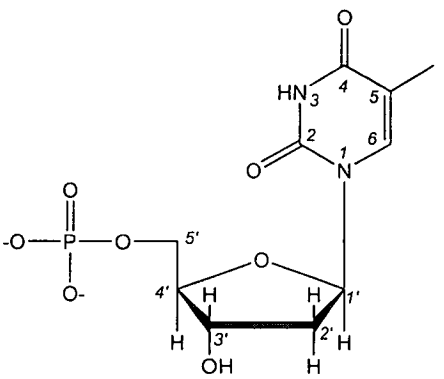

5'-deoxythymidine monophosphate

Figure 1.20 Structures and numbering schemes of mononucleotides used in this thesis

The acid-base behaviour of a nucleotide is its most important physical characteristic since it determines its charge, tautomeric structure and its ability to accept and donate hydrogen bonds. The pK_a values of the four nucleosides and 5'-nucleotides are given in Table 1.6. All the bases are neutral in the physiological range $5 < pH < 9$. The same is true for the pentoses where the D-ribose loses a proton only above pH 12 and the deoxy-ribose only above pH 15. The monophosphate group loses its first proton at pH 1 and a second proton at about pH 7. The three amino bases G, A, and C all become protonated on one of the ring nitrogens rather than the exocyclic amino group since this does not interfere with delocalisation of the NH_2 electron lone pair into the aromatic system.

Base (site of protonation)	Nucleoside	5'-Nucleotide
Adenine (N-1)	3.52	3.88
Cytosine (N-3)	4.17	4.56
Guanine (N-7)	3.30	3.60
Guanine (N-1)	9.42	10.00
Thymine (N-3)	9.93	10.47

Table 1.6 pK_a values for bases in nucleosides and nucleotides at 20°C and zero salt concentration[96]

1.7.1 Metal Binding Sites

As discussed for cisplatin, the N7 purine sites provide major binding sites for Pt due to their accessibility in the major groove of DNA. In addition guanine has been shown to be the most electron rich site on DNA in studies on photoinduced DNA cleavage via electron transfer.[31] However, when looking at model bases such as nucleotides virtually any site on the base can be a potential binding site. A number of methods have been employed to study platinum-nucleobase binding such as ^1H NMR, IR, Raman, UV, CD, and X-ray crystallography. The results of these studies have been comprehensively reviewed.[95,109,110]

Guanine

A number of factors make G-N7 the most common metal binding site on all the nucleobases. Primarily its accessibility in DNA and the fact that it is not involved in the major Watson-Crick base pairing. There is also the possibility of H bonding between the O6 on guanine and auxiliary ligands on the platinum. The N7 of guanine has a somewhat higher basicity than adenine N7 and a favourable electrostatic potential. Another possible binding site on guanine is the N1 site, this can be deprotonated in an N7-metallated species at high pH. In kinetically labile complexes a competition between the Pt(II) ion and the proton exists and a Pt bound to N7 at acidic pH can transfer to N1 if the pH is raised.

In all the bases exocyclic amine groups are metal binding sites only following removal the removal of one or both protons, i.e. after deprotonation or shift of a proton to another site of the base corresponding to a change in tautomeric structure. This is because the N lone pair of electrons is not free for donation but delocalised into the hetrocyclic ring.

Adenine

At physiological pH, adenine provides three unprotonated endocyclic nitrogen atoms: N1, N7 and N3. The order of basicity of the sites is N1 > N7 > N3, and while in duplex DNA the N7 site is preferred due to its accessibility, in nucleotides there is strong competition between N7 and N1 binding. Only at strongly acidic pH when the N1 site is fully protonated, is metal binding preferentially through the N7. Binding at N3 can only be achieved by blocking both the N7 and N1 sites.

Cytosine

Cytosine can have many different binding motifs for metal ions including through N3, O2, N4, and C5. In isolated cytosine base the binding is predominantly through N3 and O2 depending on the softness/hardness of the metal ion and possible steric effects. For this reason platinum generally prefers the N3 site. Coordination of a second platinum through the deprotonated N1 site has also been observed by NMR coupling.[111] Bridging and chelating via N3 and N4 has also been observed.[112]

Thymine

The nucleobase thymine has not been identified in any of the established cisplatin crosslinks with DNA. This is a consequence of the kinetic preference of Pt for other sites such as N7 of purines and the unfavourable location of the N3 site in the helix interior due to its involvement in H bonding. Platinum binding is possible in model nucleotides and in single stranded DNA, for example aquated cisplatin reacts with polyU (U is the RNA analogue of T, differing by loss of the methyl group at the C5 position) at pH to give a platinum-blue species.[113] Platinum blues are a class of intensely-coloured platinum antitumour compounds derived form *cis*-$[Pt(NH_3)_2(H_2O)_2]^{2+}$ and uracil, thymine or related ligands, first discovered by Rosenberg's group in 1975. N3 is the major binding site for platinum on thymine and numerous X-ray crystal structures have been determined of Pt bound to an N1

blocked model base (1-MeT) showing N-3 binding.[114] (The N1 site is blocked to mimic nucleotide/DNA binding since this site is where the sugar ring would be bound.)

Binding of platinum to one of the exocyclic oxygens in thymine is not uncommon since replacement of the N3 proton by less electron-attracting Pt(II) causes an increase in electron density at the oxygens, and allows easy formation of O-bound species.[115] In particular thymine can form N,O bridged dimer species bound through the N3 and O4 sites.[116] These dimers are termed *head-tail* dimers due to the opposed orientations of the two thymines and were first observed by Rosenberg and co workers[117, 118] with $[Pt(NH_3)_2]^{2+}$ and later crystallised by Lippert's group using 1-methyl thymine[119] (Figure 1.21, complex **23**).

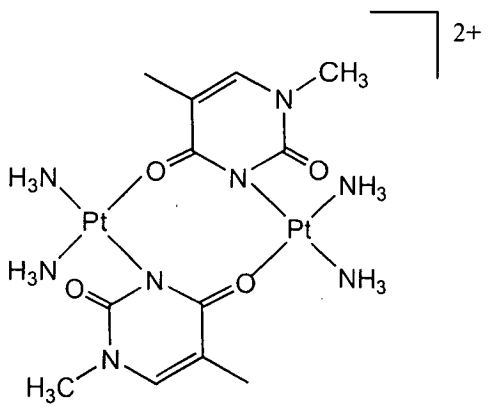

(23)

Figure 1.21 1-Methyl thymine N3,O4 bridged dimer species[119]

The reaction of platinum with DNA can be modelled at various levels of complexity from cyclic DNA or short double or single-stranded oligomers, to tri-, di- or mononucleotides or even just nucleosides or nucleobases. The use of the mononucleotides in this work allows a variety of spectroscopic techniques to be employed and information about the rate and base specificity of binding to be determined. The effect of the negatively charged phosphate may also play a role in the complex binding so can not be ignored.

1.8 Aims of this Thesis

The overall aim of this thesis is to synthesis a range of Pt(II) aminophosphine complexes and investigate their interactions with nucleotides. Such complexes could have potential as new anticancer agents with improved therapeutic properties, in particular overcoming factors which limit the use of current drugs: narrow spectrum of activity, resistance and toxic side effects

The initial challenge is to synthesise a series of ligands of the type: $\mathbf{R_2N(CH_2)_3PPh_2}$. These are similar to the ligands discussed in Section 1.5.2 but with a three carbon backbone giving the potential to form six-membered chelate rings. The alkyl groups (R) on the amine of the ligand will be varied, in order to investigate the influence of these groups on chelation. The ligands produced will then be used in the synthesis of Pt(II) aminophosphine complexes. The compounds formed will be characterised by use of NMR, mass spectrometry and X-ray crystallography techniques. The ring-opening equilibria of the complexes under different conditions will also be investigated.

Since DNA is the major target for Pt(II) complexes in the body, the interactions of the aminophosphine complexes with nucleotides (models for DNA binding) will also be studied. NMR will be used to study individual complex-nucleotide reactions whilst CE and HPLC will be employed to study competition reactions between the complexes and a mixture of nucleotides to determine the selectivity in binding site. The effect of pH on the binding to nucleotides will also be considered. The results for the Pt(II) aminophosphine complexes will be compared to those for cisplatin-nucleotide binding in order to determine if the mode of action is likely to be the same.

The effect of binding these complexes to polynucleotides will also be studied as the non-chelated "dangling arm" aminophosphines may have an impact on interactions with DNA.

Since it has been indicated that complexes of this type may have an affinity for thymine binding, the reactions of the complexes with the anti-HIV drug AZT (a thymine analogue) will be investigated. Pt-AZT adducts have the potential to act as multifunctional antiviral agents incorporating the cytotoxic properties of the platinum complex.

1.9 References

1 J. C. Chaston, *Plat. Met. Rev.* **1980**, *24*, 70

2 D. T. Thompson, *Chem. Br.* **1984**, 333

3 G. Wilkinson (Ed.), *Complete Coordination Chemistry*, Pergamon Press, Oxford, **1987**, *5*. 353

4 W. C. Fernelius (Ed.), *Inorg. Synth.* McGraw-Hill Book Company Inc., New York, **1946**, *2*, 247

5 F. A. Cotton, G. Wilkinson, *Advanced Inorganic Chemistry*, 5th Edition, John Wiley and Son, New York, **1988**, 1299

6 N. A. Campbell, *Biology*, 4th Edition, The Benjamin/Cummings Publishing Co. Inc. **1998**, pp217-219

7 Encyclopædia Britannica on-line: *www.britannica.com/eb/article?eu=108742*

8 R. B. Weiss and M. C. Christian, *Drugs*, **1993**, *46*, 360

9 M. Gordon, S. Hollander, *J. Med.* **1993**, 209

10 M. Peyrone, *Ann. Chem. Pharm.* **1845**, *51*, 1

11 B. Rosenberg, L. van Camp, T. Kringas, *Nature*, **1969**, *205*, 698

12 B. Rosenberg, L. van Camp, E. B. Grimley, A. J. Thompson, *J. Biol. Chem.* **1967**, *242*, 1347

13 B. Rosenberg, L. van Camp, J. E. Trosko, V. H. Monsour, *Nature*, **1969**, *222*, 385

14 B. Rosenberg, L. van Camp, *Cancer Res.* **1970**, *30*, 1799

15 D. J. Higby, H. J. Wallace, D. J. Albert, J. F. Holland, *Cancer*, **1974**, *33*, 1219

16 P. J. Loehrer, L. H. Einhon, *Ann. Intern. Med.* **1984**, *100*, 704

17 C. F. J. Barnard, *Plat. Met. Rev.* **1989**, *33*, 162

18 T. Esaki, S. Nakono, T. Tatsumoto, M. Kurolki-Migita, K. Mitsugi, M. Nakamura, Y. Niho, *Cancer Res.* **1992**, *52*, 6501

19 G. Daugaard, U. Abildgaard, *Cancer Chemother. Pharmacol.* **1989**, *25*, 1

20 R. F. Borch, M. Markman, *Pharmac. Ther.* **1989**, *41*, 371

21 J. Reedijk, *J. Chem. Soc., Chem. Commun.* **1996**, 801

22 H. C. Harder, B. Rosenberg, *Int. J. Cancer*, **1970**, *6*, 207

23 J. Arpalahti, M. Mikola, S. Mauristo, *Inorg. Chem.* **1993**, *32*, 3327

24 T. G. Appleton, J. R. Hall, S. F. Ralph, C. S. M. Thompson, *Inorg. Chem.* **1989**, *28*, 1989

25 S. J. Berners-Price, T. A. Frenkiel, U. Frey, J. Ranford, P. J. Sadler, *J. Chem. Soc., Chem. Commun.* **1992**, 789

26 D. M. Orton, V. A. Gretton, M. Green, *Inorg. Chim. Acta.* **1993**, *204*, 265

27 R. B. Martin in *Cisplatin : Chemistry and Biochemistry of a Leading Anticancer Drug*, B. Lippert Ed., **1999**, Wiley-VCH Weinheim, p 188

28 S. Mansy, B. Rosenberg, A. J. Thompson, *J. Am. Chem. Soc.* **1973**, *95*, *5*, 1633

29 A. M. J. Fichtinger-Schepman, J. L. van der Veer, J. H. J. den Hartog, P. H. M. Lohman, J. Reedijk, *Biochemistry,* **1985**, *24*, 707

30 F. Legendre, J.-C. Chottard in *Cisplatin : chemistry and biochemistry of a leading anticancer drug*, B. Lippert Ed., **1999**, Wiley-VCH Weinheim, p 240

31 I. Saito, M. Takayama, H. Sugiyama, K. Nakitani, *J. Am. Chem. Soc.* **1995**, *117*, 6406

32 D. P. Bancroft, C. A. Lepre, S. J. Lippard, *J. Am. Chem. Soc.* **1990**, *112*, 6860

33 K. J. Barnham, S. J. Berners-Price, T. A. Frenkiel, U. Frey, P. J. Sadler, *Angew. Chem., Int. Ed. Engl.* **1995**, *34*, 1874

34 F. Reeder, Z. Guo, P. del S. Murdoch, A. Corazza, T. W. Hambley, S. J. Berners-Price, J.-C. Chottard, P. J. Sadler, *Eur. J. Biochem.* **1997**, *249*, 370

35 A. Gelaso, S. J. Lippard, in *"Topics in Biological Inorganic Chemistry"* M. J. Clarke, P. J. Sadler, Eds.; Springer-Verlag : Heidelberg, **1999**, *1*, 1-43

36 S. E. Sherman, D. Gibson, A. H.–J. Wang, S. J. Lippard, *Science*, **1985**, *230*, 412

37 G. Admiraal, J. L. van der Veer, R. A. G. de Graaff, J. H. J. den Hartog, J. Reedijk, *J. Am. Chem. Soc.* **1987**, *109*, 592

38 J. A. Rice, D. M. Crothers, A. L. Pinto, S. J. Lippard, *Proc. Natl. Acad. Sci. USA*, **1988**, *85*, 4158

39 P.M. Takahara, A. C. Rosenzweig, C. A. Frederick, S. J. Lippard, *Nature,* **1995,** *377*, 649

40 P.M. Takahara, C. A. Frederick, S. J. Lippard, *J. Am. Chem. Soc.* **1996**, *118*, 12309

41 A. Gelasco, S. J. Lippard, *Biochemistry*, **1998**, *37*, 9230

42 D. Yang, S. S. G. E. van Boom, J. Reedijk, J. H. van Boom, A. H.–J. Wang, *Biochemistry* **1995**, *34*, 12912

43 S. U. Dunham, C. J. Turner, S. J. Lippard, *J. Am. Chem. Soc.* **1998**, *120*, 5395

44 H. Huang, L. Zhu, B. R. Reid, G. P. Drobny, P. B. Hopkins, *Science*, **1995**, *270*, 1842

45 C. J. van Garderen, L. P. A. van Houte, *Eur. J. Biochem.* **1994**, *225*, 1169

46 E. R. Jamieson, S. J. Lippard, *Chem. Rev.* **1999**, *99*, 2467

47 C. H. Hardman, R. W. Broadhurst, A. R. Raine, K. D. Grasser, J. O. Thomas, E. D. Laue, *Biochemistry*, **1995**, *34*, 16596

48 S. U. Dunham, S. J. Lippard, *Biochemistry*, **1997**, *36*, 11428

49 U.-M. Uhndorf, M. A. Rould, Q. He, C. O. Pabo, S. J. Lippard, *Nature*, **1999**, *399*, 708

50 Q. He, C. H. Liang, S. J. Lippard, *Proc. Natl. Acad. Sci. USA*, **2000**, *97, 11*, 5768

51 G. Chu, *J. Biol. Chem.* **1994**, *269*, 787

52 J. Reedijk, *Chem. Rev.* **1999**, *99*, 2499

53 T. W. Hambley, *Coord. Chem. Rev.* **1997**, *166*, 181

54 S. Neidle, I. M. Ismail, P. J. Sadler, *J. Inorg. Biochem.* **1980**, *13*, 205

55 L. Canovese, L. Cattalini, G. Chessa, M. L. Tobe, *J. Chem. Soc. Dalton Trans.* **1988**, 2135

56 E. Wong, C. M. Giandomenico, *Chem. Rev.* **1999**, *99*, 2451

57 Y. Chen, Z. Guo, S. Parsons, P. J. Sadler, *Chem. Eur. J.* **1998**, *4*, 672

58 N. Farrell, T. T. B. Ha, J.-P. Souchard, F. L. Wimmer, S. Cros, N. P. Johnson, *J. Med. Chem.* **1989**, *32*, 2240

59 M. Van Beusichem, N. Farrell, *Inorg. Chem.* **1992**, *31*, 634

60 L. R. Kelland, C. F. J. barnard, K. L. Mellish, M. Jones, P. M. Goddard, M. Valenti, A. Bryant, B. A. Murrer, K. R. Harrap, *Cancer Res.*, **1994**, *54*, 5618

61 M. Coliccia, A. Nassi, F. Loseto, A. Boccarelli, M. A. Mariggio, D. Gordano, F. P. Intini, P. Caputo, G. Natile, *J. Med. Chem.* **1993**, *36*, 510

62 M. Coluccia, A. Boccarelli, M. A. Mariggio, N. Cardellicchio, P. Caputo, F. P. Intini, G. Natile, *Chem. Biol. Int.*, **1995**, *98*, 251

63 M. Coluccia, M. A. Mariggio, A. Boccarelli, F. Loseto, N. Cardellicchio, P. Caputo, F.P. Intini, C. Pacifico, G. Natile, *Platinum and other Metal Coordination Compounds in Cancer Chemotherapy 2,* H. M. Pinedo, J. H. Schornagel, Ed., Plenum, New York, **1993**, 27

64 N. Farrell, Y. Qu, M. P. Hacker, *J. Med. Chem.* **1990**, *33*, 2179

65 S. B. Hartley, W. S. Holmes, J. K. Jaques, M. F. Mole, J. C. McCoubrey, *Quart. Rev.*_**1963**, *17*, 204

66 K. K. Chow, W. Levason, C. A. McAuliffe, in *"Transition metal Complexes of P, As, Sb, and Bi ligands"*, C. A. McAuliffe, Ed.; MacMillan, London 1973

67 P. J. Sadler, R. E. Sue, *Metal-Based Drugs*, **1994**, *1*, 2-3, 107

68 J. Forestier, *Bull. Mém. Soc. Méd. Hôp. (Paris),* **1929**, *53*, 3231

69 M. A. Mazid, M. T. razi, P. J. Sadler, G. N. Greaves, S. J. Hurman, M. H. J. Koch, J. C. Phillips, *J. Chem. Soc. Chem Commun.* **1980**, 1261

70 R. C. Elder, M. K. Eidsness, M. J. Heeg, K. G. Tepperman, C. F. Shaw III, N. Schaeffer, *ACS Symposium Series*, **1983**, *209*, 385

71 D. T. Walz, M. J. DiMartino, B. M. Sutton, A. Misher, *J. Pharm. Exp. Ther.*, **1972**, *181*, 292

72 D. J. Ecker, J. C. Hempel, B. M. Sutton, R. Kirsch, S. T. Crooke, *Inorg. Chem.* **1986**, *25*, 3139

73 A. A. Issab, A. L. Hormann, D. T. Hill, D. E. Griswold, M. J. DiMartino, C. F. Shaw III, *Inorg. Chem.* **1989**, *28*, 1321

74 T. M. Simon, D. H. Kunishima, D. H. Vibert, A. Lorber, *Cancer Res.* **1981**, 41, 94

75 C. K. Mirabelli, R. K. Johnson, C. –M. Sung, L. F. Faucette, K. Muirhead, S. T. Crooke, *Cancer Res.* **1985**, 45, 32

76 C. K. Mirabelli, R. K. Johnson, D. T. Hill, L. F. Faucette, G. R. Girard, G. Y. Kuo, C.-M. Sung, S. T. Crooke, *J. Med. Chem.* **1986**, *29*, 218

77 S. J. Berners-Price, P. J. Sadler, *Struct. Bonding (Berlin)*, **1988**, *70*, 27

78 S. J. Berners-Price, M. A. Mazid, P. J. Sadler, *J. Chem. Soc. Dalton Trans.* **1984**, 969

79 S. J. Berners-Price, P. J. Sadler, *Inorg. Chem.* **1986**, *25*, 3822

80 S. J. Berners-Price, C. K. Mirabelli, R. K. Johnson, M. R. Mattern, F. L. McCabe, L. F. Faucette, C.-M. Sung, S. M. Mong, P. J. Sadler, S. T. Crooke, *Cancer Res.* **1986**, *46*, 5486

81 C. K. Mirabelli, D. T. Hill, L. F. Faucette, F. L. McCabe, G. R. Girard, D. B. Bryan, B. M. Sutton, J. O'L. Bartus, S. T. Crooke, R. K. Johnson, *J. Med. Chem.* **1987**, *30*, 2181

82 R. M. Snyder, C. K. Mirabelli, R. K. Johnson, C.-M. Sung, L. F. Faucette, F. L. McCabe, J. P. Zimmerman, M. Whitman, J. C. Hempel, S. T. Crooke, *Cancer, Res.* **1986**, *46*, 5054

83 G. D. Hoke, R. A. Macia, P. C. Meunier, P. J. Bugelski, C. K. Mirabelli, G. F. Rush, W. D. Matthews, *Toxicol. and Appl. Pharm.* **1989**, *100*, 293

84 G. D. Hoke, G. F. Rush, G. E. Bossard, J. V. McArdle, B. D. Jenson, C. K. Mirabelli, *J. Biol. Chem.* **1988**, *263*, 11203

85 S. J. Berners-Price, R. J. Bowen, P. Galettis, P. C. Healy, M. J. McKeage, *Coord. Chem. Rev.* **1999**, *185*, 823

86 F. A. Cotton, G. Wilkinson, *Advanced Inorganic Chemistry*, 5th Ed. John Wiley and Sons, Chichester, **1988**, pp1299

87 A. Tongni, L. M. Venanzi, *Angew. Chem. Int. Ed. Eng.* **1994**, *33*, 497

88 G. K. Anderson, R. Kumar, *Inorg. Chem.* **1984**, *23*, 4064

89 S. Naili, J.-F. Carpenter, F. Agbossou, A. Mortreux, G. Nowogrocki, J.-P. Wignacourt, *Organometallics*, **1995**, *14*, 1, 401

90 M. Basset, D. L. Davies, J. Neild, L. J. S. Prouse, D. R. Russell, *Polyhedron,* **1991**, *10*, 501

91 G. P. C. M. Dekker, A. Buijs, C. J. Elsevier, K. Vrieze, P. W. N. M. van Leeuwan, W. J. J. Smeets, A. L. Spek, Y. F. Wang, C. H. Stam, *Organometallics,* **1992**, *11*, 1937

92 S. Chatterjee, D. C. R. Hockless, G. Salem, P. Waring, *J. Chem. Soc., Dalton Trans.* **1997**, 3889

93 A Habtemariam, P. J. Sadler, *J. Chem. Soc., Chem. Commun.* **1996**, 1785

94 N. Margiotta, A. Habtemariam, P. J. Sadler, *Angew. Chem. Int. Ed. Engl.* **1997**, *36*, 11, 1185

95 B. Lippert, *Prog. Inorg. Chem.* **1989**, *37*, 1

96 G. M. Blackburn in *Nucleic Acids in Chemistry and Biology*, G. M. Blackburn, M. J. Gait; Eds. Oxford University Press, Oxford, **1996**, pp16-18

97 F. Reeder, F. Gonnet, J. Kozelka, J.-C. Chottard, *Chem. Eur. J.* **1996**, *2*, 1068

98 T. S. Mansour, R. Storer, *Curr. Pharm. Design*, **1997**, *3*, 227

99 A. J. Wagstaff, D. Faulds, G. L. Goa, *Drugs*, **1994**, *47*, 153

100 H. D. Langtry, D. M. Campoli-Richards, *Drugs*, **1989**, *37*, 408

101 P. A. Furman, J. A. Fyfe, M. H. St. Clair, K. Weinhold, J. L. Rideout, G. A. Freeman, S. N. Lehrman, D. P. Bolognesi, S. Broder, H. Mitsuya, D. W. Barry, *Proc. Natl. Acad. Sci. USA*, **1986**, *83*, 8333

102 P. Levantis, C. Stein, J. Oxford, *Antiviral Chem. Chemother.* **1993**, *4*, 3

103 G. Valette, A. Pompon, J.-L. Giradet, L. Cappellacci, P. Franchetti, M. Grifantini, P. Lacolla, A. G. Loi, C. Périgaud, G. Gosselin, J.-L. Imbach, *J. Med. Chem.* **1996**, *39*, 1748

104 M. B. Snyder, L. D. Saravolatz, N. Markowitz, D. Pohlod, R. C. Taylor, S. G. Ward, *J. Antimicrob. Chemother.* **1987**, *19*, 815

105 R. C. Taylor, S. G. Ward in *Lectures in Bioinorganic Chemistry*, M. Nicolini, L. Sindellari, Eds.; Raven Press, New York, **1991**, pp63-90

106 A. Pasini, F. Zunino, *Angew. Chem. Int. Ed. Engl.* **1987**, *26*, 615

107 M. Coluccia, A. Boccarelli, C. Cermelli, M. Portolani, G. Natile, *Metal Based Drugs*, **1995**, *2*, 5, 249

108 Z. Balcarová, J. Kašpárková, A. á k o vská, O. Nováková, M. F. Sivo, G. Natile, V. Brabec, *Mol. Pharm.* **1998**, *53*, 846

109 R. B Martin, in *Cisplatin: Chemistry and Biochemistry of a Leading Anticancer Agent*, B. Lippert, Ed., VHCA Zurich and Wiley-VCH Weinheim, **1999**, pp133-183

110 B. Lippert, *Coord. Chem. Rev.* **2000**, *200-202*, 487

111 S. Jaworski, H. Schollhorn, P. Eisenmann, U. Thewalt, B. Lippert, *Inorg. Chim. Acta,* **1988**, *153*, 31

112 H. Schollhorn, R. Beyerle-Pfnur, U. Thewalt, B. Lippert, *J. Am. Chem. Soc.* **1986**, *108*, 3680

113 J. P. Davidson, P. J. Faber, R. G. Fischer, S. Mansey, H. J. Peresie, B. Rosenberg, L. van Camp, *Cancer Chemother. Rep.* **1975**, *59*, 287

114 H. Schöllhorn, U. Thewalt, B. Lippert, *Inorg. Chim. Acta,* **1985**, *106*, 177

115 B. Lippert, *Inorg. Chim. Acta,* **1981**, *55*, 5

116 B. Lippert, *Platinum, Gold and Other Metal Chemotherapeutic Agents,* S.J. Lippard, Ed., ACS Symposium Series 209, American Chemical Society, Washington DC, **1983**, pp147

117 C. J. L. Lock, H. J. Peresie, B. Rosenberg, G. Turner, *J. Am. Chem. Soc.* **1978**, *100*, 3371

118 R. Faggini, C. J. L. Lock, R. J. Pollock, B. Rosenberg, G. Turner, *Inorg. Chem.* **1981**, *20*, 804

119 D. Neugebauer, B. Lippert, *Inorg. Chim Acta,* **1982**, *67*, 151

Chapter Two

Materials and Methods

2.1 Materials

The reagents used in this work were purchased from the following companies listed in Table 2.1.

Reagent	Company
ethyl formate, methylene oxide, *tert*-butylamine, lithium aluminium hydride, lithium tetrafluoroborate, guanosine 5'-monophosphate (sodium salt) - 5'-GMP	Acros
$Me_2N(CH_2)_3Cl.HCl$, $H_2N(CH_2)_3Cl.HCl$, potassium *tert*-butoxide, thionyl chloride, 1,5-cyclooctadiene - COD, $Pt(COD)Cl_2$, tetramethyl tin	Aldrich
sodium phosphate, potassium phosphate adenosine 5'-monophosphate (sodium salt) – 5'-AMP, cytidine 5'-monophosphate (sodium salt) - 5'-CMP, deoxythymidine 5'-monophosphate (sodium salt) - 5'-dTMP, 3'-azido,3'-deoxythymidine - AZT	Sigma
$Pt(COD)Cl_2$	Strem
tetrabutyl ammonium hydrogen sulfate - TBAHS	Fluka
diphenyl phosphine	Flurochem
3-amino-1-propanol	Lancaster
potassium tetrachloroplatinate	Johnson Matthey

Table 2.1 Materials and sources

2.2 Methods

2.2.1 Nuclear Magnetic Resonance Spectroscopy

NMR signals were first recorded in 1946 and can now routinely be detected for almost any magnetic nucleus. Many textbooks have been published describing the theory and applications of NMR.[1,2,3]

Angular Momentum and Nuclear Magnetism

Nuclear magnetic moments are very sensitive to their surroundings yet interact very weakly with them making them ideal tools to investigate the structures and motions of molecules.

Magnetic nuclei possess an intrinsic angular momentum known as *spin*, arising largely from the number of unpaired protons and neutrons they contain. The spin quantum number of a nucleus *(I)* may have one of the following values

$$I = 0,\ 1/2,\ 1,\ 3/2,\ 2,\ldots,$$

with quantum numbers greater than 4 being very rare. Nuclei having spins greater than ½ are called *quadrupolar* and normally give broad NMR lines making them difficult to study. The spinning of a nucleus (a charged body) generates a magnetic moment, the *nuclear magnetic moment,* μ (μ is a vector quantity). The moment is proportional to the spin with a constant of proportionality, γ, called the *gyromagnetic ratio*. Every isotope has a different characteristic value of γ.

$$\mu = \gamma I$$

The number of m_I states (energy levels) for a nucleus with spin I is $2I + 1$. In the absence of a magnetic field the m_I states are all degenerate. When a nucleus is placed in an applied field, different states will have different energies depending on how the

nuclear magnetic moment is orientated relative to the applied field. For a spin- ½ nucleus such as ^1H there are two energy levels which correspond to nuclei having their spins aligned with or opposed to the magnetic field.

The energies (E) of the allowed orientations of the nuclear magnetic moment depend on the strength of the applied field (B_0), the size of the nuclear magnetic moment (γ), and on the orientation of the moment in the applied field (m_I)

$$E = m_I \gamma B_0$$

Resonance Frequencies

Transitions of nuclei between different levels is possible by irradiation with electromagnetic radiation of the correct frequency. This is known as the *resonance frequency* (v). Since the separation of energy levels will also be dependent on the magnetic field strength and the gyromagnetic ratio, each different isotope will resonate at a characteristic, distinct frequency.

$$\Delta E = hv = \gamma B_0$$

$$v = \gamma B_0 / 2\pi$$

(h = Plank's constant)

The selection rule for NMR is $\Delta m_I = \pm 1$, i.e. transitions are allowed only between adjacent levels. Since all energy levels are equally spaced only a single resonance will be observed in the spectrum.

Irradiation of a sample at the resonance frequency causes the nuclear spins to both be excited from lower to higher energy levels (absorption) and relax from the higher to lower states (emission). Since these are both transitions of the same energy, the NMR signal depends on the *difference* between the numbers of absorptions and emissions that occur. This is in turn dependent on the population difference between

the two levels which is very small (approx. 1 in 10^5) so NMR signals are therefore very weak. One way to improve the sensitivity of NMR as a technique is to make B_0, the field strength as large as possible so the separation of the energy levels is large. NMR spectrometers are usually classified by their proton frequencies (since this is the most popular NMR nucleus) rather than their magnetic field, e.g. in 9.4 T field $\nu(^1H) = 400$ MHz.

The magnetic properties of some useful NMR active nuclei are displayed in Table 2.2.

Nucleus	Spin Quantum Number, I	Magnetic Moment, μ	Gyromagnetic ratio, γ ($10^8 radT^{-1}s^{-1}$)	Resonance Frequency, ν (MHz)	Relative sensitivity (versus ^1H at constant field)	Natural Abundance %
^1H	½	2.798	2.675	42.577	1.000	99.98
^{13}C	½	0.702	0.673	10.705	0.016	1.108
^{15}N	½	-0.283	-0.271	4.315	0.001	0.365
^{31}P	½	1.132	1.083	17.235	0.066	100.00
^{195}Pt	½	0.606	0.580	9.238	0.003	33.8

Table 2.2 Selected NMR properties of common nuclei (in a 1 T magnetic field)

Experimental Methods

An NMR spectrum is measured by applying a radio frequency as a powerful pulse for a certain time over a range of frequencies. This excites all the resonances within a sample and as a result the macroscopic magnetisation of the sample is displaced by an angle θ. The intensity of the excitation pulse determines how much the magnetisation is tipped. A pulse producing $\theta = 90^\circ$ will give the maximum intensity of NMR signal. The tipped magnetisation precesses around its axis and a receiver

coil picks up the resultant oscillation which decays away to zero during the acquisition period a process known as free induction decay (FID). Fourier transformation then converts the FID in the time domain into a spectrum in the frequency domain resulting in a spectrum of signal intensity versus frequency.

Integration

The intensity of an NMR signal is proportional to the number of nuclei resonating at that frequency so we can quantify the relative numbers of nuclei in different chemical environments by comparing the areas under peaks. This area is measured by integration.

Chemical Shifts

As well as depending on γ and B_0 the frequency at which a nucleus resonates is also dependent, to a lesser extent, on the local electron distribution within the molecule. This distinguishes individual nuclei according to their position in a molecule.

The external magnetic field applied to a sample causes the electrons to circulate in their atomic orbitals, generating a small magnetic field B' which reinforces or opposes the existing magnetic field. A nucleus in a molecule then experiences a different magnetic field (B) depending on its surrounding electron distribution.

$$B = B_0 \pm B'$$

This effect is referred to as *nuclear shielding*. The resonance frequency of the nucleus is then shifted from that for a bare nucleus with no electrons. The chemical shielding is reported as the shift of the resonance line from that of a resonance compound, the *chemical shift*. This is given as a fraction of the applied magnetic

field, in parts per million, on the δ scale which is then independent of the applied field. δ increases as the amount of shielding increases. Conventionally the δ scale increases from right to left in an NMR spectrum. The left-hand side is known as the downfield end and is the high frequency end. The opposite is true for the right-hand side.

Several factors influence the shielding of nuclei in complexes and hence their chemical shift.[4] It is however difficult to establish general trends for these effects as often many independent factors with competing effects are present in a single complex.

1. *Geometry* – geometric factors can make otherwise equivalent nuclei distinct e.g. *cis* or *trans*, *fac* or *mer*. The position of a nucleus in a complex determines its electronic environment and hence its chemical shift.
2. *Electronegativity, charge and oxidation state* – all of these factors affect the electron density around the nucleus and so alter the chemical shift. The shielding becomes smaller as the electron density decreases and the chemical shift produced is larger. Thus electronegative substituents, positive charge or an increase in oxidation state all result in a downfield shift.
3. *Co-ordination number* – The chemical shift can be diagnostic of the co-ordination number of a nucleus in a complex, shifting upfield as the co-ordination number increases. This is well illustrated in work by J. Errington using ^{17}O NMR to distinguish between terminal and bridging oxygen atoms in $W_6O_{19}^{2-}$ structures.[5]

Spin-Spin Coupling

Coupling arises because the nuclear magnetic moments of other NMR active nuclei surrounding the nucleus under observation produce small magnetic fields in addition to those due to the spectrometer magnet and the chemical shift. Thus the observed

nucleus sees not one resultant field but several depending on the number and nature of the surrounding NMR active nuclei.

If the neighbouring nucleus is aligned with the field, the total effective field will be larger than the applied field of the spectrometer causing the resonance frequency to be higher. Conversely if the nucleus is aligned opposed to the field, the effective field will be reduced and the resonance will be at a lower frequency. Since there is an almost equal probability of the nucleus being in either spin state, this results in two lines of equal intensity in the NMR spectrum instead of a single resonance. The same principle of splitting can be applied to larger numbers of nuclei in the same molecule resulting in multiplet patterns of resonances.

The difference between resonance frequencies of the split lines is called the *coupling constant* (*J*). This is independent of the spectrometer field used and so is measured in Hertz (Hz). The size of *J* diminishes as the number of bonds between the two active nuclei increases.

Many factors, discussed below, affect the coupling constant,[4] some general trends can be identified allowing structural and chemical information to be determined. In general it is the *s-character* of the bond(s) between the coupling nuclei that controls the magnitude *J*. The coupling between nuclei is transmitted via the bonding electrons rather than directly through space. Only s-electrons have a finite density at the nucleus so the amount of *s*-character in the valence hybrids used to form the chemical bond influences the strength of the coupling. Percentage *s*-character is determined by the following:

1. *Hybridisation* – coupling constants increase in the order of $sp^3 < sp^2 < sp$ hybridised nuclei as *s*-character increases
2. *Co-ordination number* – increasing co-ordination number leads to a decrease in coupling constant, the *s*-character of the bond to any given ligand decreases as the number of ligands increases

3. *Electronegativity* – Coupling constants increase with increasing electronegativity of the substituents
4. *Trans influence* – The magnitude of couplings between a ligand and acceptor is strongly influenced by the other ligands in the complex. The nature of the *trans* group affects the covalency or *s*-character of the metal-ligand bond. A ligand with a high *trans influence* will weaken the bond *trans* to it and lower the coupling constant, conversely a ligand with low *trans* influence will produce a higher *J* value.
5. *Interbond angles* – as the bond angle increases between coupling nuclei the *s*-character of the bonds increases until a maximum at 180°. Hence the magnitude of the coupling constant can be correlated to the interbond angle between nuclei, e.g. *trans* couplings will normally be larger than *cis* couplings.

Natural Abundance

Elements can exist as more than one isotope. These isotopes need not all have the same spin so will not necessarily all be NMR active. Even those which are active will have different gyromagnetic ratios, γ, and hence different resonance frequencies. The different isotopes will therefore show different coupling constants and different coupling patterns. To understand the NMR spectra of compounds containing an element possessing more than one NMR active isotope it must be considered as a combination of the spectrum containing only inactive isotopes of the element and spectra containing each of the active isotopes.

2.2.1.1 NMR of Platinum(II) Complexes with Phosphine Ligands

Platinum Satellites

A number of the NMR effects described above can be used to great effect in the study of platinum complexes. Platinum contains only one NMR active isotope – ^{195}Pt, which is only 33.8% abundant. When coupling to other active nuclei this produces a distinctive pattern of *satellites*. (Figure 2.1) The central unsplit line is

due to molecules containing the non-active Pt isotopes. This is flanked by a doublet of peaks from molecules containing the ^{195}Pt spin-1/2 molecule.

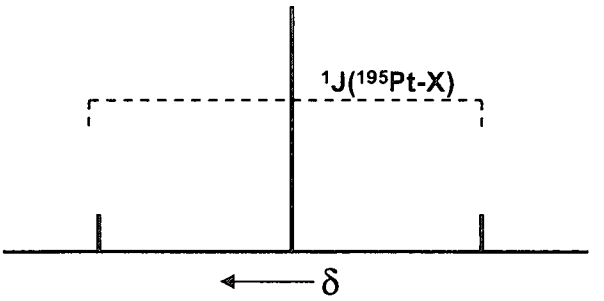

Figure 2.1 Satellites produced by coupling of ^{195}Pt to an NMR active nucleus

Phosphorus-31 NMR

Due to its favourable nuclear properties (I = ½, high NMR frequency and high receptivity), the ^{31}P nucleus is easy to observe and very useful in structure determination.

The properties of the ^{31}P nucleus are described in Table 2.3.

Natural abundance, %	100
Nuclear spin, *I*	½
Magnetic moment, μ	1.1316
Gyromagnetic ratio, γ (10^7radT^{-1}s^{-1})	10.8394
NMR frequency at 2.35 T (MHz)	40.480
Receptivity relative to that of ^{1}H	6.63×10^{-2}

Table 2.3 NMR Properties of ^{31}P [6]

Phosphorus-31 chemical shifts have been observed over a range exceeding 1000 ppm.[7] The chemical shift can be indicative of the coordination number of the phosphorus atom as it is determined by the bond angles to the neighbouring nuclei, the electronegativity of the substituents and the extent of π-bonding. Phosphorus-31 shifts are reported relative to the signal for 85% phosphoric acid as an external reference. Being present in 100% abundance, and having a spin quantum number of ½, ^{31}P imparts spin-spin coupling information analogous to a proton. Coupling information such as multiplicity and *J* value are useful aids in the identification of compound structures from spectra.

Phosphorus-Platinum Coupling

In transition metal complexes coupling of ^{31}P to platinum is one of the most widely studied NMR interactions. As previously discussed the magnitude of the coupling constant is seen to depend on the *trans* influence of the ligand opposite to P. A combination of calculations and experimental data have shown that contributions from the interaction of the nuclear spins of the atoms (P and Pt) are negligible in determining the magnitude of the coupling constant, while the Fermi contact interaction at the nucleus, between the nuclear spin and *s*-electrons, makes the dominant contribution.[8,9]

The coupling constant $J(^{31}P\text{-}^{195}Pt)$ is then given by:

$$J(^{31}P\text{-}^{195}Pt) \;\alpha\; \gamma_P\gamma_{Pt}\alpha_P^2\alpha_{Pt}^2\,|\psi_{P(3s)}(0)|^2\,|\psi_{Pt(6s)}(0)|^2\,(^3\Delta E)^{-1}$$

where γ_X is the gyromagnetic ratio for the nucleus, α_X^2 is the *s*-character of the bonding hybrid orbital used by X in the P-Pt bond, the $|\psi_{X(ns)}(0)|^2$ terms describe the electron density of the indicated orbital evaluated at the parent nuclei and $^3\Delta E$ is an average singlet-triplet excitation energy.

The variation of $J(^{31}P\text{-}^{195}Pt)$ according to the ligand in the *trans* position can then be accounted for by the effect of this ligand on the degree of covalency/*s*-character of the Pt-P bond and hence the coupling. This is very useful in the characterisation of platinum phosphine compounds indicating the nature of the coordinated ligands and *cis/trans* geometry.[10-14]

A *trans* influence series (according to increase of coupling constant) has been obtained by combining several sets of data[15]:

$$SiMePh_2 > Ph^- > Me^- > PEt_3, PBu^n_3 > PMe_2Ph > PPh_3 > P(OPh)_3, CN^- > NO_2^- >$$
$$EtNH_2 > Et_2NH > py, N_3^-, NCO^-, NCS^-, Cl^-, Br^-, I^- > ONO_2^-$$

Table 2.4 shows a rule of thumb correlation between phosphorus-platinum coupling constant and various *trans* donor atoms relevant to platinum compounds in this thesis.

increasing trans influence ←

***trans* ligand**	P	N	Cl	O
^1J ($^{31}P\text{-}^{195}Pt$) / Hz	2400-3000	3200-3600	3500-3800	>4000

Table 2.3 Effect of *trans* ligand on the ^1J ($^{31}P\text{-}^{195}Pt$) coupling in square-planar Pt(II) complexes

In addition to coupling to platinum, phosphorus can also couple to other P ligands in a square-planar Pt(II) complex. This coupling again indicates the geometry of a complex since it is only observed for two phosphorus atoms with a *cis* relationship and not with a *trans* relationship. The $^2J(^{31}P\text{-}^{31}P)$ coupling is of the order of 20 Hz.

Chelate Effect

Since the early '70s it has been known that a good correlation exists between the chemical shift of a tertiary phosphine and the change in chemical shift upon coordination to a metal. More recently a new parameter has been described, Δ_R, (the ring contribution) accounting for the change in chemical shift due to incorporation of the phosphine in a chelate ring.[16] This parameter is defined as the difference between the coordination chemical shift of a *cis*-disubstituted phosphine complex and the observed coordination chemical shift of an equivalent phosphorus atom in a chelate complex. Using the series of complexes $[Pt\{Ph_2P(CH_2)_nPPh_2\}(CH_3)_2]$ with n = 1-4, and the acyclic analogue *cis*-$[Pt(Ph_2PCH_3)_2(CH_3)_2]$ a pattern relating chelate ring size to chemical shift has been determined.[17] P atoms in four and six-membered rings have increased shielding and move slightly upfield, but in five-membered rings the P atoms are deshielded and shift downfield. A comparison of these phenomenon with the X-ray structures for an analogous Pd series show that this anomalous shift is not related to the stain in the chelate ring which is low in the five-membered case. To date this effect remains well documented but unaccounted for.[13,18]

2.2.1.2 NMR of Nucleotide Reactions with Platinum

^{1}H NMR is possibly the single most powerful technique for studying the interactions between platinum and nucleotides. It allows the study of complex formation, the assignment of binding sites and also allows structural changes such as ligand rotation and metal migration to be followed.[19]

Chemical Shift with Pt Coordination

Platinum coordination to a heteroatom in a nucleobase generally causes a downfield shift in the resonances of the nonexchangeable ring protons.[20] This downfield shift originates from the *inductive effect* - that is the effect of diminishing the electron density at these protons and deshielding them.

Ligand Rotation

The number of observed ^1H resonances as a function of temperature can often allow conclusions to be reached about the number and geometries of isomers. In complexes containing more than one nucleobase (such as GG adducts) isomers have been attributed to the restricted rotation of the Pt-nucleobase bond producing so-called *head –to-head* (HH) isomers (both guanines perpendicular to Pt square-plane and orientated in the same direction) and *head-to-tail* (HT) isomers (both guanines perpendicular to Pt square-plane and orientated in opposite directions) as shown in Figure 2.2. [21] Conformations of the cisplatin moiety $\{Pt(NH_3)_2\}^{2+}$, are difficult to elucidate by NMR since attachment of the NH_3 to Pt via a single bond allows the NH_3 ligands to adopt independently numerous orientations in which the NH groups form hydrogen bonds to the nucleotide target or avoid steric interactions with the target. As a result, multiple similar conformations co-exist and the barriers between the conformations are probably shallow making these adducts especially fluxional.[22] However, for nucleotide binding of Pt(II) moieties with larger amine groups ^1H NMR can be a useful tool for studying complex conformation.

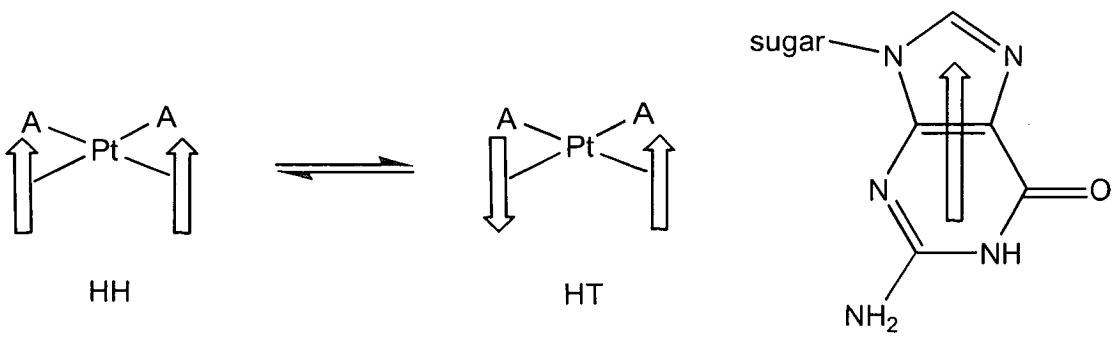

Figure 2.2 Possible isomers of complexes of the form $[PtA_2G_2]$ where A = am(m)ine ligand, G = guanine. Arrows represent an N7 bound G as shown on right hand side of the figure.

Binding Site

Monitoring the chemical shift of nonexchangeable ^{1}H protons of heterocyclic rings as a function of pH permits determination of relevant pK_a values of acid-base equilibria at the heteroatoms. This is due to the fact that protonation of the heteroatom causes a downfield shift by the *inductive effect.* The method can also be applied to platinated nucleobases. Since sites occupied by Pt can no longer be protonated as in the free nucleobase, a pH titration of the platinated product will no longer show the expected chemical shift for proton signals in the region of the heteroatoms pK_a values. Also when Pt is bound at one ring N, the pK_a values of other sites can be significantly changed, again causing a distinctive change in the chemical shift profile. For example, Pt binding at N7 of guanine can unambiguously be established on the basis of the downfield shift of the H8 resonance. [23] The pK_a of this site is ca. 2-3, but when platination occurs the chemical shift of the H8 shows no change over a wide pH range 0-6. The binding at N7 also acidifies the N1 proton (pK_a ca. 7.8-8.3) [24] which is reflected by the sensitivity of the H8 signal to pH in the range 6-10.

2.2.2 Capillary Electrophoresis

Electrophoresis is a separation method based on the differential rate of migration of charged species in a buffer solution across which has been applied a dc electric field. The classical method of electrophoretic separation is carried out on a slab of porous semisolid gel containing an aqueous buffer within its pores and is therefore referred to as *slab* electrophoresis. This technique has many disadvantages including low resolution, the requirement of large sample volumes, and the limitation of using a low electric field due to the convection currents created by Joule heating in the gel. Major efforts have been directed towards the development of new electrophoretic media to improve the technique. Capillary electrophoresis (CE) was developed only in the last 20 years by the groups of Mikkers[25] and Jorgenson.[26] CE uses a fused silica capillary, coated with a protective polyimide layer, as the separating medium.

Typical capillaries have an internal diameter of only 10–100 μm and are 40–100 cm long. CE presents many advantages over *slab* electrophoresis:

1. high resolution separations can be achieved on exceptionally small sample volumes (0.1–10 nl in contrast to volumes in the μl range required for *slab* electrophoresis),
2. the high surface-to-volume ratio allows for very efficient dissipation of Joule heat, so high voltages can be used for faster separations,
3. the separated species are eluted from the end of the capillary so quantitative detectors such as UV spectrometers can be used instead of the staining techniques of *slab* electrophoresis.

Detailed descriptions of CE theory can be found in many analytical texts and reviews,[27-30] these are summarised in the following sections.

Instrumentation for Capillary Electrophoresis

As shown in Figure 2.3 the instrumentation required for CE is very simple. The capillary is filled with the required electrolyte solution and the ends of the capillary dipped into reservoirs of electrolyte containing high voltage electrodes. The electrodes are made of an inert material such as platinum and apply a voltage of 5–30 kV across the capillary. This causes an overall movement of solution towards one electrode (usually the cathode). A detector is placed at the end of the capillary nearest this electrode and the sample for detection is introduced at the other end. The ions in the sample move at different rates (as discussed in the next section) along the capillary and are therefore separated by the time they reach the detector. A plot of the detector response (usually UV absorbance) with time is generated and is termed an electropherogram.

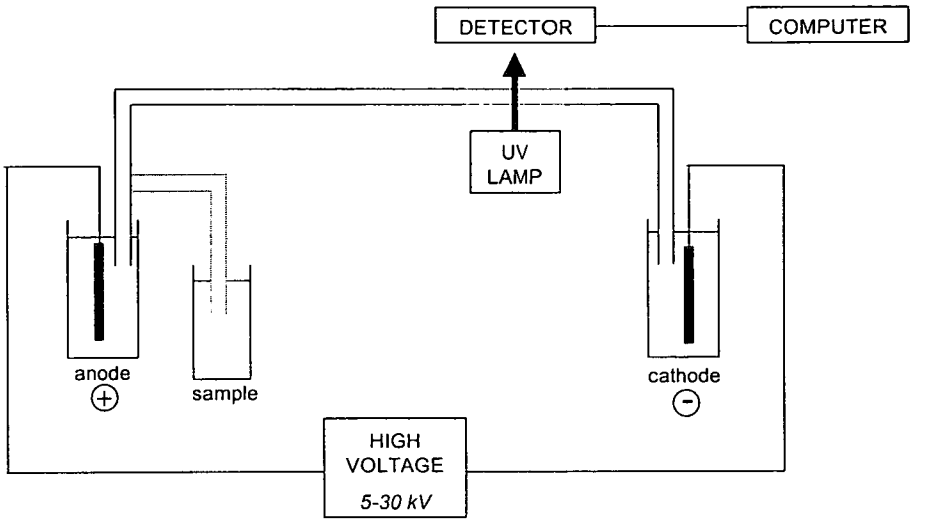

Figure 2.3 A schematic representation of capillary electrophoresis apparatus (Adapted from ref. 28)

Samples can be introduced into the capillary by three methods all of which involve immersing the capillary end into the sample solution and exerting a force to inject the sample into the capillary. All the methods are quantitative allowing reproducible analysis.

1. *Pressure Differential* - The sampling end of the tube is immersed in the solution and a pressure difference applied (positive pressure at the sample end or a vacuum at the detector end) allowing sample to be pushed or pulled into the capillary. The volume of sample will depend on the viscosity of the solution and the temperature.
2. *Gravity Injection* – The capillary, while dipping in the sample vial, is mechanically raised above the height of the detector electrolyte vial. The volume entering the capillary will depend on the height raised, and the density of the liquid.
3. *Elecrokinetic* – The sampling end of the capillary and the high-voltage electrode are both inserted into the sample solution and a voltage is applied for a set length of time allowing sample ions to enter the capillary by electrophoretic migration

and electro-osmotic flow (see next section). This can have bias effects as a greater number of more mobile ions will enter the tube.

Numerous detection methods can be employed in CE, the most usual being UV absorbance, as for HPLC, although fluorescence is also common. Due to the very small sample volumes encountered, detection occurs *on-column*. A small section of the polyimide capillary coating is removed by burning, allowing that section of the tube to act as a detection cell. The very small flow rates of under 1 µl/min from electrophoresis capillaries make it possible to couple the effluent directly to the ionisation source of a mass spectrometer for sample detection. The most common interface is electrospray, which is discussed in section 2.2.3. This method of detection is particularly useful to biologists for large biomolecules such as proteins and DNA fragments. More recently the concept of linking CE to inductively-coupled plasma-mass spectrometry (ICP-MS) has been developed allowing elemental speciation of the eluted products.[31,32] This requires an interface to link the low elution rate of the CE to the rate required for aspiration into the ICP which is of the order of 1 ml/min.

Ion Movement through the Capillary

Ions travel through the capillary by two mechanisms.

1. *Electrophoretic Migration (EM)*- This is the movement of sample ions under the influence of the applied voltage. The ion will move towards the appropriate electrode depending on its charge. The migration rate is governed by the size and charge of the ion according the following equations:

$$Migration\ velocity = \mu E\ V$$

where V is the applied voltage and μE, the ionic mobility, is given by:

$$\mu E = (q / 6\pi)\ \eta r$$

q is the number of charges, η is the solution viscosity and r is the radius of the ion.

Therefore when separating a mixture of ions in a sample, the smaller more highly charged ions will reach the detector first.

2. *Electro-osmotic Flow (EOF)*- From the set up in Figure 2.3, it appears that only cations will be detected as they pass the detector travelling to the cathode. Anions however can also be detected due to a bulk flow of the electrolyte solution towards the cathode. The walls of the capillary are coated in weakly acidic silanol groups. If the buffer has a sufficiently high pH (above 4), these groups are dissociated resulting in a negatively-charged surface. To maintain electroneutrality, cations build up near the surface in a double layer (Figure 2.4). At the wall, there is a fixed layer of cations followed by a diffuse layer to fully balance the charge. When a voltage is applied, the ions in the diffuse layer move towards the cathode. Since the cations are solvated they drag the bulk solvent with them contributing to the overall rate of migration. Since the EOF is a bulk effect, it acts on all molecules in the sample to the same extent, hence all positive, neutral and even negative species will eventually reach the cathode and the detector.

The total migration rate of an ion is the sum of its EM and the EOF, with the latter generally being the greater. In a typical capillary electrophoretic separation, cations will be eluted first since their EM and EOF are both acting towards the cathode.

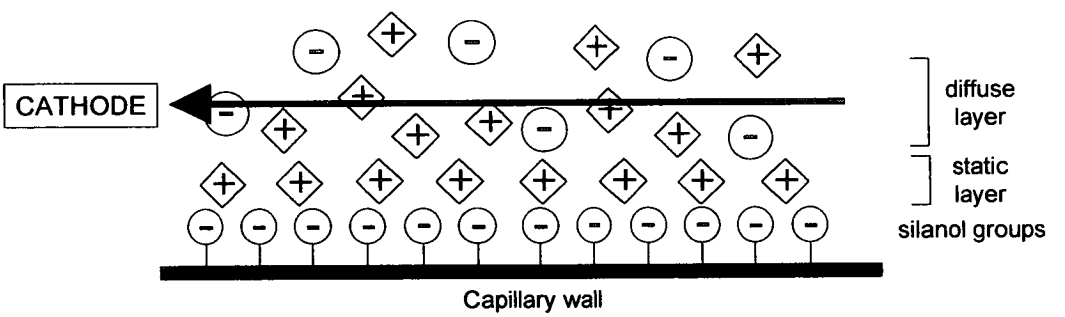

Figure 2.4 Formation of a double layer of cations at the capillary wall leading to electro-osmotic flow (Adapted from ref. 29)

The cations will be separated with the smallest and most highly charged eluting first. Secondly all the neutral molecules will elute since these have only an EOF acting on them. There will therefore be no separation between different neutral components. Finally the anions will be eluted since they have an EM in the opposite direction to the EOF reducing their rate of migration. These will be separated with the largest and lowest charged ions (smallest EM) eluting first. The order of elution is shown in Figure 2.5.

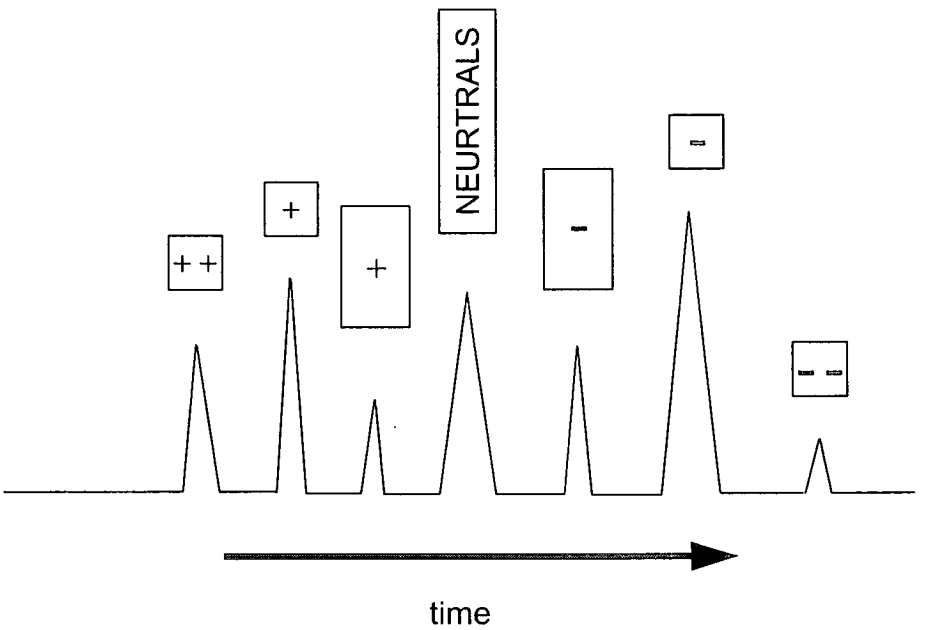

Figure 2.5 Elution order of positive, neutral and negative components in an electrophoretic separation

Modes of Capillary Electrophoresis

The simplest mode of CE, as described above, is called *Capillary Zone Electrophoresis (CZE)*. This can be used for a diverse range of separations from small organic or inorganic molecules to large biomolecules such as proteins and DNA fragments. The resolution of a separation can be maximised by varying several parameters such as the *applied voltage* to shorten analysis times and decrease line-

DNA fragments. The resolution of a separation can be maximised by varying several parameters such as the *applied voltage* to shorten analysis times and decrease line-broadening, *capillary temperature* to change the buffer viscosity, *capillary diameter* to increase detector sensitivity, *capillary length* to vary detection time and separation, and *buffer* to determine pH. This basic technique can also be modified further for more specific applications.

1. *Micellar Electrokinetic Capillary Chromatography (MECC)* was initially developed for the resolution of uncharged compounds which all co-elute in CZE.[33] The electrolyte solution contains relatively high levels of a surfactant, such as sodium dodecyl sulphate, which self-aggregates forming micelles in which the hydrophilic head groups form the outer shell and the hydrophobic tails form a non-polar core. Sample species can partition into this core in a similar fashion to retention on a stationary phase in HPLC. The differential partitioning between the buffered aqueous mobile phase and the micellar phase is the basis for separation of neutral molecules.
2. *Capillary Gel Electrophoresis (CGE)* is used to analyse large biomolecules such as DNA which have very similar charge to mass ratios so are difficult to separate by CZE. The capillary is filled with a porous gel matrix, the pores of which contain the separation buffer. This provides a molecular sieving action, which retards the migration of analyte species to various extents depending on the pore size of the polymer and the size of the analyte anions.
3. *Capillary Isoelectric Focusing (CIEF)* is used to separate amphiprotic species, such as amino acids and proteins containing both acid and base groups. These species have a pI value, a pH at which they form a zwitterion and hence possess no net charge, so will have no tendency to migrate. The capillary is filled with a pH gradient that remains fixed during the application of the separation voltage. The sample is injected at the low pH end and so is positively-charged and moves towards the detector. When the solute reaches the point where the pH matches its pI value it will remain in a fixed position. The various components of the mixture will therefore be separated according to pI value. Pressure is then

applied across the capillary to force the pH gradient along allowing detection of all the separated zones.

4. *Capillary Isotachophoresis (CITP)* can sharpen the resolution of analytes with similar migration velocities. The sample is injected between two buffers, a leading buffer with a high mobility and a terminating buffer with a low mobility. The difference in migration rates results in separation of the various analyte species into adjacent bands, with the fastest located just after the leading buffer. After the bands have formed they all move at the same velocity because the potential field becomes smaller for the more mobile bands and greater for the slower bands so the current is the same in all parts of the buffer. The boundaries formed are very sharp giving high resolution.

A recent development by Knox and Grant[34] is *Capillary Electrochromatography* where a capillary is filled with a reversed-phase HPLC packing. A polar solvent is driven by electro-osmotic flow through the capillary. Separation depends on the distribution of the analyte species between the mobile phase and the liquid stationary phase held on the packing. This has advantages over both parent techniques; it is applicable to uncharged species like HPLC but can provide efficient separations from very small sample volumes. It also does not require high-pressure pumps, so simplifying the system. The electro-osmotic pump has a flat flow profile as opposed to the parabolic flow profile from hydrodynamic pressure, which significantly reduces the line-broadening effect seen in HPLC.

2.2.2.1 Capillary Electrophoresis of Nucleotides

Nucleotides have been quantified by HPLC for approximately 30 years, however HPLC analyses do have limitations. Due to their negative charge, nucleotides can be readily separated by capillary electrophoresis, which has the advantage of using smaller quantities of both sample and buffer.

As detailed in Section 1.7, the total charge on a nucleotide is derived from the charges on the phosphate, the base and the sugar. At pH values close to neutral, the four DNA nucleotides will all have the same charge derived only from the phosphate group since their bases are all neutral. They can therefore only be separated according to their different sizes in the basic CZE mode. At high pH the guanosine N-1 and thymidine N-3 will be deprotonated and will be further distinguished from the other two bases due to an increased charge and electrophoretic mobility. Conversely at low pH adenosine N-1, cytosine N-3 and guanine N-7 can be protonated reducing the overall charge and reducing the migration rate.

The analysis of nucleotides by CE has become widespread in recent years and has been recently reviewed.[35] The separations have been performed in both CZE and MECC modes under a variety of conditions. In the CZE mode, separation has been achieved in acidic, neutral and basic conditions. Commonly-used buffers include sodium salicylate, acetic acid, ammonium acetate and sodium formate, for acidic separations in the range pH 2-6. Neutral separations are generally carried out in sodium phosphate buffer. Alkaline buffers provide a good separation medium for a mixture of mono- di- and tri- phosphates since ionisation of the additional phosphates occurs at around pH 6 giving differently charged species. The most common alkaline buffer is sodium borate. Buffer composition becomes more complicated when MECC is used. Sodium dodecyl sulphate is usually the surfactant added in combination with phosphate and borate salts.

UV detection is ideal for nucleotides since it is inexpensive and can detect species on-column. The detection limit for nucleotide separations by CE is in the picomolar range and is restricted only by the very small pathlength since the UV cell is the capillary. The usual wavelength used for detection is 254 nm. All the nucleotides have a strong absorbance in the region around 260 nm due to π-π^* transitions from the aromatic rings in the bases.

CE has also been used to study the interaction of platinum complexes with nucleotides. Sharma *et. al.*[36] used MECC to separate a dansylated mixture of normal nucleotides and platinated cross-link adducts of d(pGpG) and d(pApG). The use of a laser-induced fluorescence (LIF) detector gave very high sensitivity allowing quantitation of platinated DNA to be determined. The study compared the adducts formed by cisplatin and carboplatin on calf thymus DNA. After Pt binding, the DNA was enzymatically digested and the resulting nucleotide mixture was analysed. A comparison of HPLC and CE as techniques for the separation and identification of platination products of oligonucleotides has been published.[37] The conclusion was that CE was much more sensitive for the resolution of the very similar Pt-products but that adduct identification was much more difficult due to the very small amounts of material eluted from the capillary. The binding of cisplatin to individual nucleotide monophosphates has also been investigated using CE separations in a sodium phosphate buffer using an instrument equipped with a diode array detector.[38] This technique allowed the selectivity of the complex for each nucleotide to be determined as well as the kinetics of binding.

2.2.3 Electrospray Ionisation Mass Spectrometry

Mass spectrometry (MS) is a versatile technique that can provide information on the elemental composition of samples of matter and the structures of inorganic, organic and biological molecules. The general principle of mass spectrometry is the conversion of an analyte sample into gaseous ions which are attracted through the slit of a mass spectrometer and separated according to their mass-to-charge ratios. A spectrum is produced which is like a bar chart depicting the relative intensity of mass peaks according to this ratio. The components of a mass spectrometer are shown in Figure 2.6.

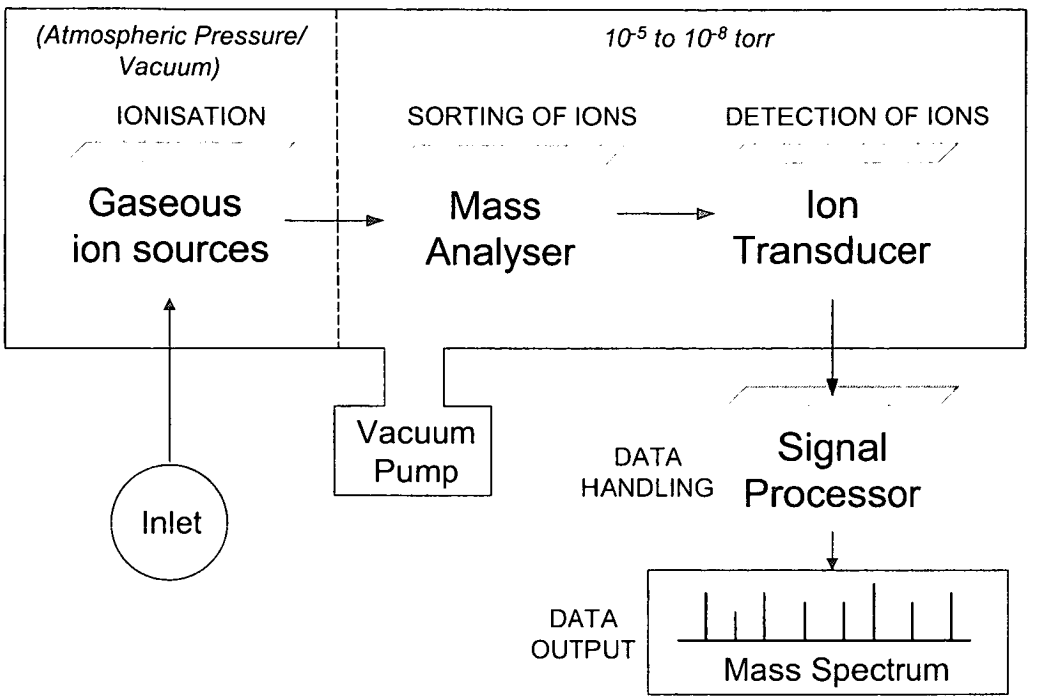

Figure 2.6 Components of a mass spectrometer

Ionisation

The classical methods of ionisation used in MS are based on gas phase encounters of the molecule (having already been vaporised) with electrons, photons, other ions, or electronically excited atoms. Such encounters can remove a negatively or positively charged entity from a neutral molecule transforming it into an ion. These methods are not suitable for large biomolecules, which undergo extensive decomposition by fragmentation of the analyte molecules. Electrospray ionisation[39-42] (ESI) is a desporption ion source where a sample in solution is converted directly into gaseous ions. It is a *soft* ion source in that it does not impart enough energy to the analyte molecules to fragment ions during analysis. The technique was first developed over 30 years ago by Dole and co-workers.[43] ESI takes place under atmospheric pressures and temperatures in an apparatus such as that shown in Figure 2.7. A solution of the sample is pumped through a stainless steel capillary needle at a rate of a few microlitres per minute. The needle is maintained at several kilovolts with respect to

a cylindrical electrode that surrounds the needle. The resulting field at the needle tip charges the surface of the emerging liquid, dispersing it by Coulomb forces into a fine spray of charged droplets. Driven by the electric field, the droplets migrate towards the inlet end of the glass capillary at the end wall of the chamber. A drying gas at 320 to 350 K, encourages evaporation of solvent from each droplet, decreasing its diameter. Consequently, the charge density at its surface increases until the *Rayleigh limit* is reached at which point the Coulomb repulsion becomes of the same order as the surface tension. The resulting instability tears the droplet apart, producing charged daughter droplets that also evaporate. This sequence of events repeats until the radius of curvature of the daughter droplet becomes small enough that the field due to the surface charge density is strong enough to desorb ions from the droplet into the ambient gas.

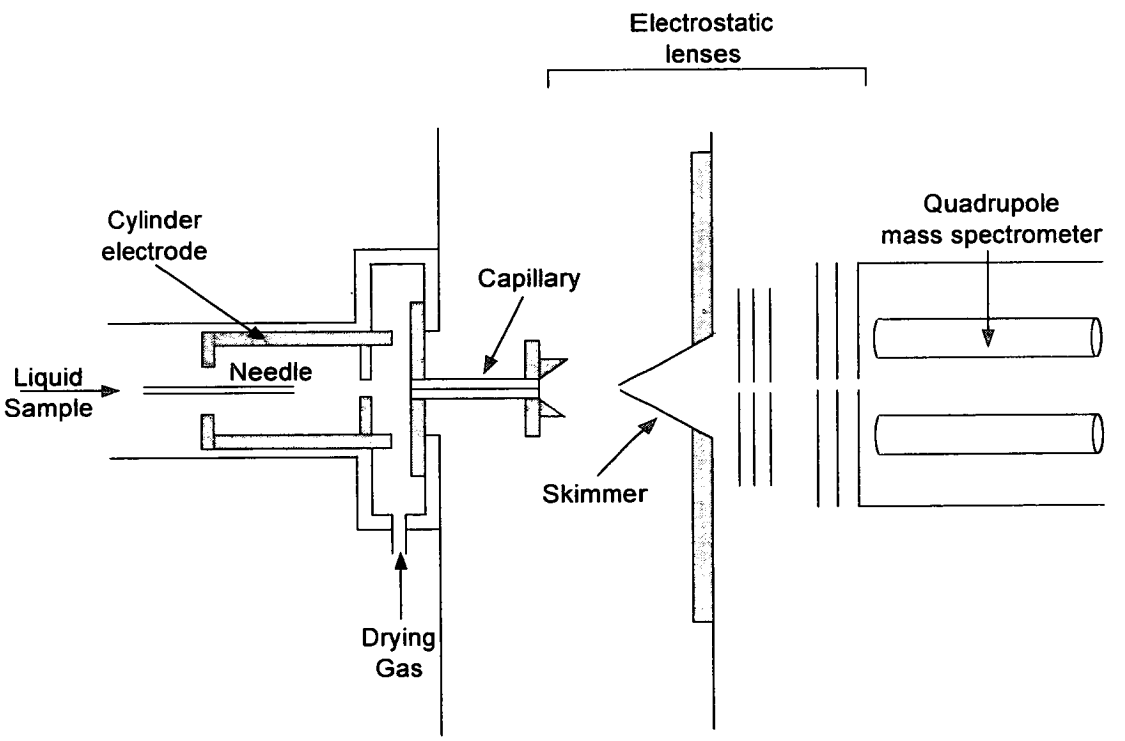

Figure 2.7 Apparatus for electrospray ionisation (Adapted from ref. 40)

A useful feature of ESI is the formation of multiply charged ions so that even very large molecules, such as proteins, have *m/z* values small enough to be detected with a quadrupole instrument with a range of only 4000. In these spectra, adjacent peaks are for analyte ions that differ by one charge. The charge state corresponding to each peak can be determined from peak distribution, thus making it possible to determine the molecular weight of the protein.

Mass Analyser

The most commonly used analyser in MS is the quadrupole mass analyser. This instrument is based around four cylindrical rods acting as electrodes. Opposite rods are connected electrically, one pair to the positive terminal and one to the negative terminal of a variable dc source. In addition variable radio-frequency ac potentials which are 180° out of phase are applied to each pair of rods. The ions from the ESI source are accelerated into the space between the rods and the dc and ac voltages on the rods increased simultaneously while maintaining their ratio constant. This varies the trajectories of the ions passing between them. At any given moment all ions except those having a certain *m/z* value strike the rods and are converted to neutral molecules. Thus only ions with the specific *m/z* reach the transducer. As the voltages are increased, the *m/z* range will change. Quadrupole mass analysers can cover a *m/z* range of up to 4000 and can resolve ions that differ in mass by one unit. The instrument also has the advantage of high scan rates so that an entire mass spectrum can be obtained in less than 100 ms.

2.3 Experimental Methods

2.3.1 Nuclear Magnetic Resonance Spectroscopy

NMR spectra were recorded on a Bruker DMX 500 spectrometer using 5 mm tubes. The frequencies for ^{1}H and ^{31}P detection were 500 MHz and 202 MHz respectively. Typically ^{1}H spectra were acquired with 64-256 transients using a pulse width 45-60° into 16-32 K data points with a relaxation delay of 2-3 s. The water resonance was suppressed by presaturation. The ^{1}H chemical shifts were internally referenced to dioxane (3.768 ppm relative to TSP at 293 K). ^{31}P-{^{1}H} spectra were aquired with 512-2048 transients using inverse-gated decoupling and a pusle width of 90° into 16-32 K data points with a relaxation delay of 0.2 s. The ^{31}P chemical shifts were externally reference to 85% H_3PO_4.

Coupling constants (*J*) are given in Hz and NMR signals are described as singlets (s), doublets (d), triplets (t), multiplets (m) and broad (br).

Some NMR spectra for characterisation purposes were also recorded at the NMR service, University of Edinburgh.

2.3.2 Capillary Electrophoresis

All CE experiments were carried out on an ISCO Model 3850 Capillary Electropherograph instrument equipped with an in-line, wavelength detector set to 254 nm.

The nucleotide separations were run at 25 kV (90-100 μA) with a fused silica capillary from Composite Metal Services Ltd. of 100 μm internal diameter. The total capillary length was 94 cm (71 cm to detector).

The capillary was conditioned with 0.1 M NaOH overnight before use, then flushed with distilled water and buffer before use. It was then washed with 0.1 M NaOH, water and buffer to recondition the capillary after every four runs.

The separation buffer was 20 mM Na_2HPO_4 at pH 7.75 prepared by dissolving Na_2HPO_4 (1.42 g, 10 mmol,) in 500 ml of water and adjusting the pH with HCl (1 M). All water for CE was purified using a Millipore Elix 5 system, followed by an Elgastat UHQ II deioniser. The buffer solution was then filtered using Varian 0.45 μm filter paper and degassed by bubbling with nitrogen gas. Samples were injected into the capillary by applying a vacuum at the detector end for 5 s.

2.3.3 Electrospray Ionisation Mass Spectrometry

Negative and positive ion electrospray mass spectrometry was performed on a Platform II mass spectrometer (Micromass, Manchester, U.K.). The samples were infused at a flow rate of 0.48 ml h^{-1} and the ions produced in an atmospheric pressure ionisation (API)/ESI ion source. The temperature was 338 K and the drying gas flow rate 300 lh^{-1}. A potential of 3.0 kV was applied to the probe tip and a cone voltage of 70 V over 500-2000 Da was used. The quadrupole was scanned at 100 amu s^{-1}. The acquisition and deconvolution of data was performed on Mass Lynx (V. 2.3) Windows NT PC data system using the Max Ent Electrospray software algorithm and calibrated versus a NaI calibration file.

2.3.4 X-ray Crystallography

X-ray crystal structure analyses were performed by Dr. Simon Parsons, Dr. Robert Coxhall and Mr. Andrew Parkin of the University of Edinburgh. X-ray data were recorded on either a Bruker SMART APEX CCD diffractometer or a Stoe Stadi-4 diffractometer, equipped with an Oxford cryosystem low-temperature device, using graphite-monochromated Mo-Kα radiation.

2.3.5 High Performance Liquid Chromatography

The following equipment was used: a Hewlett-Packard Series 1100 Chemstation, HP 1100 series quaternary pumps, HP 1100 series vacuum degasser, HP variable wavelength D_2 lamp UV/Vis detector, HP enhanced integrator, Rheodyn sample injector with 100 µl loop, Hamilton microlitre syringes. All water for HPLC was purified using a Millipore Elix 5 system, followed by an Elgastat UHQ II deioniser. All solvents were filtered prior to use using Varian 0.45 µm filter paper from Anachem. The data were analysed using HP chemstation for Windows '95. The mode of HPLC employed was reverse-phase and the column used was a Nucleosil 100 –5 C18 column purchased from Hichrom.

2.3.6 Microanalyses

CHN analyses were performed by the CHN service at the University of Edinburgh, Department of Chemistry.

2.3.7 Mass Spectrometry

Samples were run by the service at the University of Edinburgh on a Kratos M.S. 50TC instrument using fast atom bombardment. Xenon gas was used at 7kV and the matrix was CH_3CN/3-NOBA.

2.3.8 pH Measurements

These were made using a Corning 145 pH meter equipped with an Aldrich micro combination electrode calibrated with standard buffer solutions at pH 4, 7 and 10. Readings of the pH meter for D_2O solutions were not corrected for deuterium isotope effects and are designated as pH* values.

Values of pK were obtained by plotting the relative concentrations of species (from NMR peak integrals) against pH and fitting to the Henderson-Hasselbalch equation using the programme KALEIDAGRAPH[44].

2.4 References

1 P. J. Hore, *Nuclear Magnetic Resonance*, Oxford University Press, New York, **1995**

2 R. J. Abraham, J. Fisher, P. Loftus, *Introduction to NMR Spectroscopy,* John Wiley and Sons Ltd., Chichester, **1988**

3 H. Günther, *NMR Spectroscopy – Basic Principles, Concepts, and Applications in Chemistry*, 2nd Ed., John Wiley and Sons Ltd., Chichester, **1995**

4 J. A. Iggo, *NMR Spectroscopy in Inorganic Chemistry*, Oxford University Press, New York, **1999**

5 J. Errington, *J. Chem. Soc., Dalton Trans.*, **1996**, 681

6 K. Karaghiosoff, *Phosphorus-31 NMR*, in *Encyclopedia of NMR*, D. M. Grant, R. K. Harris, Eds., John Wiley and Sons, Chichester, **1996**, Vol. 6

7 J. G. Verkade, L. D. Quin, Eds., *Phosphorus-31 NMR Spectroscopy in Stereochemical Analysis*, from *Methods in Stereochemical Analysis*, A. P. Marchand, Series Ed., VCH Publishers Inc. **1987**, *8*

8 A. Pidock, R. E. Richards, L. M. Venanzi, *J. Chem. Soc. A*, **1966**, 1707

9 G. G. Mather, A. Pidock, G. J. N. Rapsey, *J. Chem. Soc., Dalton Trans.* **1973**, 2095

10 F. H. Allen, A. Pidock, *J. Chem. Soc. A.* **1968**, 2700

11 B. T. Heaton, A. Pidock, *J. Organomet. Chem.* **1968**, *14*, 235

12 G. K. Anderson, H. C. Clark, J. A. Davies, *Inorg. Chem.* **1983**, *22*, 427

13 G. K. Anderson, R. Kumar, *Inorg. Chem.* **1984**, *23*, 4064

14 G. Salem, S. B. Wild, *Inorg. Chem.* **1992**, *31*, 581

15 F. H. Allen, S. N. Sze, *J. Chem. Soc. A*, **1971**, 2055

16 P. E. Garrou, *Chem. Rev.* **1981**, *81*, 229

17 S. Heitkamp, D. J. Stufkens, K. Vrieze, *J. Organomet. Chem.* **1979**, *169*, 107

18 P. S. Pregosin, *Coord. Chem. Rev.* **1982**, *44*, 247

19 L. G. Marzilli *Prog. Inorg Chem.* **1977**, *23*, 255

20 D. Lemaire, M.-H. Fouchet, J. Kozelka, *J. Inorg. Biochem.* **1994**, *53*, 261

21 R. Cramer, P. Dahlsrom, *Inorg. Chem.* **1985**, *24*, 3420

22 S. O. Ano, Z. Kuklenyik, L. G. Marzilli, in *Cisplatin: Chemistry and Biochemistry of a Leading Anticancer Agent*, B. Lippert, Ed., VHCA Zurich and Wiley-VCH Weinheim, **1999**, p247

23 G. Raudaschl-Sieber, H. Schöllhorn, U. Thewalt, B. Lippert, *J. Am. Chem. Soc.* **1985**, *107*, 3591

24 B Lippert, *Coord. Chem. Rev.* **2000**, *200-202*, 487

25 F. E. P. Mikkers, F. M. Everaerts, T. P. E. M. Verheggen, *J. Chromatogr.* **1979**, *169*, 11

26 J. W. Jorgenson, K. D. Lukacs, *Anal. Chem.* **1981**, *53*, 1298

27 D. A. Skoog, F. J. Holler, T. A. Nieman, *Principles of Instrumental Analysis*, 5th Ed. Harcourt Brace College Publishing, Orlando, Florida, **1998**, p778

28 J. P. Landers, (Ed.) *Handbook of Capillary Electrophoresis*, 2nd Ed., CRC Press, Boca Raton, Florida, **1997**

29 K. D. Altria, (Ed.) *Capillary Electrophoresis Guidebook: Principles, Operation and Applications*, in *Methods in Molecular Biology*, Humana Press, Totowa, New Jersey, Vol. *52*, **1996**

30 A. G. Ewing, R. A. Wallingford, T. M. Olefirowicz, *Anal. Chem.* **1989**, *61*, 4, 292A

31 K. Sutton, R. M. C. Sutton, J. A. Caruso, *J. Chromatogr. A,* **1997**, *789*, 85

32 B. Michalke, P. Schramel, *Analusis*, **1998**, *26*, 6, 51

33 S. Terabe, K. Otsuka, K. Ichikawa, A. Tsuchiya, T. Ando, *Anal. Chem.* **1984**, *56*, 111

34 J. H. Knox, I. H. Grant, *Chromatographia*, **1991**, *32*, 317

35 S. E. Geldart, P. R. Brown, *J. Chromatogr. B.,* **1998**, *828*, 317

36 M. Sharma, R. Jain, E. Ionescu, H. K. Slocum, *Anal. Biochem.* **1995**, *228*, 307

37 H. Troujman, J.-C. Chottard, *Anal. Biochem.***1997**, *252*, 177

38 A. Zenker, M. Galanski, T. L. Bereuter, B. K. Keppler, W. Lindner, *J. Chromatogr. A.,* **1999**, *852*, 337

39 D. A. Skoog, F. J. Holler, T. A. Nieman, *Principles of Instrumental Analysis*, 5th Ed. Harcourt Brace College Publishing, Orlando, Florida, **1998**, p509

40 J. B. Fenn, M. Mann, C. K. Meng, S. F. Wong, C. M. Whitehouse, *Science*, **1989**, *246*, 64

41 R. D. Smith, J. A. Loo, C. G. Edmonds, C. J. Barinaga, H. R. Udseth, *Anal. Chem.* **1990**, *62*, 882

42 P. Kebarle, L. Tang, *Anal. Chem.* **1993**, *65*, 22, 972A

43 M. Dole, L. L. Mack, R. L. Hine, R. C. Mobley, L. D. Ferguson, M. B. Alice, *J. Chem. Phys.* **1968**, *49*, 2240

44 Kaleidagraph 3.09, Synergy Software, 1997

Chapter Three

Synthesis and Characterisation of Platinum Aminophosphine Complexes

This chapter is concerned with the synthesis and crystal structures of some Pt(II) aminophosphine complexes using the ligands shown in Figure 3.1, and with their potential chelate ring-opening reactions.

3.1 Experimental

3.1.1 Synthesis of Aminophosphine Ligands

3.1.1.1 $Ph_2P(CH_2)_3NMe_2$ (DMDPPA)

PPh_2H (5.5 ml, 5.88 g, 31.6 mmol) was added via syringe to a suspension of Bu^tOK (9.0 g, 80 mmol) in dry and freshly distilled THF (150 ml). The resulting red solution was stirred at ambient temperature for 40 min. $Me_2N(CH_2)_3Cl.HCl$ crystals (5 g, 31.6 mmol), previously stored in a dessicator over P_2O_5, were added and the reaction mixture then heated under reflux for 24 hours until the solution had turned almost colourless. The solvent was removed *in vacuo* and the residue taken up in 10% HCl solution. The solution was washed with benzene and made alkaline with 10% NaOH solution. The product was extracted into benzene (3 x 50 ml), washed with brine and dried over Na_2SO_4. After filtration and rotary evaporation, a colourless oil was obtained. This was purified by distillation under vacuum: B.p. = 403 K (0.05 mm Hg).

Yield = 5.72 g, 21.1 mmol, 66.8%.

^1H NMR ($CDCl_3$): δ 1.54-1.63 (2 H, m, $-CH_2-$), 2.06 (2 H, t, *P*-CH_2), 2.16 (6 H, s, 2 CH_3), 2.34 (2 H, t, *N*-CH_2), 7.25-7.45 (10 H, m, 2 Ph)

^{31}P NMR ($CDCl_3$): δ -15.18

3.1.1.2 $Ph_2P(CH_2)_3NH_2$ (DPPA)

This was prepared by an analogous procedure to that described in Section 3.1.1.1 replacing $Me_2N(CH_2)_3Cl.HCl$ with $H_2N(CH_2)_3Cl.HCl$.

Distillation of product: B.p. = 388 K (0.01 mm Hg)

Yield = 2.41 g, 9.92 mmol, 40.2%

^1H NMR ($CDCl_3$): δ 1.10 (2 H, s, H_2N), 1.51-1.65 (2 H, m, -CH_2-), 2.01-2.09 (2 H, m, *P*-CH_2), 2.74 (2 H, t, *N*-CH_2), 7.23-7.50 (10 H, m, 2 Ph)

^{31}P NMR ($CDCl_3$): δ -15.47

3.1.1.3 $Ph_2P(CH_2)_3N(H)Me$ (MDPPA)

$CHO(H)N(CH_2)_3OH$

3-Amino-1-propanol (50 ml, 0.66 mol) was placed in a flame-dried flask under argon. An excess of ethyl formate (150 ml, 1.86 mol) was added dropwise and the mixture heated under reflux for 20 h. After cooling, the excess ethyl formate and ethanol by-product were removed under vacuum to leave an oily product.

Yield = 65.37 g, 0.64 mol, 96.6%

^1H NMR ($CDCl_3$): δ 1.75 (2 H, m) 3.4 (2 H, m), 3.6 (2 H, m), 6.5 (1 H, br, s), 8.1 (2 H, s)

$C_4H_9NO_2$ (103.14) Calc. %C = 46.60 %H = 8.74 %N = 13.58

Found %C = 44.92 %H = 8.45 %N = 13.02

m/z (FAB): 103

$Me(H)N(CH_2)_3OH$

$LiAlH_4$ (18.4 g, 0.49 mol) was placed in a flame dried flask under argon. Dry and freshly distilled THF (150 ml) was added slowly and the mixture cooled to 273 K. $HO(CH_2)_3N(H)CHO$ (32.39 g, 0.31 mol) in dry THF (50 ml) was added dropwise with mechanical stirring and the reaction heated under reflux for 3 h. Excess $LiAlH_4$

was hydrolysed by addition of a 1:1 diethyl ether/water mixture (ca.100 ml) and the solution was made basic with 20% NaOH. The remaining slurry was filtered to a give clear liquid, which was purified by distillation. B.p. = 313 K (0.2 mm Hg).

Yield = 18.34 g, 0.21 mol, 65.6%

^{1}H NMR ($CDCl_3$): δ 1.6 (2 H, q, -CH_2-) 2.35 (3 H, s, CH_3), 2.7 (2 H, t, CH_2), 3.2 (1 H, br, NH), 3.7 (2 H, t, CH_2)

m/z (FAB): 90

$Me(H)N(CH_2)_3Cl.HCl$

$Me(H)N(CH_2)_3OH$ (9.24 g, 0.10 mol) was placed in a flame-dried and argon filled flask. Dry and freshly distilled chloroform was added slowly and the reaction cooled to 0°C. Thionyl chloride (60 ml, 0.82 mol) was added to the solution, dropwise with stirring. The reaction vessel was allowed to warm slowly and then heated under reflux for 3 h. After cooling, the solvent and excess thionyl chloride were removed under vacuum leaving a brown oily residue. After repeated recrystallisation from ethanol/diethyl ether, a white solid product was obtained.

Yield = 10.40 g, 0.07 mol, 69.5%

^{1}H NMR ($CDCl_3$): δ 2.3 (2 H, q, -CH_2-) 2.7 (3 H, s, CH_3), 3.1 (2 H, t, CH_2), 3.7 (2 H, t, CH_2), 9.6 (1 H, br, NH)

$C_4H_{10}NCl_2$ (144.06) Calc. %C = 33.33 %H = 7.64 %N = 9.72

Found %C = 32.25 %H = 7.32 %N = 9.27

m/z (FAB): 108 {$Me(H)N(CH_2)_3Cl$}

$Ph_2P(CH_2)_3NHMe$

This was prepared by in an analogous procedure to that described in Section 3.1.1.1 replacing $Me_2N(CH_2)_3Cl.HCl$ with $Me(H)N(CH_2)_3Cl.HCl$.

Distillation of product: B.p. = 403 K (0.01 mm Hg)

Yield = 2.79 g, 0.01 mol, 39.2%

^{1}H NMR ($CDCl_3$): δ 1.6 (2 H, m, -CH_2-), 2.1 (2 H, m, *P*-CH_2), 2.4 (3 H, s, CH_3), 2.6 (2 H, m, *N*-CH_2), 7.3 (10 H, m, 2 Ph)

^{31}P NMR ($CDCl_3$): δ -15.45

$C_{16}H_{20}NP$ (257.34) Calc. %C = 74.71 %H = 7.78 %N = 5.45

Found %C = 74.62 %H = 7.62 %N = 5.27

m/z (FAB): 258

3.1.1.4 $Ph_2P(CH_2)_3N(H)^tBu$ (BDPPA)

$^tBu(H)N(CH_2)_3OH$

Trimethylene oxide (3.25 ml, 49.97 mmol) was added to freshly distilled acetonitrile (50 ml), via a syringe, under argon. *Tert*-butylamine (10.5 ml, 0.1 mol) was dried by refluxing over CaH_2 and also added to the mixture together with lithium tetrafluoroborate (10.00 g, 0.11 mol). The reaction mixture was stirred at room temperature for 84 h. The solution was diluted with 36% aqueous ammonia (200 ml) and a saturated NaCl solution (50 ml). The product was extracted with chloroform (4 x 60 ml), washed with saturated NaCl solution and dried over Na_2SO_4. Filtration and rotary evaporation yielded a crude product, which was recrystallised from ethanol/diethyl ether to give white crystals.

Yield = 4.39 g, 33.4 mmol, 67.1%

^1H NMR ($CDCl_3$): δ 1.1 (9 H, s, ^tBu), 1.7 (2 H, m, CH_2), 2.8 (2 H, t, CH_2), 3.8 (2 H, t, CH_2)

$C_7H_{17}NO$ (131.25) Calc. %C = 64.12 %H = 12.98 %N = 10.69

Found %C = 63.78 %H = 13.44 %N = 10.42

m/z (FAB): 132

$^tBu(H)N(CH_2)_3Cl.HCl$

The chloride was prepared by an analogous procedure to that described in Section 3.1.1.3, replacing $Me(H)N(CH_2)_3OH$ with $^tBu(H)N(CH_2)_3OH$. A shiny off-white solid was obtained from recrystallisation from ethanol/diethyl ether.

Yield = 4.05 g, 21.8 mmol, 79.0%

^{1}H NMR ($CDCl_3$): δ 1.5 (9 H, s, ^{t}Bu), 2.5 (2 H, m, CH_2), 3.1 (2 H, m, CH_2), 3.7 (2 H, t, CH_2) 9.3 (1 H, br, NH)

$C_7H_{16}NCl.HCl$ (186.15) Calc. %C = 45.16 %H = 9.14 %N = 7.53

Found %C = 45.07 %H = 9.31 %N = 7.30

m/z (FAB): 150 {^{t}Bu(H)N$(CH_2)_3Cl$}

$Ph_2P(CH_2)_3N(H)^tBu$

This was prepared as described in Section 3.1.1.1 replacing $Me_2N(CH_2)_3Cl.HCl$ with ^{t}Bu(H)N$(CH_2)_3Cl.HCl$.

Distillation of product: B.p. = 416 K (0.01 mm Hg)

Yield = 3.48 g, 11.6 mmol, 55.7%

^{1}H NMR ($CDCl_3$): δ 1.1 (9 H, s, ^{t}Bu), 1.6 (2 H, m, -CH_2-), 2.1 (2 H, m, *P*-CH_2), 2.7 (2 H, t, *N*-CH_2), 7.2 (10 H, m, 2 Ph)

^{31}P NMR ($CDCl_3$): δ -15.3

$C_{19}H_{26}NP$ (299.43) Calc. %C = 76.25 %H = 8.70 %N = 4.68

Found %C = 75.05 %H = 8.65 %N = 4.35

m/z (FAB): 301

3.1.2 Synthesis of Platinum Complexes

3.1.2.1 [Pt(1,5-cyclooctadiene)Cl_2]

Potassium tetrachloroplatinate (1.04 g, 2.76 mmol) was dissolved in 16 ml distilled water and filtered. Glacial acetic acid (24 ml) was added to the deep red filtrate followed by 1,5 cyclooctadiene (1.00 ml, 8.00 mmol), via a syringe, under argon. The reaction mixture was then stirred rapidly and heated to 363 K. Over 30 min, the red solution became pale yellow and some fine off-white crystals were deposited. Some solvent was removed under vacuum to leave a volume of about 15 ml. The product formed as pale yellow needle-like crystals, which were filtered off and washed with water, ethanol and diethyl ether.

Yield = 0.80 g, 2.13 mmol, 85.4%

$C_8H_{12}Cl_2Pt$ (374.18) Calc. %C = 25.67 %H = 3.21

Found %C = 25.46 %H = 3.13

3.1.2.2 [Pt{$Me_2N(CH_2)_3PPh_2$-*P*}$_2Cl_2$] (**24**)

$Me_2N(CH_2)_3PPh_2$ (0.11 g, 0.30 mmol) and $Pt(COD)Cl_2$ (0.16 g, 0.59 mmol) were dissolved in the minimum amount of dichloromethane. The resulting solution was stirred at room temperature overnight, then diethyl ether was added to precipitate the product. A small amount of product was filtered off and the filtrate left overnight to allow more solvent to evaporate. White crystals formed.

Yield = 0.22 g, 0.28 mmol, 92.8%.

^{1}H NMR ($CDCl_3$):δ 1.71-1.73 (2 H, m), 2.11 (6 H, s, 2 CH_3), 2.16-2.11 (2 H, m), 2.26-2.32 (2 H, m), 7.25-7.53 (10 H, m, 2 Ph)

^{31}P NMR ($CDCl_3$): δ 8.45 ^{1}J(P-Pt) 3643 Hz

$C_{34}H_{44}N_2P_2Cl_2Pt$ (808.72) Calc. %C = 50.50 %H = 5.45 %N = 3.47

Found %C = 50.29 %H = 5.44 %N = 3.39

m/z (FAB): 773 (M^+-Cl)

The following complexes were prepared by an analogous method to that described for complex **24**.

3.1.2.3 [Pt{$H_2N(CH_2)_3PPh_2$-*P,N*}$_2$]Cl_2 (**25**)

DPPA ligand (0.129 g, 0.53 mmol) was used as described in Section 3.1.2.2. The reaction solution was refrigerated overnight after addition of diethyl ether and a white powdery product was formed which was filtered and washed with diethyl ether. Crystals suitable for X-ray structure determination were obtained by slow evaporation of a nitromethane solution at room temperature.

Yield = 0.177 g, 0.26 mmol, 98.1%

^{1}H NMR ($CDCl_3$):δ 1.84-1.99 (2 H, m), 2.60-2.69 (2 H, m), 3.18-3.20 (2 H, m), 6.06-6.21 (2 H, br, NH_2) 7.25-7.53 (10 H, m, 2 Ph)

^{31}P NMR ($CDCl_3$): δ -2.47 ^{1}J(P-Pt) 3285 Hz

$C_{30}H_{36}N_2P_2Cl_2Pt$ (752.60) Calc. %C = 47.87 %H = 4.83 %N = 3.72

Found %C = 47.26 %H = 5.04 %N = 3.71

3.1.2.4 [Pt{Me(H)N(CH$_2$)$_3$PPh$_2$}$_2$Cl]Cl (**26**)

MDPPA ligand (0.139 g, 0.54 mmol) was used as described in Section 3.1.2.2. The product yielded on addition of diethyl ether was an oily residue. The solvent was removed under vacuum and the product washed with more diethyl ether. After repeated washing and decanting a white solid remained. The product was recrystallised from dichloromethane and diethyl ether, filtered and washed. A single crystal suitable for X-ray diffraction was obtained from the $CDCl_3$ NMR solution.

Yield = 0.121 g, 0.15 mmol, 55.5%

^{31}P NMR ($CDCl_3$): δ 3.82 (d) ^{1}J(P-Pt) 3728 Hz, 4.89 (d) ^{1}J(P-Pt) 3166 Hz

$C_{32}H_{40}N_2P_2Cl_2Pt$ (780.66) Calc. %C = 49.23 %H = 5.18 %N = 3.59

Found %C = 48.84 %H = 5.63 %N = 3.18

3.1.2.5[Pt{^{t}Bu (H)N(CH$_2$)$_3$PPh$_2$-*P*}$_2$Cl$_2$] (**27**)

BDPPA ligand (0.165 g, 0.55 mmol) was used as described in Section 3.1.2.2. After addition of diethyl ether a white precipitate formed slowly. After 24 h the product was filtered and washed with more ether. Crystals suitable for X-ray structure determination were obtained by slow diffusion of diethyl ether into a dichloromethane solution at 277 K.

Yield = 0.127 g, 0.15 mmol, 54.6%

^{31}P NMR ($CDCl_3$): δ 8.85 (s) ^{1}J(P-Pt) 3665 Hz

$C_{38}H_{52}N_2P_2Cl_2Pt$ (864.83) Calc. %C = 52.78 %H = 6.02 %N = 3.24
Found %C = 52.93 %H = 6.09 %N = 3.01

3.1.2.6 [Pt(1,5-cyclooctadiene)MeCl]

A slight excess of $SnMe_4$ (0.2 ml, 1.47 mmol) was added to a suspension of $Pt(COD)Cl_2$ (0.50 g, 1.34 mmol) in a 1:1 mixture of dichloromethane and methanol. The solution was left to stir for 72 h. The solvent was then removed under vacuum at 273 K to give a white powdery product, which was washed three times with diethyl ether. The product was recrystallised from dichloromethane and diethyl ether.

Yield = 0.285 g, 0.81 mmol, 60.1%.

^{1}H NMR ($CDCl_3$): δ 0.89 (3 H, t, CH_3) ^{2}J(Pt-H) = 71.2 Hz, 2.1-2.7 (8 H, m, 4 CH_2), 4.50 (2 H, t, 2 CH,) ^{2}J(Pt-H) = 76.5 Hz, 5.59 (2 H, t, 2 CH) ^{2}J(Pt-H) = 35.4 Hz

$C_9H_{15}ClPt$ (353.77) Calc. %C = 30.55 %H = 4.28
Found %C = 29.98 %H = 3.87

3.1.2.7 [Pt{$Ph_2P(CH_2)_3NMe_2$-*N,P*}MeCl] (**28**)

Pt(COD)MeCl (0.222 g, 0.63 mmol) was dissolved in dichloromethane. DMDPPA ligand (0.167 g, 0.62 mmol) was dissolved in the minimum amount of dichloromethane and added dropwise. The mixture was left to stir at room temperature overnight. The same volume of diethyl ether was then added yielding a cloudy precipitate. The flask was stored at 277 K overnight and a white crystalline product was obtained which was filtered and washed with ether. Crystals suitable for X-ray diffraction were obtained by slow diffusion of diethyl ether into a dichloromethane solution at 277 K.

Yield = 0.211 g, 0.41 mmol, 65.1%

^{1}H NMR ($CDCl_3$): δ 0.36 (3 H, t, *Pt*-CH_3) ^{2}J(Pt-H) = 70.1 Hz, 2.79 (6 H, t, 2 *N*-CH_3) ^{3}J(Pt-H) = 12.1 Hz

$C_{18}H_{25}NPClPt$ (516.94) Calc. %C = 41.82 %H = 4.84 %N = 2.71
Found %C = 41.11 %H = 4.55 %N = 2.39

3.1.2.8 [Pt{$Ph_2P(CH_2)_3NMe_2$-*N,P*}Cl_2] (**29**)

Pt{$Ph_2P(CH_2)_3NMe_2$-N,P}MeCl (0.050 g, 0.096 mmol) was dissolved in THF and a 3-fold excess of 5 M HCl (0.055 ml, 0.287 mmol) was added dropwise. An immediate yellow cloudy precipitate was formed. The reaction mixture was left to stir overnight. The yellow product was then filtered off, washed with diethyl ether and dried at 373 K.

Yield = 0.039 g, 0.072 mmol, 74.7%

$C_{17}H_{22}NPCl_2Pt$ (537.35) Calc. %C = 37.99 %H = 4.10 %N = 2.61
$C_{17}H_{22}NPCl_2Pt.HCl$ (573.81) Calc. %C = 35.57 %H = 3.84 %N = 2.44
Found %C = 34.94 %H = 3.63 %N = 2.21

3.2 Results and Discussion

3.2.1 Preparation and Properties of Ligands

A series of ligands of the form **$Ph_2P(CH_2)_3NRR'$** was prepared, with various R groups, the structures of which are shown in Figure 3.1. A number of methods has been reported for the preparation of aminophosphine ligands.[1-4] In this work the favoured starting materials were amino-chlorides which were either commercially available (see Section 2.3.1) or prepared as described below. The phosphination of the amino-chloride was achieved by reaction with the diphenylphosphine anion (formed *in situ* by the reaction of *tert*-potassium butoxide and diphenylphosphine) in THF under argon, affording the ligand. (Scheme 3.1)

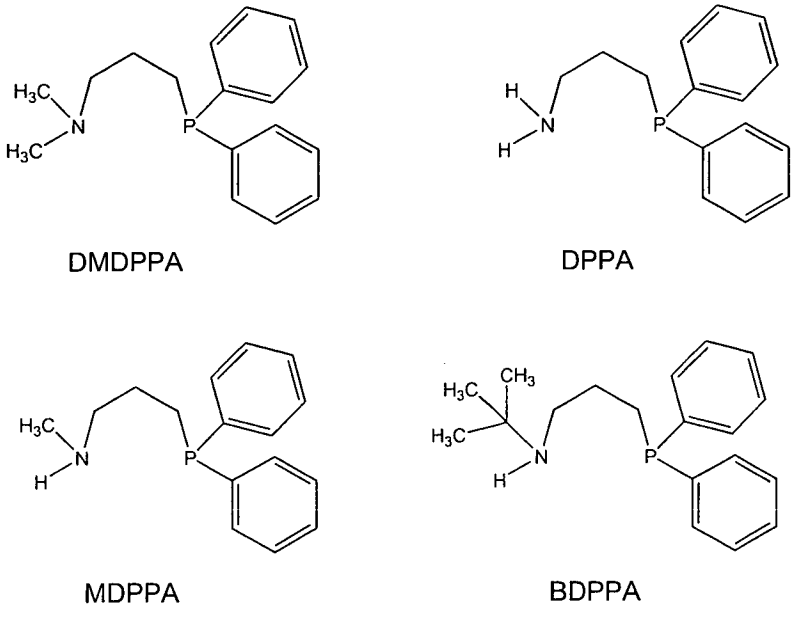

Figure 3.1 Structures of ligands and abbreviations

$$Ph_2PH + RR'N(CH_2)_3Cl.HCl \xrightarrow{{}^tBuOK,\ THF} RR'N(CH_2)_3PPh_2 + 2HCl$$

Scheme 3.1 Preparation of ligands from the amino-chloride

For the preparation of the MDPPA ligand, the 3-aminopropanol was reacted with ethyl formate to give N-formyl-3-hydroxypropylamine which was then reduced to form N-methyl-3-hydroxypropylamine.[5] This was chlorinated with thionyl chloride to yield the amino-chloride starting material for the phosphination reaction. (Scheme 3.2)

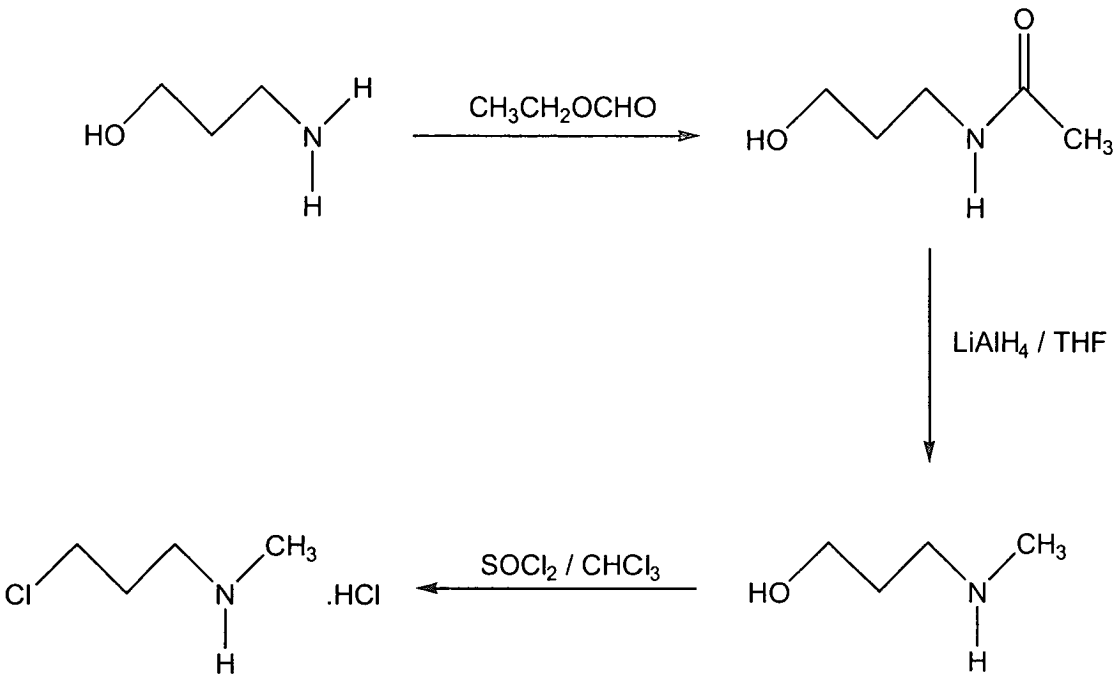

Scheme 3.2 Preparation of N-methyl-3-chloropropylamine

For the BDPPA ligand, the amino-alcohol was prepared by using $LiBF_4$ to promote the ring-opening aminolysis of methylene oxide.[6] This was then chlorinated in the same manner as for MDPPA above to give the necessary amino-chloride (Scheme 3.3).

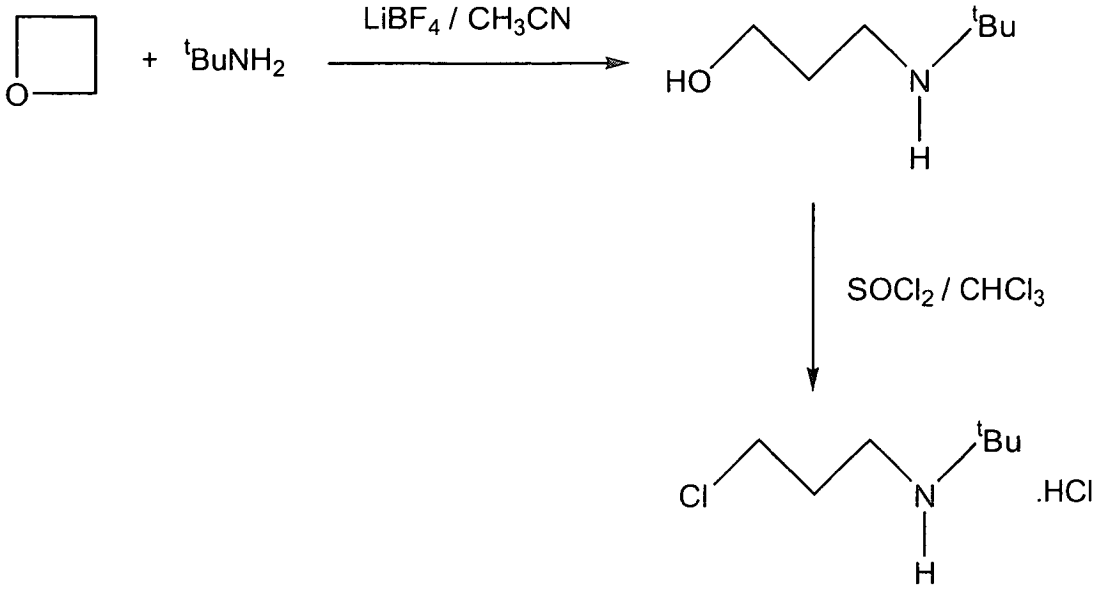

Scheme 3.3 Preparation of N-(*tert*-butyl)-3-chloropropylamine

The ligands were obtained as viscous oils, which were all soluble in organic solvents. The oily ligands were easily purified by distillation, with boiling points ranging from 388-416 K (at 0.01 mm Hg).

The ^{1}H NMR spectra of the ligands in $CDCl_3$ showed the expected peaks with the backbone $-CH_2-$ giving multiplets and the R groups on the amine giving singlet resonances. The $^{31}P\{^{1}H\}$ NMR also showed singlet resonances in the region of δ -15 ppm. In some cases minor impurities were observed with δ ~35 ppm. These were attributed to the formation of oxidised phosphine product and were seen to increase with time if the ligands were not stored in an inert atmosphere.

3.2.2 Structures and Properties of Platinum Aminophosphine Complexes

The ligands prepared in Section 3.1 were used to prepare square planar platinum(II) complexes by reaction with platinum(1,5 cyclooctadiene) starting materials.

3.2.2.1 *Bis*-aminophosphine Complexes

Complexes **24-27** were prepared by reaction of two mole equivalents of the appropriate ligand with $[Pt(COD)Cl_2]$ in dichloromethane solution. (Scheme 3.4) The $[Pt(COD)Cl_2]$ used in this work was either prepared as described in Section 3.1.2.1[7] or purchased commercially. Since the resulting complexes are more polar than either starting material they could be precipitated from the reaction mixture by the addition of diethyl ether.

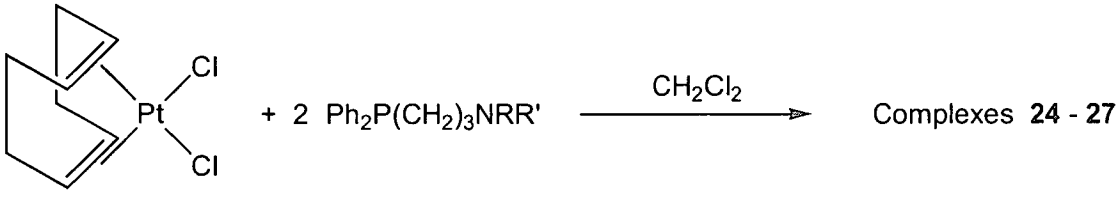

Scheme 3.4 Preparation of *bis*-aminophosphine Pt(II) complexes

Complexes **24-27** were initially characterised by elemental analysis, which established a stoichiometry of two ligands per platinum. Further analysis, by ^{31}P NMR, allowed the detection of chelate ring formation. All the ^{31}P resonances shifted downfield upon coordination to Pt from –15 ppm for the free ligands to –2.5 to 8.9 ppm for the bound ligands. The value of the $^{1}J(P\text{-}Pt)$ coupling constants allowed assignment of the atom in the *trans* position as N or Cl (see Section 2.1.1.1). This indicated whether the ligands were chelated or not as detailed below.

$[Pt\{Me_2N(CH_2)_3PPh_2\text{-}P\}_2Cl_2]$ (**24**) – The ^{31}P NMR spectrum showed only a singlet resonance and ^{195}Pt satellites with a $^{1}J(P\text{-}Pt)$ of 3643 Hz. The single peak indicated that the two ligands are equivalent. This could be achieved by having both ligands chelated (bound through P and N) or ring-opened (bound only through P). The large coupling constant suggests that the *trans* ligand is most likely to be Cl^- due to its

lower *trans influence* compared to N (Section 2.2.1.1). This suggests that both ligands are ring-opened.

$[Pt\{H_2N(CH_2)_3PPh_2\text{-}P,N\}_2]Cl_2$ (**25**)– As for complex **24**, both ligands are equivalent and only a single resonance was observed. The coupling constant in this case is 3285 Hz suggesting N in the trans position (higher *trans influence* than Cl). The structure of **25** is therefore fully chelated.

$[Pt\{Me(H)N(CH_2)_3PPh_2\}_2Cl]Cl$ (**26**)– The spectrum of this complex contained two resonances, both doublets with ^{195}Pt satellites, indicating two inequivalent P ligands. Resonance **A** at 3.82 ppm had a ^1J(P-Pt) of 3768 Hz (^{31}P *trans* to Cl) and resonance **B** had a ^1J(P-Pt) of 3166 Hz (^{31}P *trans* to N). This suggested a species with one chelated ligand (**A**) and one ring-opened ligand (**B**). The splitting of each peak to form a doublet is due to the ^2J(P-P) coupling of the two P, confirming the *cis* geometry of the complex. (see Section 2.2.1.1)

$[Pt\{^tBu\ (H)N(CH_2)_3PPh_2\text{-}P\}_2Cl_2]$ (**27**) – As for complex **24**, a single resonance was observed with a ^1J(P-Pt) of 3665 Hz (^{31}P *trans* to Cl) indicating a fully ring-opened species.

The structures of *bis*-aminophosphine complexes **24** – **27** are shown in Figure 3.2.

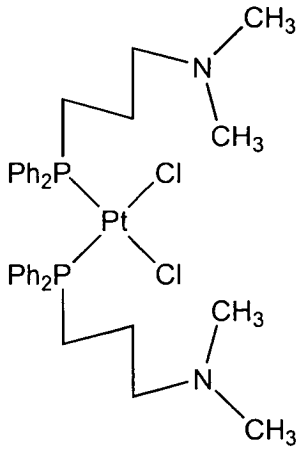

Complex **24**

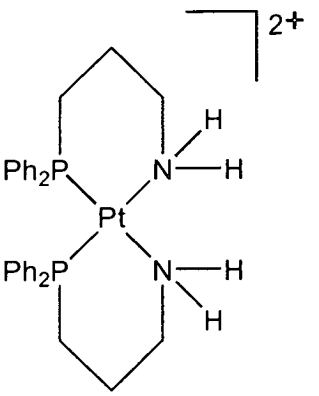

Complex **25**

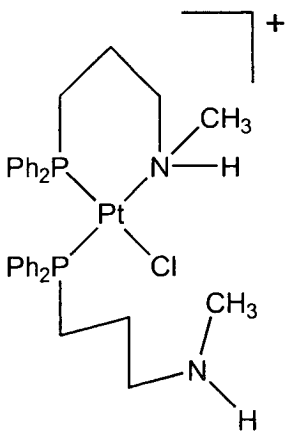

Complex **26**

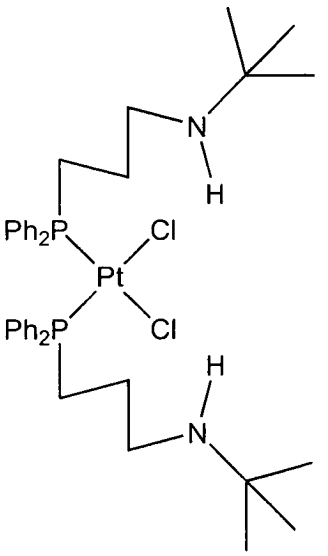

Complex **27**

Figure 3.2 Structures of platinum aminophosphine complexes **24** - **27**

Based on the ^{31}P NMR assignments the structures of the complexes formed by aminophosphine ligands with platinum(II) vary from fully ring-opened (for DMDPPA and BDPPA ligands) to fully ring-closed (for DPPA) with an intermediate open/closed complex (for MDPPA). This variation reflects the increasing steric bulk of the R groups on the amine of the ligand, which hinders the coordination of the N. (Figure 3.3)

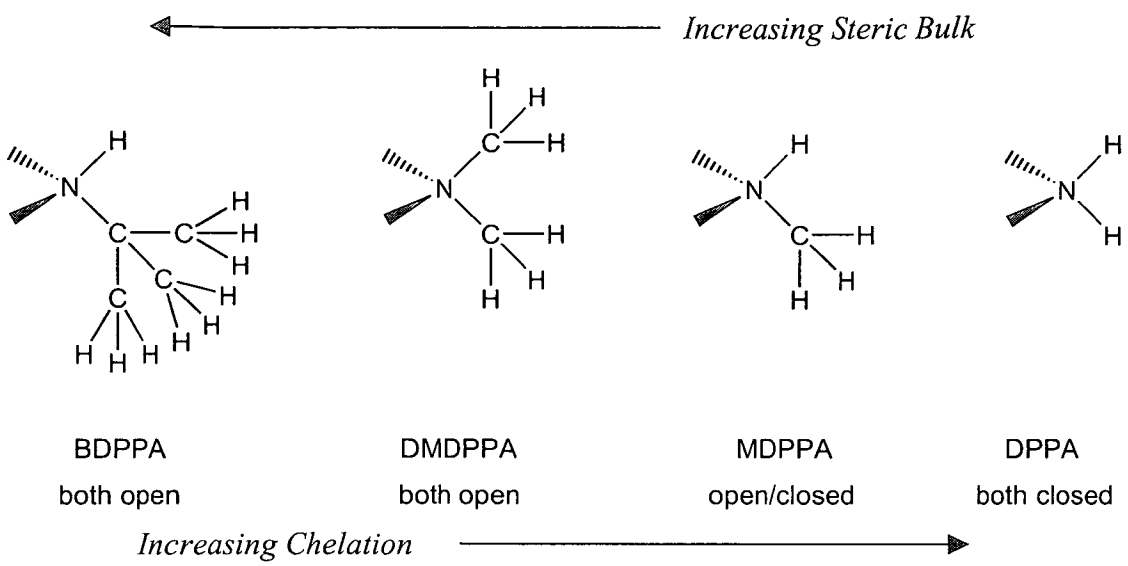

Figure 3.3 Relationship between steric bulk on amine and chelate formation

Most of the complexes showed good solubility in organic solvents such as dichloromethane, but were also water soluble to varying extents. Complexes **25** and **26** were the most soluble at concentrations in excess of 20 mM, while complex **24** could only be dissolved up to 5 mM. Complex **27** was not soluble in water, probably due to the presence of the bulky, non-polar *tert*-butyl groups. Water solubility could be achieved for this complex by lowering the pH of the solution to allow protonation of the amine groups in the ligands. Solutions of 20 mM were easily be obtained by adjusting to pH~4.

3.2.2.2 *Mono*-aminophosphine Complexes

As described in the previous section, reaction of the aminophosphine ligands with $[Pt(COD)Cl_2]$ always afforded the *bis*-aminophosphine complexes. When $[Pt(COD)Cl_2]$ was reacted with only one mole equivalent of ligand, the *bis* product was still formed, and some Pt starting material remained. The preparation of a *mono*-aminophosphine complex was therefore undertaken by a different route

(Scheme 3.5). [Pt(COD)MeCl] was prepared according to a published procedure[2] and characterised according to previous ^{1}H NMR data.[8] The methyl group was clearly distinguished as a sharp singlet with a shift of 0.89 ppm. This peak had satellites due to ^{195}Pt coupling with $^{2}J(Pt\text{-}H)$ = 71.2 Hz. Two distinct resonances were also observed for the olefinic hydrogens. The peak at higher field (4.50 ppm) had an associated $^{2}J(Pt\text{-}H)$ value of 76.5 Hz and was assigned to the olefinic group *trans* to chloride. The second peak (5.59 ppm) had a $^{2}J(Pt\text{-}H)$ value of 35.4 Hz and was assigned to the olefinic group *trans* to methyl. This was determined by the higher *trans* influence of Me leading to a smaller coupling constant.

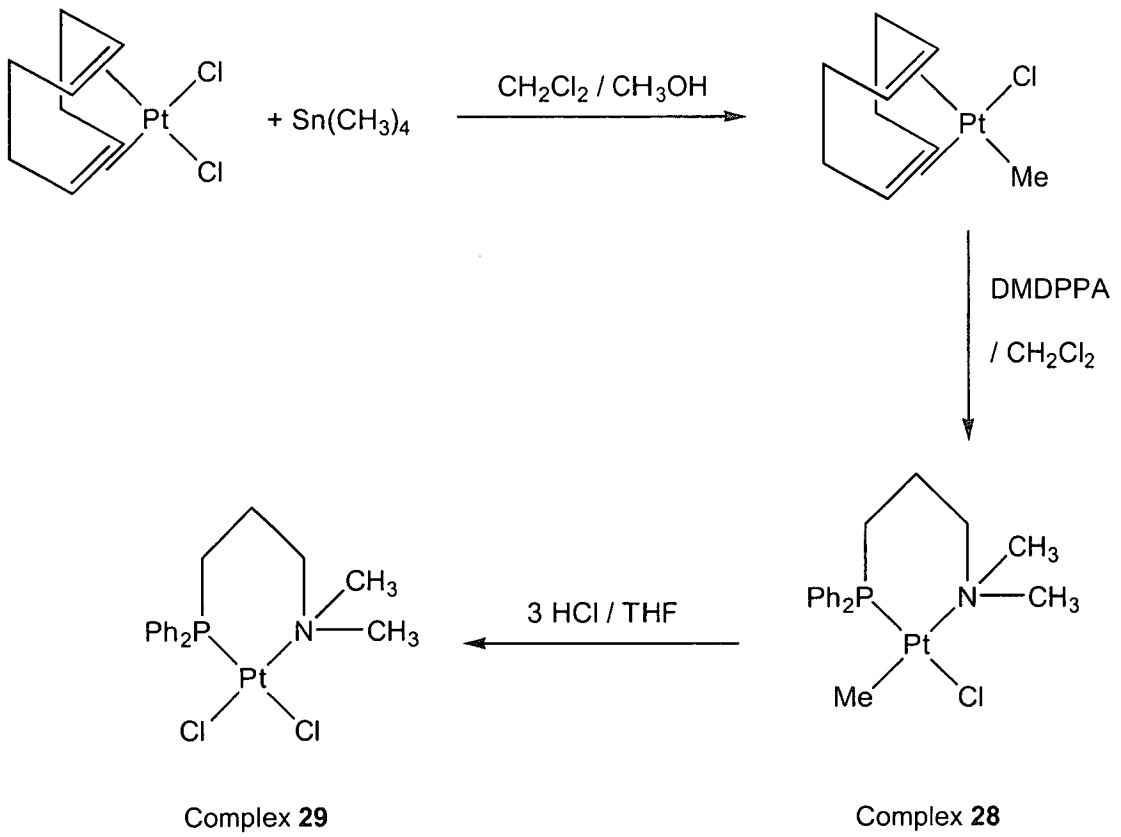

Complex **29** Complex **28**

Scheme 3.5 Synthesis of [Pt{$Ph_2P(CH_2)_3NMe_2$-*P,N*}Cl_2]

The DMDPPA ligand was then reacted with the [Pt(COD)MeCl] in a dichloromethane solution. Microanalysis confirmed that the mono complex had been formed. The ^{1}H NMR spectrum showed a high frequency shift of the $N(CH_3)_2$ resonance from 2.16 ppm for free DMDPPA to 2.79 ppm, indicating that the ligand is N-bound. This was confirmed by the presence of ^{3}J(Pt-H) coupling for the $N(CH_3)_2$ peak (12.1 Hz). The Pt-CH_3 resonance was at 0.36 ppm and had an associated ^{2}J(Pt-H) coupling of 70.1 Hz, similar to the parent complex. This resonance was further split by ^{3}J(P-H) coupling (4.2 Hz) suggesting that the P from the ligand was *cis* to the methyl group on the Pt. The resulting complex **28**, is shown in Scheme 3.5.

To allow direct comparison between the *mono*-aminophosphine and the *bis*-compound (complex **24**) the methyl ligand was replaced by chloride. This procedure was based on a published method for a similar series of Pt(II)-aminophosphine complexes (*cis*-$[PtMe_2L_2]$ where L = $H_2NC_6H_4PPhR$, R = H, Me, Ph).[9] Complex **28** was reacted with a 3-fold excess of HCl in THF solution to yield a yellow solid product. This product, complex **29** (Scheme 3.5), was confirmed by microanalysis to have formed as the hydrochloride salt due to the high excess of HCl in the reaction. The methyl resonance from the ^{1}H NMR had disappeared confirming that the reaction was complete.

Both the *mono*-aminophosphine complexes **28** and **29** showed very poor solubility in water so proved to be unsuitable for biological studies such as nucleotide and DNA binding.

3.2.2.3 X-ray Structure Determination

The X-ray crystal structures determined for complexes **24**, **25** and **27** confirmed the structures proposed on the basis of ^{31}P NMR data (Figure 3.2). Complex **26** turned out to be a mono-aminophosphine complex with a chelated ligand and two chloride ligands *trans* to P and N (Figure 3.4).

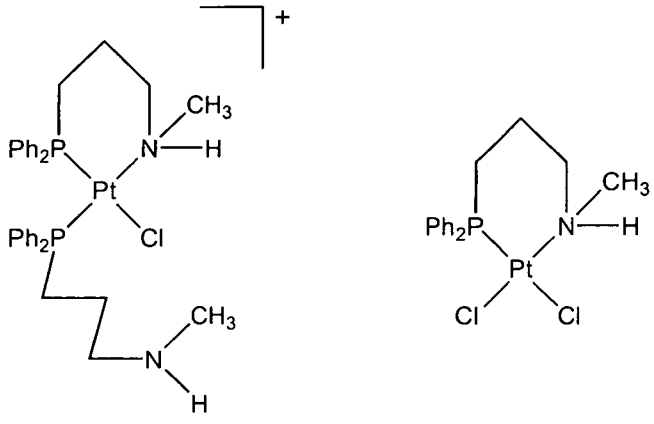

Complex **26A** Complex **26B**

Figure 3.4 *Bis-* and *mono-*Pt(II) complexes formed by MDPPA ligand

It likely that the *mono*-complex **26B** was present as a minor species in the NMR solution and that this species crystallised in preference to the *bis*-complex **26A** despite this species being in a high excess as observed from the ^{31}P NMR spectrum. This seems probable since further preparations of complex **26** have always produced a mixture of complexes **26A** and **26B** and the *bis*-complex has proved difficult to isolate (see Section 3.2.2.1).

All data collection and refinement details for the *bis*-aminophosphine complexes are given in Table 3.1, and for the *mono*-aminophosphine complexes in Table 3.2 The X-ray structures were solved by Dr Simon Parsons, Dr Robert Coxall and Mr Andrew Parkin of the University of Edinburgh.

Full atomic coordinates for all the structure determined are given in the Appendix to this thesis.

Complex	**24**	**25**	**27**
Empirical Formula	$C_{35}H_{46}Cl_4P_2N_2Pt$	$C_{34}H_{44}Cl_2N_4O_5P_2Pt$	$C_{38}H_{52}Cl_2N_2P_2Pt$
M	893.61	892.64	864.75
Temperature/K	220	150(2)	150(2)
Space Group	P 1 21/c 1	P-1	C2 / c
Crystal System	Monoclinic	Triclinic	Monoclinic
Wavelength λ/Å	0.71073	0.71073	0.71073
a/Å	10.141(1)	9.4849(8)	29.896(4)
b/Å	18.817(2)	11.3914(9)	13.5697(17)
c/Å	20.230(2)	17.8243(15)	20.927(3)
α/°	90	95.7700(10)	90
β/°	101.25(1)	96.9850(10)	118.091(2)
γ/°	90	109.0030(10)	90
Volume/Å^3	3786.31	1787.1(3)	7489.6(17)
Reflections for cell	54	7806	6864
Z	4.00	2	8
Density/g cm^{-3}	1.57	1.659	1.534
Absorption coefficient μ/mm^{-1}	4.14	4.209	4.004
F(000)	1777.39	892	3488
Crystal Description	Colourless tablet	Colourless lath	Colourless block
Crystal Size/mm	0.16 x 0.16 x 0.04	0.38 x 0.10 x 0.05	0.19 x 0.17 x 0.06
θ range/°	2.50-25.00	1.91-26.38	1.54-26.40
Index Ranges (h,k,l)	-12-11, 0-22, 0-24	-11-11, -14-14, -22-22	-37-37, -16-16, -26-20
Reflections collected	11044	12153	21038
Independent reflections	6096	7160	7648
Scan Type	ω-θ	ψ-ω	ψ-ω
Data/restraints/parameters	4543/0/398	7160/0/423	7648/125/449
Goodness of fit on F^2	1.0742	0.940	0.939
Conventional/weighted R	0.0530/0.0547	0.0296/0.0669	0.0348/0.0809
Maximum Δ/σ	0.078326	0.001	0.002

Table 3.1 Details of X-ray data collection and refinements for *bis*-aminophosphine complexes

Complex	**26B**	**28**
Empirical Formula	$C_{19}H_{23}Cl_{11}NPPt$	$C_{18}H_{25}ClNPPt$
M	881.39	516.90
Temperature/K	220(2)	150(2)
Space Group	P-1	P21/n
Crystal System	Triclinic	Monoclinic
Wavelength λ/Å	0.71073	0.71073
a/Å	11.089(4)	9.027(2)
b/Å	11.223(4)	18.889(4)
c/Å	15.198(5)	10.928(2)
α/°	91.440(17)	90
β/°	109.712(16)	94.772(18)
γ/°	117.034(14)	90
Volume/Å^3	1549.7(9)	1857.0(7)
Reflections for cell	53	78
Z	2	4
Density/g cm^{-3}	1.889	1849
Absorption coefficient μ/mm^{-1}	5.539	7.783
F(000)	848	1000
Crystal Description	Colourless block	Colourless block
Crystal Size/mm	0.31 x 0.31 x 0.31	0.23 x 0.21 x 0.18
θ range/°	2.79-30.03	2.51-25.00
Index Ranges (h,k,l)	-15-14, -15-15, 0-21	-10-10, 0-22, 0-12
Reflections collected	9034	3680
Independent reflections	9031	3260
Scan Type	ω-θ	ω-θ
Data/restraints/parameters	9031/12/302	3260/0/203
Goodness of fit on F^2	1.013	1.008
Conventional/weighted R	0.0527/0.1171	0.0270/0.0570
Maximum Δ/σ	0.002	0.002

Table 3.2 Details of X-ray data collection and refinements for *mono*-aminophosphine complexes

Selected bond angles and lengths from the X-ray structures are listed in Table 3.3 and are discussed further in the following sections.

	24	**25**	**27**	**26B**	**28**
Pt-P(1)	2.247(2)	2.2565(11)	2.2570(11)	2.2064(17)	2.1849(14)
Pt-P(2)	2.251(2)	2.2543(11)	2.2534(12)		
Pt-Cl(1)	2.354(3)		2.3510(11)	2.3747(17)	2.3815(14)
Pt-Cl(2)	2.361(2)		2.3588(12)	2.2978(17)	
Pt-N(1)		2.116(3)		2.060(5)	2.220(4)
Pt-N(2)		2.129(3)			
Pt-C(1)					2.055(5)
P1-Pt-Cl1	169.84(9)		173.71(4)	178.95(6)	170.28(5)
P2-Pt-Cl2	173.61(9)		170.99(4)		
P1-Pt-N2		171.67(10)			
P2-Pt-N1		171.43(10)			
N1-Pt-Cl2				174.18(17)	
N1-Pt-C1					176.02(18)
P1-Pt-P2	99.76(9)	98.16(4)	102.03(4)		
P2-Pt-Cl1	89.12(9)		84.06(4)		
Cl1-Pt-Cl2	87.78(9)		87.07(4)	89.82(6)	
Cl2-Pt-P1	83.84(9)		86.79(4)	91.14(7)	
P1-Pt-N1		89.60(10)		93.75(16)	95.58(12)
P2-Pt-N2		86.69(10)			
N1-Pt-N2		86.04(13)			
N1-Pt-Cl1				85.32(16)	89.63(12)
P1-Pt-C1					88.36(16)
C1-Pt-Cl1					86.40(16)

Table 3.3 Selected bond lengths/Å and angles/° for complexes **24**, **25**, **26B**, **27**, and **28** with estimated standard deviations in parentheses

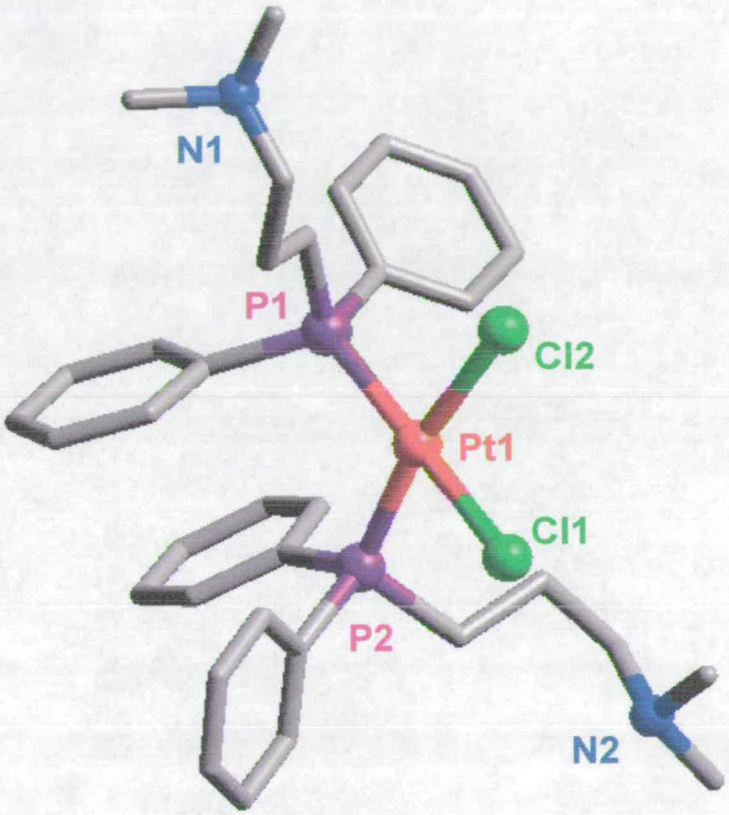

Figure 3.5 X-ray crystal structure of [Pt{$Me_2N(CH_2)_3PPh_2$-***P***}$_2Cl_2$ (**24**) plotted using Cerius2[10], H atoms omitted

[Pt{$Me_2N(CH_2)_3PPh_2$-*P*}$_2Cl_2$].CH_2Cl_2 (**24**)

The structure of complex **24** is shown in Figure 3.5. It is square-planar with a small degree of distortion. The structure was also shown to contain a molecule of dichloromethane from the recrystallisation solvent. The P1-Pt-P2 angle, 99.76°, is rather larger than expected for a square-planar complex. This is caused by the steric crowding around the phosphorus atoms due to the presence of the phenyl rings. The opening up of this angle has resulted in the reduction of the other three angles in the

square plane to less than 90°. The *trans* angles, P1-Pt-Cl1 and P2-Pt-Cl2, of 169.84° and 173.61°, respectively, also show deviations from the ideal value of 180°. The distortion around the platinum can be considered by looking at the displacement of the two chloride ions from a plane defined by the Pt and two P atoms. This would be zero for an ideal square-planar arrangement, a larger displacement indicating more distortion in the complex. The least-squares plane through Pt1, P1 and P2 was calculated using SHELXTL[11] and the deviations of Cl1 and Cl2 were shown to be 0.2029 Å and –0.2170 Å respectively. Both the Pt-P bond lengths of ~2.25 Å are consistent with average lengths reported from a compilation of data from the Cambridge Structural Database.[12] The Pt-Cl bond lengths of 2.354(3) and 2.361(2) Å are longer than average (2.32 Å[12]) due to the high *trans* influence of the P ligands. The orientation of the DMDPPA ligands appears to be fixed by the presence of intramolecular π-π interactions between the phenyl rings of each of the ligands in the structure (Figure 3.6).

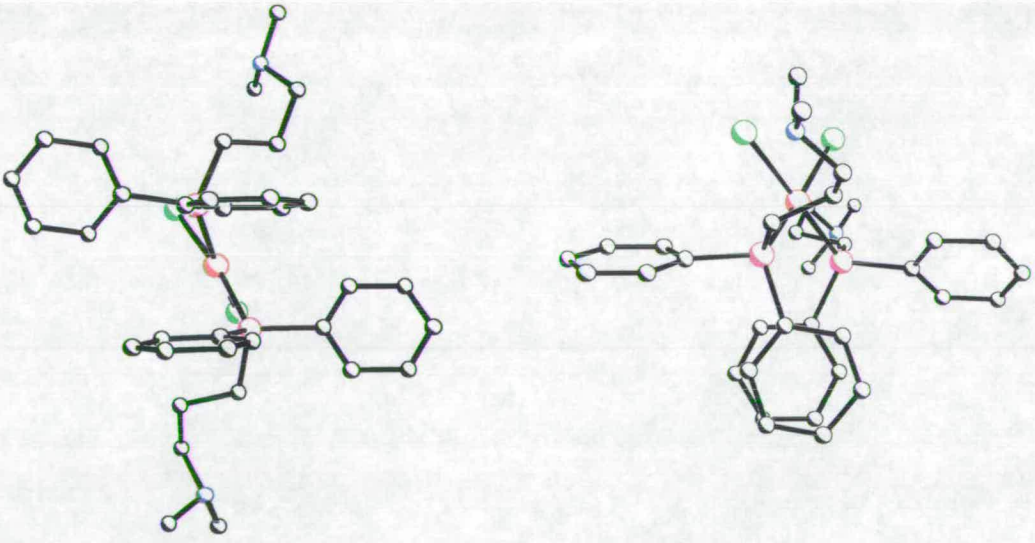

Figure 3.6 View of complex **24** showing π-stacking between ligands (plotted using SHELXTL[11])

As can be seen from Figure 3.6 the two aromatic rings are not directly aligned in a face-to-face geometry but are offset from one another. This parallel displacement can be described by the positioning of a vector from the central point of one ring to the central point of the other. (Figure 3.7)

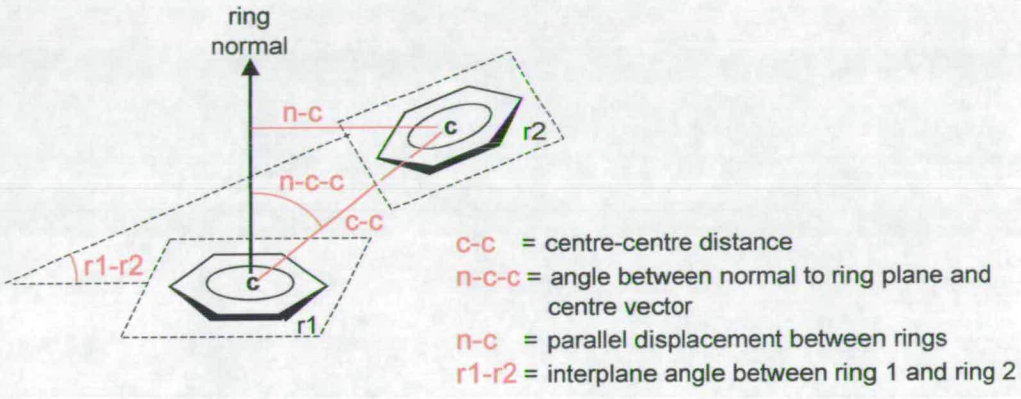

Figure 3.7 Definitions of angles and distances relating two π-stacked phenyl rings

The centre-centre distance (c-c) is 3.57 Å which is typical for π-interactions.[13] The two rings are offset by an angle of 22.5° from the normal to the lower plane (n-c-c) which gives a parallel displacement (n-c) of 1.37 Å between the two rings. The upper ring is not completely co-planar with the lower ring but is tilted at a slight angle (r1-r2) of 7.3°

The two planes are sufficiently separated that there is a favourable van der Waals interaction between the atoms in the two rings. However the geometry of the overlap is predominantly due to electrostatic interactions. This interaction has been described by Hunter and Sanders[14] based on a simple model of charge distribution in a π-system which is summarised in Figure 3.8. The phenyl ring is considered to be made up of a positively charged σ framework sandwiched between two negatively charged π electron clouds. The dominant interaction between two stacked phenyl rings will be the repulsion of the closest approaching π-clouds (Figure 3.8(a)). If the two rings are then offset from one another favourable interactions can occur by attraction between the σ-framework of one ring and the π-electron cloud from the

other. (Figure 3.8 (b)). This attraction is further optimised in the case of the phenyl rings by the polarisation of the C-H bond giving a δ+ charge over the electron cloud. The repulsion between the π-clouds is also reduced due to the electron withdrawing nature of the P atom attached to the ring reducing the electron density in the π-cloud.

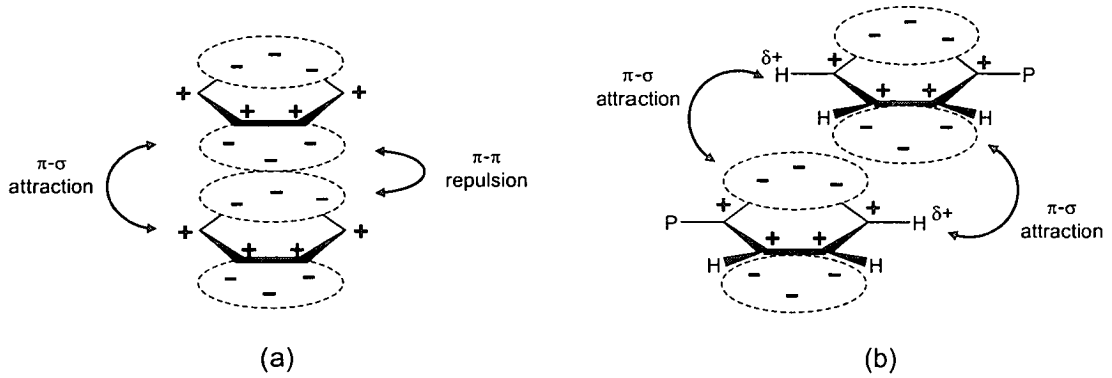

Figure 3.8 Schematic illustration of the attractive electrostatic interaction between the σ framework and the π electron density in an offset π-stacked geometry (adapted from reference 13)

The offset of 1.37 Å and interplane angle of 7.3° are within the limiting geometries required for attractive interactions between the rings, as determined in reference 14 from studies on porphyrin π-π interactions in solution and solid state.

$[Pt\{H_2N(CH_2)_3PPh_2\text{-}P,N\}_2]Cl_2.2CH_3NO_2.H_2O$ (**25**)

The structure of complex **25** is shown in Figure 3.9 and confirms the presence of two six-membered chelate rings in the complex. The resulting species is a dianion and hence two chloride counter ions are present. The structure also contains two molecules of nitromethane and a molecule of water. Despite the chelation of the aminophosphine ligands, the structure shows many features similar to complex **24**. The P1-Pt-P2 angle is opened up to 98.16° and the other *cis* angles reduced below 90° accordingly. The *trans* angles are distorted from square-planar at 171.67(10)°

and 171.43(10)° for P1-Pt-N2 and P2-Pt-N1, respectively. A least-squares plane was calculated through Pt1, P1 and P2 and the two N atoms are displaced from this plane by –0.2519 Å and 0.1347 Å. This shows the complex to be distorted from square-planar to a similar extent to complex **24**.

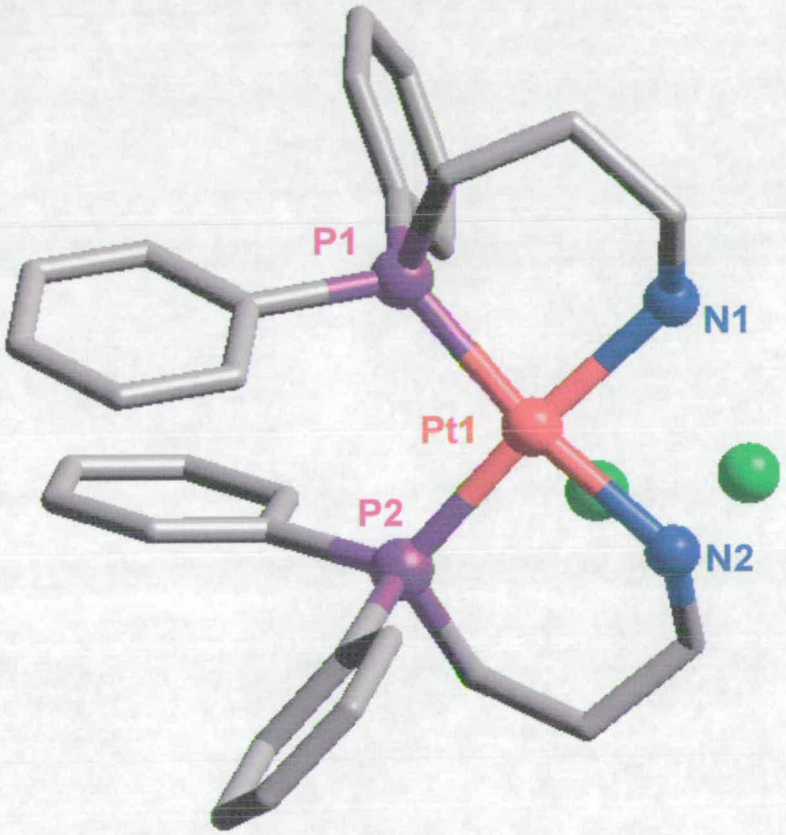

Figure 3.9 X-ray crystal structure of $[Pt\{H_2N(CH_2)_3PPh_2\text{-}P,N\}_2]Cl_2$ **(25)** plotted using Cerius2[10], H atoms omitted

The six-membered rings show some steric strain as indicated by the bond angles in the alkyl chain which show deviations from ideality. In ring 1, these angles are 115.6(3)°, 113.3(4)° and 112.19°, and in ring 2 they are 113.6(3), 113.5(4)° and

112.7(3). Both rings are in chair conformations as shown in Figure 3.10, one orientated above the Pt plane and one below. The Pt-P bond lengths are again close to the mean reported values, as for complex **24** despite the change of ligand in the *trans* position from Cl to N. The N bond lengths are longer than the reported mean value for primary amines coordinated to platinum (2.04 Å[12]), at 2.116(3) and 2.129(3) Å. This is again due to the high *trans* influence of the P ligands. The structure showed no π-stacking. This is because the Pt-P bond is constrained in a chelate ring and not free to rotate, aligning the phenyl rings.

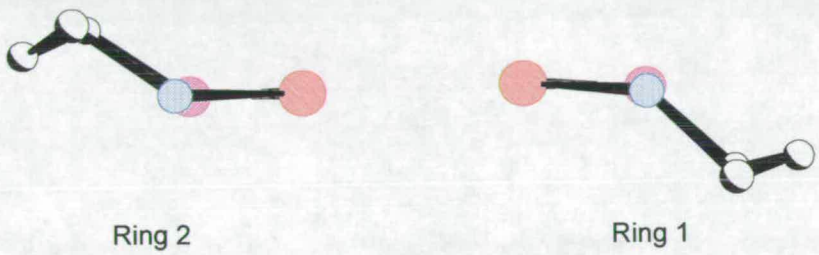

Figure 3.10 Ring conformations of chelate rings in complex **25**
(red = Pt, pink = P, blue = N, white = C)

[Pt{^{t}Bu (H)N(CH$_2$)$_3$PPh$_2$-*P*}$_2$Cl$_2$] (**27**)

The structure of complex **27** is shown in Figure 3.11 and shows the same ring-opened structure as complex **24**. Again distortion from the ideal square-planar geometry can be observed with an increased P1-Pt1-P2 bond angle of 102.03(4)°. The *trans* angles P1-Pt-Cl1 and P2-Pt-Cl2 are 173.71 (4)° and 170.99(4)°, respectively. Calculation of a least-squares plane through Pt1, P1, P2 shows the displacement of Cl1 to be 0.0756 Å and Cl2 to be 0.0650 Å from the plane. This shows the distortion to be much less than for the analogous complex **24**. The Pt-P bond lengths are as expected at 2.2570(11) Å and 2.2534(12) Å and the Pt-Cl bond lengths are again longer than mean values due to the P *trans* influence. In contrast to

24, no π-stacking between the two ligands is observed and this could be the reason for the reduced distortion around the platinum. Ligand 2 lies almost in the platinum square-plane, while ligand 1 lies almost perpendicular above the plane. This is also different from structure **24** in which the molecule is close to C2 symmetric with both the ligands adopting the same orientation.

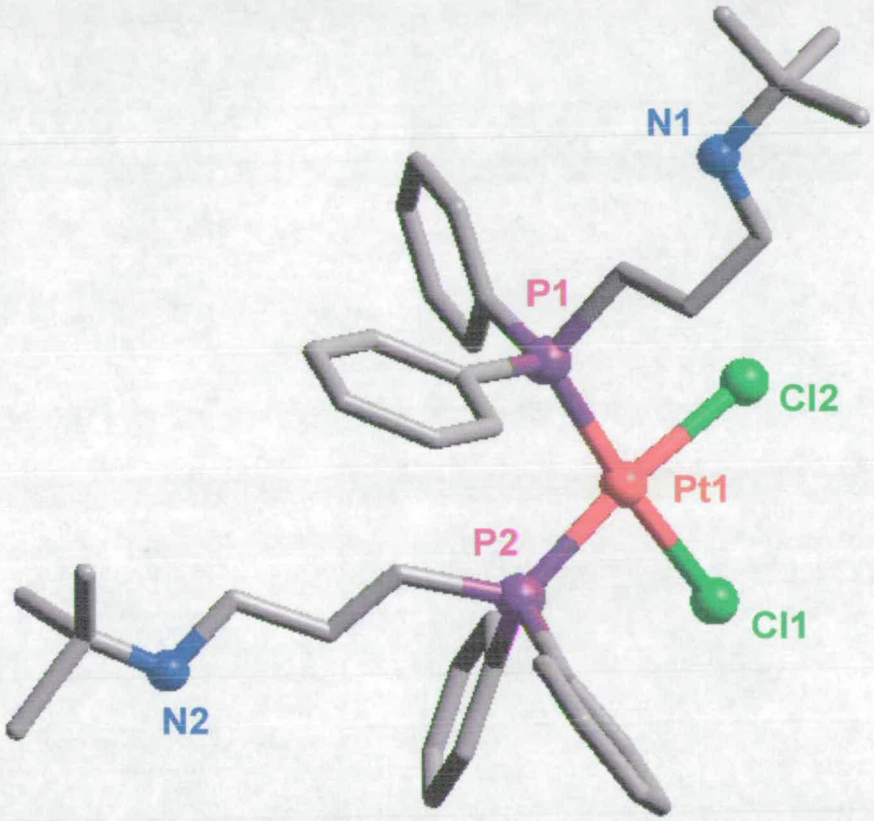

Figure 3.11 X-ray crystal structure of [Pt{^{t}Bu (H)N$(CH_2)_3PPh_2$-***P***$\}_2Cl_2$] (**27**) plotted using Cerius2[10], H atoms omitted

$[Pt\{Ph_2P(CH_2)_3NMe(H)\text{-}P,N\}Cl_2].3CHCl_3$ (**26B**)

The structure determined for complex **26B** showed a *mono*-aminophosphine complex with one MDPPA ligand chelated, forming a six-membered ring, and two *cis* chloride ligands (Figure 3.12). The structure contained three molecules of $CDCl_3$ from the NMR solvent in which the crystal was formed. The geometry is still distorted from square-planar since the P1-Pt-N1 angle is increased to 93.75(16)° to minimise strain in the ring. The *trans* angles are 178.95(6)° for P1-Pt-Cl1 and 174.18(17)° for N1-Pt-Cl2. These values are closer to the ideal values than for the *bis*-structures. The Cl1 and Cl2 ligands are displaced from the P1-Pt-N1 least-squares plane by 0.0199 Å and 0.1272 Å, respectively. This distortion is less than observed for the *bis*-chelated complex **25**. The six-membered chelate ring is again strained as shown by the angles in the alkyl chain: 113.8(5)°, 114.6(6)° and 114.4(6)°. Again the chelate ring adopts a chair conformation as shown in Figure 3.13. The Pt-P bond length is significantly shorter than the mean reported value[12] and the values determined for the previous *bis*-aminophosphine complexes, at 2.2064(17) Å. This is unexpected because it cannot be attributed to the inclusion of the P in a six-membered ring, since this does not affect the bond length in complex **25**. Also it cannot be attributed to the Cl ligand in the *trans* position which did not affect the bond length in complexes **24** and **27**. The Pt-N bond length is the same as the mean reported value for a secondary amine (2.06 Å[12]) at 2.060(5) Å. This is shorter than in complex **25** since the *trans* ligand is Cl which has a much smaller *trans* influence than P.

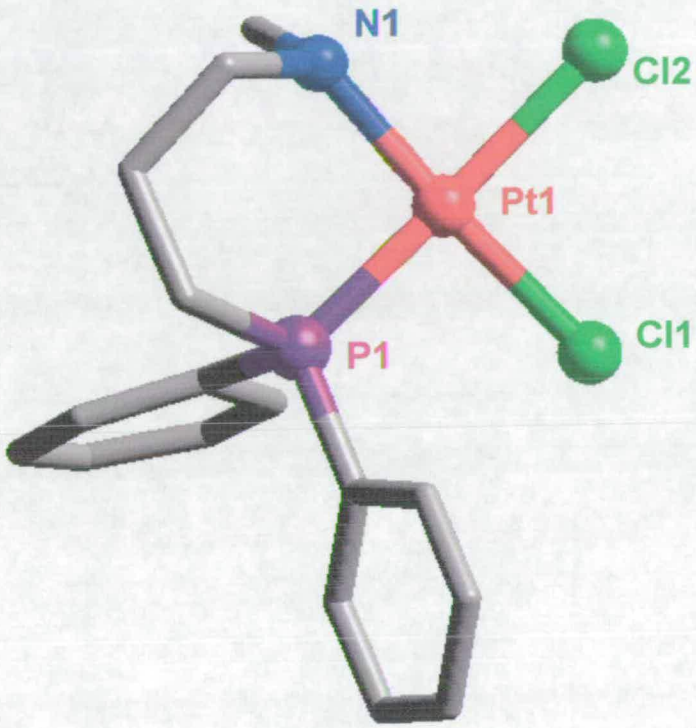

Figure 3.12 X-ray crystal structure of [Pt{$Ph^2P(CH_2)_3NMe(H)$-*P,N*}Cl_2] **(26B)** plotted using Cerius2[10], H atoms omitted

Complex **26B** Complex **28**

Figure 3.13 Ring conformations of chelate rings in *mono*-aminophosphine complexes (red = Pt, pink = P, blue = N, white = C)

[Pt{$Ph_2P(CH_2)_3NMe_2$-*P,N*}MeCl] (**28**)

Complex **28** (Figure 3.14) has a structure analogous to complex **26B**. The DMDPPA ligand is chelate ring-closed with a methyl ligand present *cis* to the P and a Cl ligand *cis* to the N. The P1-Pt-N1 bond angle is increased to 95.58(12)° as for complex **26B** and the *trans* angles are 170.28(5)° for P1-Pt-Cl1 and 176.02(18)° for N1-Pt-C1. The least-squares plane for Pt1, P1 and N1 was calculated and the Cl1 and C1 atoms are displaced from this by –0.3405 Å and –0.0189 Å, respectively. This structure is therefore more distorted from an ideal square-plane than complex **26B**. The angles for the alkyl chain in the six-membered ring are 113.6(4)°, 113.4(5)° and 117.7(4)°, the ring is again a strained chair conformation (Figure 3.13). The unexpectedly short Pt-P bond is again a feature and the long Pt-N bond length of 2.20(4) Å indicates the high *trans*-influence of the methyl ligand. This is greater even than that seen for P in the *trans* position in complex **25**. The reported mean length for a tertiary amine to platinum is only 2.108 Å[12]. The Pt-C(methyl) bond length, 2.055(5) Å is shorter than average (2.107 Å[12]).

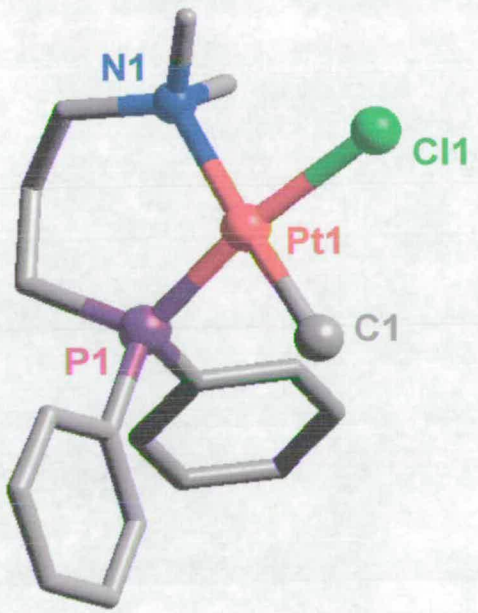

Figure 3.14 X-ray crystal structure of [Pt{$Ph_2P(CH_2)_3NMe_2$-*P,N*}MeCl] (**28**) plotted using Cerius2[10], H atoms omitted

3.3 Chelation of Aminophosphine Ligands

3.3.1 pH Titrations

In order to determine the effect of pH on the chelation of the ligands in complexes **24-27**, pH titrations were undertaken. Only the results for complexes **25** and **26A** are reported here since the titrations were not successful for complexes **24** and **27**. Complex **24** underwent unusual hydrolysis reactions in aqueous solution and these are detailed further in the next section, while complex **27** was soluble only in water under conditions of low pH. It can be assumed that under these conditions the free amine arms of the ligand are protonated resulting in a charged species with increased water solubility compared to the parent complex. When the pH was increased above 4, the complex precipitated out of solution making NMR detection impossible.

For the pH titrations, a 20 mM solution of each complex in D_2O was prepared and the pH adjusted with 0.1 M DNO_3 and 0.1 M NaOD. Details of pH measurement and NMR parameters are given in Section 2.2. ^{31}P spectra were recorded at several different pH values and the results are discussed in the following sections.

$[Pt\{H_2N(CH_2)_3PPh_2$-*P,N*$\}_2]Cl_2$ (25)

The ^{31}P spectra at various pH values are shown in Figure 3.15. At high pH only one single peak (A) can be seen at ca. -1.89 ppm. This corresponds to the fully ring-closed species, as observed in the $CDCl_3$ spectrum. The ^1J(Pt-P) coupling constant of 3199 Hz confirmed the presence of N in the *trans* position. As the pH was lowered two doublets emerged at 4.25 (C) and 0.56 (B) ppm. These correspond to the species formed by the opening of one of the chelate rings. The two P are thus inequivalent and have ^2J coupling giving two doublets. The ^1J(Pt-P) coupling constants are 3272 Hz and 3625 Hz, confirming N and Cl, respectively, in the *trans* positions. The relative amount of each species was determined from the peak integrals and plotted against pH (Figure 3.16). The pK value for the ring-closing reaction was determined to be 2.93 ± 0.05 using Kaleidagraph[15]. This means that the pH must be lowered to less than 3 before half of the complex present is ring-

opened. This is in contrast to the analogous $[Pt(H_2N(CH_2)_2PPh_2)_2]Cl_2$ which contains two five-membered and shows no ring-opening even below pH 2.[16] This reflects the lower stability of the six-membered chelate ring in contrast to the five-membered ring.

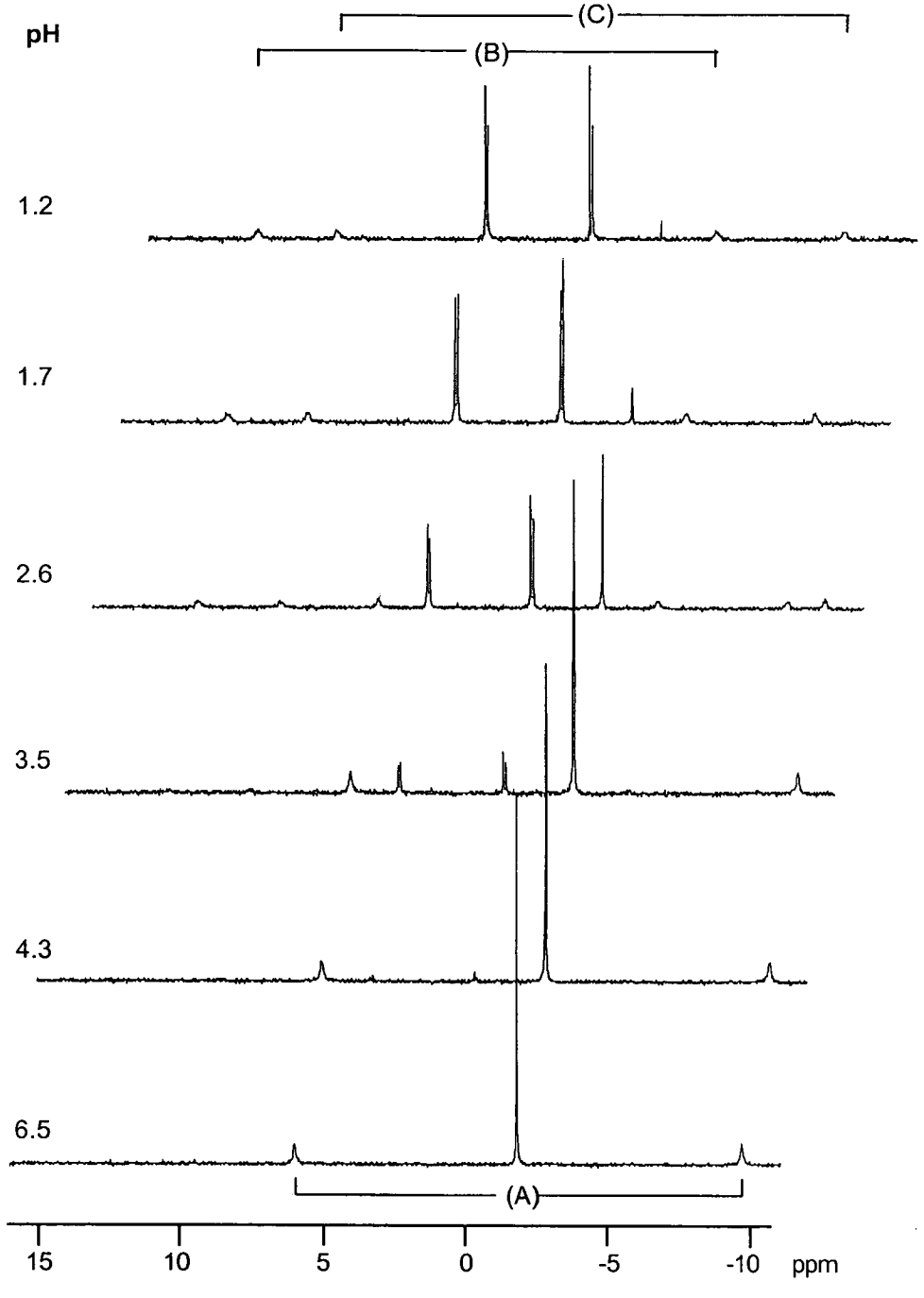

Figure 3.15 ^{31}P NMR spectra showing pH titration of complex **25**
(A = fully ring-closed species, B/C = ring-closed/open species)

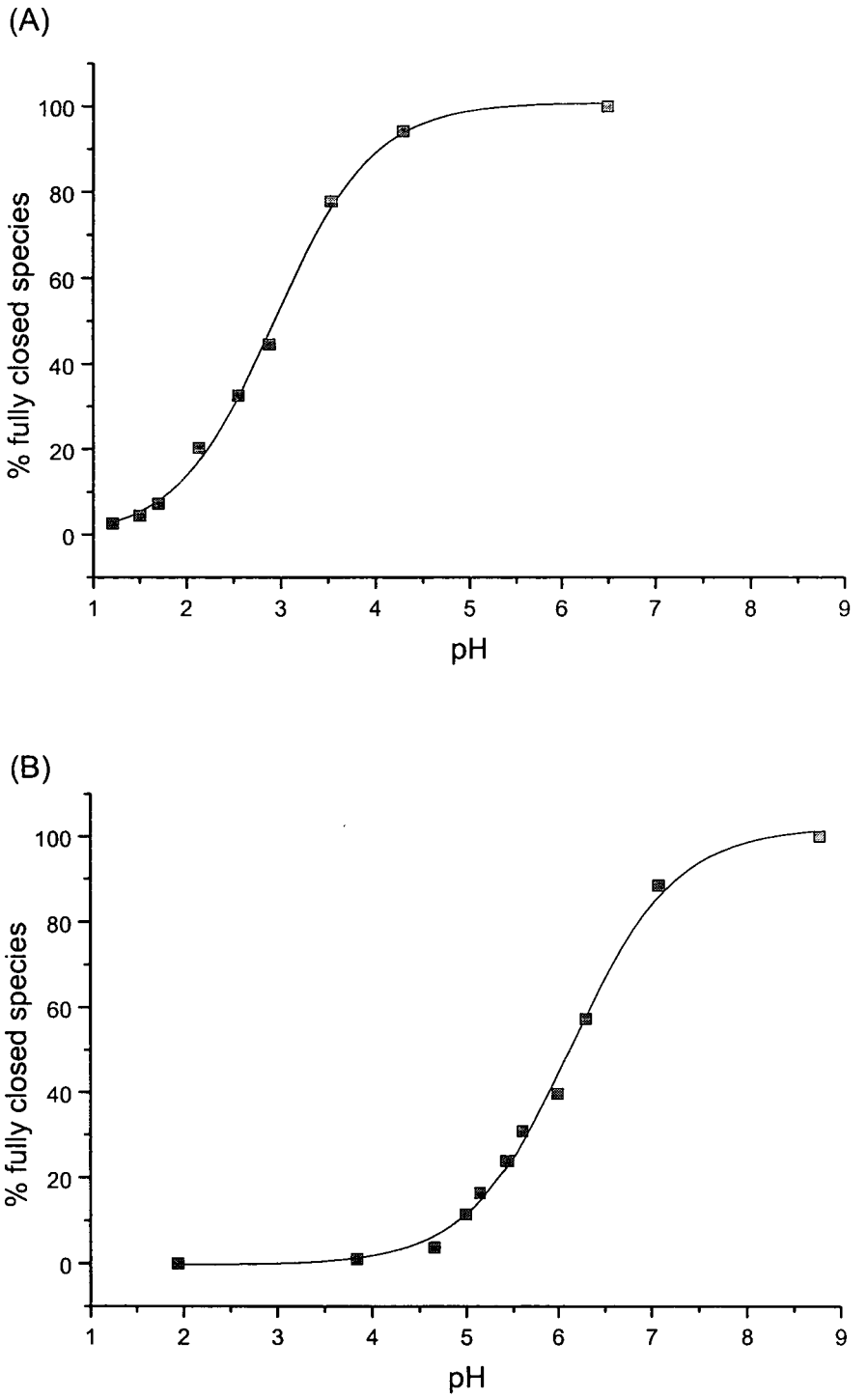

Figure 3.16 Graphs showing formation of fully ring-closed species with increasing pH for compex **25** (A) and complex **26A** (B)

$[Pt\{Me(H)N(CH_2)_3PPh_2\}_2Cl]Cl$ (**26A**)

The ^{31}P NMR spectra of this complex at various pH values are shown in Figure 3.17. The pH titration for this complex showed a similar profile to that for complex **25**. At high pH the fully ring-closed species was observed with a single peak (A) (^1J(Pt-P) = 3178 Hz, *trans* to N) and at lower pH the ring-opened species formed with two doublets (^1J(Pt-P) = 3166 Hz, *trans* to N (B) and 3728 Hz, *trans* to Cl (C)). The peak integrals were again used to determine the amount of each species and these were plotted against pH (Figure 3.16). The pK for the closing of this species was determined to be 6.14 ± 0.06. This value is much higher than for complex **25** indicating that the chelate ring can be opened much more easily. Almost half the complex present will be ring-opened when the pH is lowered to 6. This increase in pK reflects the increase in steric bulk on the amine which destabilises the chelate ring formation.

A scheme depicting the pH dependent ring-opening reaction is shown in Scheme 3.6.

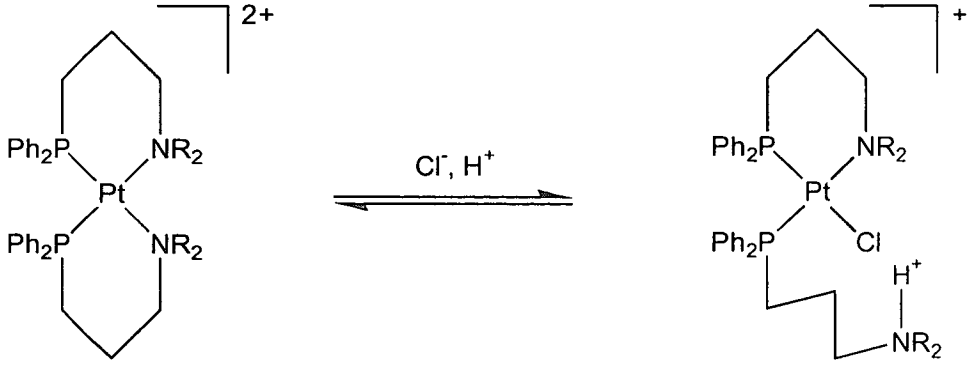

Scheme 3.6 pH-dependent equilibrium between ring-opened and closed forms of the *bis*-aminophosphine complexes

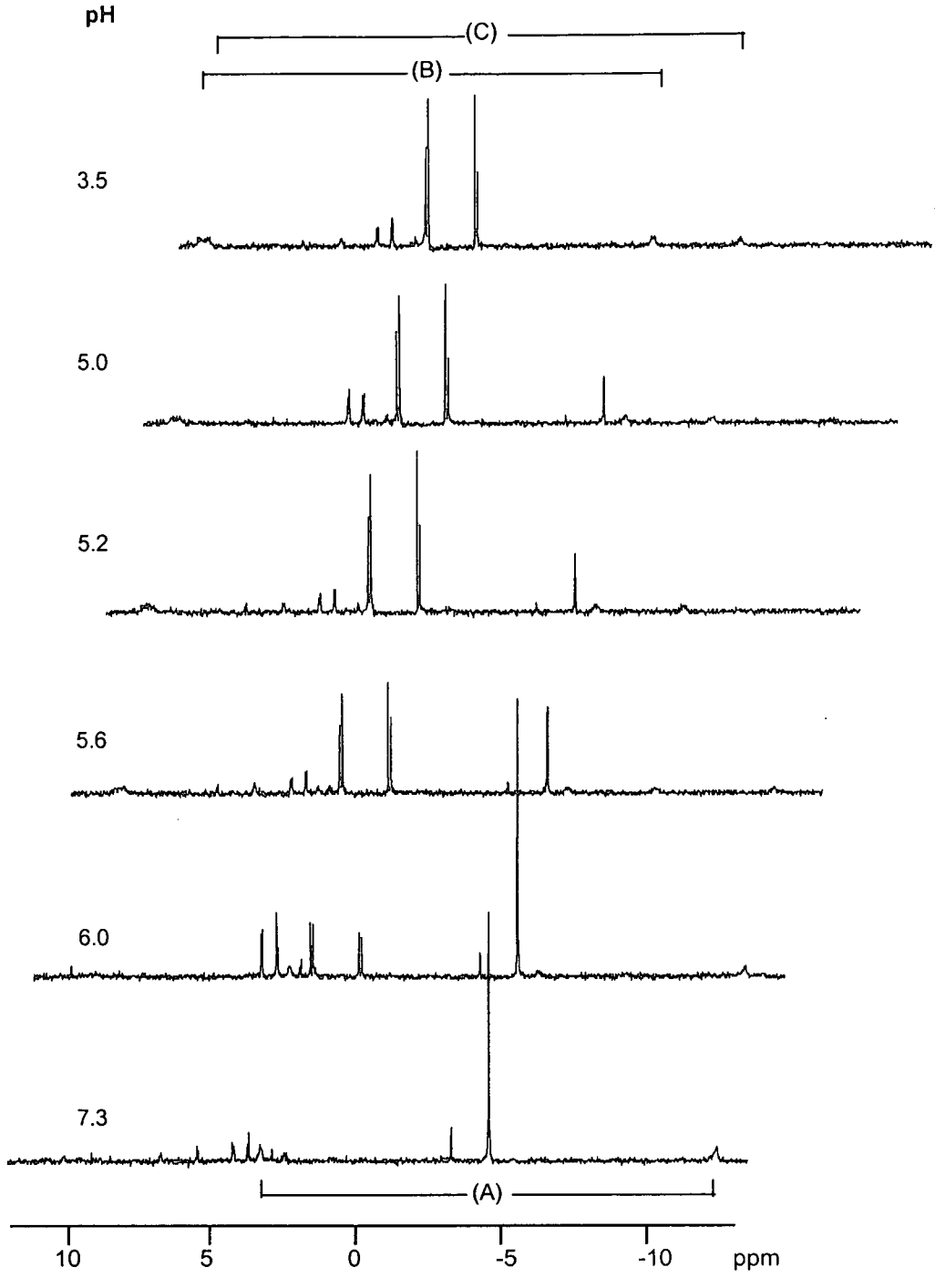

Figure 3.17 ^{31}P NMR spectra showing pH titration of complex **26A**
(A = fully ring-closed species, B/C = ring-closed/open species)

3.3.2 Hydrolysis of [Pt{$Me_2N(CH_2)_3PPh_2$-*P*}$_2Cl_2$] (24)

Whilst following aqueous reactions of complex **24** with nucleotides (see chapter 4), it was observed that the molecular ion peak for the complex [Pt{$Me_2N(CH_2)_3PPh_2$-*P*}$_2Cl_2$] was not present but appeared to be replaced by a number of peaks at lower mass. The aqueous behaviour of this complex was therefore investigated further.

3.3.2.1 Electrospray Ionisation Mass Spectrometry

An aqueous solution of complex **24** was prepared at a concentration of 50 μM. The solution was kept at room temperature (298 K) and electrospray ionisation mass spectra recorded at various time intervals over a two day period. Experimental parameters for ESI-MS are detailed in Section 2.3.3.

In the initial spectrum, recorded after the complex had been in solution for only 15 min, the molecular ion peak (808) was already not present. Three main peaks were observed at 737 (A), 754 (B), and 773 (C) (Figure 3.18). As further spectra were recorded these three peaks were all seen to decrease with time, whilst another peak gradually appeared at m/z = 709 (D). No further change was observed after about 40 hours and peak (D) then remained constant and was still observed when the solution was analysed over a week later.

In order to aid identification of the species present in the solution several isotope models for possible complexes were calculated using Mass Lynx software. These models are shown in Figure 3.19 along with the recorded spectrum from the solution at 15 min. The initial species were thus identified as [Pt{$Me_2N(CH_2)_3PPh_2$}$_2$] - **A**, [Pt{$Me_2N(CH_2)_3PPh_2$}$_2$OH] - **B**, and [Pt{$Me_2N(CH_2)_3PPh_2$}$_2$Cl] - **C**. Similarly the end product **D** was identified as [Pt{$Me(H)N(CH_2)_3PPh_2$}$_2$]. This seems to indicate that a hydrolysis takes place which results in the eventual formation of the fully ring-closed species (Scheme 3.7).

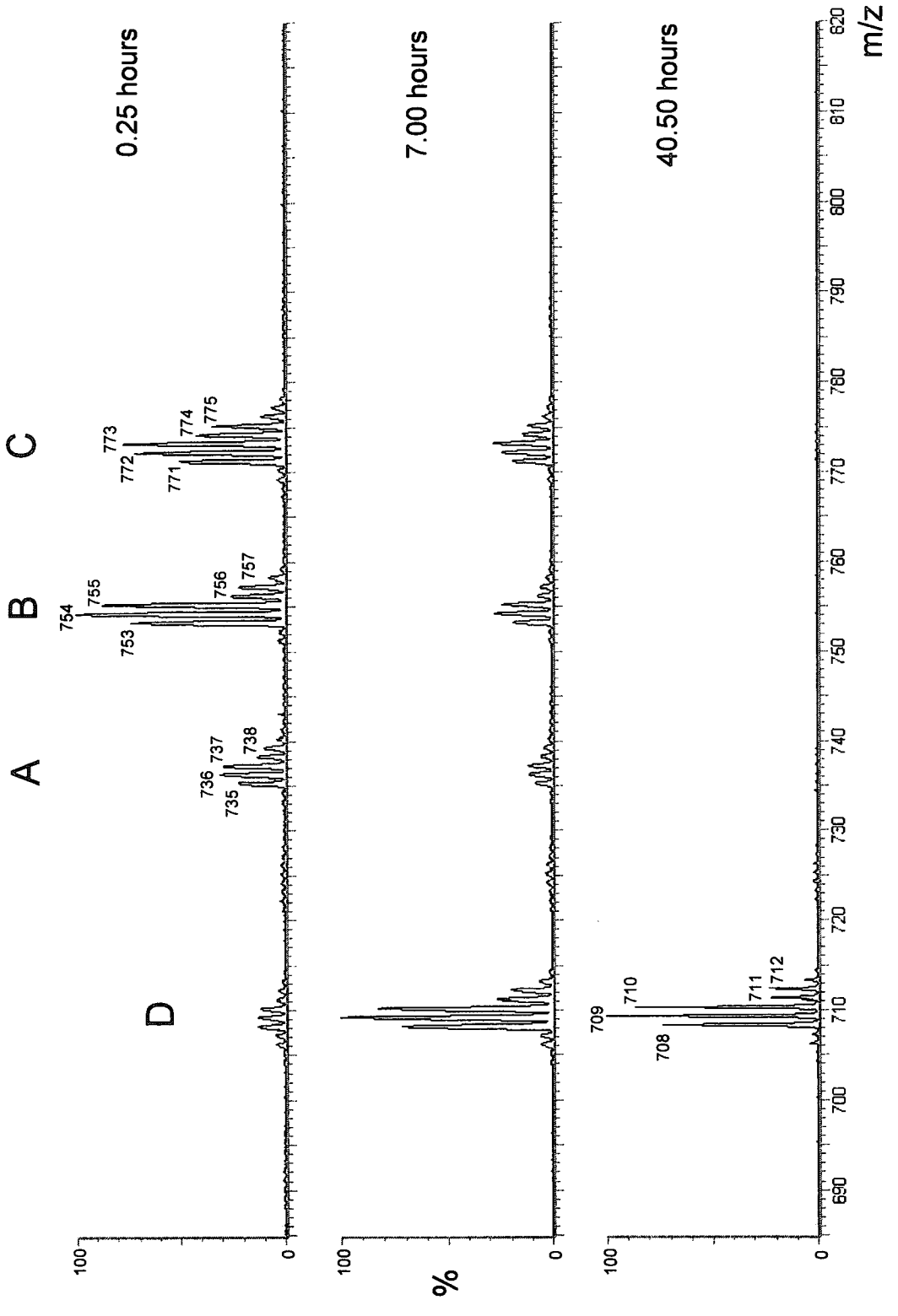

Figure 3.18 Electrospray ionisation mass spectra of complex **24** in aqueous solution after various time intervals

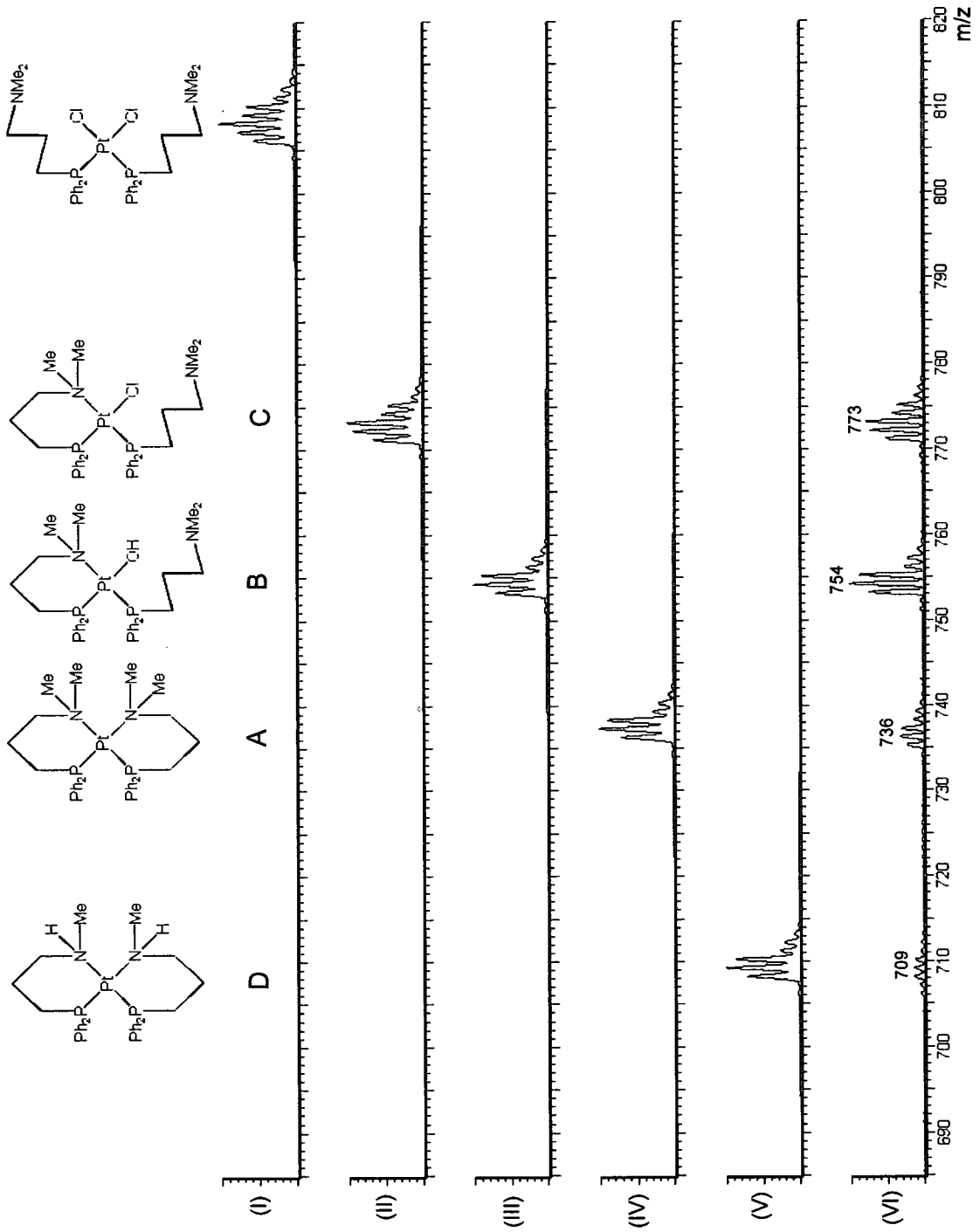

Figure 3.19 (I) – (V) = Calculated mass spectra for possible species formed from complex **24** in aqueous solution (VI) = observed mass spectrum after 0.25 hours

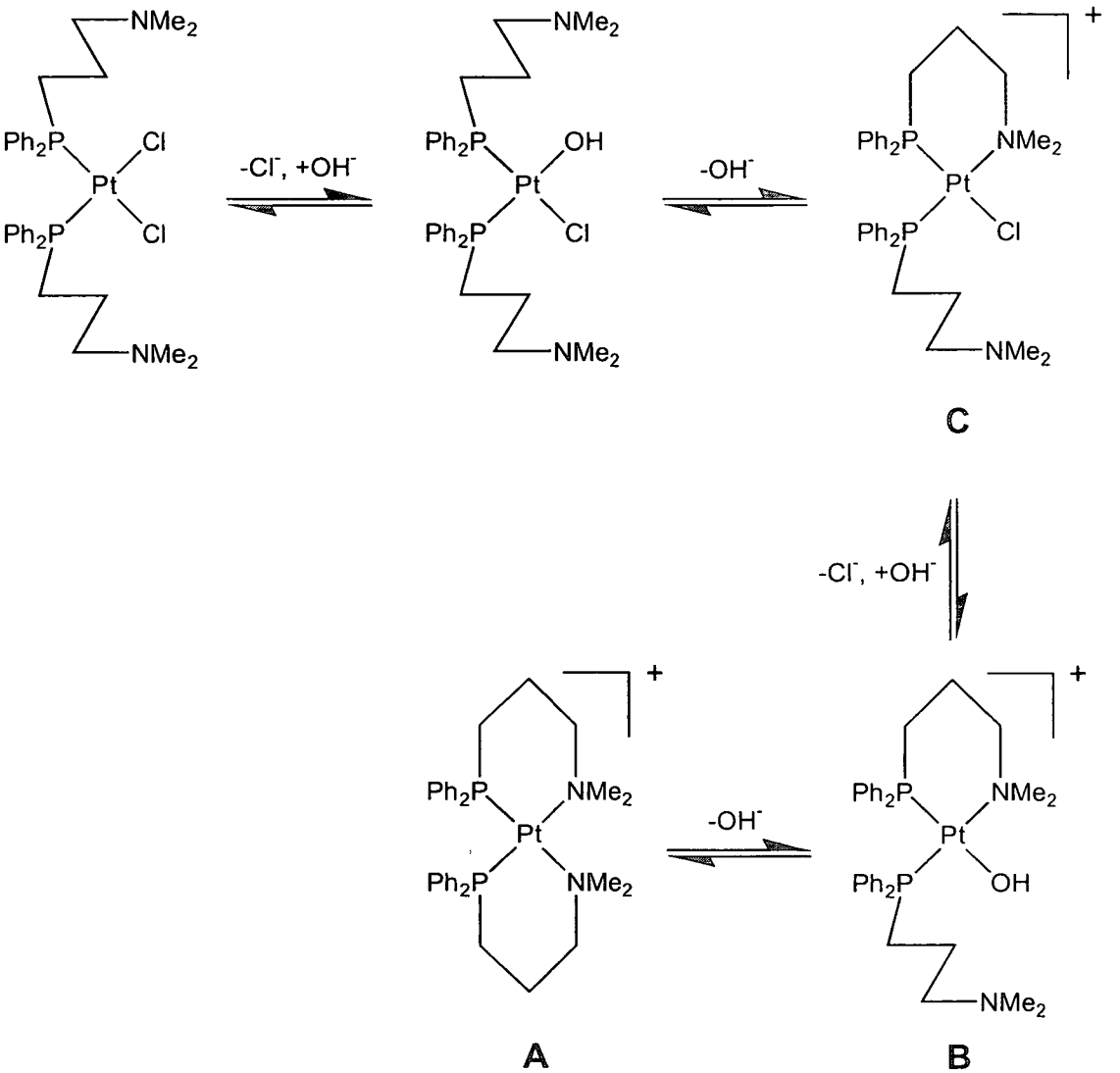

Scheme 3.7 Possible hydrolysis scheme for $[Pt\{Me_2N(CH_2)_3PPh_2\text{-}P\}_2Cl_2]$ (**24**) as shown by ESI-MS

Since neither of the fully ring-opened species can be observed in the ESI-MS after 15 minutes, it can be assumed that the rates of the first substitution and ring closure steps in the scheme are very fast and the closure of the first ligand has already occurred prior to analysis. Both the chloro- and hydroxy species **C** and **B** respectively are then observed and also the fully closed species **A**. The equilibria of the second chloride removal and second ring closure steps must be such that these

three species are all observed concurrently. These species do however eventually disappear to produce a new species **D**.

Product **D** has a mass lower than that of the fully closed species by 28 mass units. This could be accounted for by the loss of two methyl groups from the ligands to leave secondary rather than tertiary amines. This was confirmed by the calculated isotope model for $[Pt\{Me(H)N(CH_2)_3PPh_2\}_2]$ which matched the observed peak (Figure 3.19). This reaction is not expected and has not been observed for any of the other Pt-aminophosphine complexes studied. The N-C bond cleavage is likely to have been mediated by a nucleophilic OH^- ligand from the Pt with the formation of MeOH as a driving force. This is not unprecedented and can be likened to Pd-activated OH reactions used in catalysis, such as the Wacker Process. It seems likely therefore that it is species **B** that is converted to species **D** as in Scheme 3.8.

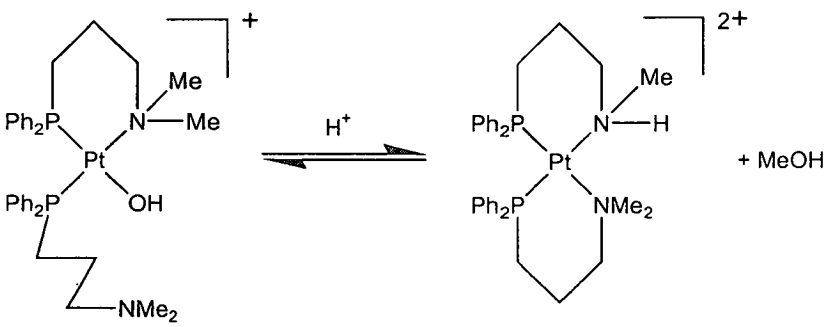

Scheme 3.8 Possible conversion of tertiary to secondary amine via hydroxy- species

Further work would be needed to understand more fully this unusual dealkylation mechanism.

3.3.2.2 NMR Spectrospcopy

In order to obtain more information about the aqueous reactions of $[Pt\{Me_2N(CH_2)_3PPh_2\text{-}P\}_2Cl_2]$ (**24**), ^{31}P NMR spectra were recorded of a 5 mM

solution in D_2O. Experimental parameters for ^{31}P are detailed in Section 2.3.1. An external reference of free ligand $\{Ph_2P(CH_2)_3NMe_2\}$, 35 mM/$CDCl_3$ in a sealed glass capillary was used.

As described in section 3.2.2.1, a ^{31}P NMR spectrum of complex **24** in $CDCl_3$ showed the presence of only a fully ring-opened species (singlet), the same species as was observed in the solid state by X-ray crystallography. When a spectrum was recorded immediately after dissolution of the complex in D_2O, four doublets were observed (Figure 3.20). These disappeared with time and two new doublets and a singlet emerged suggesting the changes in species observed by ESI-MS.

Measurement of the integrals of the initial peaks showed that they comprised two pairs of doublets. The coupling in each doublet was 19 Hz corresponding to $^2J(P\text{-}P)$ for two P atom *cis* to each other. Each pair of doublets can therefore be attributed to a species with two inequivalent P in a *cis* orientation. Species **W** has doublets at 4.15 and -1.74 showing $^1J(Pt\text{-}P)$ couplings of 3403 Hz and 3357 Hz, respectively. These values suggest P atoms with nitrogen atoms in the *trans* position in the complex. These peaks could therefore correspond to the fully closed species **A** seen in the mass spectra. It would, however, be expected that a species in which both ligands are ring-closed would result in both P being equivalent and would hence be observed as a singlet in ^{31}P NMR. Another anomaly between the NMR and ESI-MS results is the presence of only two species as opposed to the previously observed three species. The second NMR species **X**, had doublet peaks at 8.68 and 4.65 ppm. The platinum satellites for these peaks were too weak to observe. It is therefore impossible to correlate this to any specific complex from the mass spectra.

Further ^{31}P NMR spectra were recorded over the next 3 days and the changes in species present were monitored. Figure 3.20 shows spectra from various points during the time course experiment. Species **X** appeared to be stable and the integrals of the peaks only reduced slightly over the time. The peaks for species **W** were seen to decrease gradually with the emergence of a singlet at 0.53 ppm and two new

doublets at 0.53 and –3.25 ppm, for species **Y** and **Z** respectively. Again the two doublets represent a species with two inequivalent P atoms in a *cis* arrangement (^{2}J(P-P) = 19 Hz). The ^{1}J(Pt-P) couplings for these peaks were 3417 Hz and 3446 Hz respectively, indicating that both P atoms are again *trans* to nitrogen. The platinum satellites for the singlet peak **Y** are at the same shift as for the upfield doublet from **Z**, suggesting nitrogen to be the trans ligand in this species too. Species **Y** is therefore likely to be a fully ring-closed species with two equivalent P atoms.

The observed behaviour of complex [Pt{$Me_2N(CH_2)_3PPh_2$-*P*}$_2Cl_2$] (**24**) under NMR conditions is clearly not the same as under electrospray ionisation mass spectrometry conditions. This could be due to the large difference in the concentrations of the solutions used in each experiment, 5 mM for NMR and 50 μM for ESI-MS. Since the reactions of the complex are likely to involve hydrolysis it would be expected that concentration would be an important factor. It is clear that while ^{31}P NMR is an extremely useful tool, it is still relatively insensitive in the study of Pt-P containing complexes due to the high concentrations/long acquisition times needed to observe the ^{1}J(Pt-P) coupling constants.

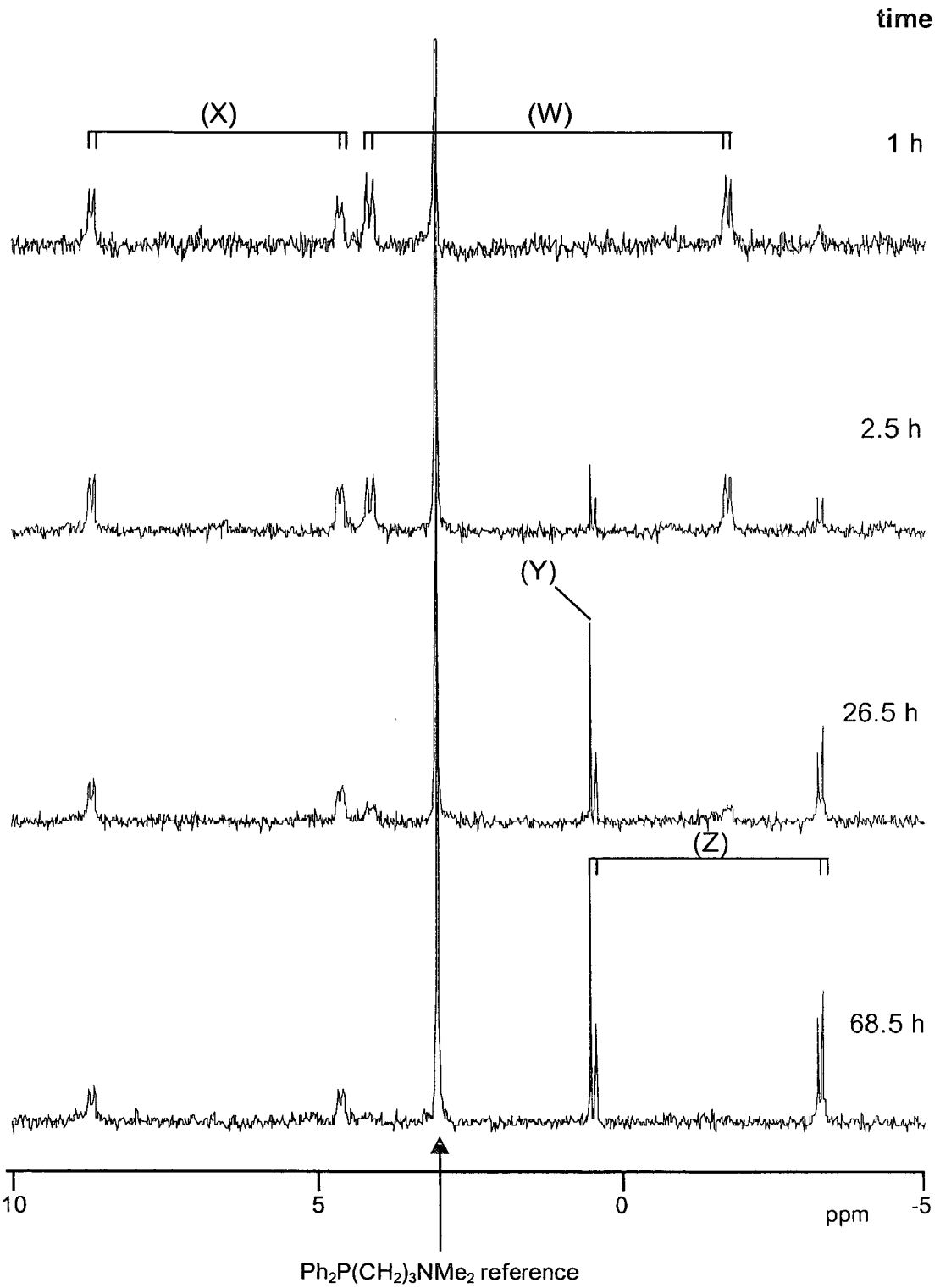

Figure 3.20 ^{31}P spectra of $[Pt\{Me_2N(CH_2)_3PPh_2\text{-}P\}_2Cl_2]$ (**24**) recorded at various times after dissolution in D_2O at ambient temperature

3.4 Conclusions

A series of aminophosphine ligands $\{Ph_2P(CH_2)_3RR'\}$ has been prepared from amino-chloride and diphenylphosphine starting materials, with varying levels levels of substitution on the amine group. The preparations used were successful but did not yield particularly large quantities of products due to their ease of oxidation during the reaction. Distillation was therefore required to purify the aminophosphine products.

The aminophosphines were then complexed to platinum via a $Pt(COD)Cl_2$ starting material. This lead predominantly to the formation of complexes with two ligands bound per Pt, with binding through the phosphorus atom in the ligand occuring preferentially over nitrogen atom binding. Analysis of the complexes by ^{31}P NMR showed that binding of the nitrogen was influenced by the steric bulk of the groups on the amine(R, R'). The complexes therefore ranged from fully ring-closed (both ligands bound through both P and N) for low steric bulk to fully ring-opened (both ligands bound through P only) for high steric bulk. One anomaly in the preparation of these complexes was for the ligand $Ph_2P(CH_2)_3NMeH$ which formed a mixture of the *bis*-aminophosphine complex and a *mono*-aminophosphine complex with the ligand ring-closed. In general the preparation of *mono*-aminophosphine complexes was achieved by the use of Pt(COD)MeCl starting material. The *mono*-aminophosphine complexes had very poor water-solubility and were not suitable candidates as Pt anticancer agents.

The X-ray crystal structures of the complexes prepared have been solved and show that the structure in the solid state is the same as that in solution as determined by NMR. The *bis*-aminophosphine structures all show Pt to exist in a distorted square-planar geometry with an increased bond angle between the two ligand phosphines due to the presence of the bulky phenyl groups. The structure of complex **24** $[Pt\{Ph_2P(CH_2)_3NMe_2\text{-}P\}_2Cl_2]$ also showed π-stacking between the phenyl rings of

the two ligands. The ring-closed structures contained six-membered rings in a chair conformation.

Further studies on the *bis*-aminophosphine complexes showed that their solution structures are pH-dependent. Low pH values cause protonation of the amine groups of the ligands and force them into a ring-opened conformation. High pH values promoted deprotonation of the ligand and allowed ring-closing to occur, dependent on the steric bulk on the amines.

The most interesting complex studied was complex **24** [Pt{$Ph_2P(CH_2)_3NMe_2$-*P*}$_2Cl_2$], which underwent unusual reactions in aqueous solution leading to hydrolysis and ring-closure of the complex and eventually to de-methylation of the tertiary amine ligands. This could open a number of new possibilities for these complexes as potential catalysts.

3.5 References

1 G. K. Anderson, R. Kumar, *Inorg. Chem.* **1984**, *23*, 4064

2 G. P. C. M. Dekker, A. Buijs, C. J. Elsecier, K. Vrieze, P. W. N. M. van Leeuwan, W. J. J. Smeets, A. L. Spek, Y. F. Wang, C. H. Stam, *Organometallics,* **1992**, *11*, 1937

3 M. Basset, D. L. Davies, J. Neild, L. J. S. Prouse, D. R. Russell, *Polyhedron*, **1991**, *10*, 501

4 S. Naili, J.-F. Carpenter, F. Agbossou, A. Mortreux, G. Nowogrocki, J.-P. Wignacourt, *Organometallics,* **1995**, *14*, 1, 401

5 S. Koepke, R. Kupper and C. Michejda, *J. Org. Chem.* **1979,** *44*, 2718

6 M. Chini, P. Crotti, L. Favero and F.Macchia, *Tetrahedron Letters*, **1994,** *35*, 761

7 J. McDermott, J. White, G. Whitesides, *J. Am. Chem. Soc.* **1976**, *98*, 6525

8 H. C. Clark, L. E. Manzer, *J. Organomet. Chem.* **1973**, *59*, 411

9 S. Chatterjee, D. C. R. Hockless, G. Salem, P. Waring, *J. Chem. Soc., Dalton Trans.*, **1997**, 3889

10 CERIUS^2, Molecular Simulations Incorporated, San Diego, California, 1997

11 G.M Sheldrick, SHELXTL, Bruker Analaytical X-Ray, Madison, Wisconsin, 1995

12 A. G. Orpen, L. Brammer, F. H. Allen, O. Kennard, D. G. Watson, R. Taylor, *J. Chem. Soc., Dalton Trans.*, **1989**, S1

13 C. Janiak, *J. Chem. Soc., Dalton Trans.*, **2000,** 3885

14 C. A. Hunter, J. K. M. Sanders, *J. Am. Chem. Soc.*, **1990**, *112*, 5525

15 Kaleidagraph 3.09, Synergy Software, **1997**

16 A. Habtemariam, B. Watchman, B. S. Potter, R. Palmer, S. Parsons, A. Parkin, P. J. Sadler, *J. Chem. Soc. Dalton Trans.*, **2001**, 1306

Chapter Four

Interactions of Platinum Aminophosphine Complexes with Nucleotides

In this Chapter the reactions of the platinum aminophosphine complexes, prepared and characterised in Chapter 3, with nucleotides are investigated. As discussed in Section 1.7, nucleotides are the building blocks of DNA and as such are ideal for simplifying and studying the potential reactions of platinum drugs with DNA, their major biological target.[1] In this work the selectivity and rate of binding of complexes **24**, **25**, and **27** (shown in Figure 4.1) have been studied in particular.

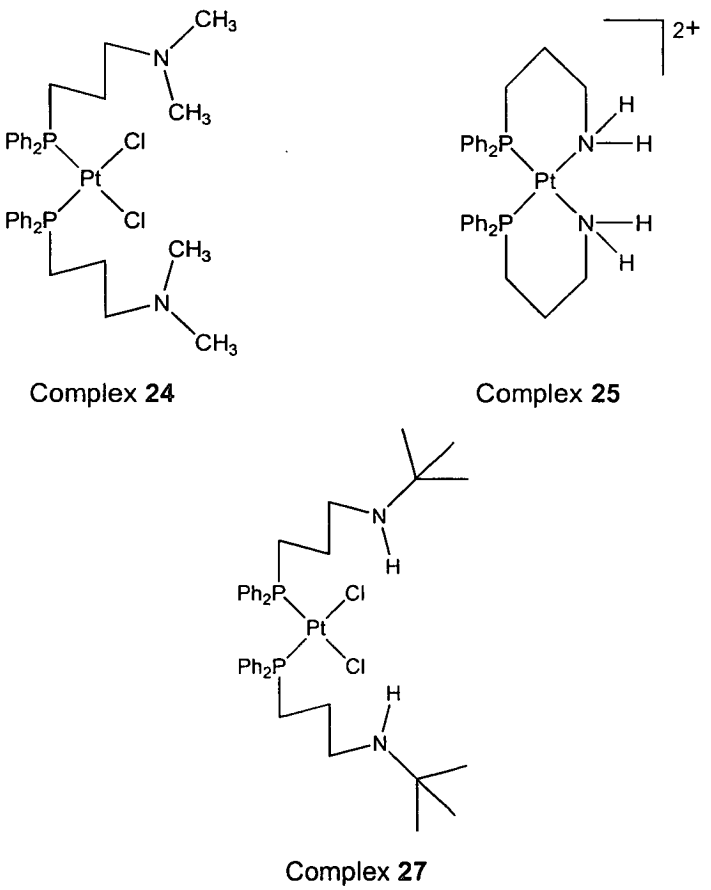

Complex **24** Complex **25**

Complex **27**

Figure 4.1 Structures of platinum aminophosphine complexes **24**, **25** and **27**

4.1 Experimental

4.1.1 NMR Spectroscopy – Reactions with Nucleotides

Acquisition details for NMR spectroscopy are given in Section 2.3.1. Samples containing the relevant complex at a concentration of 5 mM and the relevant nucleotide at either 5 mM or 10 mM, depending on the reaction ratio, were prepared in D_2O. The pH* values of the samples were measured as described in Section 2.3.7 and adjusted using 0.1 M DNO_3 or NaOD. Dioxane solution (2 μl, 5%) was added to each sample to act as a reference. The samples were all placed in a water bath at 310 K overnight to ensure complete reaction.

4.1.2 High Performance Liquid Chromatography – Competition Reactions

The HPLC set-up is detailed in Section 2.3.5. A mixture of all four nucleotides was separated on a reverse phase C18 column, by a method based on that described by Meynial[2] An isocratic solvent mixture was used incorporating 95% solvent I (50 mM K_2HPO_4, 2.5 mM tetrabutyl ammonium hydrogen sulphate – TBAHS, pH 7) and 5% solvent II (100 mM K_2HPO_4, 2.5 mM TBAHS, diluted with 50% acetonitrile, pH 7). The pH of both solvents was adjusted using 85% orthophosphoric acid. The nucleotides were detected by UV absorbance at 254 nm.

Calibration solutions were prepared containing equimolar amounts of all four nucleotides at concentrations ranging from 0.1 – 1 mM in water. Each sample was separated and analysed by HPLC and a calibration graph of peak area versus concentration for each nucleotide was plotted. Samples were then prepared containing the appropriate complex and all four nucleotides at 1 mM concentration. These samples were then analysed and the peak area of each nucleotide was used to determine the amount of free nucleotide remaining.

4.1.3 Capillary Electrophoresis – Competition Reactions

The CE equipment and operation parameters used are detailed in Section 2.3.2. The method used is based on a previously reported method.[3] The separation buffer used was 20 mM $NaHPO_4$ at pH 7.75. Calibration samples were prepared containing all four nucleotides in equimolar amounts at concentrations ranging from 10 –100 μM in water. The four peaks were identified by using spiked samples containing an excess of one of the nucleotides. A calibration graph was plotted of peak area versus concentration for each nucleotide.

Samples were prepared containing the appropriate complex and the four nucleotides all at 100 μM concentration in water. The pH was adjusted to close to physiological pH and the samples were incubated at 310 K in a water bath overnight, prior to analysis, to ensure complete reaction. The amount of each nucleotide bound was determined as in the HPLC method by determining the concentration corresponding to the decrease in peak area for the free nucleotide. It should be noted that the equipment used did not hold a precise voltage, so the elution times of the nucleotides varies slightly between runs, although the order of elution remains constant.

4.1.4 Electrospray Ionisation Mass Spectrometry – Detection of Nucleotide Adducts

The ESI-MS equipment and experimental parameters are described in Section 2.3.3. Samples were prepared containing the appropriate complex at 1 mM concentration and two mole equivalents of the nucleotide in water. The pH of each sample was adjusted to close to physiological pH (7.4) and the samples incubated overnight at 310 K to ensure complete reaction. Prior to analysis, the samples were diluted to 50 μM with water.

4.2 Reactions of $[Pt\{Me_2N(CH_2)_3PPh_2\text{-}P\}_2Cl_2]$ (24)

4.2.1 NMR Spectroscopy

4.2.1.1 Guanosine 5'-Monophosphate

1:1 (Nucleotide:Complex) Reaction

In the recorded ^1H NMR spectrum the resonances for all the protons in free 5′-GMP have completely disappeared, showing all the nucleotide has been bound in the reaction.

Shifts for resonances of free nucleotide:

H8: 8.21 ppm, s H1': 5.94 ppm, t dH3': 4.50 ppm, dd H4': 4.32 ppm, q 2H5': 3.99 ppm, t

New peaks appeared with an upfield shift from the free GMP signals.

2:1 (Nucleotide:Complex) Reaction

Some free GMP peaks were observed, with new peaks for Pt-bound products with upfield shifts. The ^1H spectrum of the 2:1 reaction is shown in Figure 4.2. The clearest signal to observe was that of the H1′ proton (d, 5.9 ppm) in an area of the spectrum with a flat baseline allowing integration of individual peaks. As shown in the expansion in Figure 4.2, eight new Pt-GMP resonances are produced in the reaction, with H1′ doublets in the region 5.32 – 5.76 ppm. All the doublets have a coupling of 6 Hz, the same as that in free GMP. Measurement of the integrals of the free and bound GMP H1′ peaks showed that 71% (1.42 mole equivalents) of the GMP present was bound to Pt in the reaction.

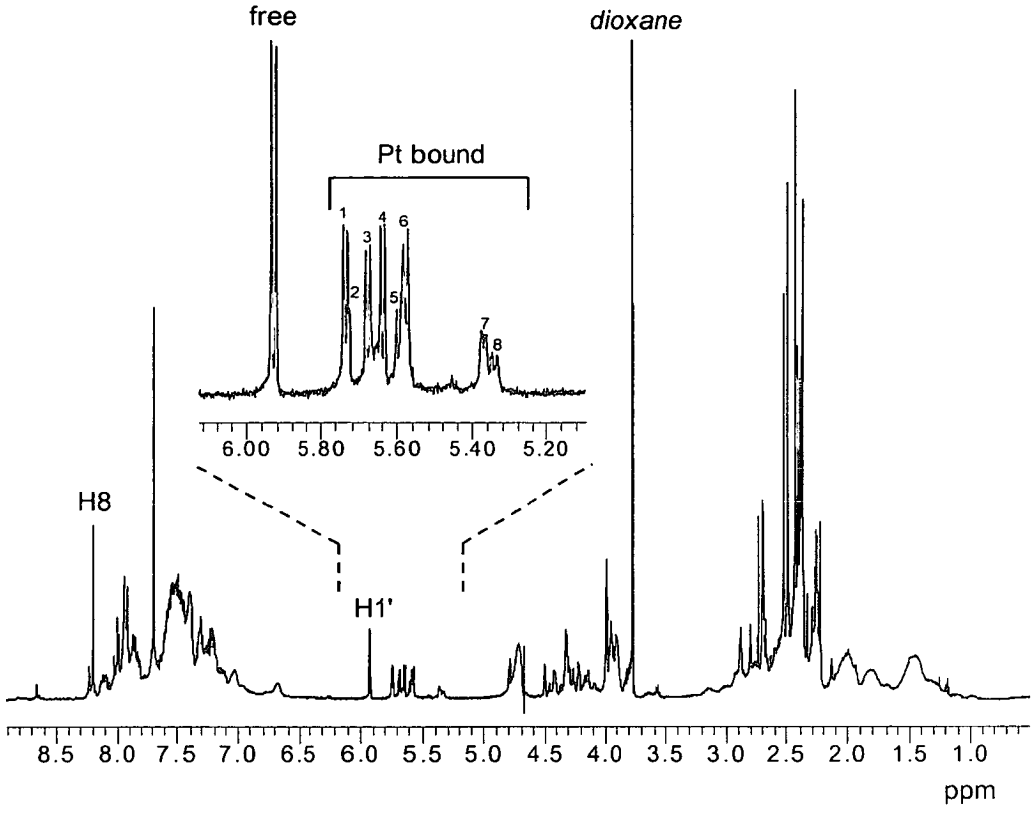

Figure 4.2 ^{1}H spectrum of [Pt{$Me_2N(CH_2)_3PPh_2$-*P*}$_2Cl_2$] (**24**) with two mole equivalents of 5'-GMP (expansion shows H1' resonances for free and bound 5'-GMP)

As described in Section 2.1.1.2 it is usual for the protons on the heterocycle of a nucleotide to shift downfield upon platination of the nucleotide.[4] In the reaction between complex **24** and 5'-GMP however these new product peaks are shifted upfield of the free GMP peaks. The H8 signals for the platinated products, which are often useful in following Pt-binding[5], are shifted into the phenyl region of the spectrum (ca. 8.0 ppm) making them difficult to observe and separate. For this reason, the H1' doublet (ca. 5.9 ppm) is used to follow the platination of the nucleotide since it appears in a clear region of the spectrum. Whilst not directly bound to the base, this proton is close enough to experience a change in electron density on platination and is also seen to undergo a chemical shift change. The upfield shift observed for proton resonances of the nucleobase is very unusual but

could be due the presence of phenyl groups in the ligand. The ring current of the π-system on the ring could be positioned over the protons in question.

As described above, virtually all the GMP was bound in the 1:1 reaction indicating that the complex is capable of forming a monofunctional GMP adduct (i.e. one GMP per platinum). The reaction was then repeated with two mole equivalents of 5'-GMP and the ^{1}H NMR spectrum is shown in Figure 4.2. By studying the H1' region, it was determined that 29% of the GMP was still free (5.93 ppm) and peaks for eight bound products (71% of the GMP present) were also seen in the region 5.32-5.75 ppm. Some bifunctional adducts (i.e. two GMP bound per platinum) must therefore have been formed. It is difficult to see if all the complex present has bound GMP since the ^{1}H NMR spectrum of $[Pt\{Me_2N(CH_2)_3PPh_2\text{-}P\}_2Cl_2]$ in D_2O is already complicated by the presence of a number of new species in solution (see section 3.3.2). It is impossible to separate the signals for nucleotide-bound species (up to 8 different forms) and non-bound species (up to 4 different forms).

If it is assumed that all the Pt binds to the nucleotide, then the 71% (1.4 mole equivalents) of GMP that is bound in a 2:1 reaction mixture suggests that 40% of the complex forms bifunctional adducts and 60% of the complex forms monofunctional adducts. However, this may not be the case, as it is possible that any fully ring-closed species present in solution would be incapable of ring-opening and therefore would not have a free binding site for the GMP. The presence of both monofunctional and bifunctional adducts would help to explain why there are so many distinct bound H1' signals observed in the spectrum. The number of distinct species produced can be accounted for by a combination of two factors: (i) monfunctional adducts can have different groups at the vacant site ($Cl^-/OH^-/NMe_2$), (ii) both monofunctional and bifunctional adducts can exist as different isomers with the GMP adopting either a head or tail conformation[6] relative to the platinum square-plane (section 2.2.1.2).

As discussed in Section 3.3.2, complex **24** is likely to undergo chelate ring-closing in aqueous solution. If this is the case then the pH is likely to have an effect on

nucleotide binding since low pH can indice ring-opening of the ligand by protonation of the amine and leave a vacant site. To investigate this possibility, a pH titration was carried out on a 1:2, complex:GMP sample and the percentage of bound nucleotide determined at each pH using the integrals of the H1' signals. The change in binding with pH is shown as a graph in Figure 4.3. The amount of GMP bound does not vary greatly with pH suggesting that the complex does not readily ring-close in the presence of GMP. The nucleotide binding reaction must be more favourable than the ring-closing mechanism in aqueous solution. The GMP present is never all bound at any pH suggesting that at least one of the Pt-species present is not capable of binding a second GMP to form a bifunctional adduct. There is a small decrease in the amount of GMP bound at ca. pH 8 followed by an increase at higher pH values. This could indicate a switch from N7 to N1 binding of the Pt as has previously been seen for the analogous complex $[Pt\{Me_2N(CH_2)_2PPh_2\}_2Cl]Cl$.[7]

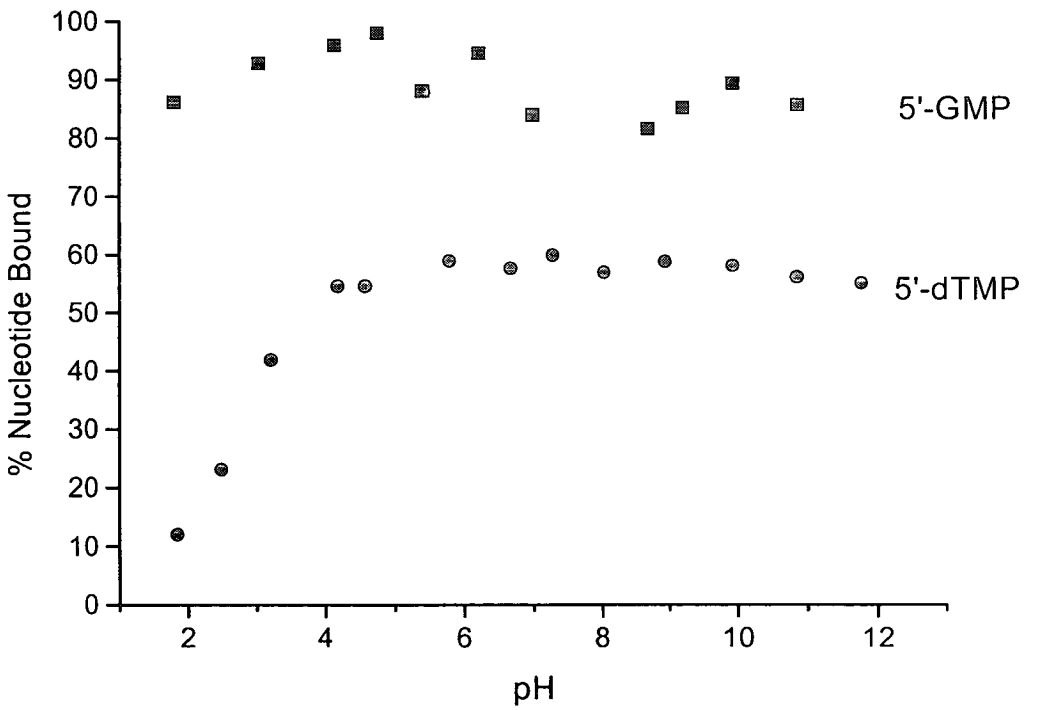

Figure 4.3 Graph showing the percentage of 5'-GMP and 5'-dTMP bound to $[Pt\{Me_2N(CH_2)_3PPh_2\text{-}P\}_2Cl_2]$ **(24)** in separate reactions, with 2:1 ratio, at various pH values

4.2.1.2 Adenosine 5'-Monophosphate

1:1 (Nucleotide:Complex) Reaction

As for 5'-GMP the reaction between [Pt{$Me_2N(CH_2)_3PPh_2$-*P*}$_2Cl_2$] (**24**) and 5'-AMP was initially carried out with one mole equivalent of the nucleotide. Strong resonances for free 5'-AMP remained after completion of the reaction (Figure 4.4).

Shifts for resonances of free nucleotide:

H2: 8.52 ppm, s H8: 8.27 ppm, s H1': 6.15 ppm, d

H3': 4.51 ppm, dd H4': 4.39 ppm, m 2H5': 4.11 ppm, m

Two small sets of peaks for new Pt-bound AMP had appeared, one shifted upfield and one downfield of free AMP. The clearest signal to observe and measure was again the H1' signal. As shown in the expansion in Figure 4.4, the H1' for free AMP was observed at 6.13 ppm and the H1' for bound AMP were at 6.57 and 5.86 ppm (a) and (b), respectively. Measurement of the integrals for these peaks showed that 25% of the AMP was bound during the reaction. The same pattern can also be seen for the H2 and H8 resonances (8.59 and 8.25 ppm) with two bound peaks for bound products (a) and (b) appearing either side of the free AMP peak.

The very low level of binding observed is not expected since N7 of adenine is usually a common binding site on DNA[8] and is favoured by Pt-amine anticancer complexes.[9] The very simple spectrum observed suggests that only one of the Pt species in solution can bind AMP and this forms two isomers in a ratio 56% (a) to 44% (b).

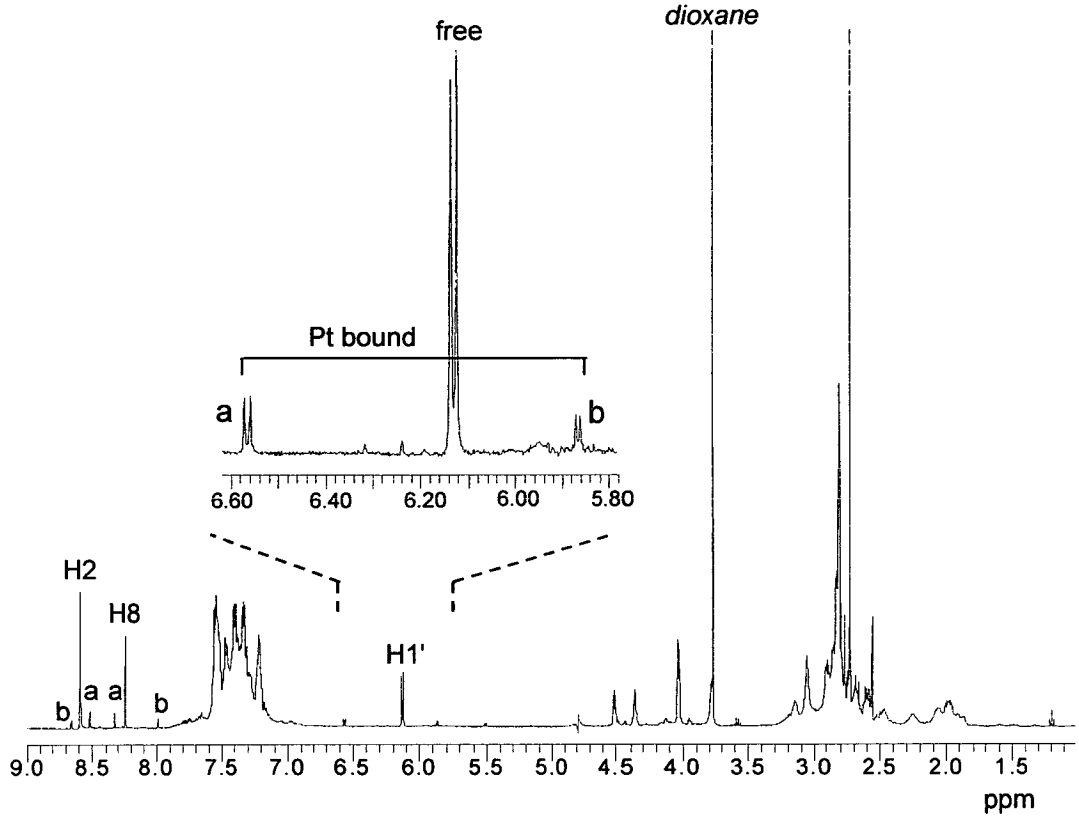

Figure 4.4 ^{1}H spectrum of [Pt{$Me_2N(CH_2)_3PPh_2$-*P*}$_2Cl_2$] (**24**) with one mole equivalent of 5'-AMP (expansion shows H1' resonances for free and bound 5'-AMP)

4.2.1.3 Cytidine 5'-Monophosphate

The reaction was carried out as described for 5'-GMP, between 5'-CMP and [Pt{$Me_2N(CH_2)_3PPh_2$-*P*}$_2Cl_2$] (**24**) in a 1:1 ratio. The signals for free 5' CMP were observed with no new product peaks.

Shifts for resonances of free nucleotide:

H6: 8.14 ppm, d H1': 6.15 ppm, d H5: 6.02 ppm, q

H3': 4.36 ppm, q H4': 4.25 ppm, br 2H5': 4.02 ppm, mm

This suggests that no binding occurs between the complex and 5'-CMP

4.2.1.4 Deoxythymidine 5'-Monophosphate

1:1 (Nucleotide:Complex) Reaction

In the ^{1}H NMR spectrum for [Pt{$Me_2N(CH_2)_3PPh_2$-*P*}$_2Cl_2$] (24) and 5′-dTMP the resonances for all the protons of free 5′-dTMP completely disappeared, showing that all the nucleotide had reacted.

Shifts for resonances of free nucleotide:

H6: 7.83 ppm, s	H1': 6.36 ppm, t	H3': 4.59 ppm, m	H4': 4.15 ppm, q
2H5': 3.97 ppm, t	H2': 2.38 ppm, mm	Me: 1.94 ppm, s	

New peaks appeared shifted upfield of free TMP signals.

2:1 (Nucleotide:Complex) Reaction)

In the reaction with two mole equivalents of 5′-dTMP some free dTMP peaks were observed, with new peaks for Pt-bound products shifted upfield. The ^{1}H spectrum of the 2:1 reaction is shown in Figure 4.5. As for GMP, the clearest signal was that of the H1′ proton (t, 6.35 ppm) where the flat baseline allowed integration of individual peaks. As shown in the expansion in Figure 4.5, only two major new Pt-TMP resonances are produced with H1′ triplets in the region 6.04 – 6.27 ppm. Products **a** and **b** are present in the ratio 1:1.4. All the product triplets have couplings of 7 Hz, the same as the coupling in free TMP. The same ratios of products can be observed for the methyl signal of TMP (s, 1.94 ppm) with **a** and **b** at 1.72 and 1.70 ppm with relative intensities 1:1.4. Measurement of the integrals of the free and bound TMP H1′ peaks showed that 58% (1.2 mole equivalents) of the TMP present was bound to Pt in the reaction.

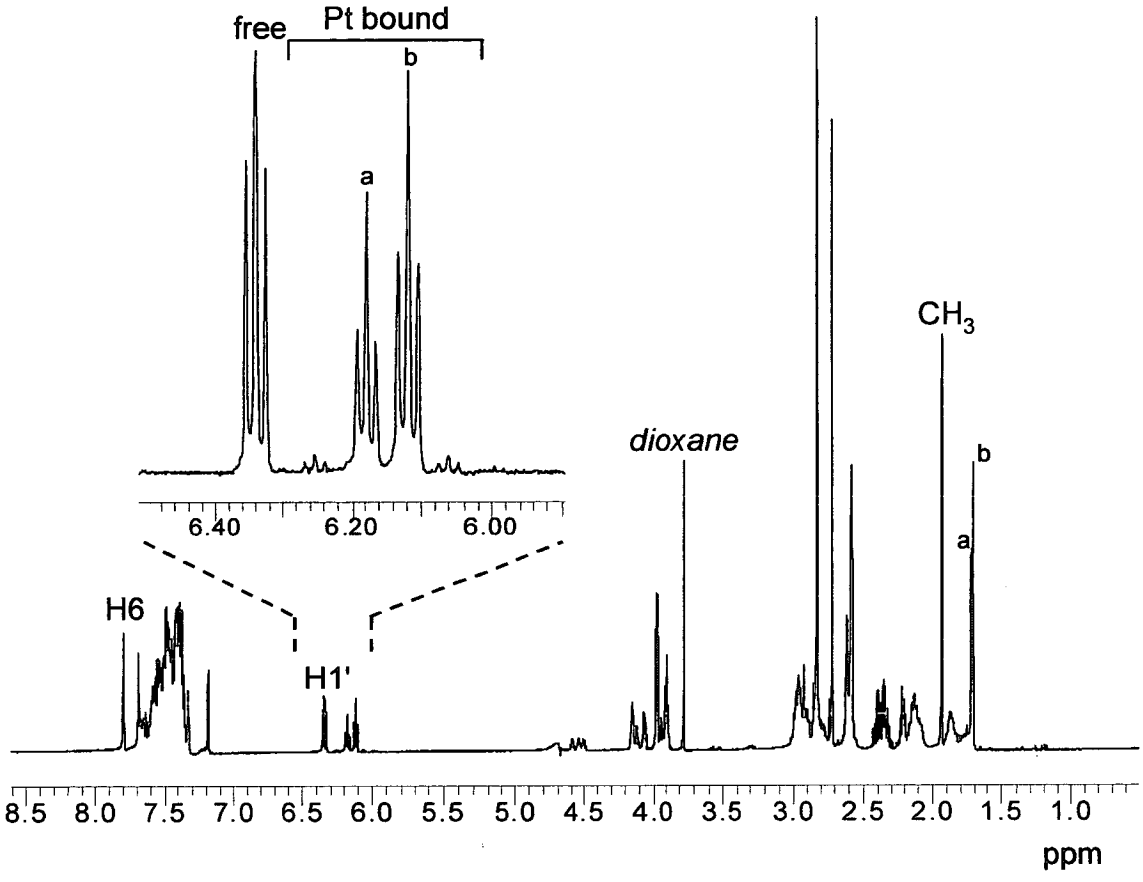

Figure 4.5 ^{1}H spectrum of [Pt{$Me_2N(CH_2)_3PPh_2$-*P*}$_2Cl_2$] (**24**) with two mole equivalents of 5'-dTMP (expansion shows H1' resonances for free and bound 5'-dTMP)

As seen from the results above, virtually all the TMP was bound in the 1:1 reaction suggesting that complex (**24**) is capable of forming monofunctional adducts with 5'-dTMP as was seen for 5'-GMP. In contrast when the reaction ratio was increased to 2:1 nearly half of the 5'-dTMP remained free in solution suggesting that very few bifunctional adducts were formed.

Binding of a platinum complex to thymine is much less common than to G or A.[10] This is largely a consequence of the kinetic preference of platinum for other sites such as N7 on G and A which are unprotonated at physiological pH and the

inaccessibility of the main T binding site, N3, in a DNA duplex structure. Binding of Pt complexes to thymine has however been obseved with poly(dT) and thymine nucleotides and nucleobases in isolation.[10]

It has been shown that with the N1 site blocked, by the ribose-linkage, the major binding site on thymine is N3.[11] Since binding to 5'-dTMP appears to require the deprotonation of the N3 site, the effect of pH on the binding to complex (**24**) was therefore investigated by means of a pH titration. ^{1}H spectra of the sample above were recorded at various pH values and the H1' signal used to determine the percentage of the nucleotide bound. The results are plotted as a graph in Figure 4.3.

The graph shows that at all pH values, the binding to 5'-dTMP occurs only in a monofunctional manner, since the percentage of nucleotide bound is limited to ca. 50%. The graph also shows that the TMP remains bound even as low as pH 4, well below the pK_a value of the N3 site. Below pH 4 the amount of thymine binding decreases but significant amounts of bound species are detected even as low as pH 2. As well as establishing the change in amount of 5'-dTMP bound, the pH titration also identified a change in the nature of the bound species, Figure 4.6.

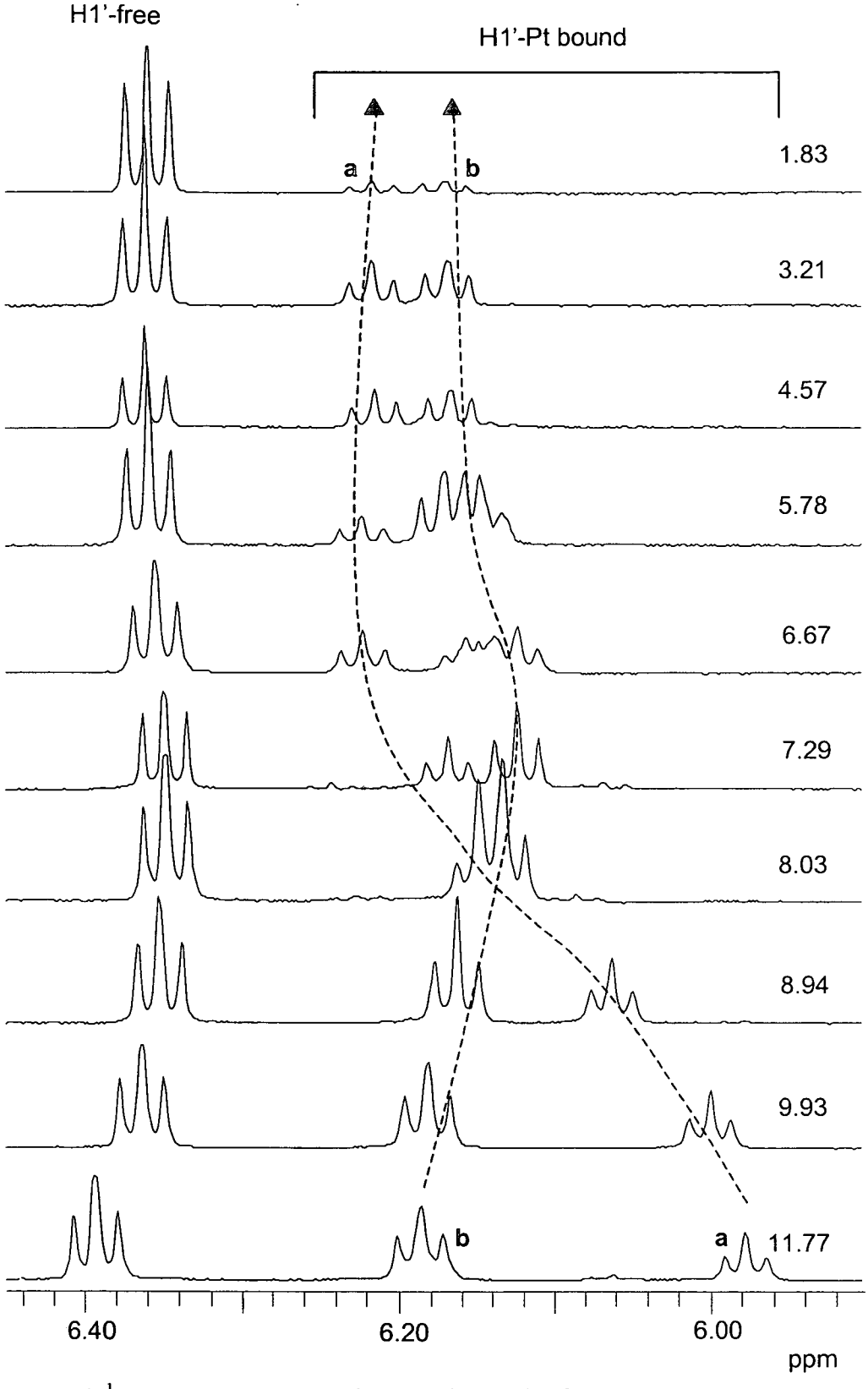

Figure 4.6 ^{1}H NMR spectra showing H1'signals for free and Pt-bound 5'-dTMP on reaction with [Pt{$Me_2N(CH_2)_3PPh_2$-*P*}$_2Cl_2$] (**24**) at various pH values

At high pH two platinum bound species are present. Measurement of the H1' signals for these species showed their relative intensities were 1:1.4. The peaks for both signals shift with pH but with very different profiles. The larger peak, **b,** at 6.19 ppm shifts upfield as the pH decreases. This shift pattern is similar to that for free 5'-dTMP. The smaller peak, **a**, at 5.98 ppm, shows a much more prominent shift downfield with decreasing pH. This is opposite to the shift exhibited by free TMP.

Between pH 8 to 5 more H1' peaks are seen suggesting a mixture of products is present in this range. At low pH there are again only 2 bound species which have the same relative intensities as the species at high pH (1:1.4). These two species **a** and **b** can be followed through the range of pH values and their chemical shift is shown at each pH in the graph in Figure 4.7.

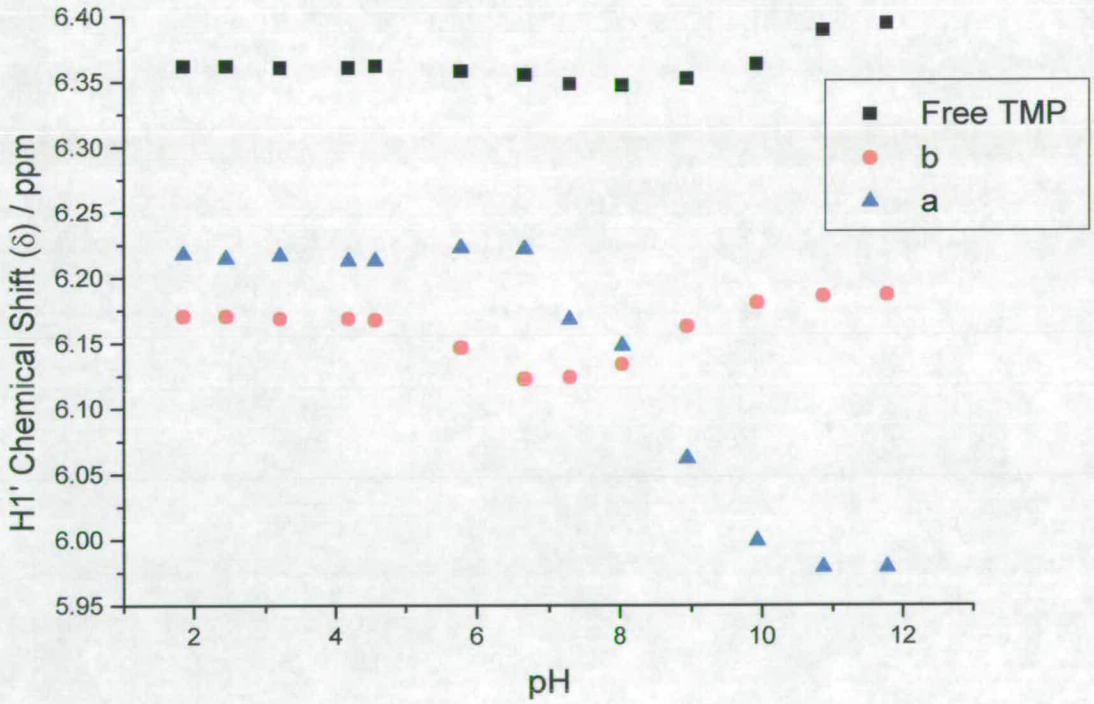

Figure 4.7 Graph showing chemical shift of H1' protons of Pt-bound TMP species **a** and **b**

At high pH the usual binding site for Pt on TMP, N3, is deprotonated (pK_a = 10.47)[12] so it is likely that the species formed are N3-bound monofunctional adducts. At low pH the N3 site would be expected to be protonated so the mode of binding could be quite different. In order to further identify the nature of the bound species ^{31}P NMR spectra were recorded at both low and high pH. (Figure 4.8)

At high pH two pairs of small doublets and two pairs of overlapping large doublets can be seen, with relative intensities 1:1.4, corresponding to species **a** and **b** observed in the ^{1}H NMR spectra. Each doublet has ^{2}J(P-P) = 17 Hz suggesting that each pair corresponds to a species with two inequivalent P in a *cis* orientation. Both species **a** and **b** have a downfield doublet at ca. –2.2 ppm with ^{1}J(Pt-P) = 3310 Hz and an upfield doublet at ca. –8.5 ppm with ^{1}J(Pt-P) = 3295 Hz. These values indicate that both species contain nitrogen atoms in the positions *trans* to both phosphorus atoms.[13,14] This is consistent with N3 binding of TMP. Since only a monofunctional adduct is formed, the adduct is likely to contain one DMDPPA ligand chelated and one 5′-dTMP molecule bound through N. (Figure 4.9). Chelation of the aminophosphine would be favoured at high pH as discussed in section 3.3. Since the two distinct species **a** and **b** exhibit very similar shifts in the ^{31}P NMR spectrum it is likely that these are two isomers of the same product. This could be caused by the restriction of rotation of the Pt-N3 bond due to the presence of the bulky aminophosphine ligands. This would lead to two head and tail isomers differing by orientation of the plane through the rings in the nucleotide relative to the platinum square-plane[15] (Figure 4.10). The isomers could be fixed in position by hydrogen bonding between either O4 or O2 on the TMP with a proton on the amine in the dangling ligand. Similar intermolecular H-bonds have been observed between NH and O2 in the 1-methyl thymine structure, $[Pt(NH_3)_2(1\text{-MeT})](NO_3)_2$.[16] It is possible that the added flexibility of the propyl amine ligand could allow intramolecular H-bonds to form.

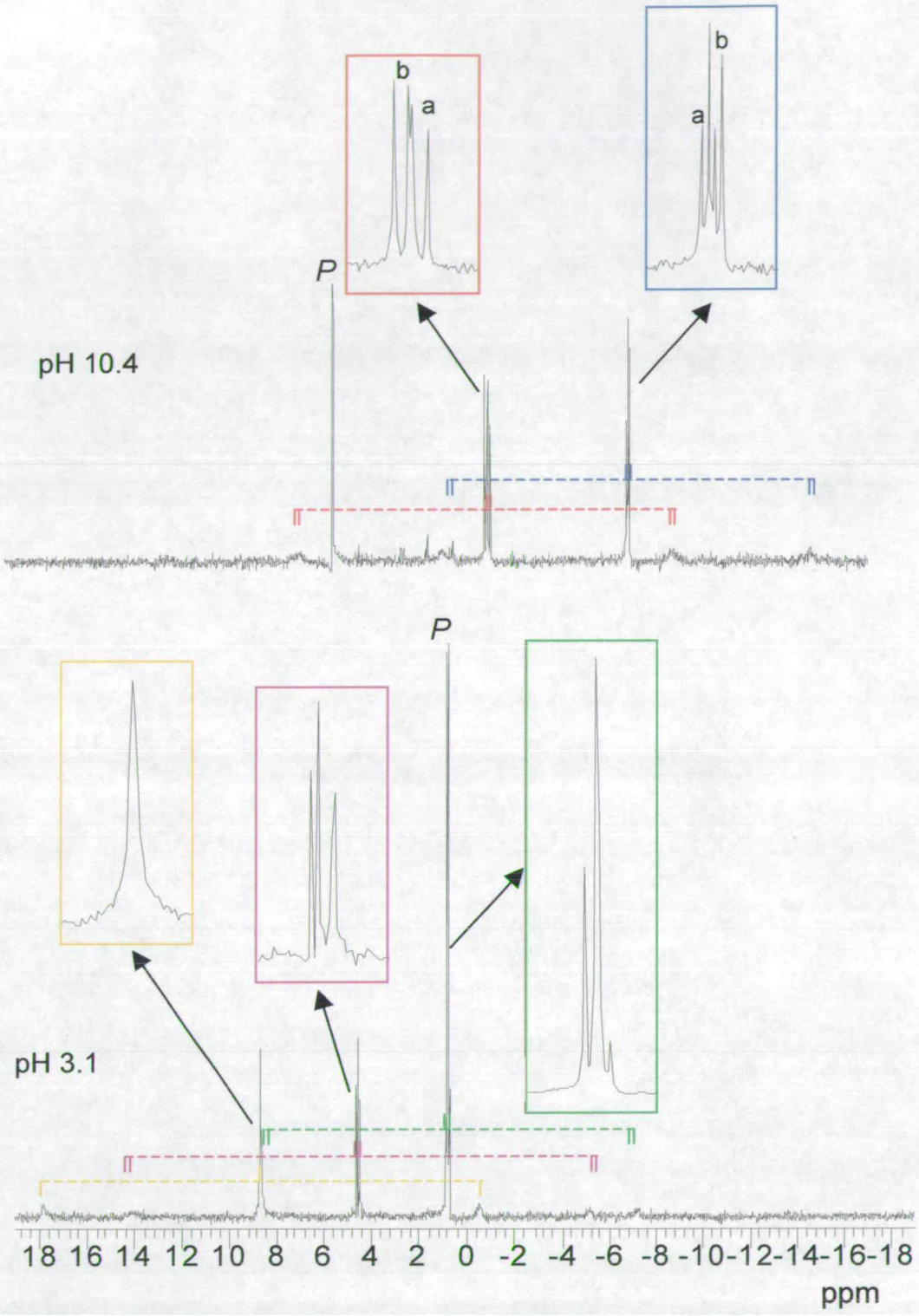

Figure 4.8 ^{31}P NMR spectra of complex **24** with 2 mole equivalents of 5′-dTMP at low and high pH values (*P* = phosphate)

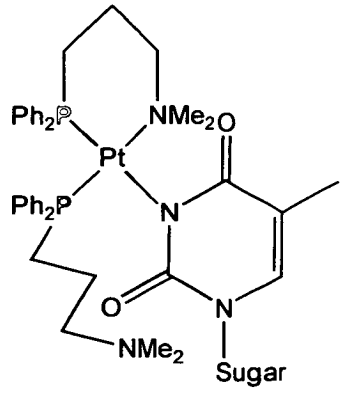

Figure 4.9 N3-bound monofunctional adduct of 5′-dTMP and complex **24** at high pH (coloured P atoms correspond to ^{31}P peaks in Figure 4.8)

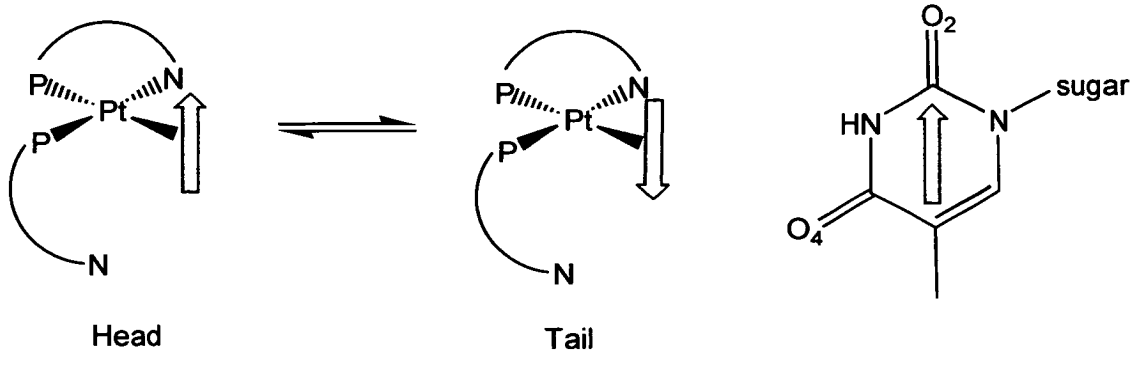

Figure 4.10 Possible head and tail isomers of N3-bound Pt-TMP species

At low pH two pairs of doublets are again observed (Figure 4.8). Again these correspond to two species, probably isomers containing inequivalent P atoms in a *cis* orientation (^2J(P-P) = 17 Hz). Each species has a downfield doublet (4.5 ppm) with ^1J(Pt-P) = 3899 Hz and an upfield doublet (0.8 ppm) with ^1J(Pt-P) = 3128 Hz, which overlaps the phosphate signal. This suggests that in each species one phosphorus atom has chloride in the *trans* position and the other phosphorus has nitrogen in the *trans* position. This is indicative of a product which is fully ring-opened and

contains TMP again bound through N3 (Figure 4.11). Ring-opening of the aminophosphine ligands is favoured at low pH due to protonation of the amine group.

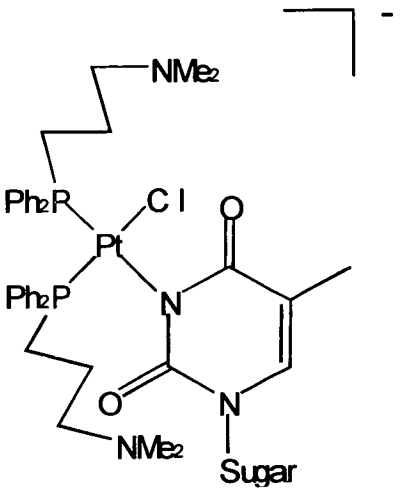

Figure 4.11 N3-bound monofunctional adduct of 5′-dTMP and complex **24** at low pH (coloured P atoms correspond to ^{31}P peaks in Figure 4.8)

The fact that TMP can bind to $[Pt\{Me_2N(CH_2)_3PPh_2\text{-}P\}_2Cl_2]$ through the N3 site over such a wide pH range is very unusual since it would be expected that the site would be protonated above pH 10.47. It is possible that the amine groups on the ligands in the complex are influential in abstracting a proton from the TMP allowing binding to occur.

In the low pH spectrum (Figure 4.8) a singlet peak at 8.5 ppm is also seen. This is likely to belong to unbound complex since at pH 3.2 only about 35% of the TMP is bound (from graph in Figure 4.3). The two P atoms are equivalent and the ^{1}J(Pt-P) coupling of 3732 Hz indicates Cl in the *trans* position as would be expected for a fully opened species at this pH.

4.2.2 High Performance Liquid Chromatography

The competitive binding of $[Pt\{Me_2N(CH_2)_3PPh_2\text{-}P\}_2Cl_2]$ (**24**) to the four nucleotides GMP, TMP, AMP and CMP was also studied by HPLC. The reverse-phase separation of the four nucleotides by the method described in Section 4.1.2 is shown in Figure 4.12 below.

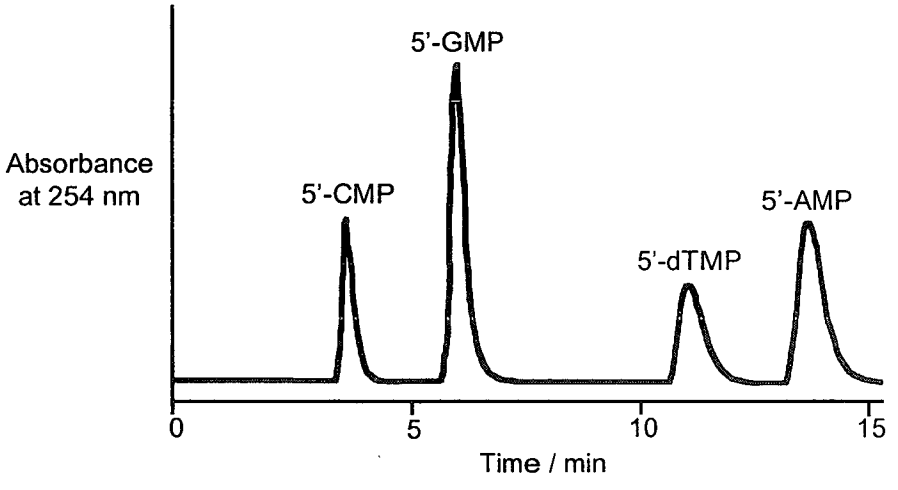

Figure 4.12 HPLC separation of nucleotides in a 1 mM sample with isocratic solvent mixture 95% I (50 mM K_2HPO_4, 2.5 mM TBAHS, pH 7), 5% II (100 mM K_2HPO_4, 2.5 mM TBAHS, diluted with 50% acetonitrile, pH 7) as described in Section 4.1.2

As described in section 4.1.2, platinum binding can be detected as a reduction in the peak area of the free nucleotide. The reaction sample was analysed at various time intervals to give an indication of the rate of reaction. A graph showing the percentage of each nucleotide bound with time is shown in Figure 4.13.

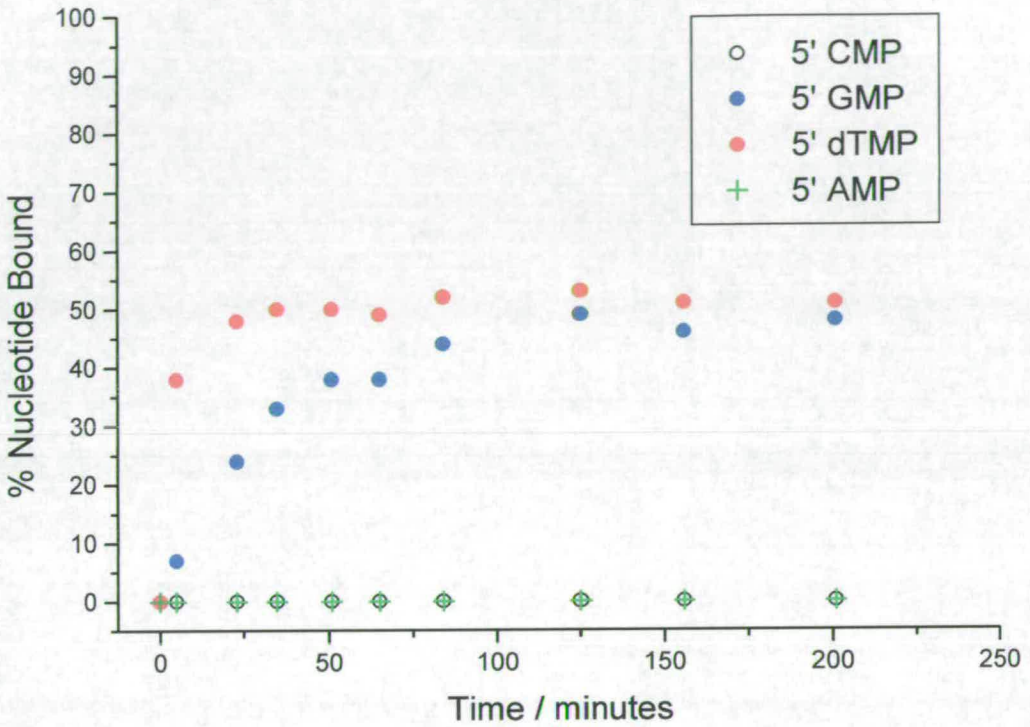

Figure 4.13 Graph showing percentage of each nucleotide bound in a competition reaction between [Pt{$Me_2N(CH_2)_3PPh_2$-*P*}$_2Cl_2$] (**24**) and equimolar amounts of all four nucleotides

It can immediately be seen from the graph that complex **24** binds neither AMP nor CMP in the presence of the other nucleotides. This is consistent with the NMR results where there were very low levels of binding observed even with the isolated nucleotides. There are two rather unexpected results from the competition reaction. Firstly that the complex appears to bind as strongly to thymine as it does to guanine both of which are bound up to about 50%. This is very unusual for platinum which tends to have a very strong preference for binding guanine residues[9] as discussed previously. Thymine binding although possible is not generally favoured in the presence of purine bases.[10] Secondly, the rate of reaction between the complex and the nucleotides is fast. There is no change in the amount of nucleotide bound after

about 25 min for TMP and after about 100 min for GMP. Again this is unusual if compared to cisplatin which undergoes relatively slow binding to nucleotides and DNA.[17] As discussed in Section 1.3.2.1 the rate determining step for cisplatin binding is hydrolysis of the complex since the dichloro form in relatively unreactive. In this complex the chloride ligands may be more labile due to the high *trans* influence of the P ligands[18], this was indicated by long Pt-Cl bond lengths in the crystal structure.[19] If the chloro complex can react directly with the nucleotides this may explain the increased rate of binding.

The method employed above for the separation of nucleotides and competitive binding studies proved not to be suitable for long term use since there was precipitation of the sample in the column which resulted in a build up of pressure. Capillary electrophoresis was therefore investigated as an alternative method of nucleotide separation.

4.2.3 Capillary Electrophoresis

The separation of the four nucleotides by the method described in Section 4.1.3 is shown in Figure 4.14 for a 100 μM sample. A reaction sample containing $[Pt\{Me_2N(CH_2)_3PPh_2\text{-}P\}_2Cl_2]$ **(24)** incubated with equimolar quantities of the nucleotides was analysed and the amount of each nucleotide bound to the complex determined by measurement of the peak area for the free nucleotide remaining. The electropherogram showing the analysis of binding to complex **24** is also shown in Figure 4.14.

The figure shows clearly that there has been no change in the peaks for AMP and CMP upon reaction with the complex. This is the same as determined in the HPLC experiment. The peaks for both GMP and dTMP have decreased in intensity showing that these nucleotides are bound to platinum. Measurement of the peak areas show that 60% of the GMP and 59% of the dTMP was bound. This is consistent with the HPLC results confirming that the complex shows high selectivity

for thymine binding, even to the same extent as the more typical guanine binding. In the electropherogram for the platinated sample a new peak appeared which eluted before the free nucleotides (10.2 min). This is likely to correspond to the platinum bound species since the incorporation of a Pt^{2+} will increase the charge on the nucleotide and hence increase its electrophoretic mobility. Thus platinated species should pass the UV detector before the free nucleotides.

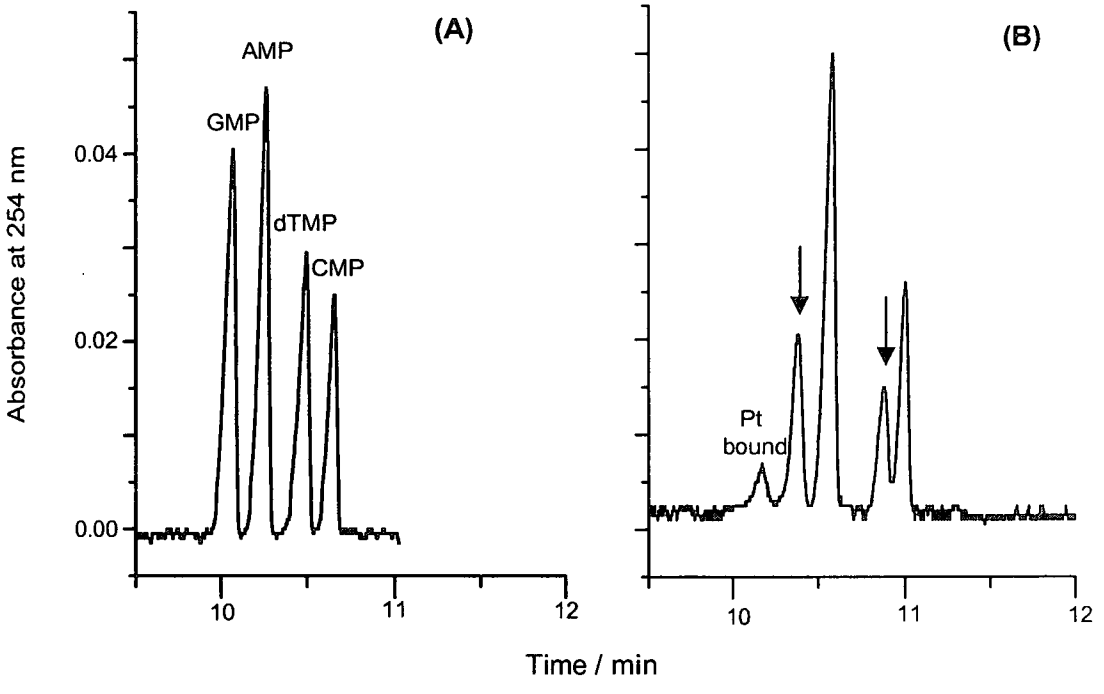

Figure 4.14 Electropherograms showing: (**A**) four nucleotides at 100 μM concentration, (**B**) four nucleotides with $[Pt\{Me_2N(CH_2)_3PPh_2\text{-}P\}_2Cl_2]$ (**24**), all at 100 μM concentration, pH 7.1, after incubation at 310 K for 12 hours.

4.2.4 Electrospray Ionisation Mass Spectrometry

4.2.4.1 Guanosine 5'-Monophosphate

A mass spectrum showing the products of the reaction between $[Pt\{Me_2N(CH_2)_3PPh_2\text{-}P\}_2Cl_2]$ (**24**) and 5'-GMP is shown in Figure 4.15. A

monofunctional adduct containing Pt with two DMDPPA ligands and one GMP is clearly seen at 1099 m/z (calculated m/z for $PtC_{44}H_{56}N_7O_8P_3$ = 1099). The assignment of this species was confirmed by the calculation of an isotope model for the corresponding compound using the Mass Lynx (V 2.3) program. This major peak is accompanied by a smaller peak at 1121 corresponding to the same species with an attached Na atom. This is because the nucleotides were all used as sodium salts, as purchased. If the resolution of the spectrum is reduced a very small set of peaks can be seen corresponding to the bifunctional adduct (two GMP bound) with a mass of 1461 (calculated m/z for $PtC_{54}H_{68}N_{12}O_{16}P_4$ = 1461). Again additional peaks can be seen in a series at 1484, 1506 and 1528 corresponding to the species with increasing numbers of sodium ions attached. This confirms the ^1H NMR results which suggested that complex **24** was capable of forming bifunctional adducts. The number of bifunctional molecules detected is very small in comparison to the number of monofunctional. It must be noted however that ESI-MS is not a quantitative technique since the number of molecules detected depends on the ability of the compound to ionise.

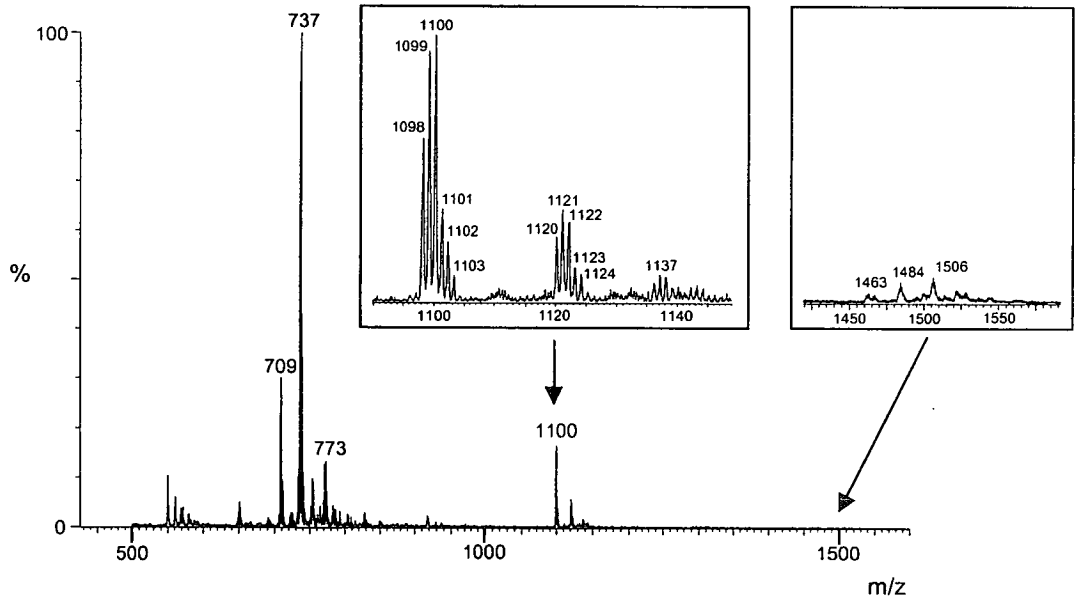

Figure 4.15 ESI-MS spectrum of $[Pt\{Me_2N(CH_2)_3PPh_2\text{-}P\}_2Cl_2]$ (**24**) after reaction with two equivalents of 5'-GMP at pH 7.3 (expansion shows isotope pattern for monofunctional and bifunctional adducts more clearly, using lower resolution)

4.2.4.2 Adenosine 5'-Monophosphate and Cytidine 5'-Monophosphate

The analysis of the reactions between complex **24** and both 5'-AMP and 5'-CMP yielded no observable platinated species. This correlates with the lack of binding observed by ^{1}H NMR.

4.2.4.3 Deoxythymidine 5'-Monophosphate

A mass spectrum showing products of the reaction between complex **24** and 5'-dTMP is shown in Figure 4.16. Again a monofunctional adduct, with one bound TMP and two DMDPPA ligands, can clearly be seen at m/z 1057 (calculated m/z for $PtC_{44}H_{56}N_4O_8P_3$ = 1057). An additional peak for the species with one Na^+ bound was also observed at 1080 and also a peak at 1096 corresponding to a monofunctional species with one coordinated chloride remaining. No bifunctional adducts, (calculated m/z for $PtC_{54}H_{68}N_6O_{16}P_4$ = 1376), can be observed even at low resolution. This corresponds to the ^{1}H NMR results which suggested that complex **24** formed only monofunctional complexes with 5'-dTMP.

4.2.4.4 Competition Reactions

As in the HPLC and CE reactions, complex **24** was incubated with all four nucleotides in equimolar amounts and the mixture analysed by ESI-MS. From the region where monofunctional adducts should be observed, the only peaks seen were those corresponding to the GMP and TMP adducts already described. This confirms that GMP and TMP binding are preferred over AMP and CMP.

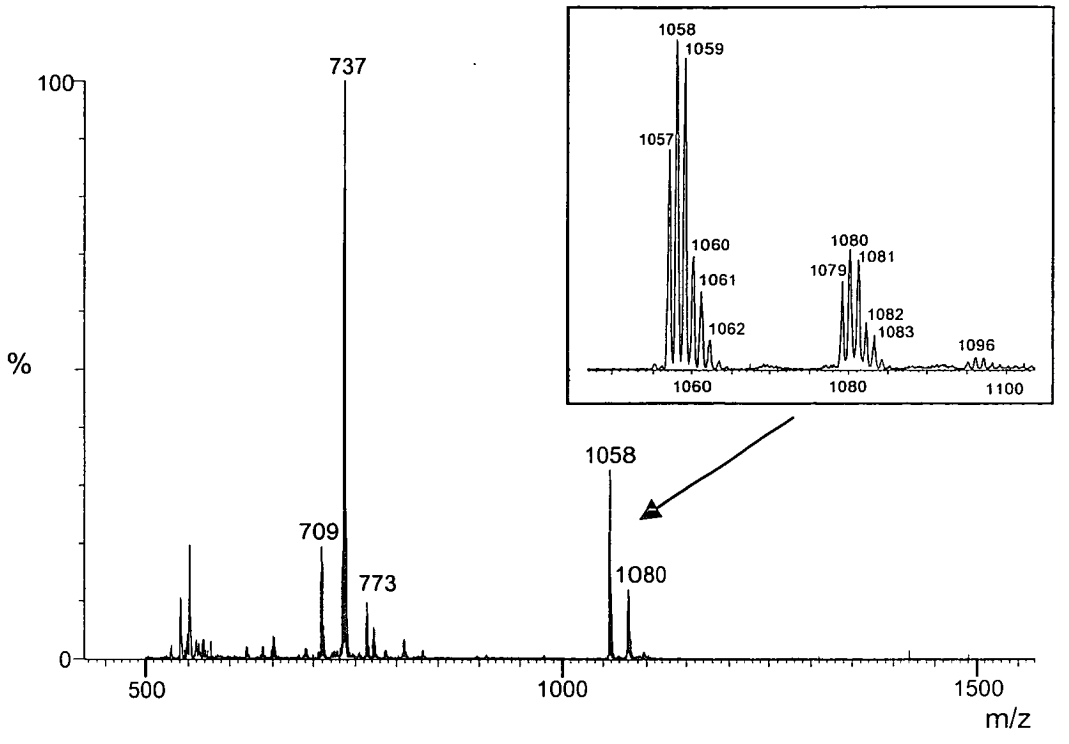

Figure 4.16 ESI-MS spectrum of [Pt{$Me_2N(CH_2)_3PPh_2$-*P*}$_2Cl_2$] (**24**) after reaction with two equivalents of 5'-dTMP at pH 7.2 (expansion shows isotope pattern for monofunctional adducts)

4.3 Reactions of [Pt{^{t}Bu(H)N(CH$_2$)$_3$PPh$_2$-*P*}$_2$Cl$_2$] (27)

4.3.1 NMR Spectroscopy

4.3.1.1 Guanosine 5'-Monophosphate

1:1 (Nucleotide:Complex) Reaction

As for the previous complex, [Pt{^{t}Bu(H)N(CH$_2$)$_3$PPh$_2$-*P*}$_2$Cl$_2$] (**27**) and GMP were initially reacted in a 1:1 ratio.

In the ^{1}H NMR spectrum, the resonances for all the protons of free 5'-GMP had completely disappeared, showing all the nucleotide had bound to Pt. Again new peaks appeared with upfield shifts from the free GMP signals.

2:1 (Nucleotide:Complex) Reaction

Some free GMP peaks were observed with new peaks for Pt-bound products shifted upfield. The ^{1}H spectrum of the 2:1 reaction is shown in Figure 4.17. As for complex **24**, the H1' signal (d, 5.9 ppm) was used to determine the amount of GMP bound to platinum in the reaction.

As shown in the expansion in Figure 4.17, the resulting spectrum from the reaction of [Pt{^{t}Bu(H)N(CH$_2$)$_3$PPh$_2$-*P*}$_2$Cl$_2$] (**27**) and GMP is less complicated than the spectrum from the analogous reaction of complex **24**. Only two major adducts are formed with H1' doublets overlapping at 5.74 ppm (**a**) and 5.72 ppm (**b**). All the doublets have a coupling of 6 Hz, the same coupling as in free GMP. Measurement of the integrals of the free and bound GMP H1' peaks showed that 85.5% (1.7 mole equivalents) of the GMP present was bound to Pt in the reaction.

As was the case for complex **24**, [Pt{^{t}Bu(H)N(CH$_2$)$_3$PPh$_2$-*P*}$_2$Cl$_2$] (**27**) must form some bifunctional adducts in the reaction with GMP since more than one mole equivalent of the nucleotide is bound. If it is assumed that all of the complex binds nucleotide (since it exists in the ring-opened form with labile chloride ligands) then

70% of the complex must have formed bifunctional adducts and 30% must have formed monofunctional adducts. This would suggest that the two predominant Pt-bound species identified from their H1' shifts in Figure 4.17 are bifunctional adducts. Again, these could correspond to the *head-head* and *head-tail* isomers[15] of the bifunctional adduct as discussed in Section 2.2.1.2.

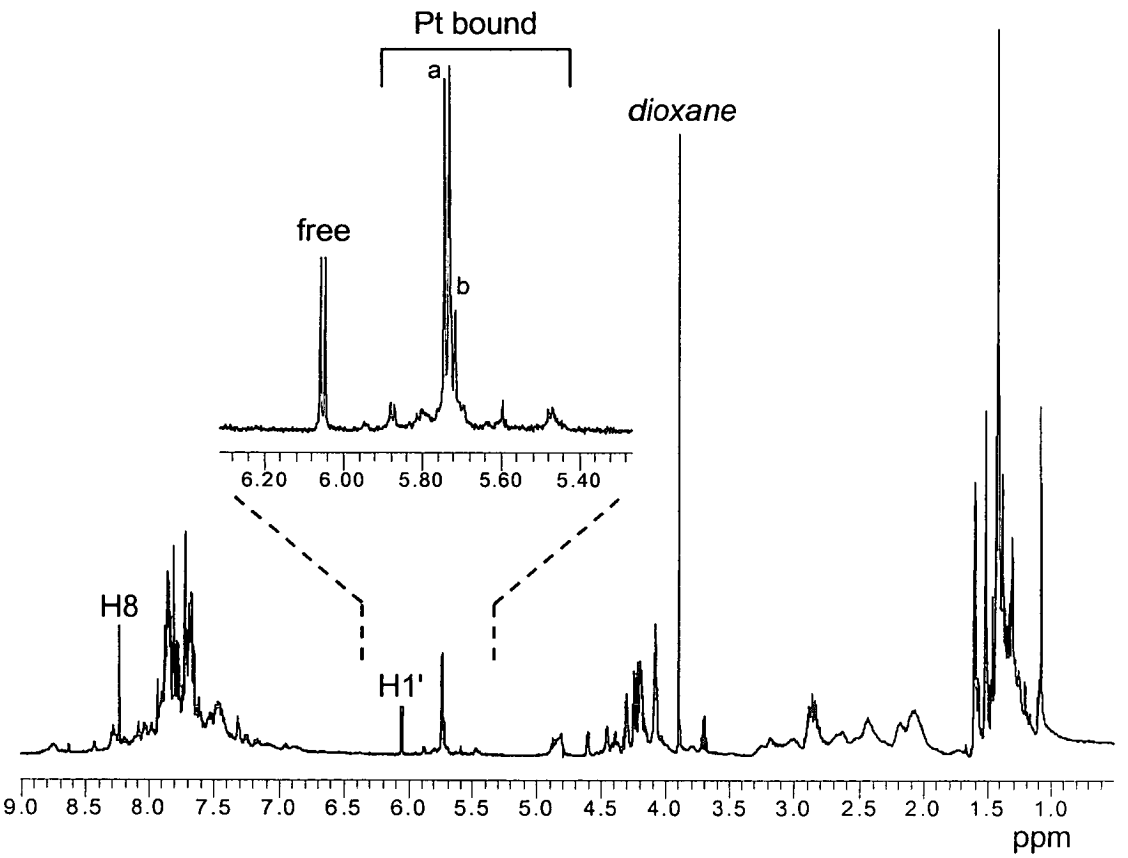

Figure 4.17 ^{1}H spectrum of [Pt{^{t}Bu(H)N(CH$_2$)$_3$PPh$_2$-*P*}$_2$Cl$_2$] (**27**) with two mole equivalents of 5'-GMP (expansion shows H1' resonances for free and bound 5'-GMP)

Again the pH dependence of GMP binding to [Pt{^{t}Bu(H)N(CH$_2$)$_3$PPh$_2$-*P*}$_2$Cl$_2$] (**27**) was investigated by recording spectra at various pH values and determining the amount of nucleotide bound from the integrals of free and bound H1' peaks. The results are shown in Figure 4.18. As was shown for complex **24**, there is little

change in the amount of binding with pH. The profile is very similar for the two complexes and again the two equivalents of GMP are never completely bound suggesting that there is a Pt species present in solution that is not capable of binding a second GMP to form a bifunctional adduct.

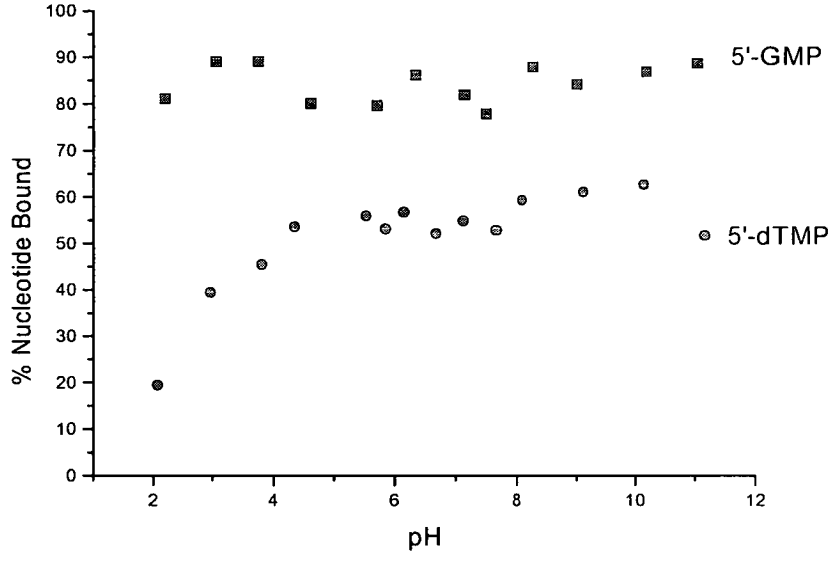

Figure 4.18 Graph showing the percentage of 5'-GMP and 5'-dTMP bound to $[Pt\{^tBu(H)N(CH_2)_3PPh_2\text{-}P\}_2Cl_2]$ (**27**) in separate reactions, with 2:1 ratio, at various pH values

4.3.1.2 Adenosine 5'-Monophosphate

As for 5'-GMP, the reaction between $[Pt\{^tBu(H)N(CH_2)_3PPh_2\text{-}P\}_2Cl_2]$ (**27**) and 5'-AMP was initally carried out with one mole equivalent of the nucleotide. Strong resonances for free 5'-AMP remained after completion of the reaction (Figure 4.19). Six bound species can be identified from the H1' signals as shown in the expansion in Figure 4.19 (6.07 – 5.61 ppm). Integration of these peaks showed that 33% of the AMP was bound during the reaction. This is higher than the amount of binding to

complex **24** (Section 4.2.1.2) but is still lower than would be expected due to the high electron density of the N7 binding site, usually favourable to Pt binding.

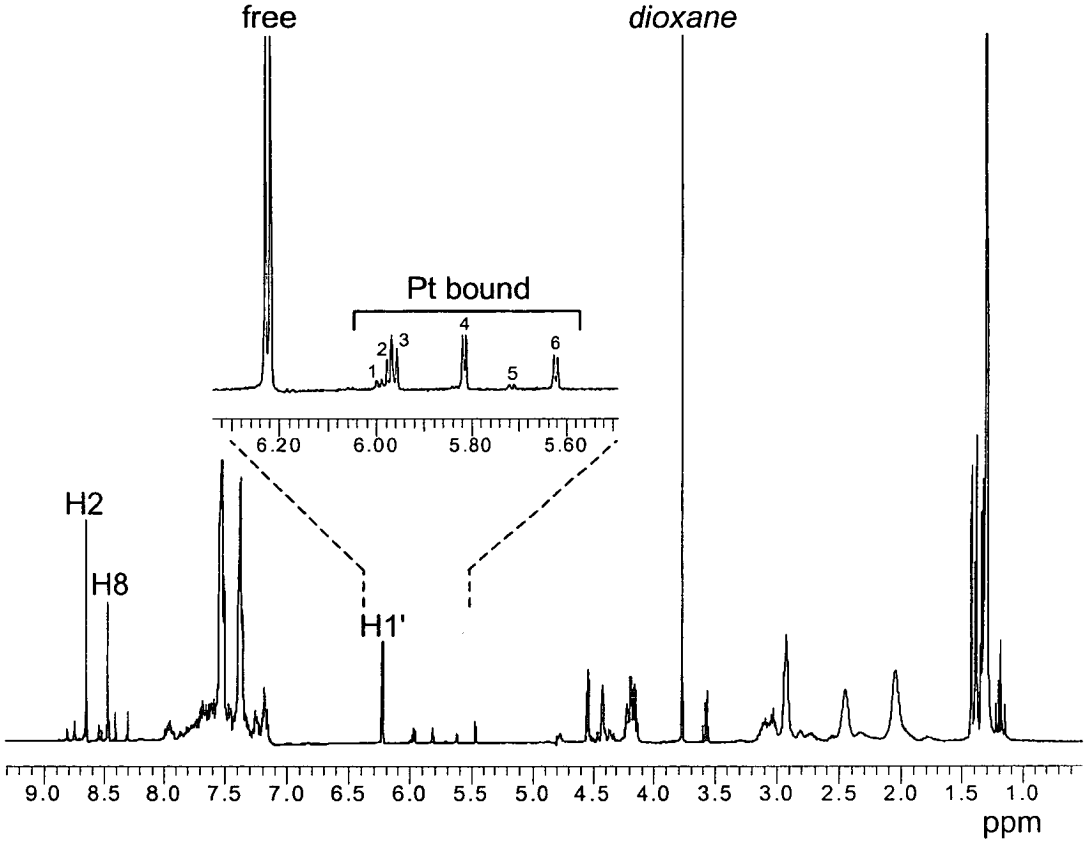

Figure 4.19 ^{1}H spectrum of [Pt{^{t}Bu(H)N(CH$_2$)$_3$PPh$_2$-*P*}$_2$Cl$_2$] (**27**) with two mole equivalents of 5'-AMP (expansion shows H1' resonances for free and bound 5'-AMP

4.3.1.3 Cytidine 5'-Monophosphate

The reaction was carried out as described for 5'-GMP, between 5'-CMP and [Pt{^{t}Bu(H)N(CH$_2$)$_3$PPh$_2$-*P*}$_2$Cl$_2$] (**27**) in a 1:1 ratio. Contrary to the spectrum obtained for complex **24** and CMP, the resulting spectrum showed new resonances for Pt-bound species with upfield shifts. The spectrum is shown in Figure 4.20.

Two distinct species can be observed by studying the H1' doublet and H5 multiplet. Species **a** and **b** are present in the ratio 1:0.9. Integration of these signals for the free and bound species shows that 56% of the CMP was bound in the reaction. This suggests that [Pt{^{t}Bu(H)N$(CH_2)_3PPh_2$-*P*}$_2Cl_2$] (**27**) can form monofunctional adducts with CMP unlike complex **24** with showed no binding under the same conditions.

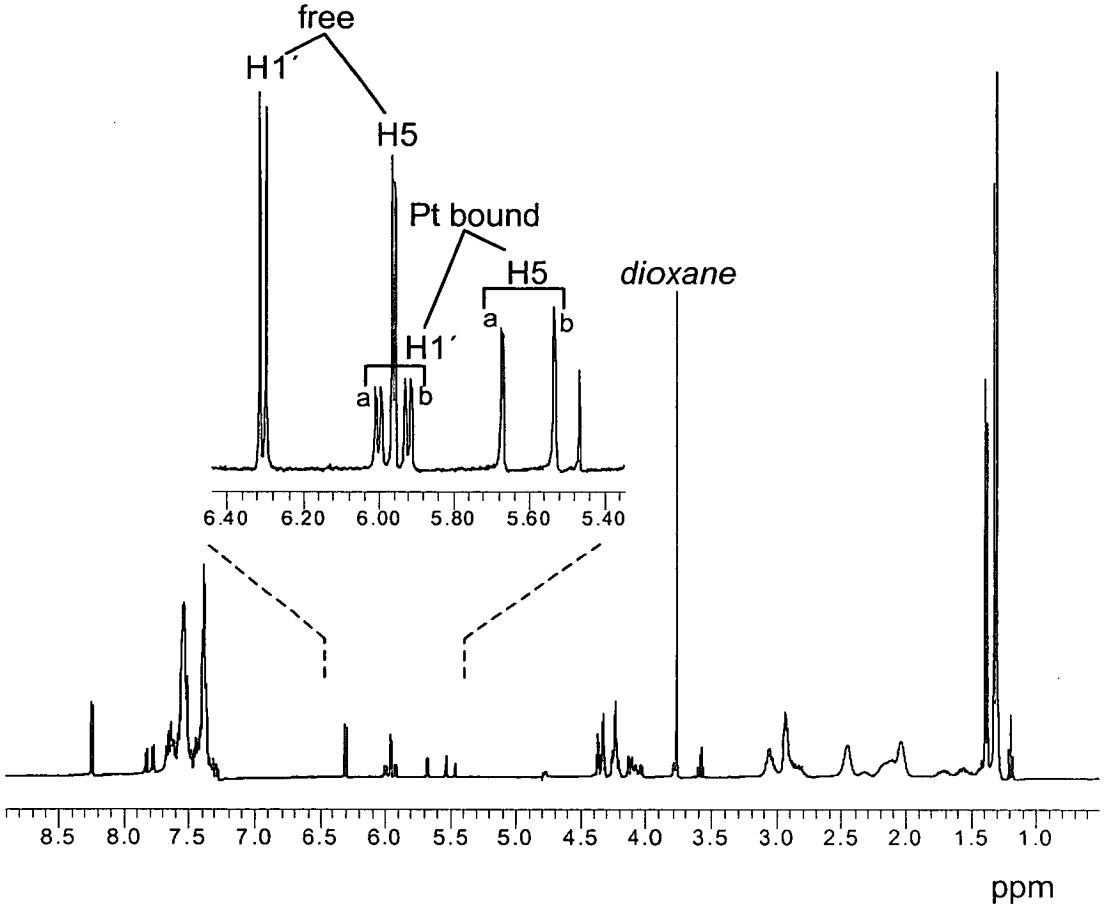

Figure 4.20 ^{1}H spectrum of [Pt{^{t}Bu(H)N$(CH_2)_3PPh_2$-*P*}$_2Cl_2$] (**27**) with two mole equivalents of 5'-CMP (expansion shows H1' and H5 resonances for free and bound 5'-CMP)

4.3.1.4 Deoxythymidine 5'-Monophosphate

1:1 (Nucleotide:Complex) Reaction

In the ^{1}H NMR spectrum of $[Pt\{^tBu(H)N(CH_2)_3PPh_2\text{-}P\}_2Cl_2]$ (**27**) with 1 mole equivalent of 5'-dTMP present the resonances for all the protons in free 5'-dTMP have completely disappeared, showing that all the nucleotide is bound.

2:1 (Nucleotide:Complex) Reaction

In the reaction with two mole equivalents of 5'-dTMP, some free dTMP peaks are observed with new peaks for Pt-bound species shifted upfield. The ^{1}H spectrum of the 2:1 reaction is shown in Figure 4.21. Integration of the H1' peak for free dTMP (6.34 ppm) and the overlapping H1' peaks for the two bound species (**a**: 6.16 ppm, **b**: 6.15 ppm) showed that 57% of the TMP is bound to Pt. Due to the overlap of the H1' signals the ratio of the two species cannot be determined, however the same pattern can also be observed for the methyl signal (1.93 ppm) with two bound species (1.70 and 1.67 ppm). Here the ratio of **a**:**b** can be measured as 0.9:1.

As seen from the results above, virtually all the TMP was bound in the 1:1 reaction suggesting that complex **27** is capable of forming monofunctional adducts with 5'-dTMP as was seen for 5'-GMP. In contrast, when the reaction ratio was increased to 2:1 nearly half of the 5'-dTMP remained free in solution suggesting that very few bifunctional adducts were formed.

The effect of pH on the binding of $[Pt\{^tBu(H)N(CH_2)_3PPh_2\text{-}P\}_2Cl_2]$ (**27**) to thymine was also investigated by means of a pH titration. The percentage of TMP bound at each pH value was determined by measuring the free and bound H1' integrals. The results are show in Figure 4.18. The graph of pH dependence of nucleotide binding to complex **27** looks very similar to that for complex **24**. Binding of 5'-dTMP seems to be restricted to the formation of monofunctional adducts in comparison to that of 5'-GMP which allows formation of a proportion of bifunctional adducts. Again the

binding to thymine occurs over an unusually wide pH range with no reduction in binding occurring in the range 4-12. Below pH 4 the binding begins to decrease, but even as low as pH 2, 10% of the TMP remains bound.

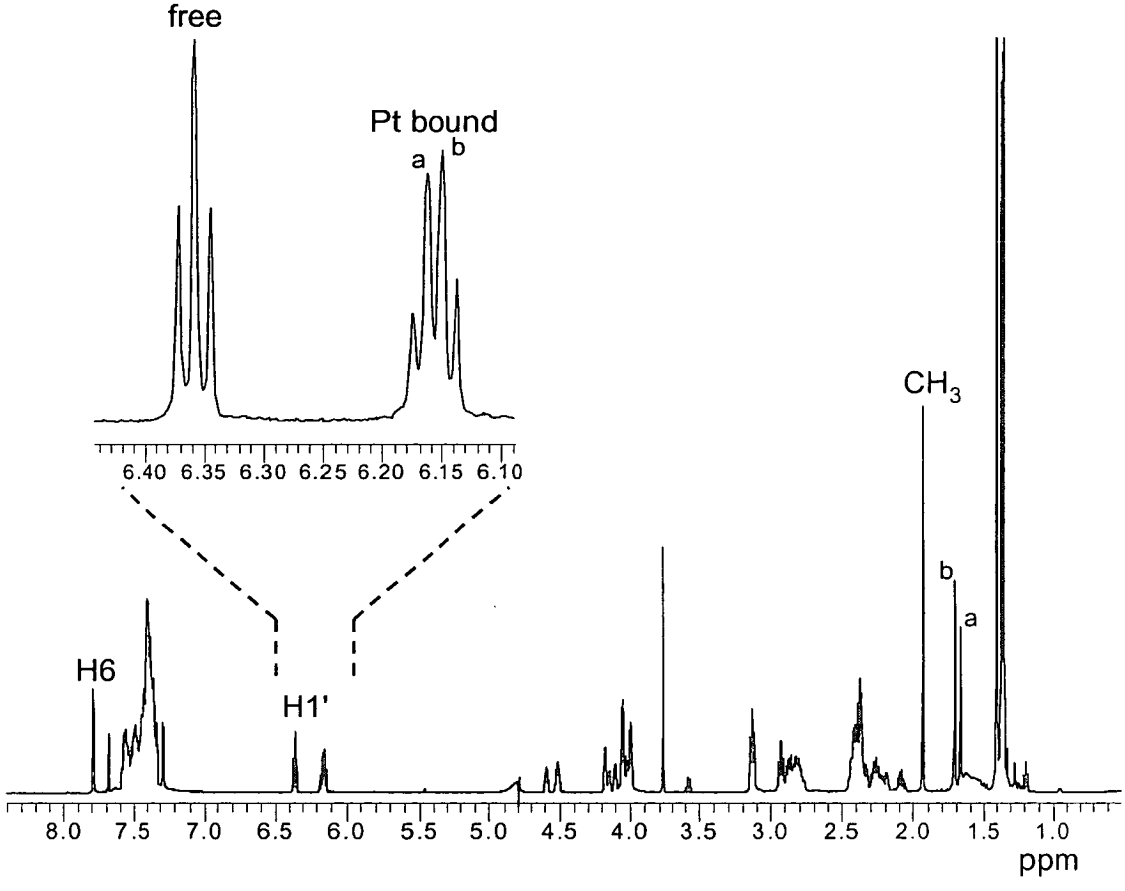

Figure 4.21 ^{1}H spectrum of $[Pt\{^{t}Bu(H)N(CH_2)_3PPh_2\text{-}P\}_2Cl_2]$ (**27**) with two mole equivalents of 5'-dTMP (expansion shows H1' resonances for free and bound 5'-dTMP)

The pH titration is shown in Figure 4.22 and shows a mixture of bound species in the region pH 6-9 but, as for complex **24**, at low and high pH values the spectra are simpler with only two peaks for bound species **a** and **b**, again probably isomers.

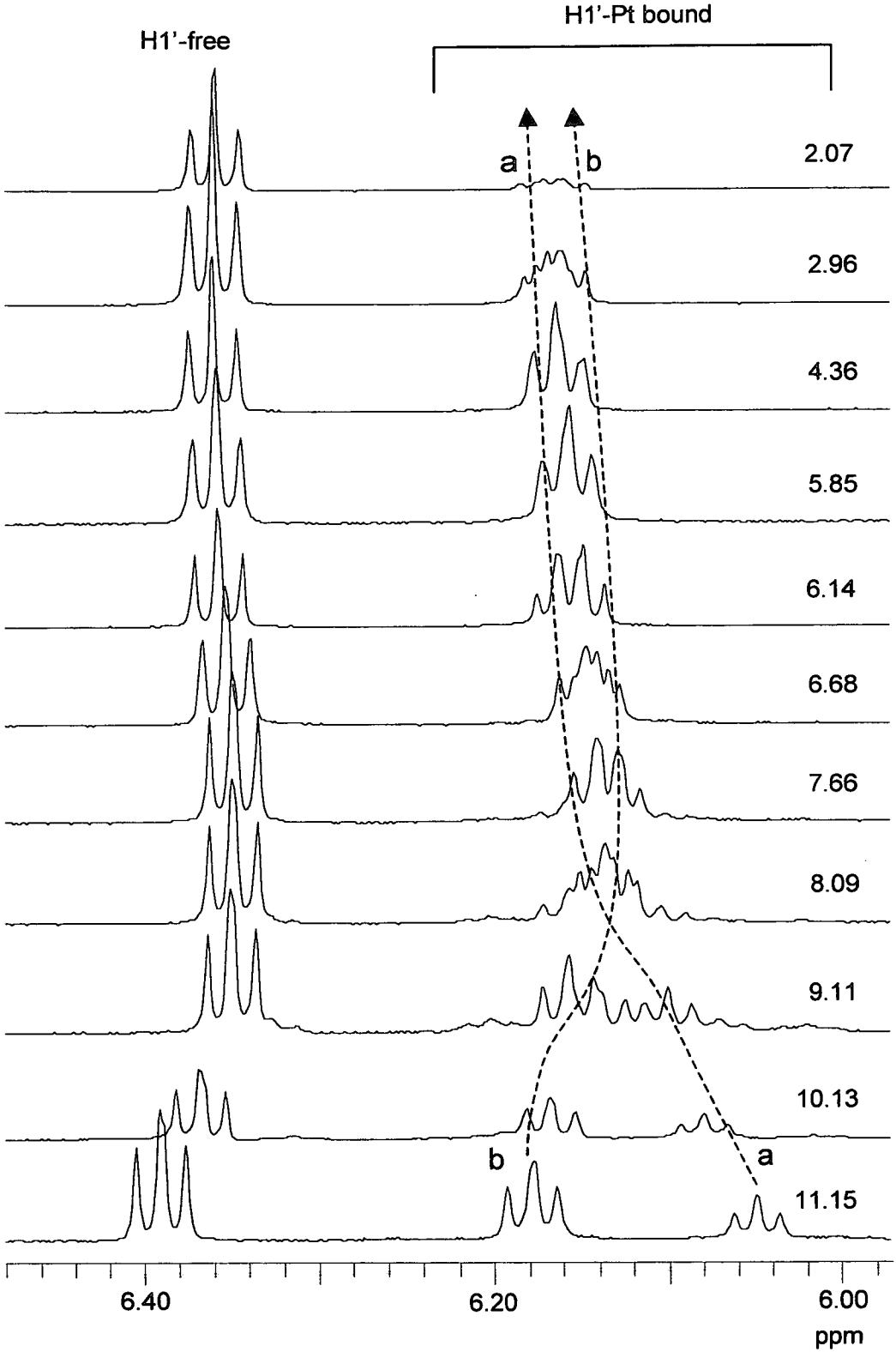

Figure 4.22 ^{1}H spectra showing H1' signals for free and Pt-bound 5'-dTMP on reaction with $[Pt\{^{t}Bu(H)N(CH_2)_3PPh_2\text{-}P\}_2Cl_2]$ (27) at various pH values

The chemical shift of H1' in the two bound species shows the same pattern as those for complex **24**. Species **b** shifts upfield with decreasing pH, following the shift of the free TMP. Species **a**, however, shifts downfield opposite to free TMP.

In order to further identify the nature of the bound species, ^{31}P NMR spectra were recorded at both low and high pH (Figure 4.23).

At high pH two pairs of overlapping doublets with ^{195}Pt satellites were observed at 2.0 ppm and -0.8 ppm. As described for complex **24**, these doublets can be attributed to the two bound species **a** and **b** observed in the ^{1}H NMR spectrum. Each species contains two inequivalent P atoms, leading to two doublets with ^{2}J(P-P) = 17 Hz, one at each chemical shift. For both species the ^{1}J(Pt-P) coupling of the downfield doublet, at 2.0 ppm, is 3474 Hz and the coupling of the upfield doublet, at – 0.8 ppm, is 3452 Hz. This indicates that in both species the two P atoms have N atoms in the *trans* position. Again this would be consistent with N3 binding of TMP at one site on Pt with one chelate ring-closed ligand, as shown in Figure 4.24. The two distinct species **a** and **b** would then be attributed to two head and tail isomers formed by restriction of rotation of the Pt-N3 bond. Hydrogen bonding between O on the TMP and the ring-opened ligand could be responsible for fixing the conformations of these isomers.[16]

At low pH, two pairs of ^{31}P doublets were observed at 4.3 ppm and 0.2 ppm. Again these correspond to two species, probably isomers containing inequivalent P atoms in a *cis* orientation (^{2}J(P-P) = 17 Hz). In each species the downfield doublet (4.3 ppm) has a ^{1}J(Pt-P) coupling of 3911 Hz indicating chloride as the *trans* ligand whilst the upfield doublet (0.2 ppm) has a coupling of 3235 Hz indicating N in the *trans* position.. This is consistent with a species in which TMP is N3 bound and both aminophosphine ligands are ring-opened with chloride bound at the vacant site (Figure 4.23). The remaining singlet peak at 8.4 ppm is likely to be due to some unbound, fully-ring-opened complex remaining (Figure 4.24). As seen in Figure

4.18 only about 40% of the TMP is bound at this pH. The ^{1}J(Pt-P) for this species is 3733 Hz showing Cl in the *trans* position.

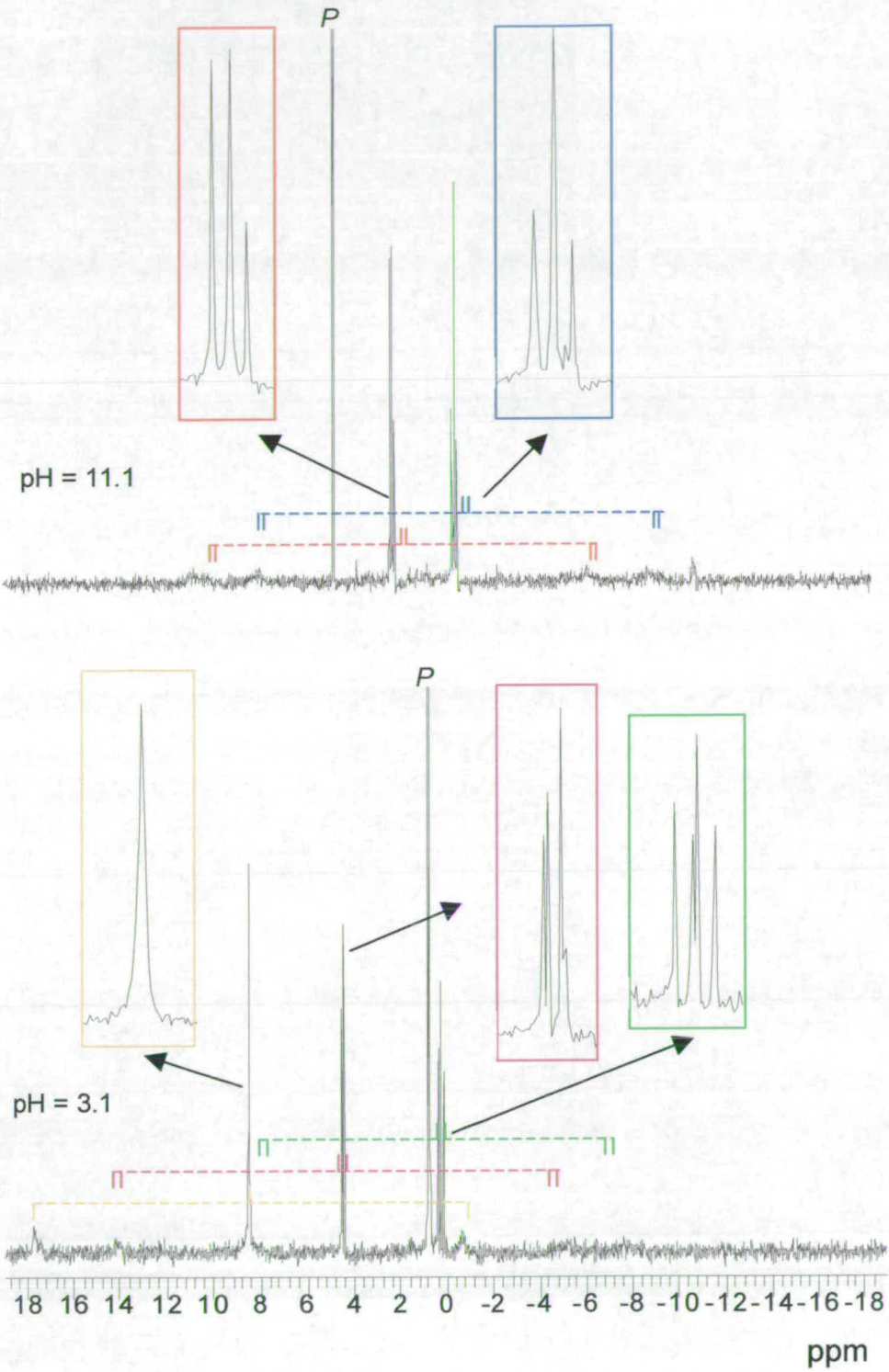

Figure 4.23 ^{31}P spectra of [Pt{^{t}Bu(H)N(CH$_2$)$_3$PPh$_2$-*P*}$_2$Cl$_2$] (**27**) with two mole equivalents of 5'-dTMP at low and high pH (*P* = phosphate)

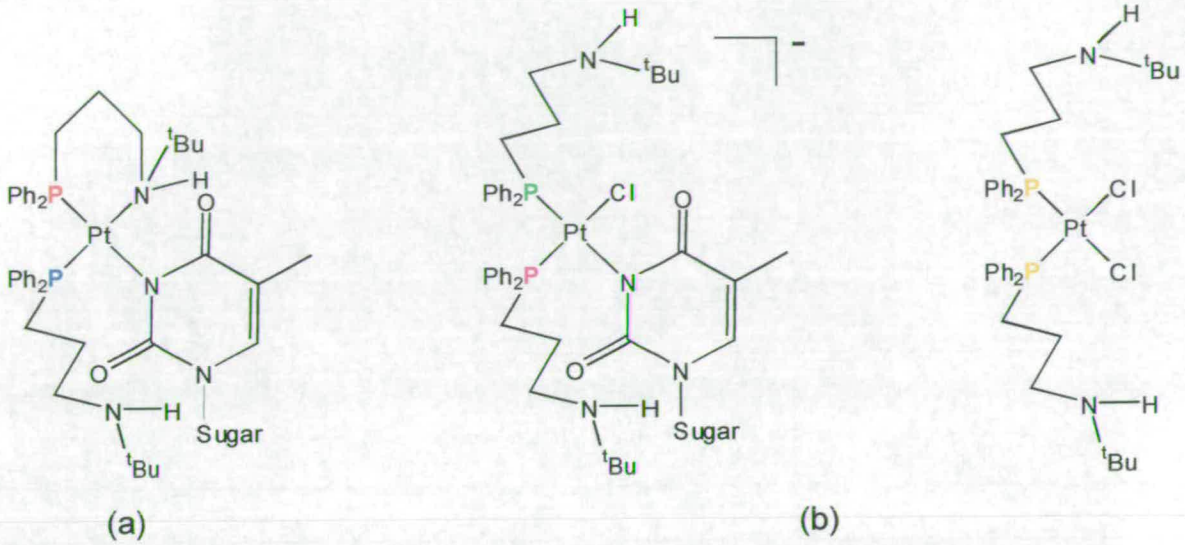

Figure 4.24 (a) N3- bound monofunctional adduct of 5'-dTMP and complex **27** at high pH, (b) N3- bound monofunctional adduct of 5'-dTMP and complex **27** and unbound fully ring-opened species at low pH (coloured P atoms correspond to ^{31}P NMR peaks in Figure 4.23)

This again demonstrates the unusual N3 binding of Pt to TMP at very low pH values well below the pK_a value for the N3 site on the nucleotide.

4.3.2 Capillary Electrophoresis

The method was used as described for complex **24** (section 4.2.3) with equimolar amounts of [Pt{^{t}Bu(H)N(CH$_2$)$_3$PPh$_2$-*P*}$_2$Cl$_2$] (**27**) and all four nucleotides incubated at physiological pH for 12 hours. The sample was then analysed and the amount of each nucleotide bound was determined from the decrease in peak area of the free nucleotides. The analysis of the reaction and a control separation with no complex present are shown in Figure 4.25.

The analysis showed that 85% of the GMP was bound, 46% of the dTMP, 20% of the AMP and 18% of the CMP. It is clear that complex **27** is much less selective in the binding of nucleotides than complex **24**. The binding of TMP is no longer to the

same extent as GMP and the more usual platinum target guanine shows the most binding. The binding of AMP is to be expected due to its favourable N7 site but the extent of this binding is low and is of the same order as CMP which showed no binding to complex **24**.

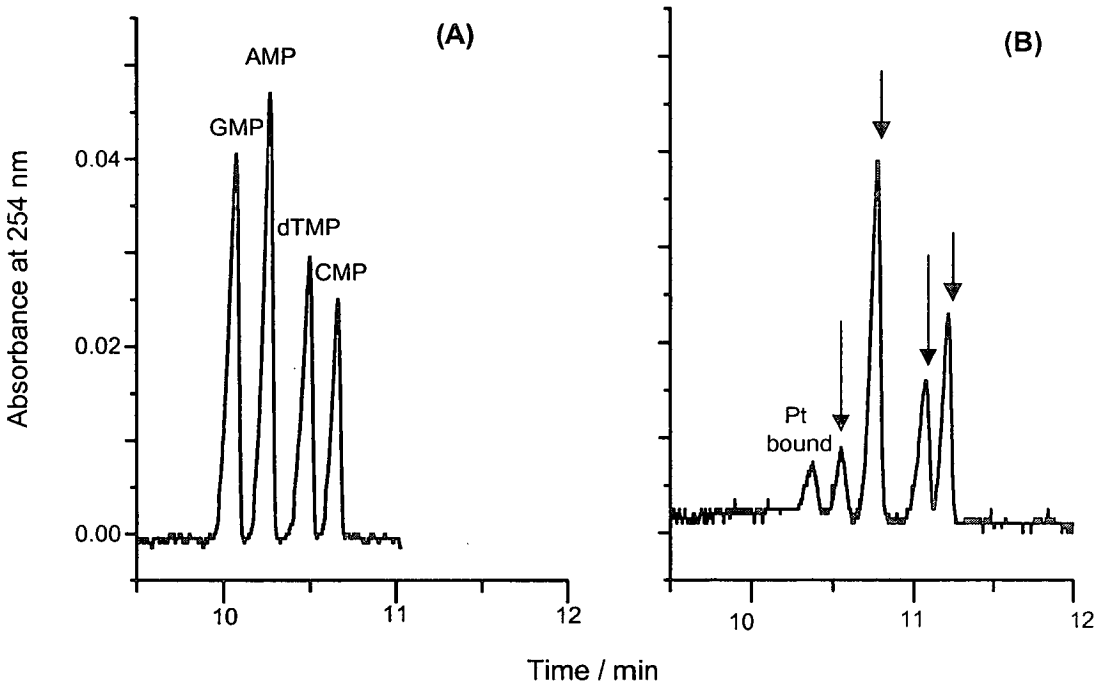

Figure 4.25 Electropherograms showing: (**A**) four nucleotides at 100 μM concentration, (**B**) four nucleotides with [Pt{^{t}Bu(H)N(CH$_2$)$_3$PPh$_2$-*P*}$_2$Cl$_2$] (**27**), all at 100 μM concentration, pH 7.1, after incubation at 310 K for 12 hours.

4.3.3 Electrospray Ionisation Mass Spectrometry

4.3.3.1 Guanosine 5'-Monophosphate

The electrospray ionisation mass spectrum of the reaction between $[Pt\{^tBu(H)N(CH_2)_3PPh_2\text{-}P\}_2Cl_2]$ (**27**) and 5'-GMP was recorded as described in Section 4.1.4 and is shown in Figure 4.26.

A monofunctional adduct containing Pt with two BDPPA ligands and one GMP is seen at 1154 m/z (calculated m/z for $PtC_{48}H_{64}N_7O_8P_3$ = 1155). This is accompanied by peaks at 1177 and 1193 corresponding to the monofunctional adduct with Na and Cl bound, respectively. When the spectrum was recorded at a lower resolution, a smaller peak for the bifunctional adduct was observed at 1516, (calculated m/z for $PtC_{58}H_{76}N_{12}O_{16}P_4$ = 1516), along with a series of peaks for the same species with 1, 2 and 3 sodium ions. These assignments were confirmed by comparing the isotope models for the predicted structures using the Mass Lynx program. The detection of bifunctional species confirms the ^1H NMR results suggesting more than one GMP was bound per platinum.

It can also be seen in the ESI mass spectra in Figure 4.26 for complex **27** that the predominant peak for the unbound complex occurs at 792 and not 864 (calculated m/z for $PtC_{38}H_{52}N_2P_2Cl_2$ = 864) as expected. From this it can be deduced that either this complex also undergoes chelate ring-closing in aqueous solution or the chloride ligands are lost under the ionisation conditions. This peak is also observed in all the following spectra for complex **27**.

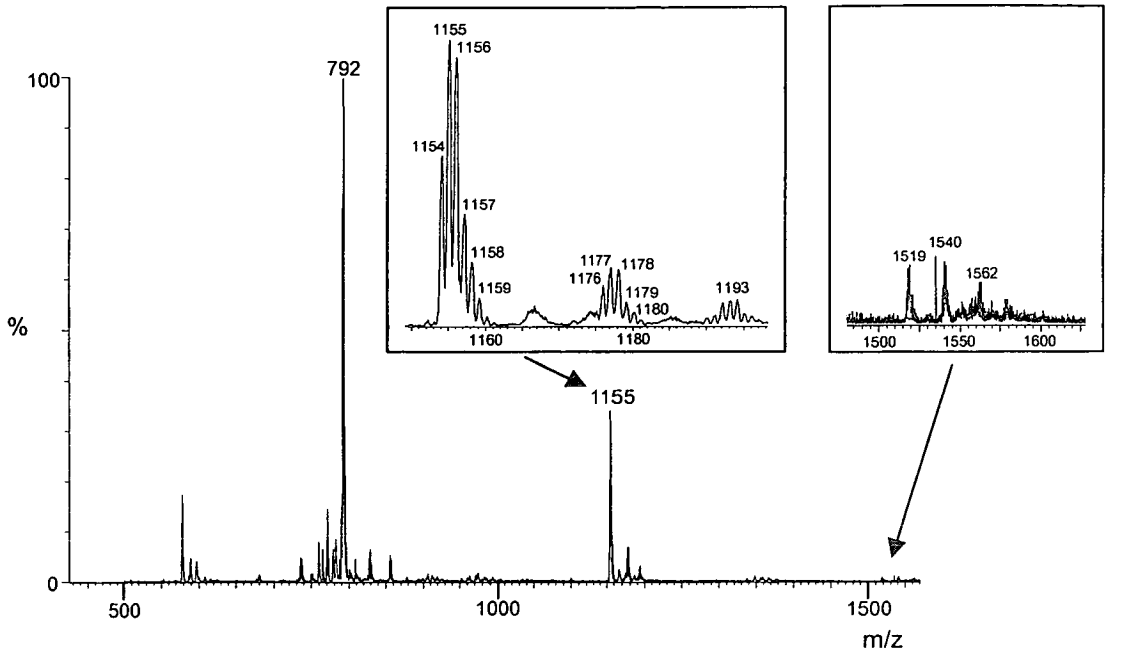

Figure 4.26 ESI-MS spectrum of[Pt{^{t}Bu(H)N$(CH_2)_3PPh_2$-*P*}$_2Cl_2$] (**27**) after reaction with two equivalents of 5'-GMP at pH 7.3 (expansion shows isotope pattern for monofunctional and bifunctional adducts)

4.3.3.2 Adenosine 5'-Monophosphate

The analysis of the ESI-MS spectra for the reaction between [Pt{^{t}Bu(H)N$(CH_2)_3PPh_2$-*P*}$_2Cl_2$] (**27**) and 5'-AMP showed the formation of monofunctional adducts which were not observed for complex **24** (Figure 4.27). The adduct is seen at m/z 1139 with additional peaks for adducts with Na and chloride bound (calculated m/z for $PtC_{48}H_{64}N_7O_7P_3$ = 1139). No bifunctional adducts, (calculated m/z for $PtC_{58}H_{76}N_{12}O_{14}P_4$ = 1484), were observed which again corresponds to the binding pattern observed by ^{1}H NMR.

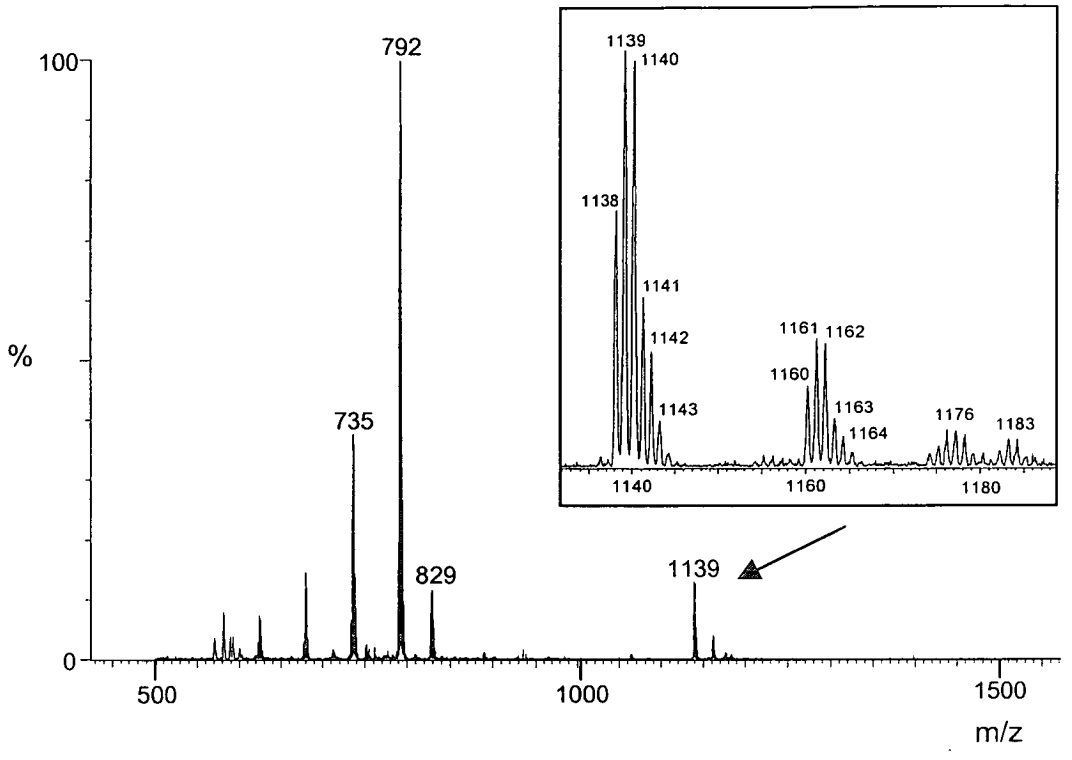

Figure 4.27 ESI-MS spectrum of [Pt{^{t}Bu(H)N$(CH_2)_3PPh_2$-*P*}$_2Cl_2$] (**27**) after reaction with two equivalents of 5'-AMP at pH 7.5 (expansion shows isotope pattern for monofunctional adducts)

4.3.3.3 Cytidine 5'-Monophosphate

Monofunctional binding was also observed for the reaction between complex **27** and 5'-CMP. The species at 1115 corresponds to Pt with 2 BDPPA ligands and one CMP (calculated m/z for $PtC_{47}H_{64}N_5O_8P_3$ = 1115). Again the Na bound species can also be seen. As for AMP, no bifunctional binding is observed, (calculated m/z for $PtC_{56}H_{68}N_8O_{16}P_4$ = 1436). The spectrum is shown in Figure 4.28.

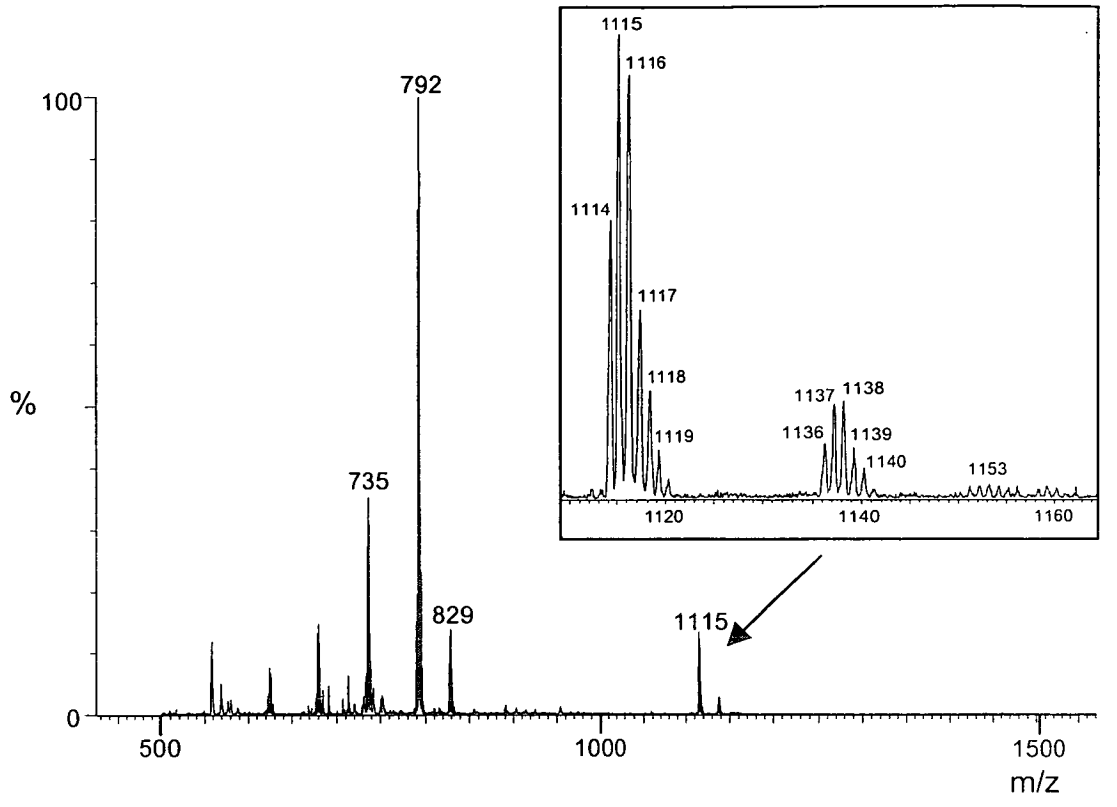

Figure 4.28 ESI-MS spectrum of $[Pt\{^tBu(H)N(CH_2)_3PPh_2\text{-}P\}_2Cl_2]$ (**27**) after reaction with two equivalents of 5'-CMP at pH 7.3 (expansion shows isotope pattern for monofunctional adducts)

4.3.3.4 Deoxythymidine 5'-Monophosphate

The mass spectrum showing products of the reaction between complex **27** and 5'-dTMP is shown in Figure 4.29. A monofunctional adduct, with one TMP and two BDPPA ligands, can be assigned to the peak at 1113 m/z (calculated m/z for $PtC_{48}H_{64}N_4O_8P_3$ = 1113). An additional peak for the sodium adduct was observed at 1136 and a species containing one remaining bound chloride remaining at m/z 1152. Again, even at low resolution, no bifunctional adducts were detected (calculated m/z for $PtC_{58}H_{76}N_6O_{16}P_4$ = 1432). This suggests that $[Pt\{^tBu(H)N(CH_2)_3PPh_2\text{-}P\}_2Cl_2]$ (**27**), as complex **24**, can form only bifunctional adducts with GMP and not the other nucleotides.

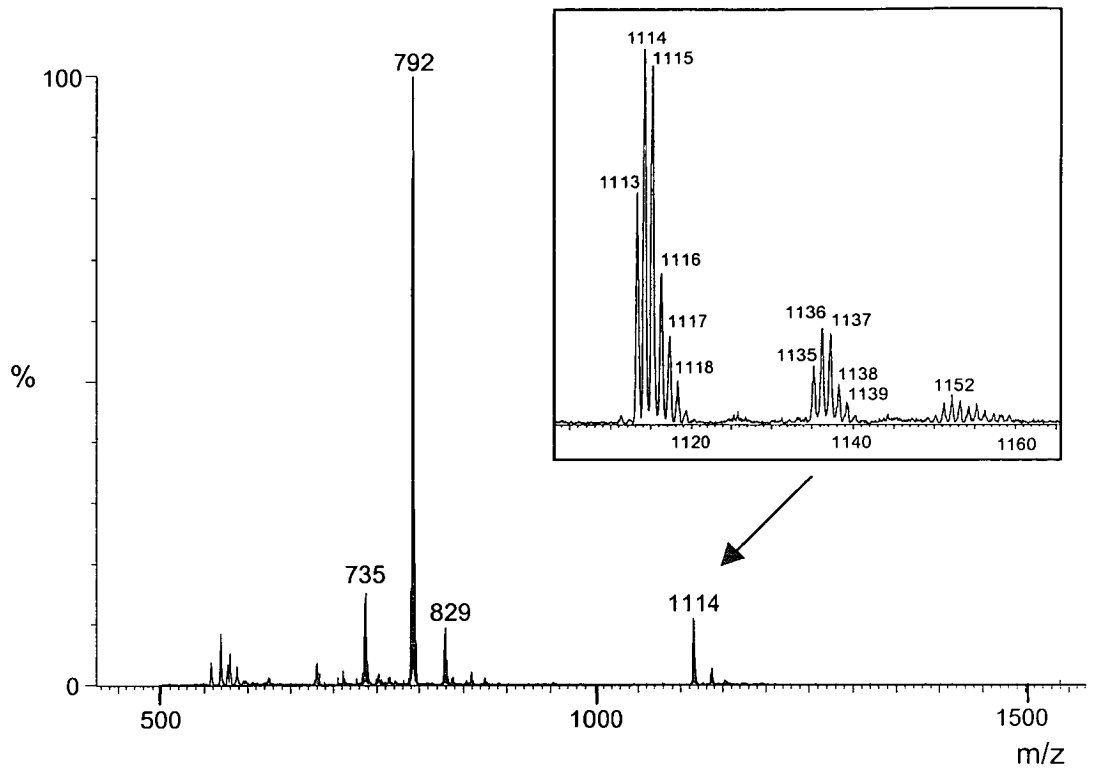

Figure 4.29 ESI-MS spectrum of [Pt{^{t}Bu(H)N$(CH_2)_3PPh_2$-*P*}$_2Cl_2$] (**27**) after reaction with two equivalents of 5'-dTMP at pH 7.4 (expansion shows isotope pattern for monofunctional adducts)

4.3.3.5 Competition Reaction

The mass spectrum of products from the reaction of [Pt{^{t}Bu(H)N$(CH_2)_3PPh_2$-*P*}$_2Cl_2$] (**27**) with all four nucleotides, showed that the only Pt bound species observed were the monofunctional adducts of GMP and TMP described previously. The CMP adduct is very close in mass to the TMP adduct (1115 and 1113). However, based on the CE results, it seems likely that the TMP adducts will be more abundant than those of CMP.

4.4 Reactions of $[Pt\{H_2N(CH_2)_3PPh_2\text{-}P,N\}_2]Cl_2$ (25)

4.4.1 NMR Spectroscopy

4.4.1.1 Guanosine 5'-Monophosphate

1:1 (Nucleotide:Complex) Reaction

In the recorded ^1H NMR spectrum of an equimolar mixture of complex **25** and 5'-GMP, the resonances for the protons in the free nucleotide could still be clearly observed. Very small peaks for Pt-bound species were observed, shifted upfield from the free nucleotide resonances. The spectrum is shown in Figure 4.30. These new peaks were too small to allow integration, so the percentage of nucleotide binding could not be determined.

The level of binding to GMP for this complex is obviously much lower than for the two complexes previously discussed. It is not surprising that this complex does not show significant binding to GMP since the pH of the sample was close to physiological and, from the pH titration in section 3.3.1, it can be seen that at this pH the complex exists in a totally ring-closed form. This means that there are no labile chloride ligands present to allow complexation of the nucleotide. For this reason the reaction was carried out at low pH values to investigate the effect on GMP binding. (Figure 4.31)

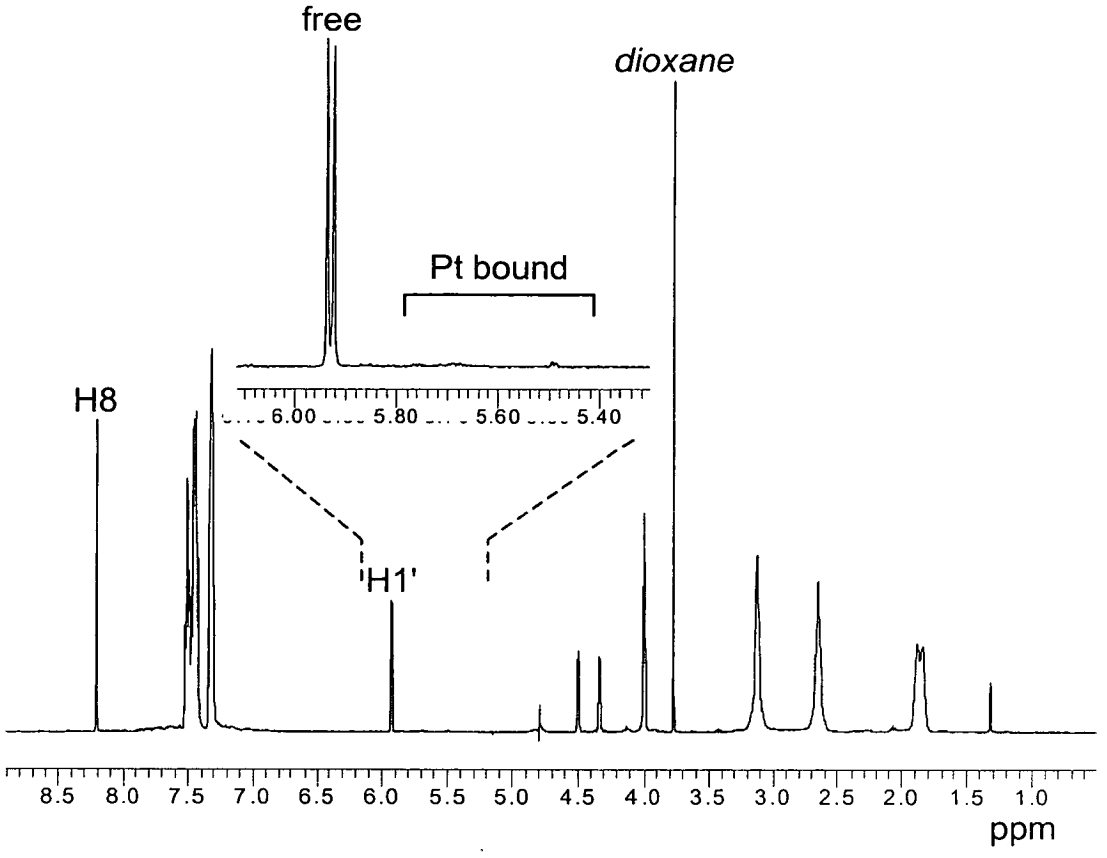

Figure 4.30 ^{1}H spectrum of $[Pt\{H_2N(CH_2)_3PPh_2\text{-}P,N\}_2]Cl_2$ (**25**) with one mole equivalent of 5'-GMP (expansion shows H1' resonances for free and bound 5'-GMP)

As can be seen in Figure 4.31, as the pH of the 1:1 reaction mixture of complex **25** and GMP is lowered the amount of nucleotide bound increases up to almost 90% at pH 1.7. The percentage of GMP bound at each pH is shown in Figure 4.32. This increase in binding reflects the fact that the complex ring-opens at low pH due to protonation of the amine groups of the ligands. (Section 3.3.1) This leaves a vacant site for binding of the nucleotide as shown in Scheme 4.1.

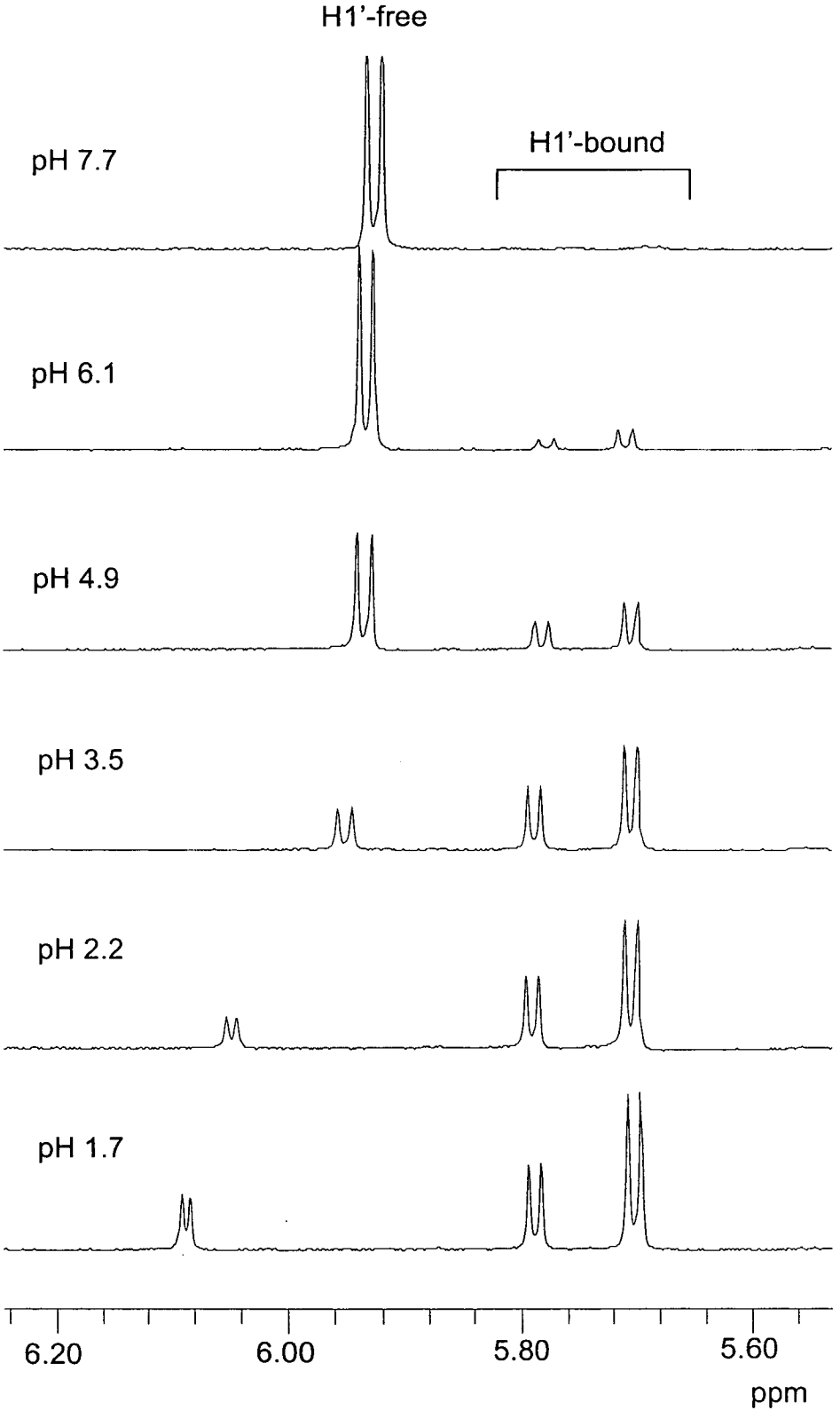

Figure 4.31 ^{1}H NMR spectra showing H1' signals for free and Pt-bound 5'-GMP after reaction with $[Pt\{H_2N(CH_2)_3PPh_2\text{-}P,N\}_2]Cl_2$ (**25**) at various pH values

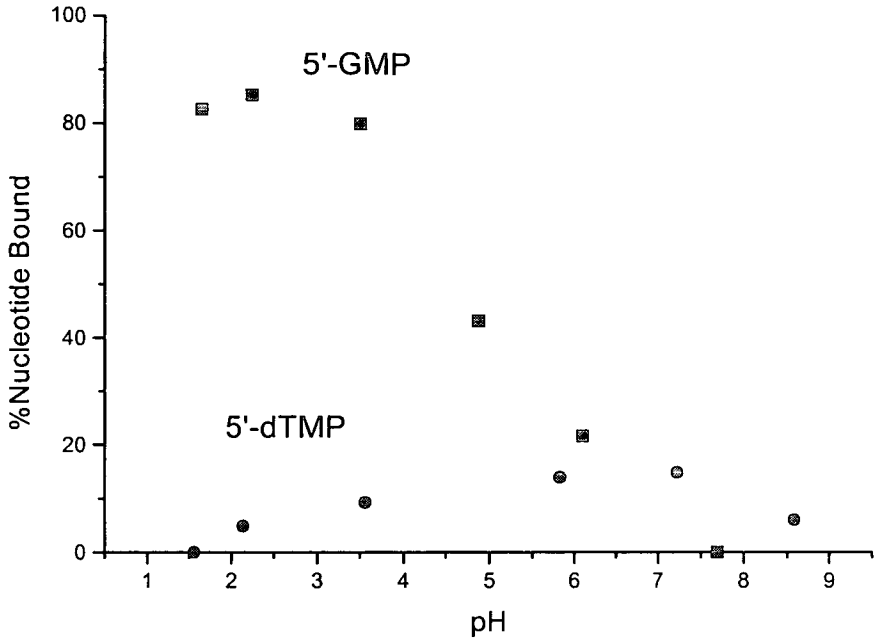

Figure 4.32 Graph showing the percentage of 5'-GMP and 5'-dTMP bound to $[Pt\{H_2N(CH_2)_3PPh_2\text{-}P,N\}_2]Cl_2$ (**25**) in separate reactions, with 1:1 ratio, at various pH values

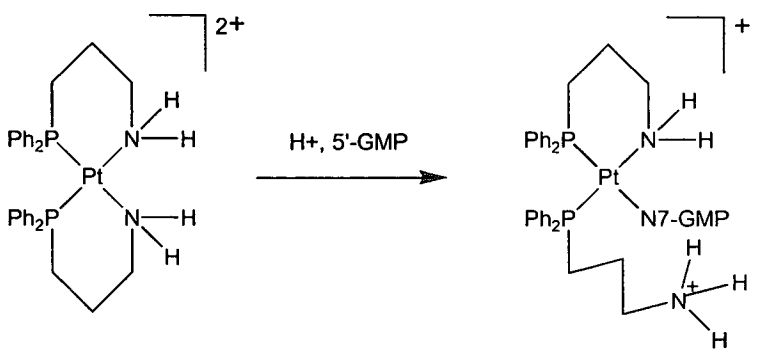

Scheme 4.1 Binding of 5'-GMP to $[Pt\{H_2N(CH_2)_3PPh_2\text{-}P,N\}_2]Cl_2$ (**25**) at low pH

4.4.1.2 Adenosine 5'-Monophosphate and Cytidine 5'-Monophosphate

$[Pt\{H_2N(CH_2)_3PPh_2\text{-}P,N\}_2]Cl_2$ (**25**) was also reacted separately with 5'-AMP and 5'-CMP, each in a 1:1 reaction. As for the ^1H spectrum of the GMP reaction, all the resonances for the protons in the free nucleotide were observed in both cases and no new peaks were observed for Pt-bound species.

4.4.1.3 Thymidine 5'-Monophosphate

1:1 (Nucleotide:Complex) Reaction

In the ^1H NMR spectrum of the reaction of complex **25** with 5'-dTMP, some Pt-bound species were observed with protons exhibiting an upfield shift from those of free TMP. The spectrum is shown in Figure 4.33. The expansion shows the H1' signals for both the free and bound TMP species and integration of these signals determined that 13% of the TMP is bound in this reaction at physiological pH (7.4). This is in contrast to the reaction with GMP where binding occurred only at lower pH values when the complex was ring-opened.

The binding of $[Pt\{H_2N(CH_2)_3PPh_2\text{-}P,N\}_2]Cl_2$ (**25**) to TMP has also been investigated at various pH values and the spectra are shown in Figure 4.34. The percentage of nucleotide bound at each pH is shown in Figure 4.32.

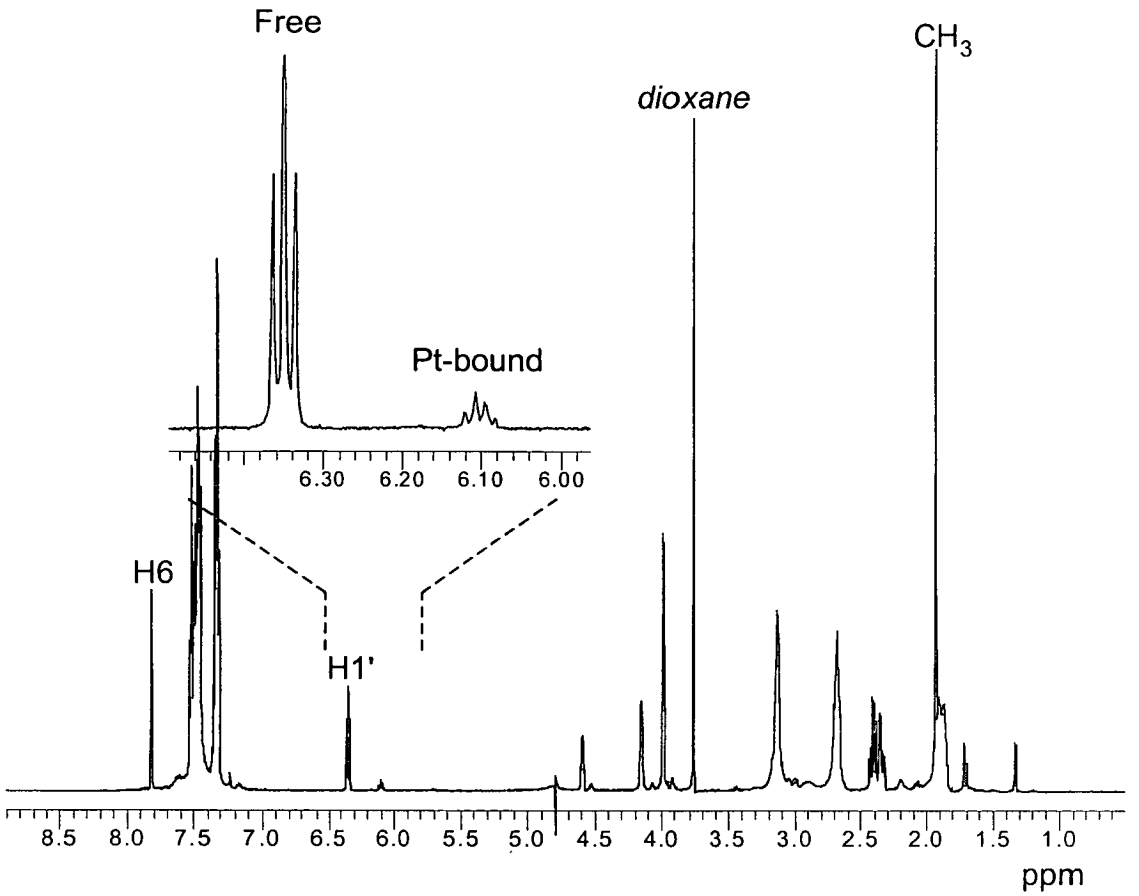

Figure 4.33 ^{1}H NMR spectrum of [Pt{$H_2N(CH_2)_3PPh_2$-*P,N*}$_2$]Cl_2 (**25**) with one mole equivalent of 5'-dTMP (expansion shows H1' resonances for free and bound 5'-dTMP)

Complex **25** does not appear to bind the nucleotide TMP to as great an extent as it does GMP. This is in keeping with traditional nucleotide binding of platinum complexes which target the more electron donating N7-site on guanine. It is not, however, in keeping with the other platinum aminophosphine complexes in this series, (**24**) and (**27**), previously discussed.

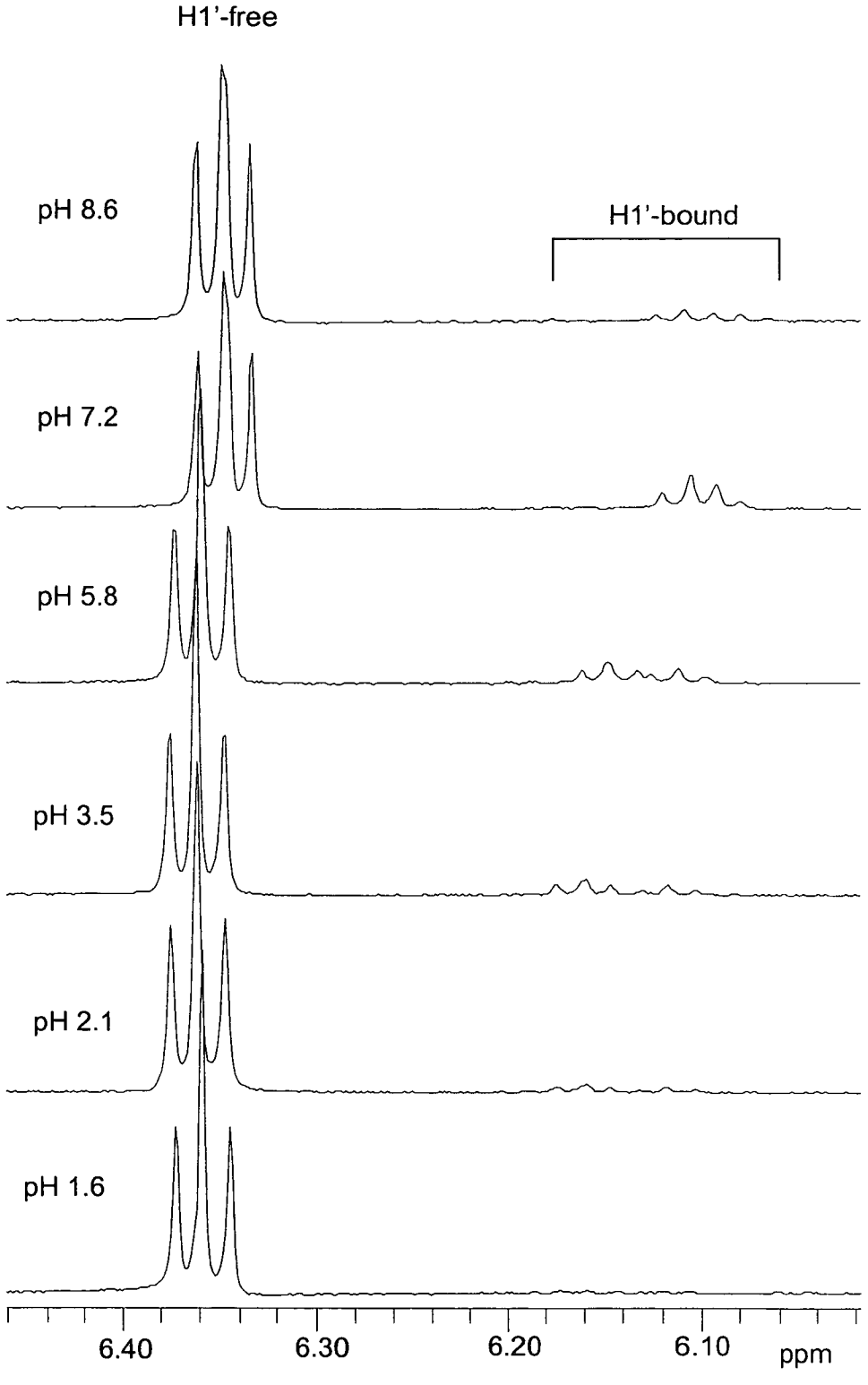

Figure 4.34 ^{1}H spectra showing H1' signals for free and Pt-bound 5'-dTMP after reaction with $[Pt\{H_2N(CH_2)_3PPh_2\text{-}P,N\}_2]Cl_2$ (**25**) at various pH values

The pH dependence of the TMP binding also shows a very different profile to the GMP binding (Figure 4.32), which increased with decreasing pH as the complex was forced to ring-open. TMP binding starts to increase as the pH is lowered from 8.5 to 6.5 but then begins to decrease below this value, until no TMP is bound at pH 1.5. This demonstrates the fact that although low pH favours ring-opening of the complex and therefore TMP binding, it also favours protonation of the N3-site on the TMP preventing binding to the Pt. These two effects are in opposition to give the resulting binding profile.

This supports the theory that TMP still binds to aminophosphine complexes through N3, even at pH values well below the usual pK_a value for the site, as has been proposed in the previous sections 4.2.1.4 and 4.3.1.4 for complexes **24** and **27**.

4.4.2 Capillary Electrophoresis

As for the previous complexes, [Pt{$H_2N(CH_2)_3PPh_2$-*P,N*}$_2$]Cl_2 (**25**) was incubated with all four nucleotides at close to physiological pH for 12 hours prior to analysis. The sample was analysed and the amount of each nucleotide bound to the complex was determined from the decrease in peak area for the free nucleotide. The resulting electropherogram is shown in Figure 4.35 with a control sample (no complex present) for comparison.

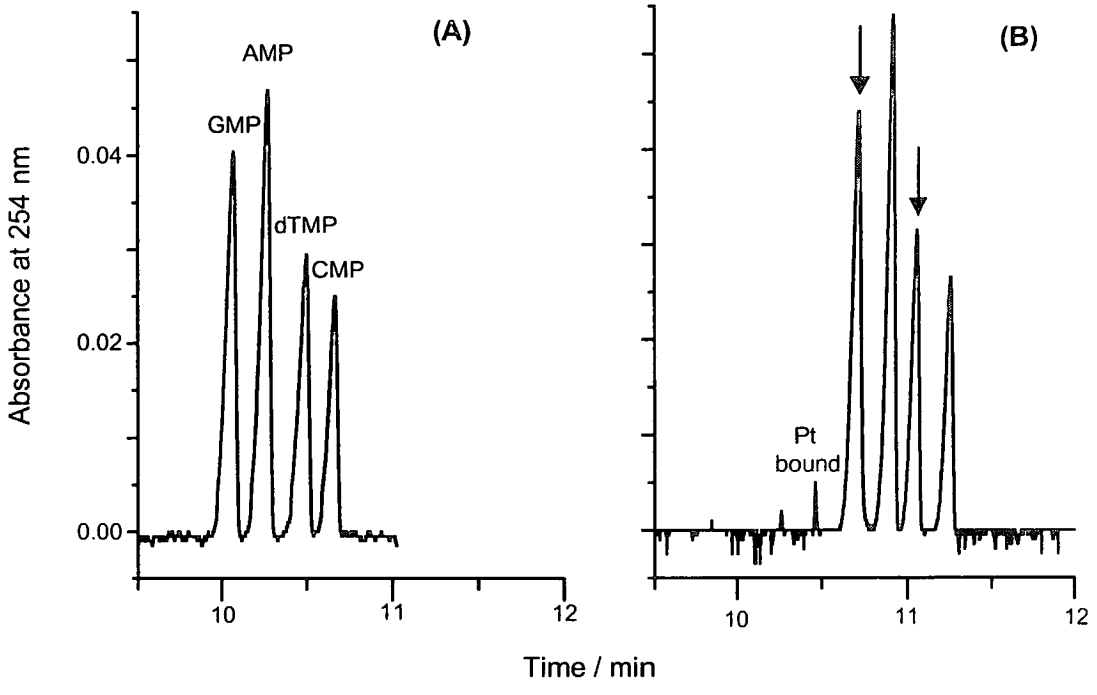

Figure 4.35 Electropherograms showing: (**A**) four nucleotides at 100 μM concentration, (**B**) four nucleotides with $[Pt\{H_2N(CH_2)_3PPh_2\text{-}P,N\}_2]Cl_2$ (**25**) all at 100 μM concentration, pH 7.0, after incubation at 310 K for 12 hours

The analysis showed that neither CMP nor AMP reacted with complex **25** as would be predicted from the NMR results. 21% and 20% of the GMP and TMP respectively were bound to the complex. This correlates to the NMR data which shows that at pH 7 similar amounts of binding to each nucleotide occur (Figure 4.32).

4.4.3 Electrospray Ionisation Mass Spectrometry

Mass spectra were recorded for $[Pt\{H_2N(CH_2)_3PPh_2\text{-}P,N\}_2]Cl_2$ (**25**) after reaction with each of the nucleotides in a 1:2 ratio. None of the resulting spectra revealed any nucleotide-bound products at all. An example of the spectrum from the reaction with GMP is shown in Figure 4.36. The major peak at 680 is for the fully ring-closed

species, (calculated m/z for $PtC_{30}H_{36}N_2P_2$ = 681), as would be expected at this pH (7.3). The absence of any bound products reflects the much lower reactivity of this complex to nucleotides compared to the previous ring-opened species **24** and **27**.

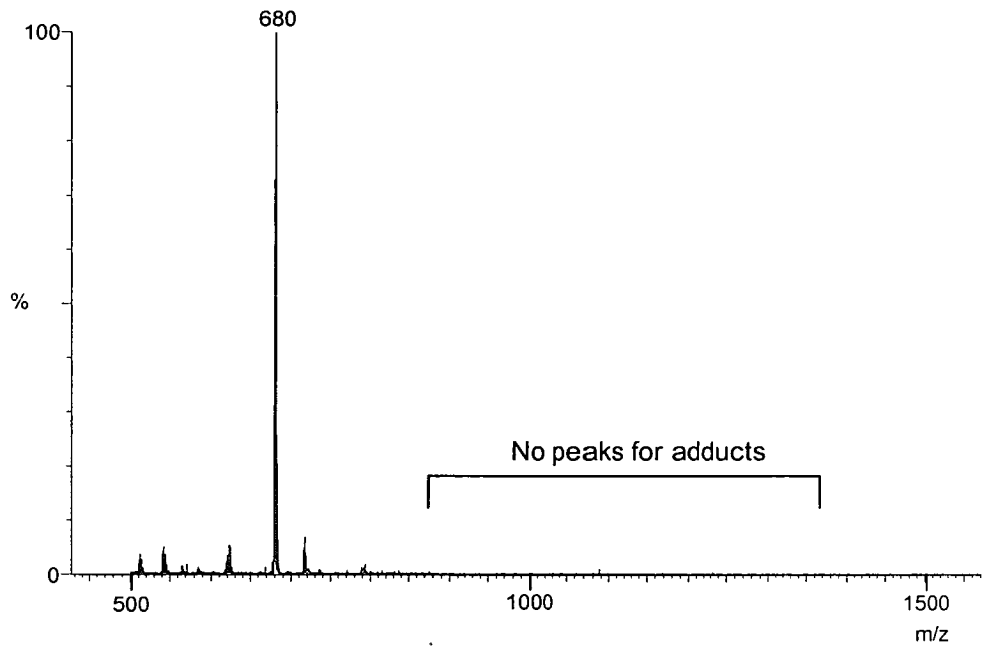

Figure 4.36 ESI-MS spectrum of $[Pt\{H_2N(CH_2)_3PPh_2\text{-}P,N\}_2]Cl_2$ (**25**) after reaction with two equivalents of 5'-GMP at pH 7.3

4.5 Conclusions

The results discussed in this chapter highlight an interesting variety of nucleotide binding for the series of aminophosphine complexes studied. As would be expected the binding is most extensive for the complexes in the chelate ring-opened form with labile chloride ligands.

Initial studies by ^1H NMR, following reactions of the complexes with each nucleotide individually, showed varying binding patterns for each complex. The reactions were all carried out at 5 mM concentration and the reaction mixtures were

incubated at 310 K overnight to ensure completion of reaction prior to analysis. The results are summarised in Figure 4.37. The pH values of the samples were not adjusted after preparation and were all in the region 6.5 – 8.5 depending on the complex and nucleotide used.

Complex **24** preferentially binds GMP and TMP with a small amount of AMP binding as well. With GMP some bifunctional adducts were formed as determined by the proportion of GMP bound and confirmed by detection of these adducts in ESI-MS. Binding to TMP however appears to be limited to monofunctional adducts. Complex **27** is able to bind to all four nucleotides and shows much less selectivity in nucleotide binding than complex **24**, but again bifunctional adducts are only formed with GMP. Complex **25** shows the least amount of binding and products are only seen in the reaction with TMP in this pH range.

CE allowed the selectivity of the complexes to be determined when reacted with all four nucleotides in competition. These results are also summarised in Figure 4.37. The reactions were carried out at pH 7.1 for complexes **24** and **27** and pH 7.0 for complex **25**.

Unexpectedly the binding to TMP is still abundant even in the presence of the purine bases which are usually the kinetically preferred sites for platinum binding. The binding profile is distinctly different to the usual platinum amine complexes such as cisplatin which show high selectivity for guanine closely followed by adenine.[20] Complex **27** shows the highest amount of overall binding with the least selectivity whilst complex **25** shows the least binding due to the high proportion of the ring-closed species present.

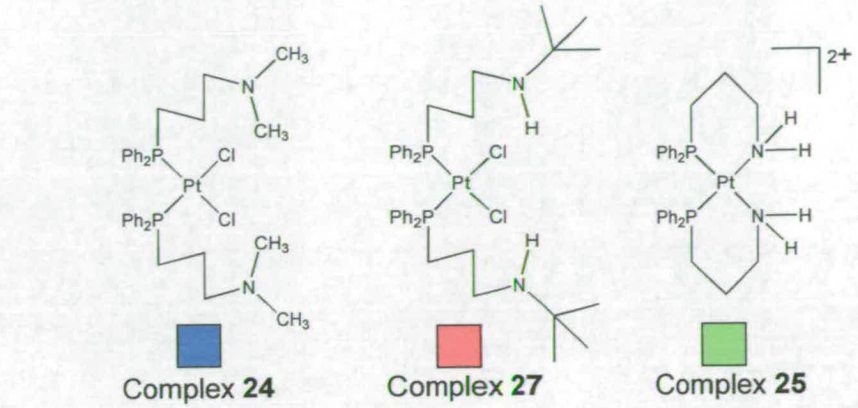

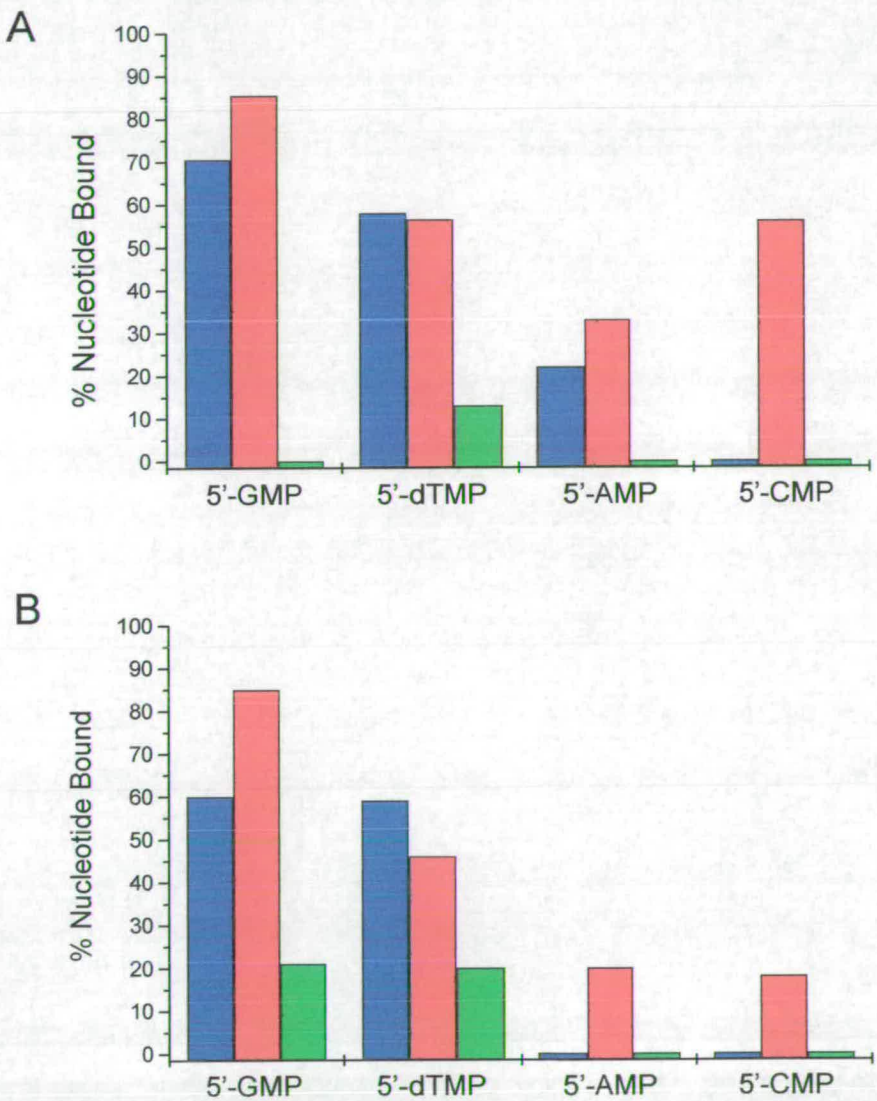

Figure 4.37 Bar charts showing binding of complexes **24**, **27**, and **25**
(A) to four nucleotides in isolation as determined by ^{1}H NMR spectroscopy
(B) to all four nucleotides in competition as determined by capillary electrophoresis

The binding to 5'-dTMP was further investigated by means of pH titrations followed by ^{1}H NMR. For both complexes **24** and **27**, TMP was seen to bind fully between pH 4 and pH 12 with binding decreasing below pH 4. A significant amount of the bound species could still be observed even as low as pH 2. The bound species was shown, by ^{31}P NMR, to still contain TMP bound via N3. This is unusual since the pK_a of N3 is 10.47, thus the nitrogen must be binding Pt preferentially instead of a proton. The N3 site seems the most likely binding site since the N1 site is blocked, however, other binding modes have previously been identified for thymine to platinum. Binding of Pt to the N3 site results in an increase of basicity at the O4 site[21,22] which promotes Pt-binding at this site. This can lead to the formation of dimers with thymine bound via both N3 and O4.[16,23-25] The NMR results did not indicate an O-bound species to be present (^{1}J(Pt-P), *trans* to O is > 4000 Hz) and the ESI-MS results did not show the presence of any dimers, so it can be assumed that the bound products are monofunctional, N3-bound species.

The unusual preference for TMP binding exhibited by this series of complexes could be explained by the "dangling" amine group on the unchelated aminophosphine ligands. This group could be capable of abstracting a proton from the N3 site to allow Pt-binding. The amine could also play a role in hydrogen bonding to the nucleotide stabilising the Pt-nucleotide adduct formed. Hydrogen bonding could also play a role in the formation of the head and tail isomers of Pt-TMP adducts by restricting rotation around the Pt-N3 bond.

Since the binding profile of these complexes is so different to current cisplatin-type platinum anticancer drugs, these complexes could be useful in the quest to find a new generation of drugs which can overcome cisplatin resistance in cells.

4.6 References

1 B. Lippert, *J. Chem Soc. Dalton Trans.* **1997**, 3971

2 I. Meynial, *Anal. Chem.* **1995**, *67*, 1627

3 A. Zenker, M. Galanski, T. L. Bereuter, B. K. Keppler, W. Lindner, *J. Chromat. A,* **1999**, *852*, 337

4 D. Lemaine, M.-H. Fouchet, J. Kozelka, *J. Inorg. Biochem.* **1998**, *120*, *46*, 12017

5 S. J. Berners-Price, U. Frey, J. D. Ranford, P. J. Sadler, *J. Am. Chem. Soc.* **1993**, *115*, 8649

6 R. Cramer, P. Dahlstrom, *Inorg. Chem.* **1985**, *24*, 3420

7 A. Habtemariam, J. A. Parkinson, N. Margiotta, T. W. Hambley, S. Parsons, P. J. Sadler, *J. Chem. Soc. Dalton Trans.* **2001**, 362

8 B. Lippert, *Prog. Inorg. Chem.* **1989**, *37*, 43

9 A. M. J. Fichtinger-Schepman, J. L. Van der Leer, J. H. J. Den Hartog, P. H. M. Lohman, J. Reedijk, *Biochemistry,* **1985**, *24*, 707

10 B. Lippert, *Prog. Inorg. Chem.* **1989**, *37*, 61

11 R. Pfab, P. Jandik, B. Lippert, *Inorg. Chim. Acta.* **1982**, *66*, 193

12 G. M. Blackburn in *Nucleic Acids in Chemistry and Biology*, G. M. Blackburn, M. J. Gait: Eds. Oxford University Press, Oxford, **1996**, pp 16-18

13 G. K. Anderson, H. C. Clark, J. A. Davies, *Inorg. Chem.* **1983**, *22*, 427

14 G. K. Anderson, R. Kumar, *Inorg. Chem.* **1984**, *23*, 4064

15 R. Cramer, P. L. Dahlstrom, *Inorg. Chem.* **1985**, *24*, 3420

16 D. Neugebauer, B. Lippert, *Inorg. Chim. Acta.* **1982**, *67*, 151

17 R. B. Martin, in *Cisplatin : Chemistry and Biochemistry of a Leading Anticancer Drug,* B. Lippert Ed., **1999**, Wiley-VCH, Weinheim, p 183-205

18 F. A. Cotton, G. Wilkinson, *Advanced Inorganic Chemistry,* 5th Edition, John Wiley and Son, New York, **1988**, p 1299-1300

19 A. G. Orpen, L. brammer, F. H. Allen, O. Kennard, D. G. Watson, R. Taylor, *J. Chem. Soc. Dalton Trans.* **1989**, S1

20 S. Mansy, G. Y. H. Chu, R. E. Duncan, R. S. Tobias, *J. Am. Chem. Soc.* **1978**, *100* 607

21 B. Lippert, *Inorg. Chim Acta.* **1981**, *55*, 5

22 O. Krizanovic, B. Lippert, *Platinum and other Metal Coordination Complexes in Cancer Chemotherapy*, M. Nicolini, Ed., **1988**, Nijhoff, Boston/Dordnecht /Lancaster, p 700

23 B. Lippert, D. Neugebauer, G. Randaschl, *Inorg. Chim Acta,* **1983**, *78*, 161

24 U. Thewalt, D. Neugebauer, B. Lippert, *Inorg. Chem.* **1984**, *23*, 1713

25 C. J. L. Lock, H. J. Presie, B. Rosenberg, G. Turner, *J. Am. Chem. Soc.* **1978**, *100*, 3371

Chapter Five

Interactions of [Pt{Me$_2$N(CH$_2$)$_3$PPh$_2$}$_2$Cl$_2$] with Natural and Synthetic Nucleic Acids

5.1 Background

In collaboration with the group of Professor V. Brabec at the Academy of Sciences of the Czech Republic, the interactions of [Pt{Me$_2$N(CH$_2$)$_3$PPh$_2$}$_2$Cl$_2$] (**24**) with natural and synthetic DNAs in cell-free media were studied using various biomedical and biophysical techniques.[1]

Complex **24** (Figure 5.1) was chosen as a representative of the aminophosphine series of complexes since it is bifunctional with two leaving chloride ligands in *cis* positions, making it ideal for comparison to cisplatin binding.

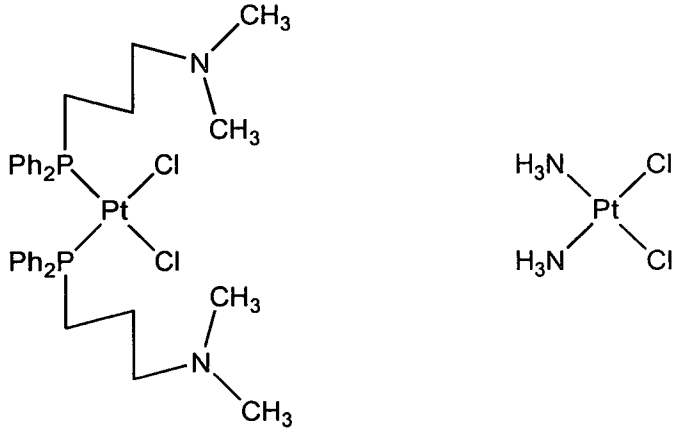

(24) Cisplatin

Figure 5.1 Structures of [Pt{Me$_2$N(CH$_2$)$_3$PPh$_2$}$_2$Cl$_2$] (**24**) and cisplatin

5.1.1 Rate and Selectivity of Binding to Nucleic Acids

Double helical calf thymus (CT) DNA was incubated with complex **24** at a molar ratio of 0.08 (Pt:nucleotide phosphates), in 10 mM $NaClO_4$ (pH 7), at 310 K. At various time intervals the amount of Pt bound to the DNA was determined by differential pulse polarography (DPP). The results are shown in Figure 5.2.

The amount of Pt bound increased with time until after 48 h approximately 100% of the complex was bound to the DNA. The time taken to bind 50% of the available Pt under these conditions (T_{50}) was ca. 3 h. This compares to a T_{50} value of ca. 4 h for cisplatin[2] (structure shown in Figure 5.1) suggesting that the presence of the aminophosphine groups increases the rate of coordination of Pt (II) complexes to natural double helical DNA.

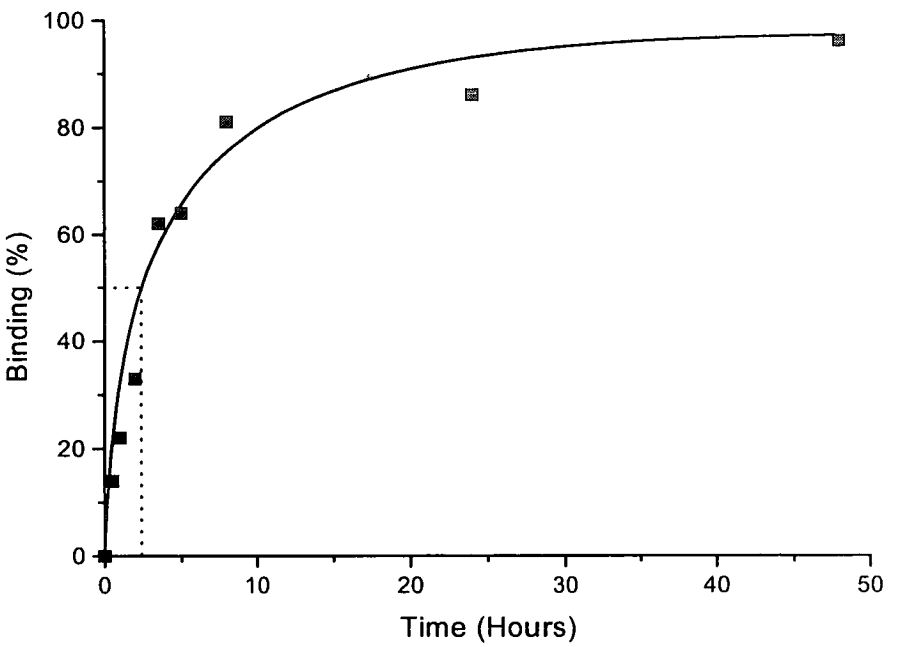

Figure 5.2 Formation of DNA adducts by [Pt{$Me_2N(CH_2)_3PPh_2$}$_2Cl_2$] (**24**) as a function of incubation time, determined by differential pulse polarography

The binding of [Pt{$Me_2N(CH_2)_3PPh_2$}$_2Cl_2$] (**24**) to several synthetic single-stranded homopolydeoxyribonucleotides and double-stranded synthetic alternating polydeoxyribonucleotides, was also investigated under the same conditions as for the CT DNA above. The percentage of Pt bound in each case was determined DPP. The results are shown in Table 5.1.

Complex **24** was shown to bind readily to single-stranded poly (dG), poly (dA) and poly (dC), with approximately the same rate, but not to poly (dT). The complex bound to double-stranded poly (dA-dT) and poly (dG-dC) with markedly higher rates than to the single-stranded polynucleotides.

Nucleic Acid	T_{50} / h	Binding after 48 h / %
ds CT DNA	3.0	99
poly (dA)	2.2	89
poly (dC)	1.9	79
poly (dG)	2.0	83
poly (dT)	-	0
poly (dA-dT)	0.3	90
poly (dG-dC)	0.7	96

Table 5.1 The binding of [Pt{$Me_2N(CH_2)_3PPh_2$}$_2Cl_2$] (**24**) to CT DNA and synthetic polydeoxyribonucleotides determined by DPP

These results suggest that complex **24** has different base sequence preference to cisplatin which binds predominantly to guanine residues and to a lesser extent adenine residues.[3,4,5]

5.1.2 Characterisation of DNA adducts

In order to further characterise the coordination mode of complex **24**, a 40 base-pair (bp) deoxyribonucleic duplex modified by reaction with the complex (in 0.1 M $NaClO_4$) was enzymatically digested to mononucleotides and analysed by HPLC. By comparison to an enzymatically digested control sample (no Pt) the reduction in peaks for the free mononucleotides allowed determination of the proportion of each nucleotide that was bound to the complex in the reaction. The results are shown in Table 5.2 along with comparative results for cisplatin.[4,5]

	Mononucleotide Peak	% reduction in peak after reaction with **24**	Number of residues in 40 bp duplex	Number of residues platinated
Complex **24**	GMP	28	17	5
	AMP	21	23	5
Cisplatin	GMP	70	17	12
	AMP	5	23	1

Table 5.2 Nucleotide specificity of binding complex **24** and cisplatin to a 40 bp DNA duplex, as determined by enzymatic digestion and HPLC analysis

As shown in Table 5.2, the 40 bp sequence contained 5 platinated guanine residues and 5 platinated adenine residues after reaction with [Pt{Me$_2$N(CH$_2$)$_3$PPh$_2$}$_2$Cl$_2$] (**24**). Since the ratio of bound Pt to nucleotide (r_b) in the reaction was 0.09, this suggests that there were only 7.2 Pt-adducts on average per DNA strand. The formation of 10 platinated nucleotides must therefore be due to the presence of 3 bifunctional adducts per DNA strand.

When the same analysis was carried out with cisplatin, 12 guanine residues and 1 adenine residue were platinated on the 40 bp strand (Table 5.2) suggesting that 80% of all adducts were bifunctional. This is in good agreement with previous analyses on the nature of cisplatin-DNA adducts.[4,5]

These results again suggest that complex **24** has less nucleotide specificity than cisplatin, forming more adenine adducts. The complex also forms less bifunctional lesions than cisplatin.

5.1.3 Effect of Binding on Global DNA Conformation

The effect of binding complex **24** to DNA was also investigated by circular dichroism (CD) spectroscopy. This reflects changes in the global DNA conformation. Previous studies[6,7] have shown that the intensity of the positive CD band yielded by B-DNA at ca. 280 nm is increased as a consequence of DNA modification by complexes containing the *cis*-[$PtCl_2$(amine)$_2$] unit, up to an r_b value of ca. 0.05. With higher levels of platinum modification the band then decreases again. This trend is shown in Figures 5.3 and 5.4 for cisplatin. On the other hand, modification of the DNA by the clinically inactive transplatin only slightly decreased this positive band.[6,7] It has been suggested that the enhancement of the CD band at 280 nm by cisplatin and active analogues reflects distortions in DNA of a non-denaturational nature. At higher Pt concentrations the decrease in the band is consistent with the occurrence of short segments containing unpaired bases.

When complex **24** was bound to DNA, the effect on the CD spectrum was great, but distinctly different to that of cisplatin binding (Figure 5.3). There was a marked loss in the intensity of the positive CD band as a linear function of r_b (ratio of bound Pt to DNA nucleotides). This was accompanied by a reduction in the intensity of the negative band at 245 nm. The changes in intensity are shown in the Figure 5.4. The changes observed are reminiscent of the DNA transformations seen in the presence of high concentrations of electrolyte or by the reaction with a variety of amines.[8,9]

For instance at the level of DNA binding corresponding to r_b = 0.13, the reduction in rotational strength of the positive band in the CD spectrum in 10 mM $NaClO_4$, was similar to that obtained for underivatised DNA in ca. 6 M LiCl or at ca. 0.1 mol of *n*-butylamine covalently fixed per mol of nucleotide. This transformation has been demonstrated to be roughly correlated with the reduction of the electrostatic repulsive interactions in the DNA molecule. It is possible therefore that the two positively-charged amine groups in the dangling ligands of complex **24** could position close to the DNA negatively charged phosphate groups, reducing the electrostatic repulsion within the molecule.

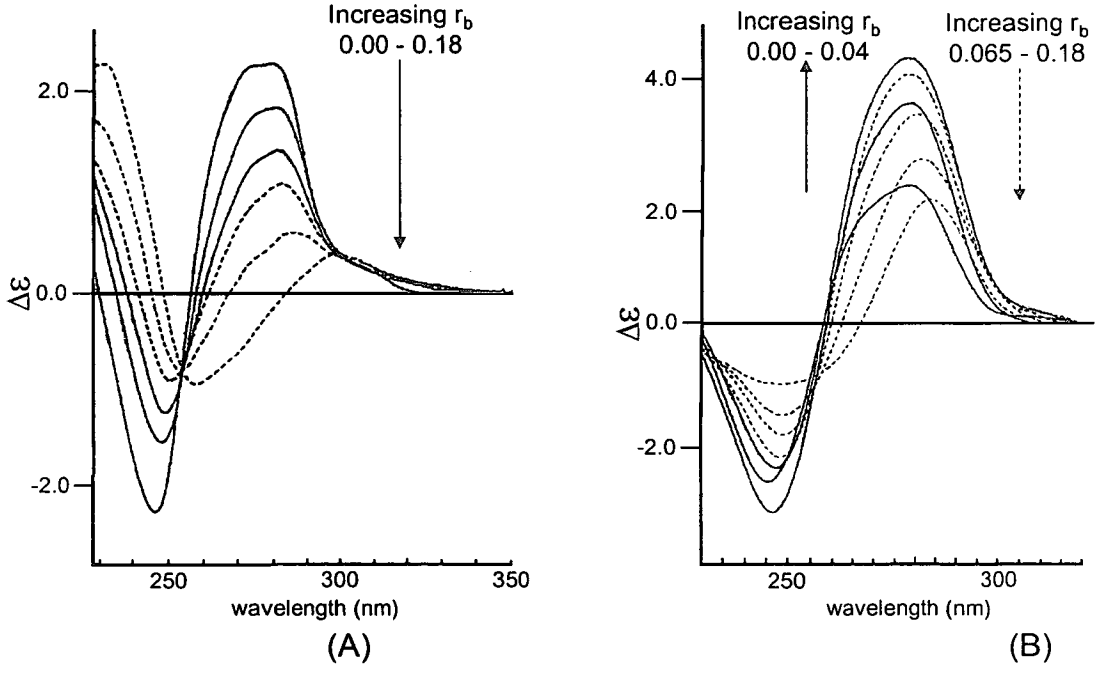

Figure 5.3 CD Spectroscopy of calf thymus DNA modified by (A) [Pt{Me$_2$N(CH$_2$)$_3$PPh$_2$}$_2$Cl$_2$] (**24**) and (B) cisplatin at various ratios of Pt:DNA phosphates (r_b)

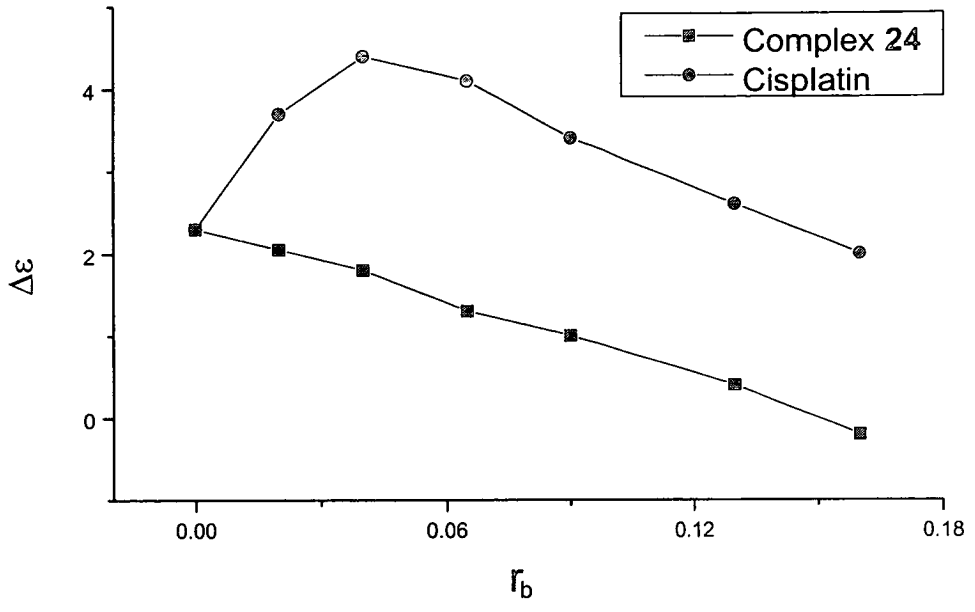

Figure 5.4 Graph showing changes in intensity of positive CD band for DNA (280 nm) with modification by complex **24** and cisplatin at increasing r_b values

5.1.4 Aims of Collaborative Visit to Czech Republic

The collaborative work discussed above, whilst providing a useful insight into the formation of DNA adducts by [Pt{Me$_2$N(CH$_2$)$_3$PPh$_2$}$_2$Cl$_2$] (**24**) also highlights some different trends to those observed when binding the complex to individual nucleotides, as discussed in Chapter 4.

The most notable differences are:

1. the lack of binding to poly (dT) shown by DPP, although binding to dTMP is highly favoured for complex **24** even when in the presence of the purine nucleotides, the more common Pt binding targets
2. the rate of binding to nucleotides is very fast as shown by HPLC (Section 4.2.2) with $T_{50} < 1$ h. whilst the rate of binding to DNA is much longer with $T_{50} > 3$ h, shown by DPP.

In order to try to account for these discrepancies between the Czech work and the results already discussed in this thesis, a working visit to the Institute of Biophysics, The Academy of Sciences of the Czech Republic in Brno was undertaken for further collaboration work with Prof. Brabec's group. This visit was part of the Cost D8 programme – Chemistry of Metals in Medicine (working group D8/0009 – Platinum Binding to Nucleic Acids), and took place in March 1998.

The aims of this visit were:

1. to study the effect of pH on the binding of [Pt{$Me_2N(CH_2)_3PPh_2$}$_2Cl_2$] (**24**) to poly (dT), to see if this accounts for the differences in binding between the DPP experiment and the reported dTMP experiments,
2. to study the effect of concentration on binding to 5'-dTMP (since the NMR experiments were carried out at 10 mM, whilst the DPP experiments were carried out at 10 μM) to see if this accounts for the differences in binding to thymine,
3. to study the kinetics of binding of complex **24** to CT DNA by following the changes in the CD spectrum, and
4. to study the effect of pH on the changes induced in the CD spectrum by binding complex **24**, in order to prove the postulate that the changes are caused by interaction of protonated amine groups from the ligands on the Pt.

5.2 Experimental

All samples contained 10 μM complex and 100 μM nucleic acids in 10 mM $NaClO_4$ unless otherwise stated.

5.2.1 Differential Pulse Polarography

All experiments were carried out on a EG and G Princeton Applied Research model 384B Polarographic analyser. A three electrode system was used comprising a EG and G PARC model 303A static mercury drop electrode and a Ag/AgCl (saturated KCl) reference electrode. All potentials were quoted vs. this electrode.

Parameters for the DPP operation were: 1s drop time, 5 mV/s voltage scan rate, -50 mV modulation amplitude, negative scanning direction, -0.6 V initial potential, -1.05 V final potential.

The electrolyte used was 0.08% formaldehyde, 0.008% hydrazine, and water, in a ratio 1:1:2. This caused the DNA to precipitate out along with any bound Pt complex. Hence only unbound Pt was detected by polarography.[10]

Reaction between [Pt{$Me_2N(CH_2)_3PPh_2$}$_2Cl_2$] (**24**) and poly (dT) at pH 8

A 1 ml sample was prepared using $NaClO_4$ with the pH kept at 8 by addition of tris buffer. The samples were incubated in the dark at 310 K. Aliquots (40 μl) were taken at regular intervals, placed in 4 ml of electrolyte and a polarogram recorded.

5.2.2 High Performance Liquid Chromatography

These experiments were performed using a Hitachi series 4 liquid chromatograph with LCI-100 computing integrator and a Waters μBondapack C18 column. The products were separated by reverse phase HPLC (isocratic elution with 0.1 M ammonium acetate, pH 5.0 in 4% acetonitrile at 1 ml/min flow rate).

[Pt{$Me_2N(CH_2)_3PPh_2$}$_2Cl_2$] (**24**) and 5′thymidine monophosphate

Samples containing complex **24** with dTMP, both at a concentration of 10 μM, were incubated at 310 K and chromatograms recorded at regular intervals up to about 24 hours.

5.2.3 Circular Dichroism Spectroscopy

CD Spectra were recorded at 310 K on a JASCO spectrapolarimeter, model J720. Parameters were : band width 2 nm, sensitivity 10 mdeg, response 0.25 sec, wavelength range 350.0 - 200.0 nm, step resolution 0.1 nm, scan speed 50 nm/min.

Kinetics of [Pt{$Me_2N(CH_2)_3PPh_2$}$_2Cl_2$] (**24**) binding to calf thymus DNA

A 2.5 ml sample of complex **24** and CT DNA was prepared in $NaClO_4$ and incubated in the spectrapolarimeter at 310 K. Spectra were recorded at regular intervals up to 48 hours.

Effect of high pH on binding of [Pt{$Me_2N(CH_2)_3PPh_2$}$_2Cl_2$] (**24**) to calf thymus DNA

Two samples of [Pt{$Me_2N(CH_2)_3PPh_2$}$_2Cl_2$] (**24**) and CT DNA were incubated for 48 hours to allow binding to occur. One sample was left unaltered as a control and

the other was adjusted to pH 9 using 0.1 M NaOH. The samples were left and spectra recorded after 1 and 6 hours for comparison.

5.3 Thymine Binding

5.3.1 Effect of pH

As previously discussed, [Pt{$Me_2N(CH_2)_3PPh_2$}$_2Cl_2$] (**24**) was seen to bind strongly and rapidly to dTMP in ^{1}H NMR experiments (Section 4.2.1.4). This was confirmed by HPLC (Section 4.2.2) and CE (Section 4.2.3) experiments which showed that binding to TMP occurred even in the presence of the more usual Pt targets GMP and AMP. However, DPP experiments on the reaction between [Pt{$Me_2N(CH_2)_3PPh_2$}$_2Cl_2$] (**24**) and synthetic poly (dT) showed no binding to occur at all (Section 5.1.1).

In order to determine if this was due to pH differences between the two experimental methods, DPP experiments were performed at pH 8 (original measurements were at pH 7) as described in Section 5.2.1. Higher pH should favour thymine binding due to deprotonation of the N3 binding site. It was difficult to increase the pH much beyond this value due to the instability of the poly (dT).

Polarograms of the sample were recorded after various time intervals and the height of the peak for the unbound Pt (at ca. –0.72 V) was measured. By comparison of the height of the peak at each time, (I_p), to that of the sample immediately after mixing, (I_o), the concentration of the complex remaining unbound, (c), at each time was calculated using the following equation;

$$c = I_p / I_o \times c_o$$

(c_o = initial concentration of Pt = 10 μM)

It was assumed that in the initial polarogram no binding had occurred and hence the peak height was taken to correspond to all Pt being free.

The amount of Pt bound at each time is shown in the graph in Figure 5.5. The maximum level of binding was 20% and this was only achieved after 9 hours. This is significantly less than the binding observed to dTMP and a much slower rate of binding, despite the thymine being in a 10 fold excess in the reaction (Pt = 10 μM, T = 100 μM). In the ^{1}H NMR experiment at pH 8 ca. 50% of the TMP was bound to Pt in a 2:1 reaction, forming monofunctional adducts (Figure 4.2, Section 4.2.1). Also, it appears from the binding curve in Figure 5.5 that there is some prereaction taking place before binding, since there is an induction period of about 8 hours before any reaction takes place. This was not observed for the NMR or HPLC experiments with dTMP previously discussed.

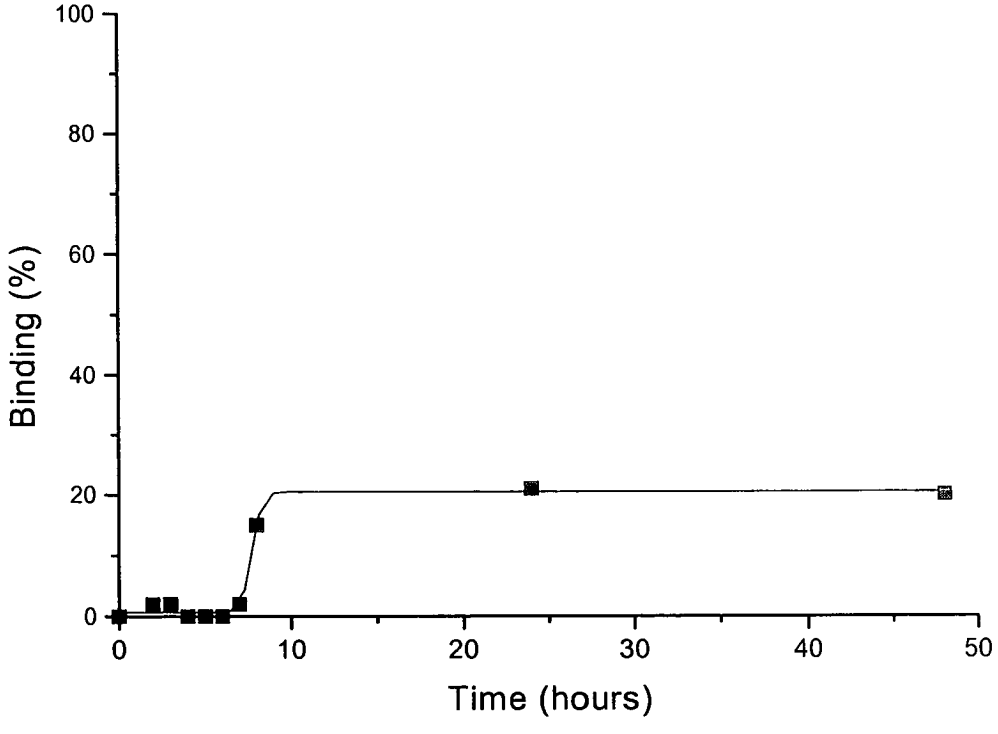

Figure 5.5 Binding of [Pt{Me$_2$N(CH$_2$)$_3$PPh$_2$}$_2$Cl$_2$] (**24**) to synthetic poly (dT) as determined by DPP

It seems from these results that pH, whilst it does affect the level of binding, does not account for the differences between the experimental data from the binding of [Pt{$Me_2N(CH_2)_3PPh_2$}$_2Cl_2$] (**24**) to poly (dT) and dTMP, by DPP and NMR respectively.

5.3.2 Effect of Concentration

The binding of [Pt{$Me_2N(CH_2)_3PPh_2$}$_2Cl_2$] (**24**) to dTMP was carried out at 5 mM concentration, for observation by NMR, whilst the binding of [Pt{$Me_2N(CH_2)_3PPh_2$}$_2Cl_2$] (**24**) to poly (dT) was carried out at 10 μM concentration, for observation by DPP. The difference between these two concentrations is very large (500x) and could have an effect on the amount of binding. For this reason the effect of concentration was investigated further.
Since it was impossible to effectively carry out NMR on these samples at 10 μM, or DPP at 5 mM, another technique had to be employed. [Pt{$Me_2N(CH_2)_3PPh_2$}$_2Cl_2$] (**24**) and dTMP were reacted in a 1:1 ratio at 10 μM and the amount of Pt bound was determined by HPLC as described in Section 5.2.2. This replicates the NMR experiments but at the concentration used in the DPP experiments.

The free dTMP peak eluted at 2.3 min and as the reaction proceeded the decrease in height of this peak corresponded to the amount of dTMP bound to Pt. The results are shown in Figure 5.6.

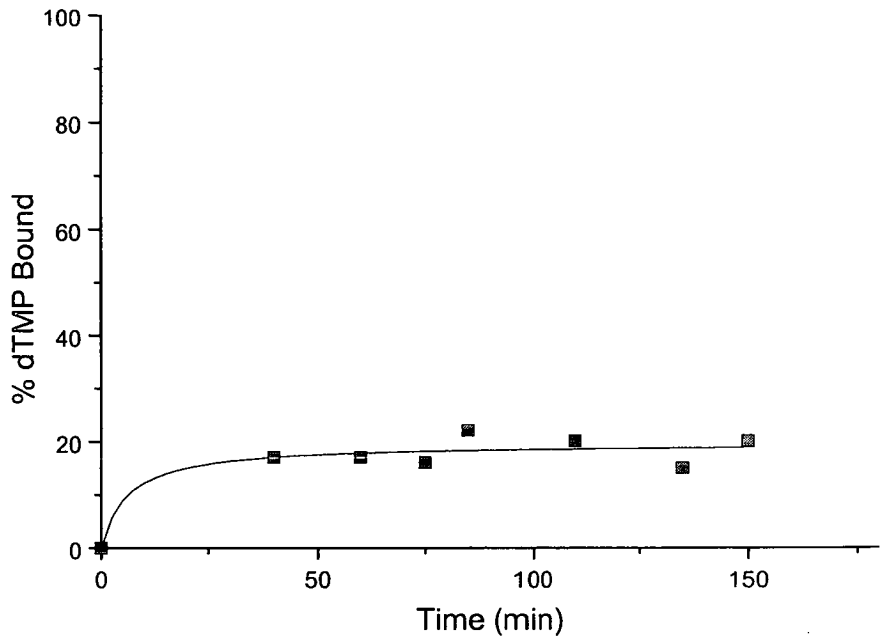

Figure 5.6 Graph showing amount of dTMP bound to [Pt{Me$_2$N(CH$_2$)$_3$PPh$_2$}$_2$Cl$_2$] (**24**) at 10 μM concentration, as determined by HPLC

In the corresponding 1:1 reaction at 5 mM, analysed by ^{1}H NMR (Section 4.2.1.4) all the TMP was bound to Pt. This result shows much lower binding with only 20% of the nucleotide being bound in total. The previous results from the HPLC competition reactions with all four nucleotides and the complex present at 1 mM also showed that 50% of the TMP was bound despite being in competition with GMP, AMP, and CMP. These results therefore suggest that the concentration of the reaction mixture has a big effect on the amount of TMP binding that occurs to complex **24**.

5.3.3 Ageing of Complex Solution

Another factor which has been identifed as influential in the thymine binding reactions of [Pt{$Me_2N(CH_2)_3PPh_2$}$_2Cl_2$] (**24**) is the length of time the complex has been in aqueous solution. As discussed in Section 3.3.2, complex **24**, changes into new species over a 3 day period in solution at ambient temperature.

The DPP and HPLC reactions described in this chapter were carried out using a stock solution of complex which was prepared and stored at room temperature in a flask, protected from sunlight. The solution was aged more than 2 weeks when used in the reactions. In order to determine the effect of time in solution on the binding of complex **24** to dTMP, the CE competition reaction as described in Section 4.2.3 was repeated using complex that had been aged in solution for 2 weeks. The results are shown in Figure 5.7.

By measuring the area of the peaks for the free nucleotides it was determined that when a fresh solution of complex **24** was used in the reaction 60% of the GMP and 59% of TMP were bound to Pt. However when the aged solution of complex **24** was used only 35% of the GMP and 22% of the TMP was bound to Pt. This shows that the new species formed change the selectivity of nucleotide binding. The overall amount of binding was reduced from 1.19 mole equivalents of nucleotide (i.e. all Pt is nucleotide bound with at least 19% bifunctional adducts formed) to 0.57 mole equivalents (i.e. only just over half the Pt has formed a nucleotide adduct at all). Also the preference for thymine binding has been reduced compared to guanine. This could be due to the demethylation of the ligands in [Pt{$Me_2N(CH_2)_3PPh_2$}$_2Cl_2$] (**24**) as proposed in Section 3.3.2. The amine groups could play an important role in thymine binding by abstracting the N3 proton to allow Pt to bind at this site.

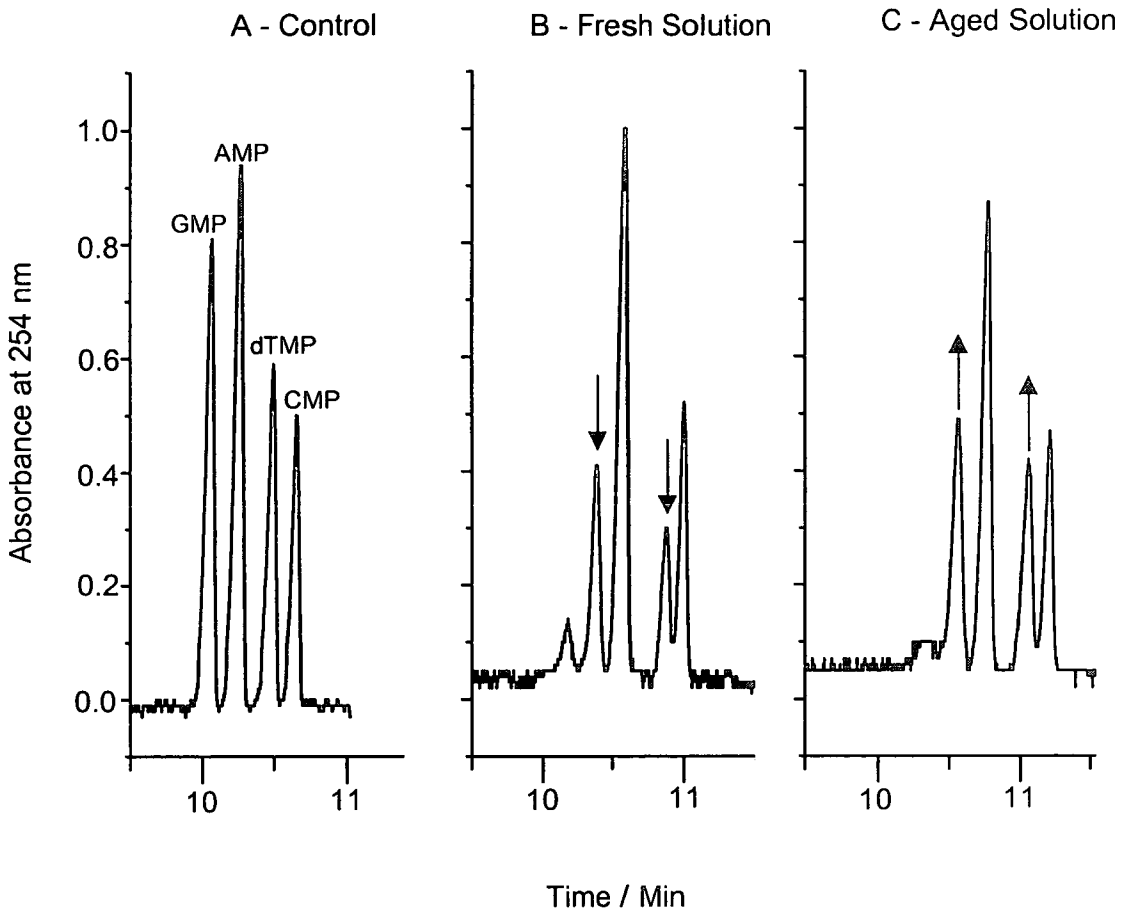

Figure 5.7 Electropherograms showing four nucleotides at 100 μM concentration with: (A) no Pt added, (B) complex **24** from fresh solution added, (C) complex **24** from aged solution added, at pH 7.1 after incubation at 310 K for 12 hours

The same trend was observed when the HPLC competition reaction as described in Section 4.2.2 was repeated using an aged complex solution. (Figure 5.8)

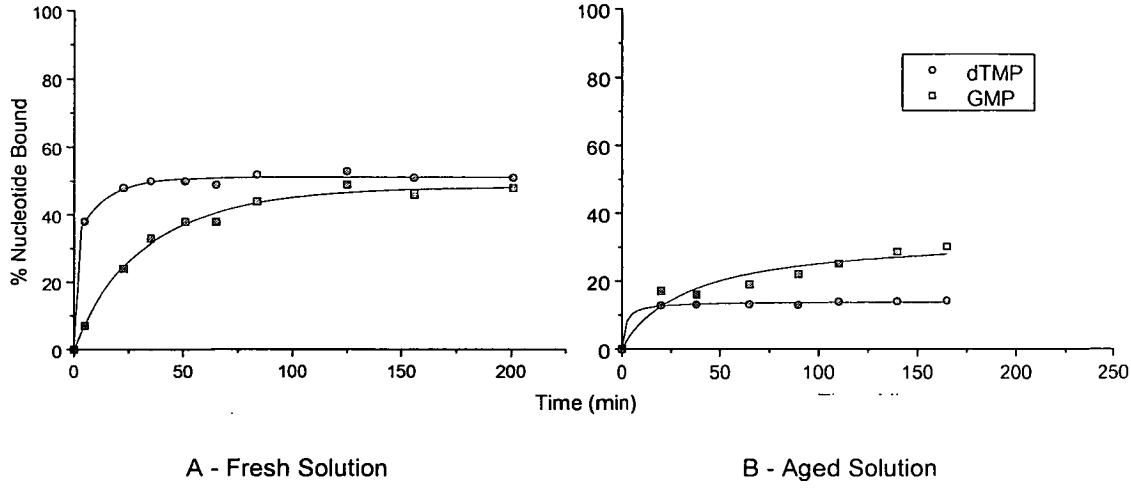

Figure 5.8 Graph showing percentage of TMP and GMP bound in a competition reaction between complex **24** and equimolar amounts of all four nucleotides: (A) using fresh complex solution, (B) using solution aged 2 weeks

With fresh solution the complex bound a maximum of 50% TMP and 48% GMP. After ageing the complex in solution for 2 weeks only 14% TMP and 30% GMP were bound. This highlights the reduction in overall binding and the loss of selectivity for thymine as the species in solution have changed.

5.4 Rate of Binding to DNA

The HPLC reactions described in Section 4.2.2 showed that binding of [Pt{Me$_2$N(CH$_2$)$_3$PPh$_2$}$_2$Cl$_2$] (**24**) to nucleotides took place rapidly (T_{50} for dTMP = 25 min) in a 1:1 reaction with all nucleotides (GMP, AMP, CMP, dTMP) present (Figure 4.12). DPP reactions with calf thymus DNA showed T_{50} = 3 h, a much lower rate of binding despite the 10 fold excess of nucleotide residues present.

Due to the inconsistencies of these results the rate of binding complex **24** to calf thymus DNA was determined by following the changes in the CD spectra with Pt binding. As discussed in Section 5.1.3, Pt binding induces a reduction of the positive

band in the spectrum (280 nm) and a corresponding reduction of the negative band (245 nm). The reaction was carried out as described in Section 5.2.3 and the results are shown in Figure 5.9.

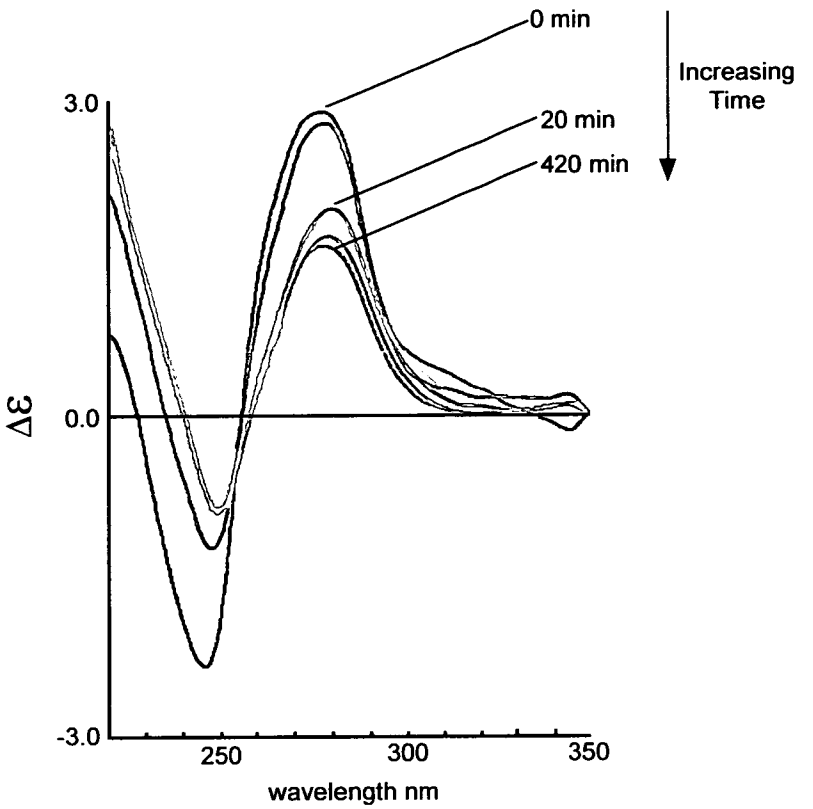

Figure 5.9 CD Spectroscopy of CT DNA modified by [Pt{$Me_2N(CH_2)_3PPh_2$}$_2Cl_2$] (**24**) at various time intervals after reaction

The reaction was seen to be complete after 24 hours as no further change was observed in the spectrum from 24 to 48 hours. The height of the band at 280 nm in the 24 hour spectrum was taken to correspond to all the Pt being bound to the DNA. In the same way the band height at 280 nm for the control spectrum was taken to correspond to no Pt binding. By plotting the peak height versus time for all the spectra at different time intervals, a T_{50} value of 20 minutes was calculated (Figure 5.10).

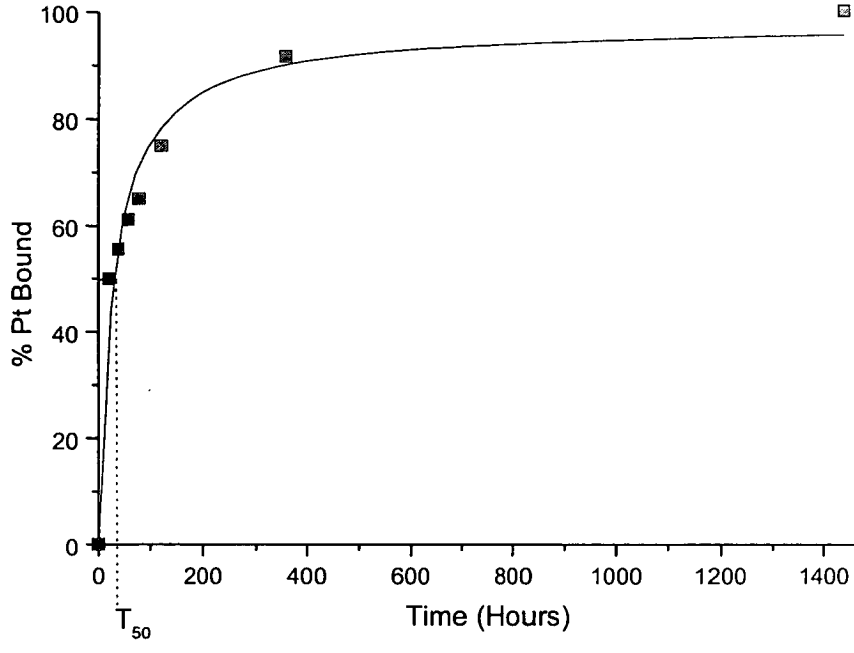

Figure 5.10 Graph showing amount of Pt bound to calf thymus DNA as determined by following changes in the CD spectrum of the DNA

This rate of binding is much lower than that observed in the DPP experiments with calf thymus DNA, with a T_{50} value similar to that seen in HPLC experiments with mononucleotides. It was therefore postulated that there are two forms of interaction between complex **24** and DNA. One is covalent binding to N-sites on the bases on DNA, which occurs relatively slowly and is observed by DPP. The other is a purely electrostatic interaction between the protonated amine arm of the ligand in the complex and the negative phosphate groups in DNA. This occurs prior to covalent binding and leads to conformational changes in the DNA leading to the observed changes in the CD spectrum as discussed in Section 5.1.3. This electrostatic interaction is not strong enough to allow the Pt to be precipitated out with the DNA in the electrolyte solution in the DPP experiment, hence Pt is seen as unbound for longer until covalent binding takes place. The electrostatic interaction may aid covalent binding by positioning the Pt in close proximity to the DNA bases. This

would account for the increased rate of covalent binding of complex **24** to CT DNA compared to cisplatin as described in Section 5.1.1.

5.4.1 Effect of pH on changes to CD Spectrum

In order to support the postulate above, that [Pt{$Me_2N(CH_2)_3PPh_2$}$_2Cl_2$] (**24**) forms electrostatic interactions with DNA, the effect of increasing pH on the changes in the CD spectrum was investigated. Higher pH should reduce the number of protonated amines on the ligand and hence reduce the amount of electrostatic attraction to the DNA phosphates. The results of increasing the pH to 9, as described in Section 5.2.3, are shown in Figure 5.11.

A blank sample was recorded at high pH to confirm that the pH was not having any effect on the DNA conformation. The platinated sample was recorded after 2 hours when DNA binding was seen to have occurred by the reduction in the positive band at 280 nm. The pH of the sample was then increased to 9 and the recorded spectra after 1 hour and 6 hours at this pH showed the band at 280 nm to have increased again. This indicated that the Pt binding had reduced allowing the conformation of the DNA to move back to that of unmodified DNA. This supports the postulate that the binding is of an electrostatic nature and is reduced by increasing pH and deprotonating the amine groups on the ligands of the complex.

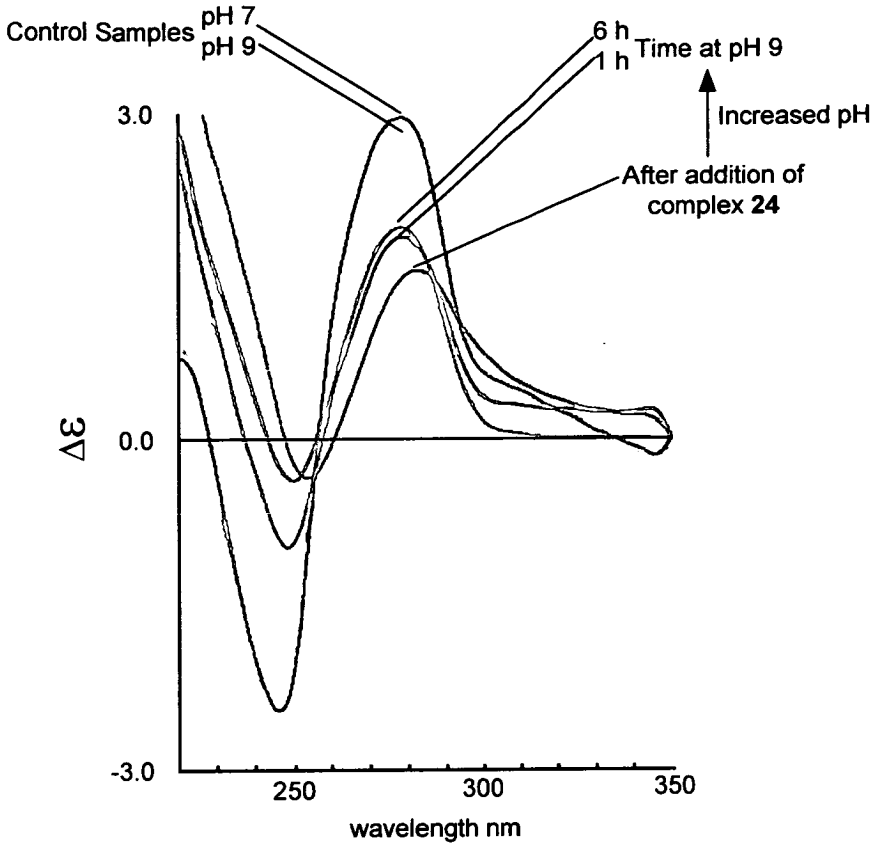

Figure 5.11 CD Spectroscopy to show effect of increased pH on changes induced in DNA by modification with [Pt{$Me_2N(CH_2)_3PPh_2$}$_2Cl_2$] (**24**)

5.5 Conclusions

The binding of [Pt{$Me_2N(CH_2)_3PPh_2$}$_2Cl_2$] (**24**) to natural and synthetic DNAs has been investigated by a variety of methods including differential pulse polarography, cicular dichroism spectroscopy and high performance liquid chromatography. The most notable result was the lack of binding to poly (dT), despite the previous evidence of strong, rapid binding to the mononucleotide dTMP. This was shown to be due to a combination of factors. Firstly the concentration plays a role – this was proved by HPLC studies reaction complex **24** with dTMP in a 1:1 ratio at a concentration of 10 μM. Only 20% of the nucleotide was bound in the reaction in

comparison to the same reaction at 5 mM followed by ^{1}H NMR in which all the dTMP was bound to Pt. Secondly the age of the complex solution used was shown to play a role. Since [Pt{$Me_2N(CH_2)_3PPh_2$}$_2Cl_2$] (**24**) changes species in aqueous solution with time, the CE and HPLC competition reactions described in Section 4.2 were repeated using complex aged in solution for 2 weeks as opposed to freshly made. The results showed that the new species formed had a much reduced level of nucleotide binding and the preference for thymine binding was greatly reduced too.

The rate of the reaction between [Pt{$Me_2N(CH_2)_3PPh_2$}$_2Cl_2$] (**24**) and calf thymus DNA was also investigated. By following the change in the CD spectrum of the DNA during the reaction, the kinetics were very fast (T_{50} = 20 min), this is due to a fast electrostatic interaction between the protonated amines in the ligands of the complex and the negative phosphates on the DNA. This was proved by a reversal of the effect induced by using a higher pH to deprotonate the amines and reduce the electrostatic attraction. By following the amount of Pt binding to CT DNA by DPP, the rate of the reaction was shown to be much slower (T_{50} = 3 h). This is due to the fact that the electrostatic interaction is too weak to cause precipitation of the Pt in the electrolyte with the DNA. The experiment therefore highlights the rate of covalent binding of the complex to DNA. This is much slower than the electrostatic interaction but still faster than that observed for cisplatin, perhaps because the initial electrostatic attraction places the Pt in close proximity to the binding sites on the DNA.

Overall [Pt{$Me_2N(CH_2)_3PPh_2$}$_2Cl_2$] (**24**) shows a comparable level of DNA binding to cisplatin but with different site selectivity. This could provide potential for the development of the next generation of Pt anticancer agents with reduced resistance compared to cisplatin.

5.6 References

1 K. Neplechová, J. Kašpárková, O. Vrána, O. Nováková, A. Habtemariam, B. Watchman, P. J. Sadler, V. Brabec, *Mol. Pharm.* **1999**, *56*, 20

2 D. P. Bancroft, C. A. Lepre, S. J. Lippard, *J. Am. Chem. Soc,* **1990**, *112*, 6860

3 N. P. Johnson, J. P. Maquet, J. L. Wiebers, B. Monsarrat, *Nucleic Acids Res.* **1982**, *10*, 5255

4 A. M. J. Fichtinger-Schepman, J. L. Van der Leer, J. H. J. Den Hartog, P. H. M. Lohman, J. Reedijk, *Biochemistry* **1985**, *24*, 707

5 A. Eastman, *Pharmacol. Ther.* **1987**, *34*, 155

6 O. Vrána, V. Brabec, V. Kleinwächter, *Anti-Cancer Drug Des.* **1986**, *1*, 95

7 V. Brabec, V. Kleinwächter, J. L. Butour, N. P. Johnson, *Biophys. Chem.* **1990**, *35*, 129

8 C. Chen, R. Kilkuskie, S. Hanlon, *Biochemistry* **1981**, *20*, 4987

9 D. M. Gray, in *Circular Dichroism and the conformational analysis of biomolecules*, G. D. Fasman; Ed. Plenum Press, New York, **1996**, pp 469-500

10 S. D. Kim, O. Vrána, V. Kleinwächter, K. Niki, V. Brabec, *Anal. Letters* **1990**, *23*, 1505

Chapter Six

Platinum–AZT Complexes as Potential Anti–HIV Agents

As discussed in the previous two chapters, the series of platinum aminophosphine complexes synthesised in this thesis have an unusual affinity for binding to thymine residues. This is in contrast to traditional platinum anticancer drugs which have been shown to bind predominantly to guanine and adenine residues on DNA.[1] For this reason it was hypothesised that these complexes would be good targets for binding the anti-viral drug 3'-azido, 3'-deoxy tymidine, AZT. This is a thymine analogue used as a drug in the treatment of HIV[2] (Section 1.6.1.2). The structure of AZT is shown in Figure 6.1.

A platinum–AZT adduct could have potential as a *multifunctional* drug with synergistic interactions between the Pt agent and the antiviral nucleoside acting via different mechanisms of action to produce a more effective drug. This idea has already been employed, and the therapeutic potential of a Pt-Acyclovir complex has been investigated. $[PtCl(NH_3)_2(acyclovir)]NO_3$ has been shown to have similar antiviral activity to that of the acyclovir parent drug whilst also exhibiting *in vivo* anticancer properties in cisplatin-resistant cell lines.[3]

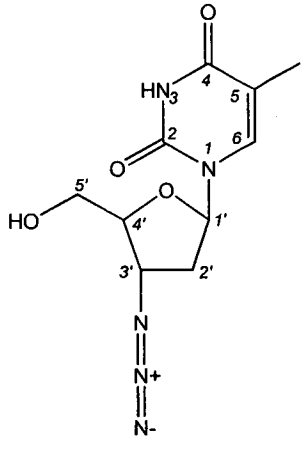

Figure 6.1 Structure and numbering scheme of the anti-HIV agent AZT

6.1 Experimental Methods

6.1 1 NMR Spectroscopy

Acquisition details for NMR spectroscopy are given in Section 2.3.1. Samples were prepared containing the relevant complex and AZT both at a concentration of 5 mM in D_2O. The pH* values of the samples were measured as described in Section 2.3.7 and adjusted as required using 0.1 M DNO_3 or NaOD. Dioxane solution (2 μl, 5%) was added to each sample to act as a reference. The samples were placed in a water bath at 310 K overnight to ensure complete reaction.

6.1.2 Electrospray Ionisation Mass Spectrometry

The ESI-MS equipment and experimental parameters are described in Section 2.3.3. Samples were prepared containing the appropriate complex at 1 mM concentration and AZT at 2 mM concentration in water. The pH of each sample was adjusted to close to physiological pH (7.4) and the samples were incubated overnight at 310 K in a water bath to ensure complete reaction. Prior to analysis the samples were diluted to 50 μM with water.

6.2 Binding of Complexes to AZT

The reaction of complexes **24**, **25**, **26**, and **27** (Figure 6.2) with AZT was carried out as described above, and studied by ^{1}H and ^{31}P NMR. Previous studies on reactions with the nucleotide dTMP (Chapter 4) showed that binding of these complexes increased with increasing pH due to deprotonation of the N3 binding site. For this reason the reactions were carried out at ca. pH 9 in order to achieve maximum binding. All the reactions were carried out at a 1:1 Pt:AZT ratio.

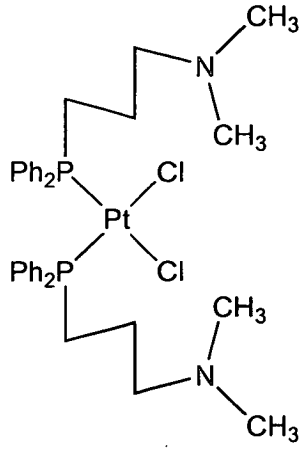

Complex **24**

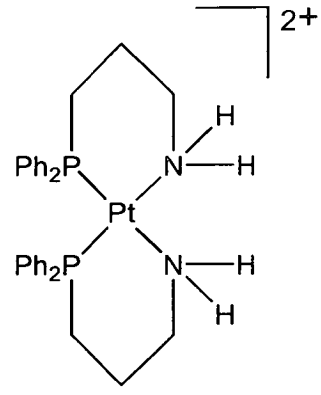

Complex **25**

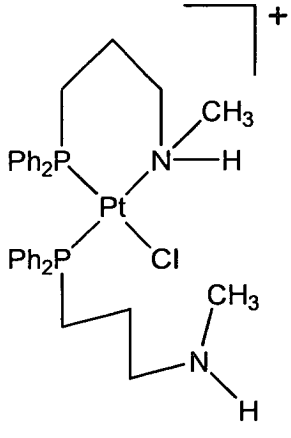

Complex **26**

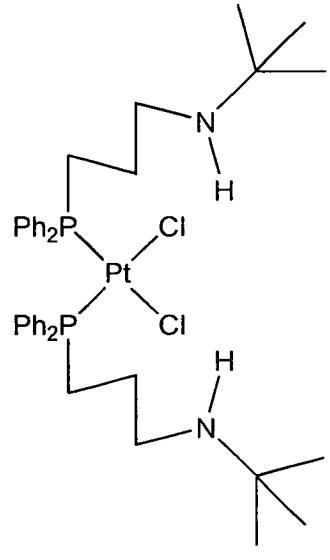

Complex **27**

Figure 6.2 Structures of platinum aminophosphine complexes **24** – **27**

In the ^{1}H spectra for each of the four reactions, Pt bound species could be identified with resonances upfield from free AZT.

Shifts for resonances in free AZT:		H6: 7.67 ppm,	H1': 6.23 ppm
H3': 4.36 ppm	H4': 4.03 ppm	H2': 3.83 ppm	2H5': 2.54 ppm
Me: 1.90 ppm			

As in the dTMP reactions, the amount of AZT bound to the complex in the reaction was determined by measurement of the integrals of the H1' signals (occurring in a clear region of the spectrum with a flat baseline) for free and bound species. The results for the four complexes are shown in Table 6.1.

Complex	% AZT Bound
25: $[Pt\{H_2N(CH_2)_3PPh_2\text{-}P,N\}_2]Cl_2$	7.0
26: $[Pt\{Me(H)N(CH_2)_3PPh_2\}_2Cl]Cl$	37.0
24: $[Pt\{Me_2N(CH_2)_3PPh_2\text{-}P\}_2Cl_2]$	86.5
27: $[Pt\{^tBu(H)N(CH_2)_3PPh_2\text{-}P\}_2Cl_2]$	95.5

Table 6.1 Amount of bound AZT determined by ^1H NMR, for complexes **24-27** in a 1:1 reaction at pH 9

These results show a clear correlation between the amount of AZT binding and the tendency for the complexes to exist in a ring-opened form. Complex **27** has shown no evidence of ring-closing, probably due to the steric bulk of the tertiary butyl groups, and binds virtually all the AZT present. This would be expected due to the presence of labile chloride leaving groups. Complex **24,** whilst prepared only as the ring-opened species, does undergo hydrolysis reactions in aqueous solution to form some ring-closed species (Section 3.3.2). The ring-closed species does not promote AZT binding since there are no labile ligands and so only 86.5% of the AZT is bound. Complex **26** undergoes ring-closing dependent on pH, as shown in Section 3.3.1, with a pK = 6.1. At high pH a large proportion of the complex is fully ring-closed preventing AZT binding, hence only 37% of the AZT is bound during this reaction. Complex **25** also undergoes ring-closing at high pH but the pK for this complex is much lower at 2.9. Hence at high pH this complex is nearly all ring-closed and virtually no AZT binding is observed, only 7%. The amount of AZT binding is therefore dependent on the amount of ring-opened species present which is

related to the steric bulk of the alkyl groups on the amine in the ligand as discussed in Section 3.3.2.

The amount of binding for all complexes is less than 100% suggesting that binding is occuring in a monofunctional manner only. The ^{31}P NMR of the four AZT reactions were also recorded to obtain further information about the binding mode.

The spectrum of the 1:1 reaction between [Pt{$Me_2N(CH_2)_3PPh_2$-*P*}$_2Cl_2$] (**24**) and AZT is shown in Figure 6.3. There are three pairs of doublets, identified by their coupling constants, all in the range 19-21 Hz, suggesting 3 species (**a**, **b** and **c**) with non-equivalent P atoms in a *cis* orientation. Species **c** corresponds to unbound complex (only 86.5% of the AZT was bound in the reaction leaving 13.5% unbound Pt). This species has two doublets at 0.6 and –3.2 ppm and corresponds to the final species produced in the hydrolysis reactions of [Pt{$Me_2N(CH_2)_3PPh_2$-*P*}$_2Cl_2$] (**24**) as described in Section 3.3.2. Species **a** and **b** are both new products with AZT bound, and both contain one P atom with a downfield doublet at ca. –2.5 ppm and another P atom with an upfield doublet at ca. –8.5 ppm. The ^{1}J(Pt-P) coupling constants for both species are 3293 Hz for the downfield peak and 3252 Hz for the upfield peak, indicating N to be present in the positions *trans* to both P.[4,5] The very similar shifts and coupling for these two species **a** and **b** suggest that they are likely to be isomers of the same product, this will be discussed further in Section 6.2.3. The bound species is likely to contain AZT bound via N3 and one ring-closed ligand (Figure 6.4), thus accounting for the coupling constants observed.

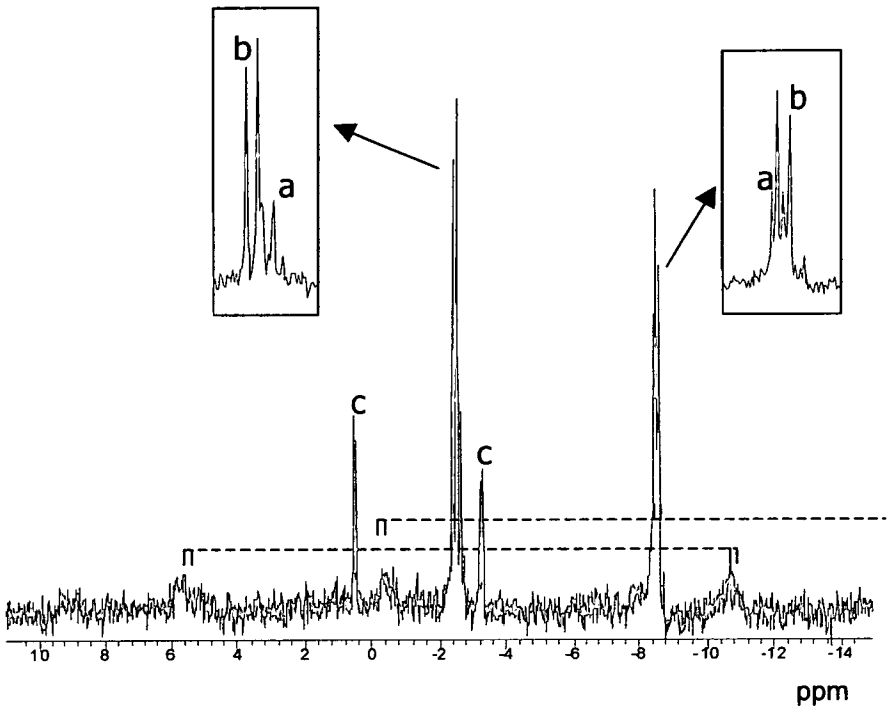

Figure 6.3 ^{31}P NMR spectrum of [Pt{$Me_2N(CH_2)_3PPh_2$-*P*}$_2Cl_2$] (**24**) with 1 mole equivalent of AZT present, pH 9

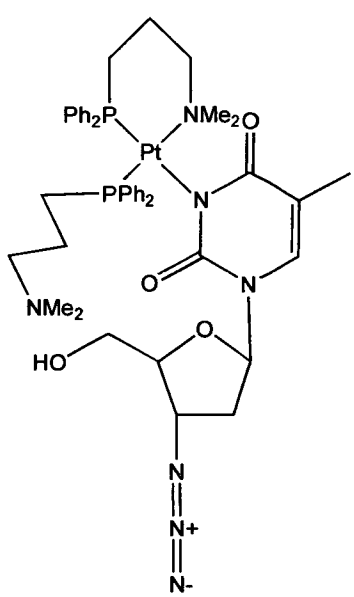

Figure 6.4 N3-bound monofunctional adduct of AZT and complex **24** (coloured atoms correspond to resonances in ^{31}P NMR spectrum in Figure 6.3)

The ^{31}P NMR spectrum for the reaction between $[Pt\{H_2N(CH_2)_3PPh_2\text{-}P,N\}_2]Cl_2$ (**25**) and AZT produced only one singlet at –1.95 ppm with platinum satellites. The singlet is due to the unbound complex, which is fully ring-closed therefore containing two equivalent P atoms. The $^1J(Pt\text{-}P) = 3205$ Hz consistent with N in the *trans* position.[4,5] This correlates to the ^1H NMR results which showed that only a very small amount of the complex was bound to AZT in the reaction.

The reaction between $[Pt\{Me(H)N(CH_2)_3PPh_2\}_2Cl]Cl$ (**26**) and AZT produced the spectrum shown in Figure 6.5. Some unbound complex can be seen as a singlet at –4.7 ppm. This is in the fully ring-closed form as would be expected at pH 9 with two equivalent P atoms. In addition to this peak, there are 4 bound species, each with 2 inequivalent *cis* P atoms producing 4 pairs of doublets (**a-d**). Each product has a downfield doublet at ca. –1.5 ppm and an upfield doublet at ca. –11.0 ppm. These four species are again likely to be isomers of an N3-bound adduct. This is discussed further in Section 6.2.3.

The spectrum from the reaction between $[Pt\{^tBu(H)N(CH_2)_3PPh_2\text{-}P\}_2Cl_2]$ (**27**) and AZT is shown in Figure 6.6. Here, no free complex can be observed as would be expected from the ^1H NMR results. As for the reaction of complex **26**, there are four bound products, **a-d**, each containing two inequivalent P atoms and producing two doublets each in the spectrum. Products **a** and **b** have a downfield doublet at ca. 4.6 ppm and an upfield doublet at ca. 0.0 ppm. Products **c** and **d** have an downfield doublet at ca. 1.5 ppm and an upfield doublet at ca. –1.0 ppm. In all four species the downfield doublet has a $^1J(Pt\text{-}P)$ coupling much greater than 3600 Hz suggesting that the ligand in the *trans* position is chloride, whilst the upfield doublet has a $^1J(Pt\text{-}P)$ coupling much less than 3600 Hz suggesting that the ligand in the *trans* position is nitrogen.[4,5] The bound species is therefore thought to contain AZT bound via N3 and both aminophosphine ligands ring-opened with a chloride in the fourth site. This structure is shown in Figure 6.7. The four distinct species are likely to be isomers of this compound, as discussed in Section 6.2.3.

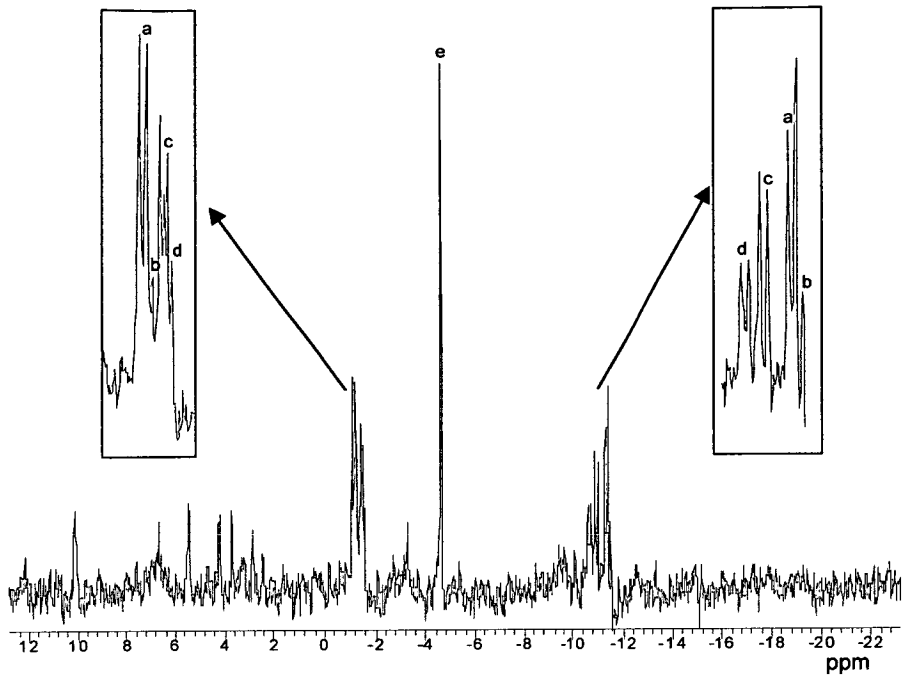

Figure 6.5 ^{31}P NMR spectrum of $[Pt\{Me(H)N(CH_2)_3PPh_2\}_2Cl]Cl$ (**26**) with 1 mole equivalent of AZT present, pH 9

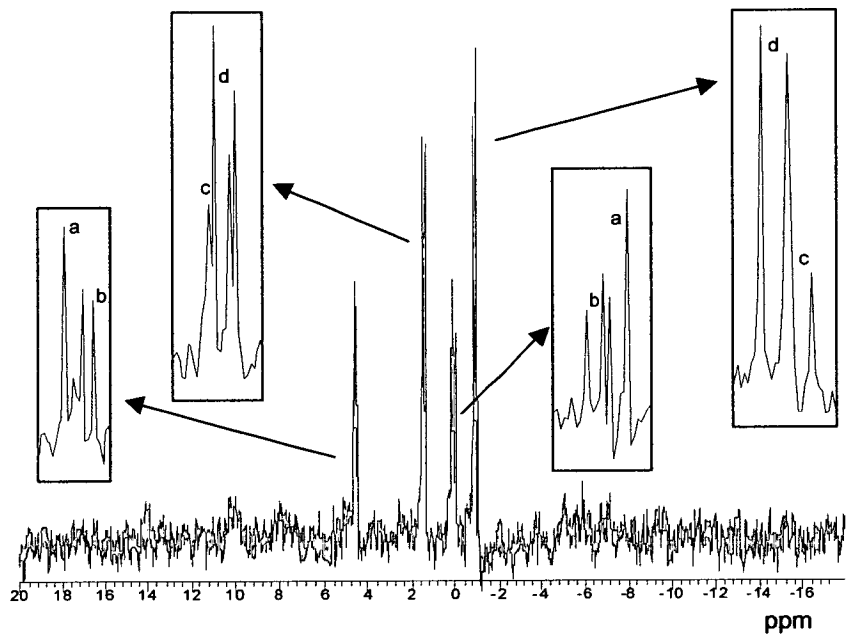

Figure 6.6 ^{31}P NMR spectrum of $[Pt\{^tBu(H)N(CH_2)_3PPh_2\text{-}P\}_2Cl_2]$ (**27**) with 1 mole equivalent of AZT present, pH 9

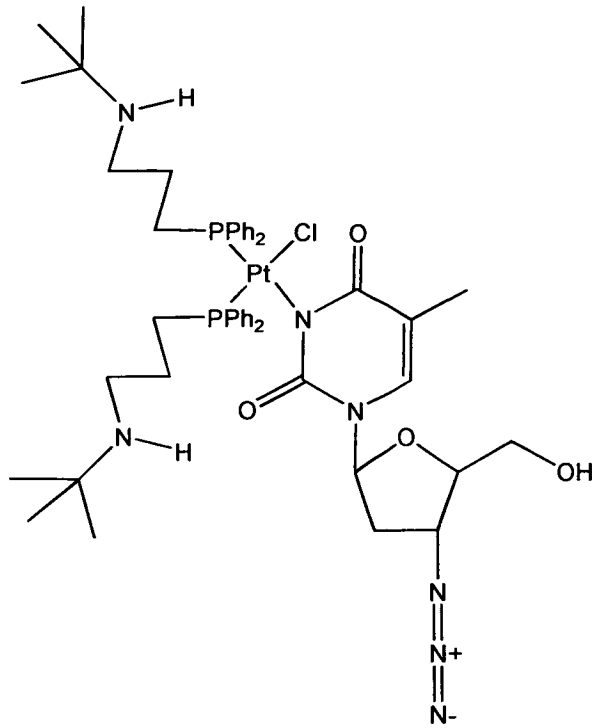

Figure 6.7 N3-bound monofunctional adduct of AZT and complex **27** (coloured atoms correspond to resonances in ^{31}P NMR spectrum in Figure 6.6)

6.2.1 Effect of pH on AZT Binding

As was seen for the reactions of the complexes with the nucleotide dTMP in Section 4.2 1, the reactions with AZT are likely to be affected by the pH of the reaction since the Pt binding site is N3 which is usually protonated up to pH values of about 10. Titrations of pH were therefore carried out on the reaction mixtures of complexes **24** and **27**. ^{1}H NMR spectra were recorded at various pH values as described in Section 6.1.1 and the amount of AZT bound was determined by integration of the H1' signal for the bound and free AZT. The results are shown in Figure 6.8 and 6.9 for complexes **24** and **27** respectively. p*K* values were obtained by fitting to the Henderson-Hasselbach equation using the program KALEIDAGRAPH.[6]

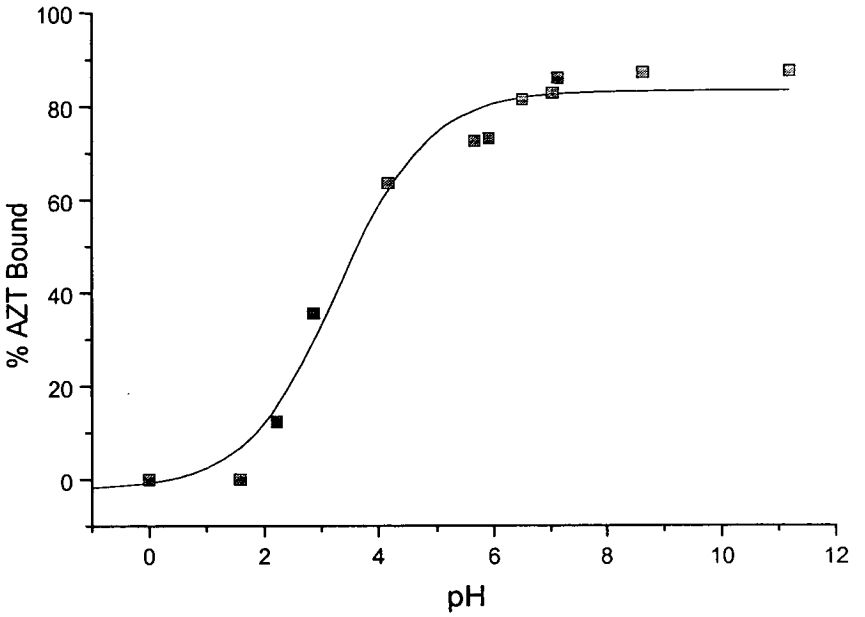

Figure 6.8 Graph showing effect of pH on amount of AZT binding to $[Pt\{Me_2N(CH_2)_3PPh_2\text{-}P\}_2Cl_2]$ (**24**) in a 1:1 reaction

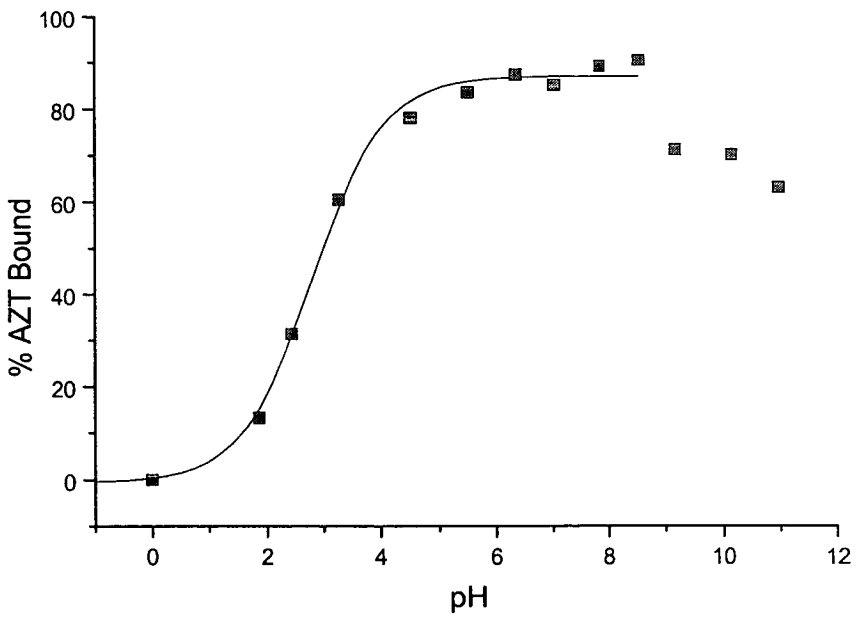

Figure 6.9 Graph showing effect of pH on amount of AZT binding to $[Pt\{^tBu(H)N(CH_2)_3PPh_2\text{-}P\}_2Cl_2]$ (**27**) in a 1:1 reaction

Both graphs clearly show an increase in the amount of AZT bound with increasing pH as predicted. Binding occurs over a large pH range starting as low as 2 and continuing up to 12. For complex **27**, a precipitate appeared in the solution above pH 9 causing a reduction in the intensities of the signals in the NMR. For complex **24**, the pK value for binding AZT was determined to be 3.29 ± 0.17 and for complex **27** the pK value was 2.80 ± 0.05. These values are remarkably low since the pK_a value for the AZT N3 site is in the region of 10. This again indicates the influence of the amine groups, in the ligands of the complex, in abstracting a proton to allow Pt binding.

6.2.2 Characterisation of AZT Adducts

As for the nucleotide adducts of complexes **24**, **25**, and **27**, electrospray ionisation mass spectrometry was used to determine the nature of the AZT adducts. The ESI-MS spectrum of the reaction between [Pt{$Me_2N(CH_2)_3PPh_2$-P}$_2Cl_2$] (**24**) and AZT was recorded as described in Section 6.1.2 and is shown in Figure 6.10.

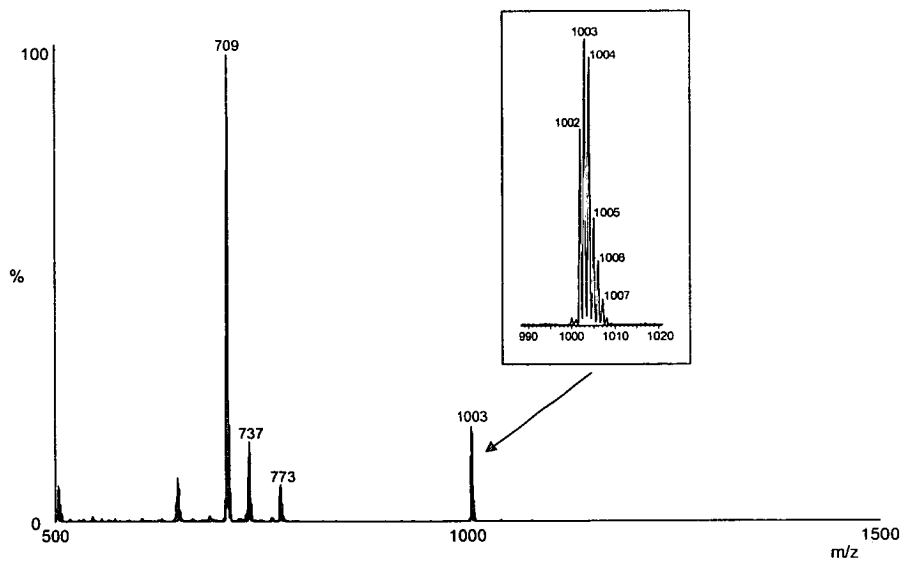

Figure 6.10 ESI-MS spectrum of [Pt{$Me_2N(CH_2)_3PPh_2$-P}$_2Cl_2$] (**24**) and AZT (expansion shows isotope pattern for monofunctional adducts)

A monfunctional adduct containing Pt with two DMDPPA ligands and one AZT is clearly seen at 1004 m/z. (Calculated m/z for $PtC_{44}H_{56}N_7O_4P_2$ = 1004) The assignment of this species was confirmed by the calculation of an isotope model for the corresponding compound in the Mass Lynx (V 2.3) program. No bifunctional adducts were observed. (Calculated m/z for $PtC_{54}H_{68}N_{12}O_8P_2$ = 1270) This confirms the assumption from the ratio of AZT bound in the ^1H NMR experiment, that complex **24** only forms monofunctional adducts with AZT.

The ESI-MS spectrum of the reaction between $[Pt\{H_2N(CH_2)_3PPh_2\text{-}P,N\}_2]Cl_2$ (**25**) and AZT was recorded as described in Section 6.1.2 and is shown in Figure 6.11.

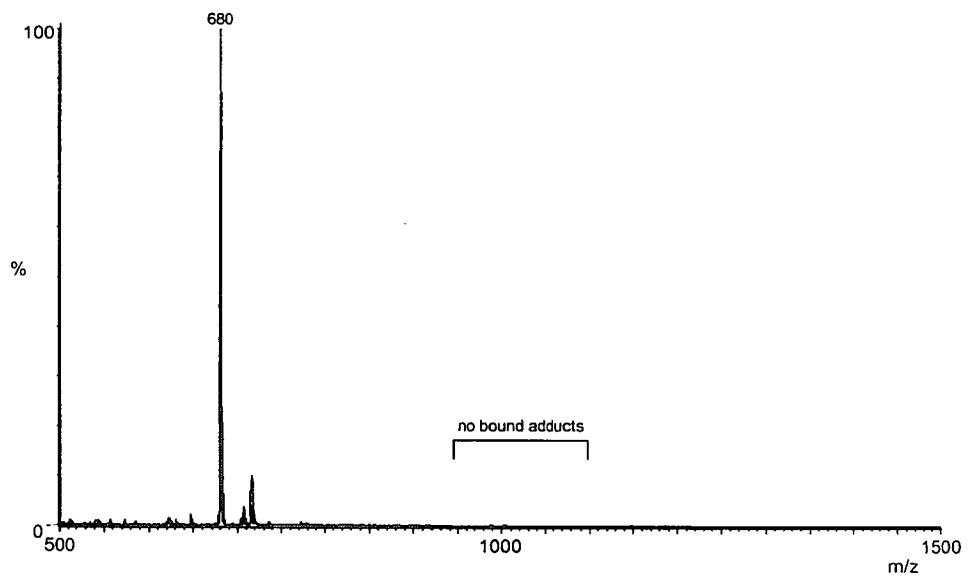

Figure 6.11 ESI-MS spectrum of $[Pt\{H_2N(CH_2)_3PPh_2\text{-}P,N\}_2]Cl_2$ (**25**) and AZT (expansion shows isotope pattern for monofunctional adducts)

Again this confirmed the ^1H NMR results, where very little binding was observed, since no Pt bound AZT adducts were detected. The major peak observed was at 680 m/z and corresponds to Pt with two DPPA ligands. (Calculated m/z for $PtC_{30}H_{36}N_2P_2$ = 680)

The ESI-MS spectrum of the reaction between [Pt{^{t}Bu(H)N$(CH_2)_3PPh_2$-*P*}$_2Cl_2$] (**27**) and AZT was recorded as described in Section 6.1.2 and is shown in Figure 6.12.

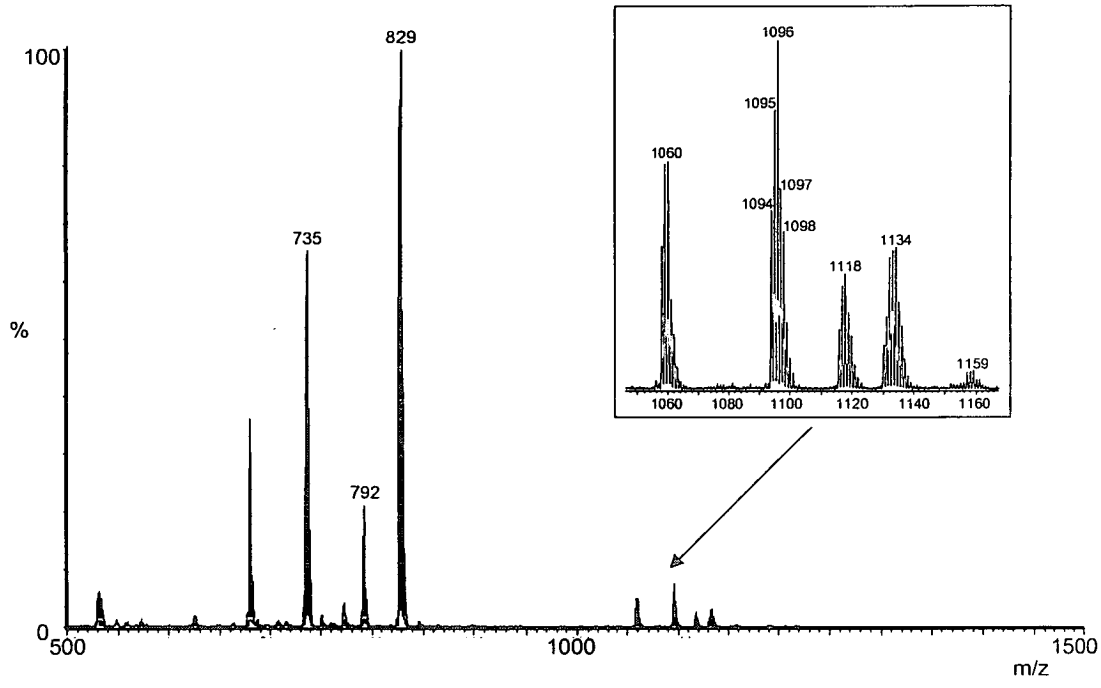

Figure 6.12 ESI-MS spectrum of [Pt{^{t}Bu(H)N$(CH_2)_3PPh_2$-*P*}$_2Cl_2$] (**27**) and AZT (expansion shows isotope pattern for monofunctional adducts)

In this spectrum quite intense signals were detected for the monofunctional adduct of complex **27** and AZT at 1096 m/z. (Calculated m/z for $PtC_{48}H_{64}N_7O_4P_2Cl$ = 1095.5) This assignment was again confirmed by the use of an isotope model. This main peak is accompanied by peaks at 1060 (adduct with loss of chloride) and 1118, 1134, 1159 m/z (addition of sodium ions). Complex **27** also seems to be limited to the formation of monfunctional adducts as was the case for complex **24**. (Calculated m/z for $PtC_{58}H_{68}N_{12}O_8P_2$ = 1328)

6.2.3 Diastereomers of AZT Adducts

It is apparent from the NMR results already discussed for the AZT reactions that AZT binding gives rise to a number of different species. The similarity in the NMR

parameters for the species produced in each reaction suggest that the adducts are very similar, probably isomers.

Whilst the complexes themselves are not chiral, an unsymmetrical incoming ligand like AZT will produce enantiomers when added, as a consequence of having head/tail directionality. Such chirality is termed *planar chirality* and is defined as the stereoisomerism resulting from the arrangement of out-of-plane groups with respect to the chirality plane.[7] This is caused by the a monodentate planar ring with only C_s symmetry orthogonally bound to a metal centre with two other different ligands *cis*-coordinated with respect to the ring.[8] In these complexes the AZT is the monodentate planar ring and can coordinate in either a "head" or "tail" position, determined by the direction the methyl group points, above or below the ring respectively creating two possible isomers.

In the cases of complexes **24** and **26** where one aminophosphine ligand in the complex is fixed in a ring-closed comformation, these two isomers can be defined as:
A: the methyl group on the AZT and the pendant aminophosphine ligand are on the same side of the Pt coordination plane
B: the methyl group on the AZT and the pendant aminophosphine ligand are on opposite sides of the Pt coordination plane
It has been shown that in analogous Pt-nucleotide complexes, that the presence of bulky ligands on the Pt can slow down rotation of the Pt-nuc bonds and create species which are distinct in their NMR observation.[9-12]

Since the AZT molecule is itself chiral, as is also the case for the nucleotide GMP, diastereomers are generated. Four energetically distinct species are possible since there are two diastereomeric forms of each rotational isomer. These species are shown in Scheme 6.1.

Previous work on a similar complex to those used in this thesis, *cis*-$[Pt\{Me_2N(CH_2)_2PPh_2\}_2Cl]Cl$, showed that the same possible isomers could be

formed with GMP.[13] Molecular modelling allowed the barriers to rotation between the isomers to be calculated. The rotation of the Pt-P bond appeared to be a relatively facile process which could occur at a significant rate but rotation of the Pt-N7(guanine) bond was impeded by interactions between the guanine and the coordination plane and would occur only at elevated temperatures. This could account for the fact that for $[Pt\{Me_2N(CH_2)_3PPh_2\text{-}P\}_2Cl_2]$ (**24**) only two bound species were identified in the ^{31}P NMR spectrum after AZT binding. If the interconversion between A and B is very fast then these two species would not be distinct in the NMR spectrum. In the case of $[Pt\{Me(H)N(CH_2)_3PPh_2\}_2Cl]Cl$ (**26**) however, 4 distinct species were observed in the ^{31}P NMR spectrum, this could be due to the presence of hydrogen bonding between the secondary amine on the dangling ligand and the exocyclic O groups on the AZT ring. This would increase the barrier to rotation around Pt-P and prevent interconversion between isomers, leading to the detection of all diastereomers. Such H-bonds have been observed in $Pt(NH_3)_2$ complexes of thymine between N-H from the amine and an exocylic oxygen from the thymine[14] but only *inter*molecular bonds. The aminophosphine ligand in this complex has the added flexibility of a propyl chain before the amine group which could allow the amine to be positioned correctly for *intra*molecular H-bonds to occur.

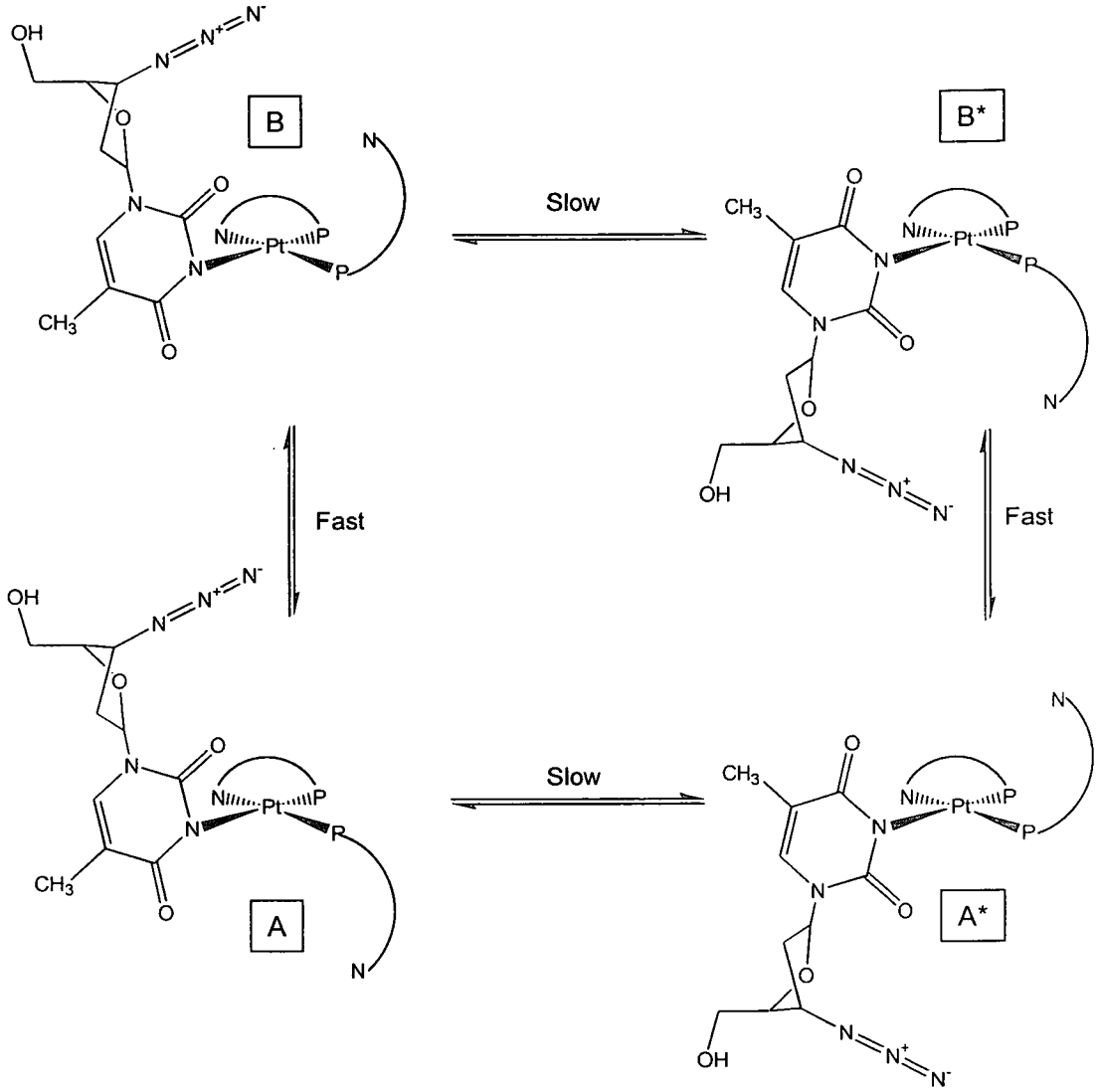

Scheme 6.1 Possible diastereomers formed with AZT and a ring-closed complex

The diastereomers produced when AZT is bound to [Pt{^{t}Bu(H)N(CH$_2$)$_3$PPh$_2$-*P*}$_2$Cl$_2$] (**27**) are further complicated by the fact that the complex contains two ring-opened ligands. This increases the number of possible diastereomers to 8 since each species in Scheme 6.1 can exist as two further rotational isomers with the second dangling ligands either above or below the Pt coordination plane. These are represented schematically in Figure 6.13.

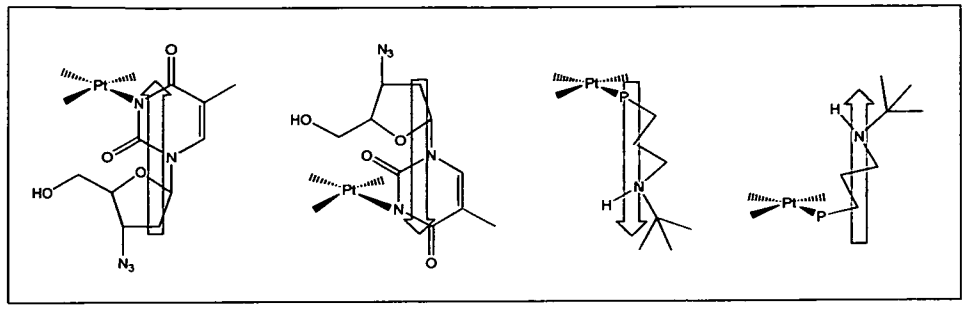

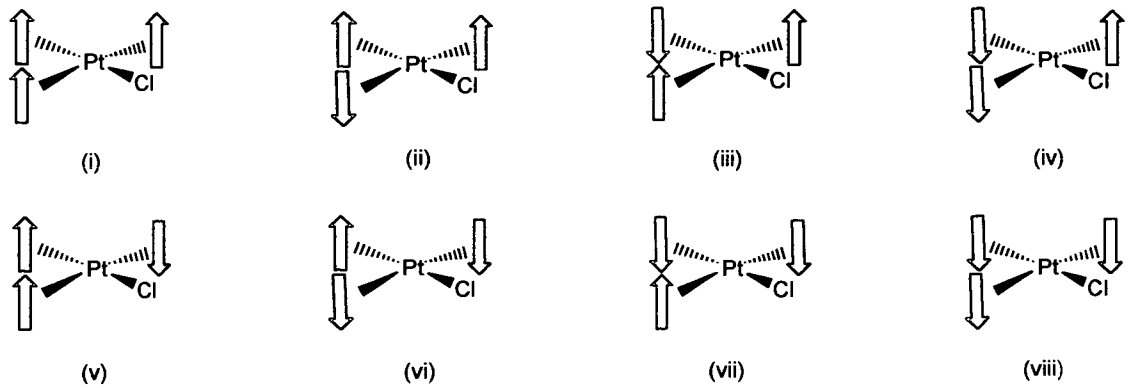

Figure 6.13 Eight possible diastereomers of the AZT adduct of complex **27**, determined by orientation of ligands relative to the Pt coordination plane

Of the eight possible diastereomers, the most favourable are likely to be ii, iii, vi and vii since in these conformations the two aminophosphine ligands are on opposite sides of the coordination plane. This will be favoured due to the steric bulk of the tertiary butyl groups in the ligands hindering the conformations with the ligands on the same side of the plane. This would account for the observation of only four distinct species in the ^{31}P NMR of the reaction between complex **27** and AZT.

In all the AZT adducts there is also the possibility for electrostatic interactions between the azide group in the AZT and the protonated amine group in the ligand. This would stabilise diastereomers with the azide and dangling arm ligand on the same side of the coordination plane. It would also be possible for hydrogen-bonding to occur between one of the exocyclic oxygens on the AZT and the NH on the ligand.

6.3 Conclusions

The binding of the complexes studied to AZT was shown by NMR experiments. The extent of binding was determined by the amount of ring-opened complex present, which is related to the steric bulk on the aminophosphine ligands. The binding was also controlled by pH, with high pH leading to increased binding due to deprotonation of the N3 binding site on the AZT. The adducts formed with AZT were all monofunctional, as determined by both NMR and ESI-MS experiments. In the binding reactions a number of different diastereomers of the bound adducts were observed. These are due to the variation of the orientation of the ligands and AZT relative to the Pt coordination plane. Different diastereomers are preferred for each complex. These may be due to the presence of hydrogen-bonding stabilising some comformations or the destabilising effects of steric hindrance.

The binding to AZT could prove to be very useful in the development of new antiviral drugs against HIV. Potentially the AZT could be used to terminate virus replication whilst the Pt could be employed to kill the damaged host cell and prevent transfer of HIV to other healthy cells. The therapeutic benefits of these Pt-AZT complexes need to be investigated further to assess their potential as multifunctional drugs.

6.4 References

1 A. M. J. Fichtinger-Schapman, J. L. van der Veer, J. H. J. den Hartog, P. H. M. Lohman, J. Reedijk, *Biochemistry*, **1985**, *24*, 707

2 H. D. Langtry, D. M. Campoli-Richards, *Drugs*, **1989**, *37*, 408

3 M. Coluccia, A. Bocarelli, C. Cermelli, M. Portolani, G. Natile, *Metal Based Drugs*, **1995**, *2, 5*, 249

4 G. K. Anderson, H. C. Clark, J. A. Davies, *Inorg. Chem.* **1983**, *22*, 427

5 G. K. Anderson, R. Kumar, *Inorg. Chem.* **1984**, *23*, 4064

6 KALEIDAGRAPH, version 3.09, Synergy Software, reading, PA, **1997**

7 G. P. Moss, *Pure Appl. Chem.* **1996**, *68*, 2193

8 M. C. Biagini, M. Ferrari, M. Lanfranchi, M. A. Pellinghelli, *J. Chem. Soc. Dalton Trans.* **1999**, 1575

9 R. E. Cramer, P. L. Dahlstrom, *J. Am. Chem Soc.* **1979**, *101*, 3676

10 R. Cramer, P. L. Dahlstrom, *Inorg. Chem.* **1985**, *24*, 3420

11 Y. Xu, G. Natile, F. P. Intini, L. G. Marzilli, *J. Am. Chem. Soc.* **1990**, *112*, 8177

12 D. Kiser, F. P. Intini, Y. Xu, G. Natile, L. G. Marzilli, *Inorg. Chem.* **1994**, *33*, 4149

13 A. Habtemariam, J. A. Parkinson, N, Margiotta, T. W. Hambley, S. Parsons, P. J. Sadler, *J. Chem. Soc. Dalton Trans.* **2001**, 362

14 D. Neugebauer, B. Lippert, *Inorg. Chim. Acta.* **1982**, *67*, 151

Appendix

A.1 X-Ray Crystallography Data for Platinum Aminophosphine Complexes

A.1.1 $[Pt\{Me_2N(CH_2)_3PPh_2\}_2Cl_2]$ (24)

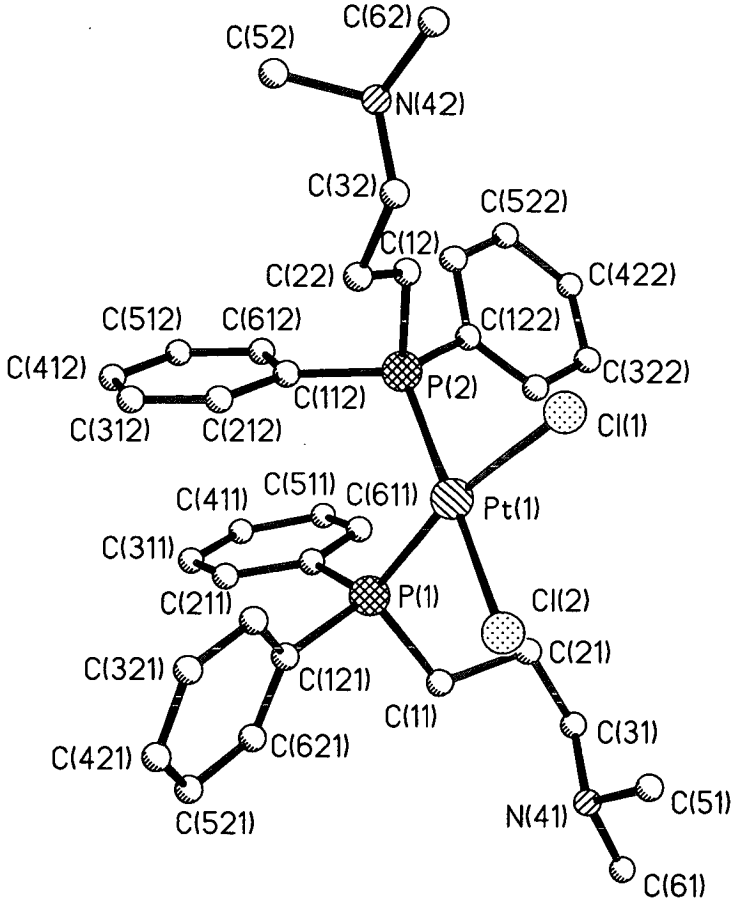

Figure A.1 X-ray crystal structure of complex **24** plotted in SHELEX showing the atom labeling scheme

Table A.1 Atomic coordinates (x 10^4), equivalent isotropic displacement parameters (A^2 x 10^3) and site occupancies for complex **24**. (U(eq) is defined as one third of the trace of the orthogonalized Uij tensor.)

	x	y	z	U(eq)	Occ
PT1	7040(1)	9485(1)	2706(1)	23	1.00
CL1	8389(3)	8569(1)	3271(1)	39	1.00
CL2	7669(3)	9096(1)	1702(1)	37	1.00
P1	6028(2)	10371(1)	2052(1)	23	1.00
C11	7232(9)	10806(6)	1605(5)	32	1.00
C21	8642(9)	10921(6)	2034(4)	37	1.00
C31	9510(10)	11359(5)	1634(5)	49	1.00
N41	9602(7)	11061(5)	1001(3)	48	1.00
C51	10290(10)	10374(8)	1091(6)	68	1.00
C61	10320(10)	11518(8)	621(6)	77	1.00
C111	5282(8)	11131(3)	2398(4)	16	1.00
C211	3959(8)	11333(4)	2172(4)	33	1.00
C311	3471(7)	11962(5)	2382(5)	35	1.00
C411	4320(10)	12400(4)	2829(5)	39	1.00
C511	5651(9)	12210(5)	3076(5)	37	1.00
C611	6114(7)	11576(5)	2864(4)	32	1.00
C121	4715(8)	10037(4)	1368(3)	25	1.00
C221	4150(10)	9371(5)	1437(4)	36	1.00
C321	3210(10)	9085(4)	917(4)	39	1.00
C421	2840(8)	9468(6)	333(4)	38	1.00
C521	3370(10)	10126(5)	265(3)	35	1.00
C621	4317(9)	10416(4)	788(4)	30	1.00
P2	6339(3)	9736(1)	3670(1)	26	1.00
C12	6200(10)	8945(4)	4171(4)	29	1.00
C22	5358(9)	8328(5)	3824(4)	32	1.00
C32	5700(10)	7646(4)	4239(4)	40	1.00
N42	5440(10)	7691(4)	4913(4)	46	1.00
C52	4000(20)	7646(9)	4902(6)	82	1.00
C62	6090(20)	7139(7)	5337(6)	69	1.00
C112	4660(6)	10125(4)	3560(4)	27	1.00
C212	3610(8)	9786(4)	3134(4)	27	1.00
C312	2321(8)	10037(5)	3048(5)	38	1.00
C412	2060(7)	10668(5)	3373(5)	39	1.00
C512	3086(9)	11021(4)	3807(5)	35	1.00
C612	4365(7)	10755(4)	3893(4)	26	1.00
C122	7501(8)	10282(5)	4251(3)	25	1.00
C222	8651(9)	10541(6)	4058(3)	33	1.00

	x	y	z	U(eq)	Occ
C322	9618(9)	10912(7)	4517(5)	49	1.00
C422	9390(10)	11036(6)	5157(5)	46	1.00
C522	8260(10)	10782(6)	5355(4)	41	1.00
C622	7305(8)	10397(5)	4905(4)	33	1.00
C20	9550(20)	3080(10)	2870(10)	104	1.00
CL21	9568(6)	2499(4)	3553(3)	124	1.00
CL22	8070(5)	3072(3)	2306(3)	92	1.00
H111	6858	11280	1442	22	1.00
H112	7322	10503	1209	22	1.00
H211	8565	11181	2455	53	1.00
H212	9079	10449	2153	53	1.00
H311	9099	11844	1554	41	1.00
H312	10433	11401	1911	41	1.00
H511	10345	10172	640	77	1.00
H512	11213	10439	1364	77	1.00
H513	9771	10041	1330	77	1.00
H611	10369	11288	180	91	1.00
H612	9845	11984	538	91	1.00
H613	11255	11598	882	91	1.00
H2111	3347	11018	1852	17	1.00
H3111	2513	12101	2214	40	1.00
H4111	3968	12858	2974	39	1.00
H5111	6257	12524	3399	40	1.00
H6111	7063	11427	3046	17	1.00
H2211	4420	9099	1867	27	1.00
H3211	2805	8607	965	36	1.00
H4211	2172	9263	-49	40	1.00
H5211	3085	10399	-163	31	1.00
H621	4700	10900	740	35	1.00
H121	5791	9094	4562	26	1.00
H122	7127	8762	4340	26	1.00
H221	4381	8439	3785	41	1.00
H222	5559	8258	3364	41	1.00
H321	6678	7541	4270	32	1.00
H322	5153	7248	3999	32	1.00
H521	3836	7678	5372	90	1.00
H522	3530	8046	4627	90	1.00
H523	3648	7183	4698	90	1.00
H621	5887	7189	5798	70	1.00
H622	7087	7174	5364	70	1.00
H623	5768	6667	5144	70	1.00
H2121	3800	9350	2886	29	1.00
H3121	1570	9772	2756	41	1.00

	x	y	z	U(eq)	Occ
H4121	1127	10866	3290	38	1.00
H5121	2893	11460	4051	41	1.00
H612	5111	11009	4198	29	1.00
H221	8787	10463	3587	50	1.00
H3221	10461	11084	4383	34	1.00
H4221	10061	11315	5483	50	1.00
H5221	8122	10873	5823	33	1.00
H6221	6487	10205	5050	41	1.00
H21	9721	3571	3042	127	1.00
H22	10277	2931	2626	127	1.00

A.1.2 $[Pt\{H_2N(CH_2)_3PPh_2\}_2]Cl_2$ (25)

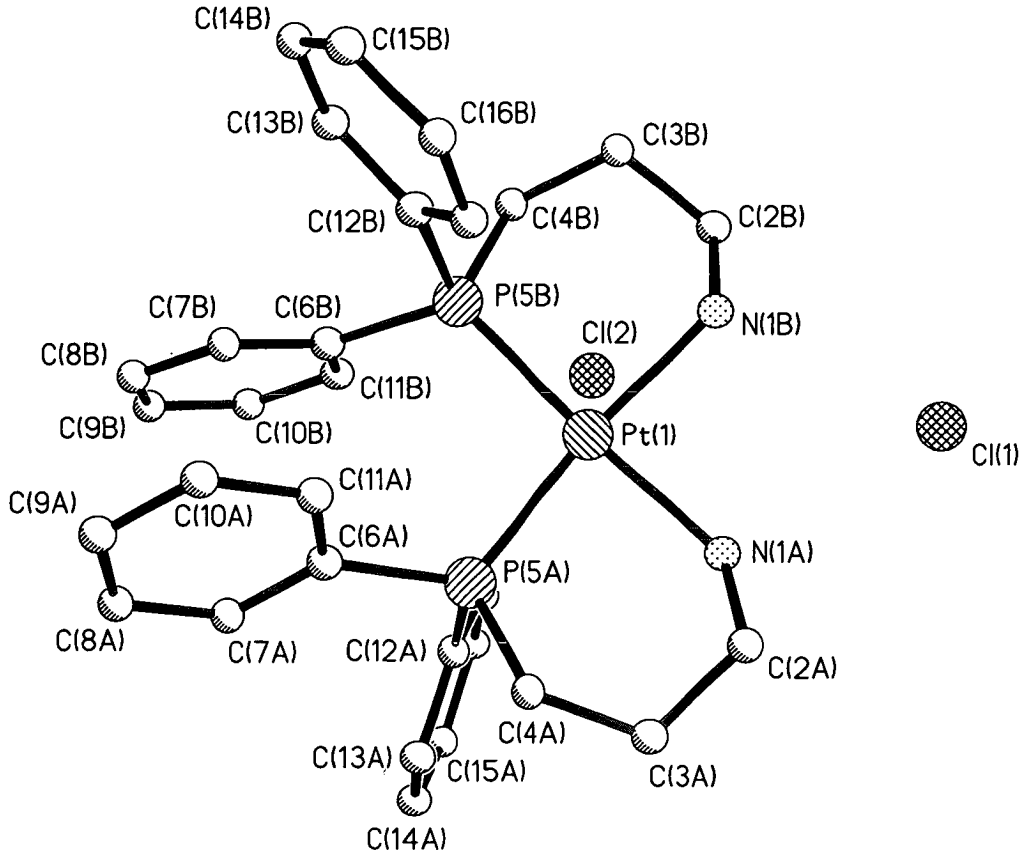

Figure A.2 X-ray crystal structure of complex **25** plotted in SHELEX showing the atom labeling scheme

Table A.2 Atomic coordinates (x 10^4) and equivalent isotropic displacement parameters (A^2 x 10^3) for complex **25**. (U(eq) is defined as one third of the trace of the orthogonalized Uij tensor.)

	x	y	z	U(eq)
Pt(1)	3167(1)	3594(1)	3034(1)	17(1)
N(1A)	2618(4)	3092(3)	4108(2)	22(1)
C(2A)	1396(5)	3366(4)	4460(2)	23(1)
C(3A)	-158(5)	2597(4)	4024(2)	25(1)
C(4A)	-459(5)	2935(4)	3223(2)	22(1)
P(5A)	700(1)	2595(1)	2557(1)	18(1)
C(6A)	-125(5)	3072(4)	1717(2)	20(1)
C(7A)	-1188(5)	2232(4)	1140(2)	26(1)
C(8A)	-1851(6)	2663(5)	541(3)	31(1)
C(9A)	-1452(6)	3945(5)	518(3)	33(1)
C(10A)	-416(5)	4780(4)	1100(3)	29(1)
C(11A)	240(5)	4353(4)	1704(3)	24(1)
C(12A)	203(5)	906(4)	2411(2)	18(1)
C(13A)	-1274(5)	104(4)	2366(2)	22(1)
C(14A)	-1588(5)	-1190(4)	2295(2)	26(1)
C(15A)	-443(5)	-1667(4)	2256(2)	27(1)
C(16A)	1022(5)	-886(4)	2292(3)	29(1)
C(17A)	1361(5)	415(4)	2379(2)	23(1)
N(1B)	5371(4)	4599(3)	3634(2)	20(1)
C(2B)	6756(5)	4441(4)	3400(2)	26(1)
C(3B)	7019(5)	4836(4)	2632(2)	24(1)
C(4B)	5905(5)	3946(4)	1968(2)	23(1)
P(5B)	4005(1)	3991(1)	1922(1)	18(1)
C(6B)	3001(5)	2893(4)	1052(2)	20(1)
C(7B)	2132(5)	3202(4)	482(2)	25(1)
C(8B)	1389(5)	2341(4)	-165(3)	29(1)
C(9B)	1501(5)	1164(4)	-242(3)	30(1)
C(10B)	2370(6)	849(4)	327(3)	32(1)
C(11B)	3135(5)	1709(4)	976(2)	26(1)
C(12B)	4226(5)	5548(4)	1686(2)	21(1)
C(13B)	4738(5)	5880(4)	1012(2)	25(1)
C(14B)	4954(5)	7082(4)	839(3)	30(1)
C(15B)	4660(5)	7950(4)	1340(3)	32(1)
C(16B)	4177(5)	7634(4)	2015(3)	27(1)
C(17B)	3949(5)	6431(4)	2190(2)	22(1)
Cl(1)	5802(1)	3598(1)	5262(1)	29(1)
Cl(2)	5393(1)	952(1)	2569(1)	29(1)

	x	y	z	U(eq)
C(1N)	3776(6)	919(5)	6016(3)	41(1)
N(1N)	2574(5)	1466(4)	5884(2)	36(1)
O(1N1)	1473(5)	882(4)	5415(3)	77(2)
O(1N2)	2726(4)	2478(3)	6245(2)	43(1)
C(2N)	8183(6)	1732(4)	5774(3)	39(1)
N(2N)	8821(5)	3022(4)	6201(2)	34(1)
O(2N1)	8494(5)	3221(4)	6823(2)	58(1)
O(2N2)	9645(4)	3830(3)	5899(2)	50(1)
O(1W)	5920(5)	8936(4)	5892(3)	45(1)
H(1A1)	2403	2239	4069	26
H(1A2)	3491	3457	4458	26
H(2A1)	1541	4269	4476	28
H(2A2)	1466	3186	4992	28
H(3A1)	-929	2723	4319	29
H(3A2)	-270	1696	3976	29
H(4A1)	-306	3843	3274	26
H(4A2)	-1533	2475	3003	26
H(7A)	-1466	1355	1155	31
H(8A)	-2579	2082	145	37
H(9A)	-1891	4242	103	40
H(10A)	-149	5657	1089	35
H(11A)	938	4937	2110	29
H(13A)	-2070	436	2383	26
H(14A)	-2594	-1740	2275	31
H(15A)	-664	-2550	2203	32
H(16A)	1804	-1230	2258	35
H(17A)	2375	959	2416	27
H(1B1)	5498	5437	3651	24
H(1B2)	5371	4436	4129	24
H(2B1)	6671	3549	3381	31
H(2B2)	7640	4946	3790	31
H(3B1)	8056	4893	2559	29
H(3B2)	6949	5684	2627	29
H(4B1)	5876	3079	2012	27
H(4B2)	6268	4159	1484	27
H(7B)	2041	4012	532	30
H(8B)	800	2565	-559	35
H(9B)	981	571	-684	35
H(10B)	2447	35	275	38
H(11B)	3743	1491	1363	32
H(13B)	4940	5284	670	30
H(14B)	5302	7307	378	36
H(15B)	4792	8769	1218	38

	x	y	z	U(eq)
H(16B)	4000	8241	2361	33
H(17B)	3605	6212	2653	26
H(1N1)	4599	1483	6407	61
H(1N2)	4164	804	5539	61
H(1N3)	3364	104	6189	61
H(2N1)	8550	1715	5284	58
H(2N2)	7078	1468	5683	58
H(2N3)	8501	1159	6073	58
H(1W1)	5610(70)	8990(50)	6300(30)	49(19)
H(1W2)	5270(80)	8320(60)	5610(40)	80(30)

A.1.3 [Pt{Me(H)P(CH$_2$)$_3$NMe$_2$}Cl$_2$] (26B)

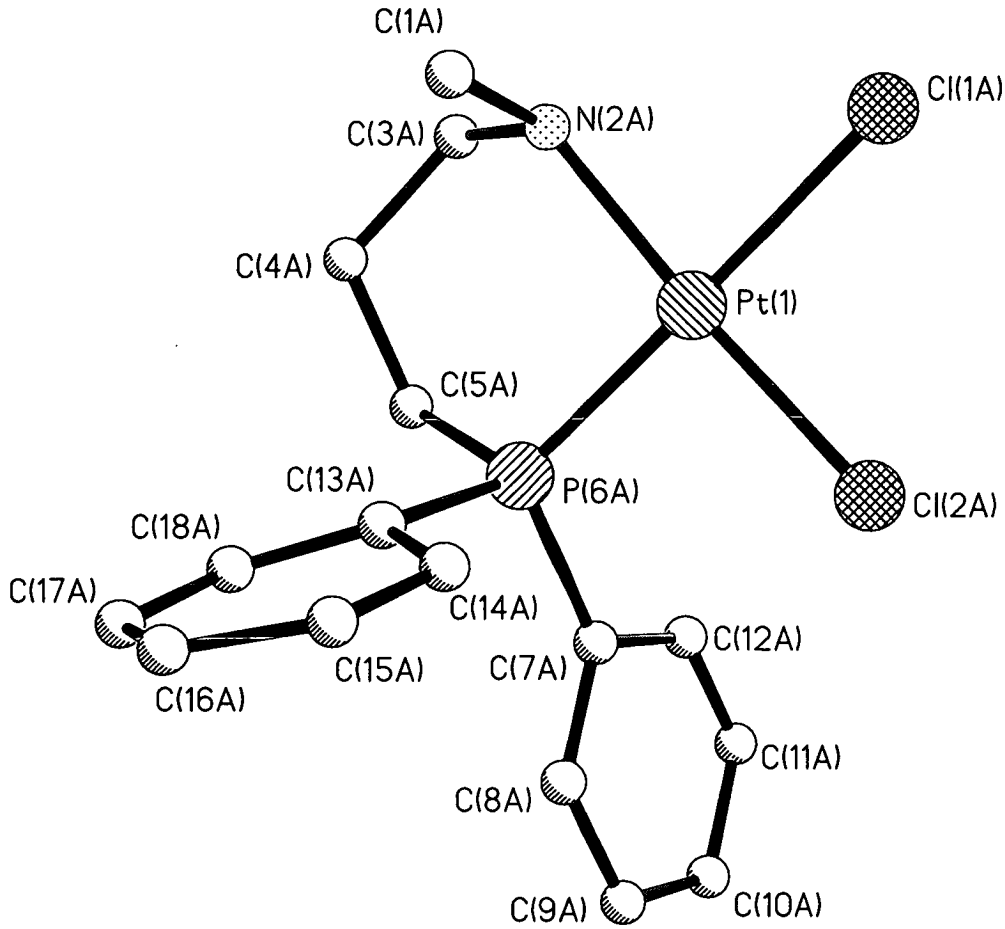

Figure A.3 X-ray crystal structure of complex **26B** plotted in SHELEX showing the atom labeling scheme

Table A.3 Atomic coordinates (x 10^4) and equivalent isotropic displacement parameters (A^2 x 10^3) for complex **26B**. (U(eq) is defined as one third of the trace of the orthogonalized Uij tensor.)

	x	y	z	U(eq)	Occ
Pt(1)	1175(1)	587(1)	2281(1)	33(1)	1
Cl(1A)	-366(2)	926(2)	909(1)	49(1)	1
Cl(2A)	1232(2)	2259(2)	3225(1)	46(1)	1
C(1A)	-380(10)	-2297(8)	1275(6)	61(2)	1
N(2A)	909(7)	-960(6)	1348(4)	47(2)	1
C(3A)	2195(9)	-1119(8)	1416(5)	53(2)	1
C(4A)	2907(9)	-1452(8)	2354(5)	51(2)	1
C(5A)	3759(8)	-268(7)	3219(5)	44(2)	1
P(6A)	2621(2)	257(2)	3538(1)	34(1)	1
C(7A)	3939(7)	1759(6)	4502(5)	39(2)	1
C(8A)	3970(8)	1789(7)	5418(5)	48(2)	1
C(9A)	5006(9)	2961(8)	6141(6)	57(2)	1
C(10A)	5974(9)	4088(8)	5930(7)	64(2)	1
C(11A)	5950(9)	4068(8)	5023(7)	64(2)	1
C(12A)	4916(5)	2937(4)	4356(3)	56(2)	1
C(13A)	1564(5)	-1120(4)	4026(3)	36(1)	1
C(14A)	438(5)	-1055(4)	4184(3)	49(2)	1
C(15A)	-388(9)	-2053(8)	4604(5)	58(2)	1
C(16A)	60(9)	-2964(8)	4966(5)	57(2)	1
C(17A)	1316(9)	-2878(7)	4921(5)	49(2)	1
C(18A)	2095(8)	-1942(7)	4490(5)	42(2)	1
C(1X)	7032(10)	9808(9)	1915(6)	65(2)	1
Cl(1X)	7074(4)	8321(4)	2233(3)	102(1)	0.80
Cl(2X)	5425(6)	9329(8)	941(3)	107(2)	0.80
Cl(3X)	7219(4)	10788(4)	2894(3)	96(1)	0.80
Cl(1W)	6770(20)	11300(20)	2295(16)	138(7)	0.20
Cl(2W)	7120(30)	9200(30)	2833(19)	163(9)	0.20
Cl(3W)	5590(50)	8960(50)	870(30)	210(20)	0.20
C(1Y)	4027(17)	3769(16)	1527(11)	131(5)	1
Cl(1Y)	3867(6)	4994(5)	776(5)	206(3)	1
Cl(2Y)	5963(6)	4753(5)	2418(3)	172(2)	1
Cl(3Y)	3834(6)	2468(4)	813(4)	162(2)	1
C(1Z)	-420(9)	-6102(9)	1735(6)	61(2)	1
Cl(1Z)	-2075(5)	-6603(6)	810(3)	113(2)	0.80
Cl(2Z)	1034(5)	-5175(4)	1342(3)	83(1)	0.80
Cl(3Z)	-193(10)	-5129(10)	2750(5)	79(2)	0.80
Cl(1V)	-2358(16)	-6850(30)	1144(15)	119(10)	0.20
Cl(2V)	401(18)	-5239(18)	1003(11)	86(5)	0.20

	x	y	z	U(eq)	Occ
Cl(3V)	90(30)	-4980(30)	2782(18)	46(4)	0.20
H(1A1)	-1184	-2151	1259	92	
H(1A2)	-100	-2678	1824	92	
H(1A3)	-691	-2928	694	92	
H(2A)	618	- 752	758	56	
H(3A1)	2938	-269	1337	64	
H(3A2)	1879	-1851	886	64	
H(4A1)	2136	-2221	2480	61	
H(4A2)	3578	-1750	2278	61	
H(5A1)	4505	516	3085	53	
H(5A2)	4274	-538	3768	53	
H(8A)	3292	1018	5557	58	
H(9A)	5036	2973	6766	69	
H(10A)	6661	4882	6412	77	
H(11A)	6636	4821	4876	77	
H(12A)	4858	2958	3726	67	
H(14A)	171	-399	3967	59	
H(15A)	-1238	-2095	4636	69	
H(16A)	-487	-3637	5240	68	
H(17A)	1644	-3474	5192	59	
H(18A)	2988	-1854	4506	51	
D(1X)	7874	10341	1734	78	
D(1Y)	3304	3458	1831	157	
D(1Z)	-385	-6935	1904	73	

A.1.4 $[Pt\{^tBu\ (H)N(CH_2)_3PPh_2\}_2Cl_2]$ (27)

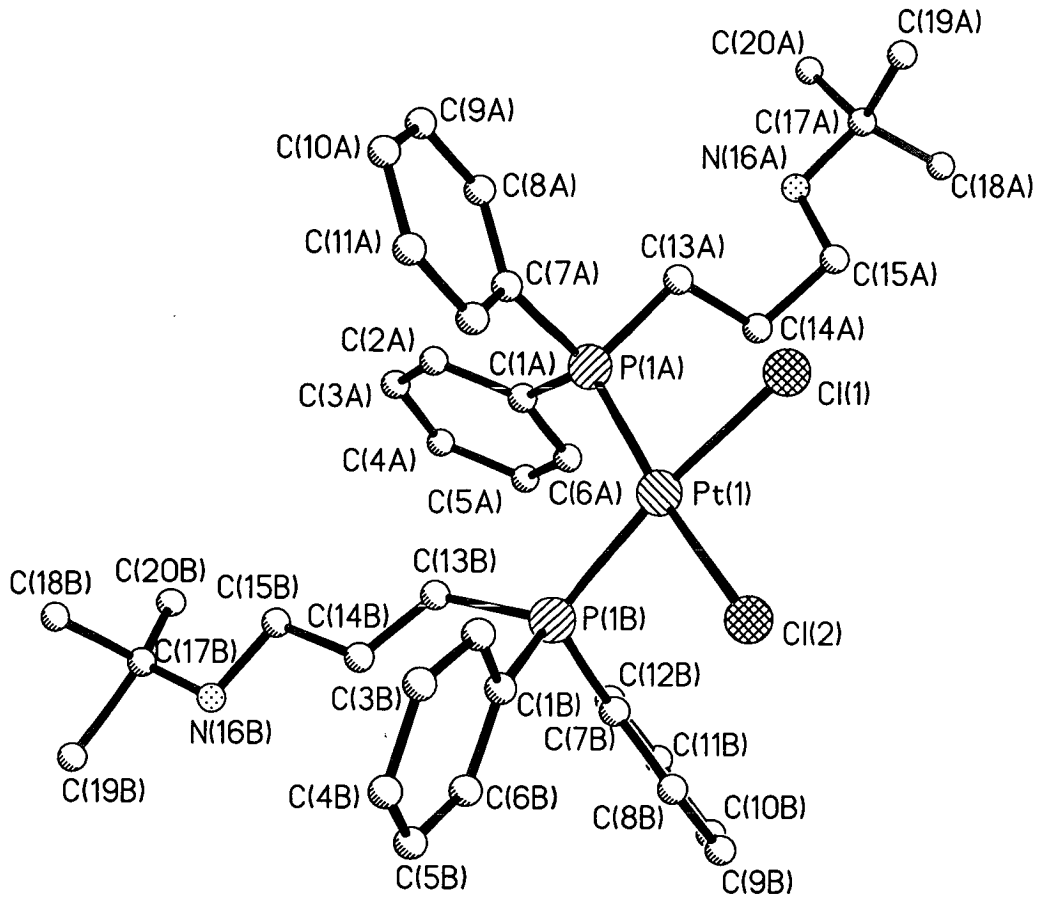

Figure A.4 X-ray crystal structure of complex **27** plotted in SHELEX showing the atom labeling scheme

Table A.4 Atomic coordinates (x 10^4) and equivalent isotropic displacement parameters (A^2 x 10^3) for complex **27**. (U(eq) is defined as one third of the trace of the orthogonalized Uij tensor.)

	x	y	z	U(eq)	Occ
Pt(1)	3513(1)	9576(1)	3784(1)	30(1)	1
Cl(1)	3280(1)	10990(1)	4214(1)	41(1)	1
Cl(2)	3904(1)	10649(1)	3315(1)	40(1)	1
P(1A)	3132(1)	8689(1)	4304(1)	30(1)	1
C(1A)	2874(2)	7483(4)	3931(2)	35(1)	1
C(2A)	2954(2)	6641(3)	4347(3)	38(1)	1
C(3A)	2733(2)	5767(4)	4030(3)	47(1)	1
C(4A)	2425(2)	5703(4)	3287(3)	45(1)	1
C(5A)	2338(2)	6535(4)	2861(3)	44(1)	1
C(6A)	2563(2)	7420(4)	3183(2)	36(1)	1
C(7A)	3549(2)	8528(3)	5267(2)	31(1)	1
C(8A)	3365(2)	8272(3)	5747(2)	37(1)	1
C(9A)	3688(2)	8246(4)	6486(3)	45(1)	1
C(10A	4195(2)	8458(4)	6752(3)	50(1)	1
C(11A)	4380(2)	8704(4)	6294(3)	57(2)	1
C(12A)	4063(2)	8745(4)	5548(3)	45(1)	1
C(13A)	2574(2)	9283(4)	4279(3)	37(1)	1
C(14A)	2171(2)	9584(4)	3519(3)	42(1)	1
C(15A)	1757(2)	10212(4)	3529(3)	46(1)	1
N(16A)	1480(2)	9682(4)	3828(3)	70(1)	1
C(17A)	1060(2)	10211(5)	3848(4)	75(1)	1
C(18A)	687(2)	10640(5)	3131(4)	83(1)	1
C(19A)	1266(2)	11027(5)	4408(4)	82(1)	1
C(20A)	781(3)	9467(5)	4061(4)	86(1)	1
P(1B)	3812(1)	8387(1)	3336(1)	35(1)	1
C(1B)	4485(2)	8538(3)	3636(3)	38(1)	1
C(2B)	4799(2)	8907(3)	4318(3)	43(1)	1
C(3B)	5319(2)	8904(3)	4600(3)	47(1)	1
C(4B)	5532(2)	8541(4)	4199(3)	58(2)	1
C(5B)	5231(2)	8180(6)	3525(3)	77(2)	1
C(6B)	4705(2)	8155(5)	3238(3)	65(2)	1
C(7B)	3491(2)	8400(3)	2346(3)	34(1)	1
C(8B)	3640(2)	9027(3)	1955(3)	37(1)	1
C(9B)	3379(2)	9056(3)	1213(3)	42(1)	1
C(10B)	2959(2)	8472(4)	838(3)	48(1)	1
C(11B)	2795(2)	7866(4)	1212(3)	57(2)	1
C(12B)	3063(2)	7820(3)	1961(3)	47(1)	1
C(13B)	3798(2)	7094(4)	3565(4)	83(3)	1

	x	y	z	U(eq)	Occ
C(14B)	4114(3)	6446(5)	3523(5)	30(2)	0.50
C(15B)	4034(4)	5396(6)	3729(6)	41(2)	0.50
N(16B)	4282(5)	4701(6)	3515(6)	59(1)	0.50
C(14)	4137(4)	6625(6)	4164(6)	52(1)	0.50
C(15)	4099(5)	5502(6)	4232(6)	54(1)	0.50
N(16)	4192(5)	4912(6)	3712(6)	58(1)	0.50
C(17B)	4202(2)	3786(4)	3722(3)	61(1)	1
C(18B)	4583(2)	3515(4)	4488(3)	68(1)	1
C(19B)	4509(5)	3030(9)	3415(6)	63(1)	0.50
C(19)	4201(5)	3477(8)	3079(6)	62(1)	0.50
C(20B)	3679(2)	3474(4)	3589(3)	74(1)	1
H(2AA)	3163	6672	4856	45	
H(3AA)	2791	5197	4322	57	
H(4AA)	2275	5092	3071	54	
H(5AA)	2126	6499	2352	53	
H(6AA)	2506	7991	2891	43	
H(8AA)	3016	8114	5566	45	
H(9AA)	3559	8083	6810	54	
H(10A)	4417	8432	7258	60	
H(11A)	4730	8849	6483	69	
H(12A)	4197	8920	5233	54	
H(13A)	2418	8826	4487	44	
H(13B)	2685	9878	4590	44	
H(14A)	2336	9955	3280	51	
H(14B)	2018	8983	3230	51	
H(15A)	1909	10811	3822	55	
H(15B)	1520	10423	3029	55	
H(16A)	1705	9496	4293	84	
H(16B)	1354	9115	3562	84	
H(18A)	858	11133	2979	125	
H(18B)	408	10953	3177	125	
H(18C)	552	10114	2768	125	
H(19A)	1437	11520	4256	123	
H(19B)	1509	10750	4877	123	
H(19C)	987	11339	4452	123	
H(20A)	665	8925	3710	129	
H(20B)	488	9782	4067	129	
H(20C)	1009	9208	4544	129	
H(2BA)	4653	9169	4599	52	
H(3BA)	5528	9155	5072	57	
H(4BA)	5890	8541	4390	70	
H(5BA)	5381	7940	3244	93	
H(6BA)	4500	7878	2773	78	

	x	y	z	U(eq)
H(8BA)	3927	9441	2206	44
H(9BA)	3490	9482	955	50
H(10B)	2782	8489	324	57
H(11B)	2498	7478	957	68
H(12B)	2953	7386	2215	56
H(13B)	3850	7074	4068	99
H(13C)	3450	6850	3250	99
H(13D)	3466	6996	3552	99
H(13E)	3784	6713	3153	99
H(14C)	4467	6655	3849	36
H(14D)	4067	6440	3022	36
H(15C)	4166	5357	4260	50
H(15D)	3667	5246	3494	50
H(16C)	4157	4722	3021	71
H(16D)	4624	4836	3731	71
H(14E)	4123	6932	4583	62
H(14F)	4478	6765	4216	62
H(15E)	4347	5301	4730	64
H(15F)	3756	5344	4165	64
H(16E)	4498	5117	3756	69
H(16F)	3949	5096	3257	69
H(18D)	4922	3729	4583	101
H(18E)	4582	2800	4550	101
H(18F)	4492	3842	4829	101
H(19D)	4295	2909	2897	95
H(19E)	4584	2403	3678	95
H(19F)	4827	3340	3493	95
H(19G)	3911	3770	2662	93
H(19H)	4176	2757	3044	93
H(19I)	4516	3690	3083	93
H(20D)	3424	3732	3120	111
H(20E)	3614	3735	3975	111
H(20F)	3659	2753	3585	111

A.1.5 [Pt{$Ph_2P(CH_2)_3NMe_2$}MeCl] (28)

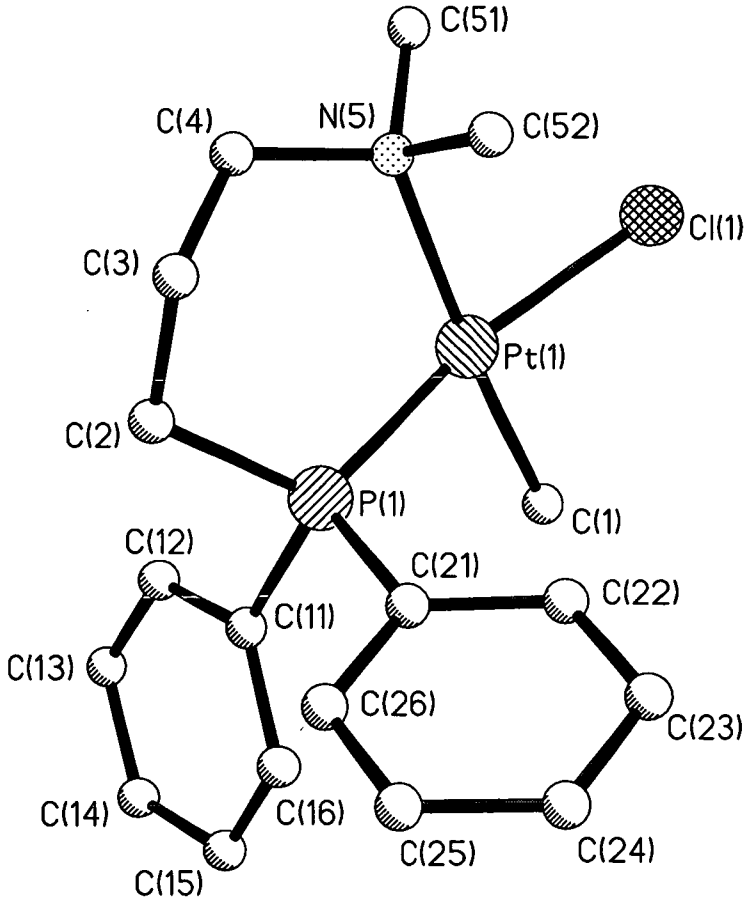

Figure A.5 X-ray crystal structure of complex **28** plotted in SHELEX showing the atom labeling scheme

Table A.5 Atomic coordinates (x 10^4) and equivalent isotropic displacement parameters (A^2 x 10^3) for complex **28**. (U(eq) is defined as one third of the trace of the orthogonalized Uij tensor.)

	x	y	z	U(eq)
Pt(1)	2567(1)	1558(1)	1493(1)	17(1)
Cl(1)	1361(1)	2202(1)	-179(1)	7(1)
C(1)	543(6)	1552(3)	2225(5)	29(1)
P(1)	3388(1)	831(1)	2949(1)	18(1)
C(11)	2795(5)	961(3)	4495(5)	20(1)
C(12)	3309(6)	1565(3)	5133(5)	27(1)
C(13)	2901(6)	1687(3)	6305(5)	33(2)
C(14)	1942(6)	1234(4)	6843(5)	34(2)
C(15)	1406(6)	644(3)	6202(5)	33(2)
C(16)	1849(6)	510(3)	5041(5)	27(1)
C(21)	2850(5)	-75(3)	2565(5)	21(1)
C(22)	1775(5)	-206(3)	1594(5)	24(1)
C(23)	1296(6)	-893(3)	1328(5)	26(1)
C(24)	1862(6)	-1454(3)	2030(5)	29(1)
C(25)	2947(7)	-1329(3)	2975(5)	34(2)
C(26)	3423(6)	-652(3)	3242(5)	29(1)
C(2)	5395(5)	803(3)	3269(5)	24(1)
C(3)	6243(6)	809(3)	2115(5)	29(1)
C(4)	6088(6)	1493(3)	1410(5)	29(1)
N(5)	4680(5)	1608(3)	592(4)	26(1)
C(51)	4869(7)	2304(4)	-5(7)	49(2)
C(52)	4560(6)	1061(4)	-365(5)	39(2)
H(1A)	431	1109	2677	44
H(1B)	-254	1588	1562	44
H(1C)	486	1954	2786	44
H(12)	3937	1891	4762	33
H(13)	3285	2088	6749	39
H(14)	1654	1327	7644	40
H(15)	738	331	6556	39
H(16)	1493	98	4612	32
H(22)	1370	177	1112	28
H(23)	575	-977	660	31
H(24)	1509	-1921	1866	35
H(26)	4158	-575	3902	35
H(2A)	5711	1216	3784	29
H(2B)	5665	371	3747	29
H(3A)	7310	722	2354	35
H(3B)	5876	416	1571	35

	x	y	z	U(eq)
H(4A)	6937	1529	894	34
H(4B)	6184	1887	2009	34
H(51A)	5787	2301	-425	74
H(51B)	4926	2677	619	74
H(51C)	4020	2393	-603	74
H(52A)	3691	1157	-939	59
H(52B)	4451	596	14	59
H(52C)	5459	1065	-810	59

A.2 Conferences Attended

Conference Title	**Dates**
Cost D8 – Chemistry of Metals in Medicine Workshop – Chelators and Metal Macromolecule Interactions in Medicine	11th – 14 th December 1997, Windsor, UK
Cost D8 - Chemistry of Metals in Medicine Workshop – The Industrial Perspective	5th – 8th December 1998, Ivrea, Italy
Universities of Scotland Inorganic Club Conference	15th – 16th September 1998, University of Strathclyde, UK
8th International Symposium on Platinum and other Metal Coordination Compounds in Cancer Therapy	28th – 31st March 1999, Oxford, UK
Royal Society of Chemistry, Scottish Dalton Meeting Macrocycles, Mechanisms and Medicine	8th April 1999, University of St. Andrews, UK
Annual Highlights of Chemistry Research and R & D by Younger Research Chemists	3rd May 1999, London, UK
Universities of Scotland Inorganic Club Conference	20th – 21st September 1999, Heriot Watt University, UK
The Royal Society of Chemistry - 14th International Meeting on NMR Spectroscopy	27th June – 2nd July 1999, University of Edinburgh, UK
The Royal Society of Chemistry - 34th International Conference on Coordination Chemistry	9th – 14th July 2000, University of Edinburgh, UK
5th European Biological Inorganic Chemistry Conference	17th – 20th July 2000, Toulouse, France

A.3 Lecture Courses Attended

Title	Dates	Duration / Hours
Medicinal Inorganic Chemistry – Prof. P. J. Sadler	10th November – 10th December 1997	10 hours
Introduction to UNIX – Edinburgh University Computing Services	14th November 1997	6 hours
Hazards in the Laboratory - Merck	6th January 1998	6 hours
Modern NMR Spectroscopy – Various Lecturers	15th January – 19th March 1998	10 hours
Techniques for Ligand Synthesis – Various Lecturers	22nd April 1998	6 hours
AMES Symposium – Biomolecular Structure and Mechanism	8th June 1998	4 hours
Computers in NMR – Dr. J. A. Parkinson	17th June 1998	3 hours
Crystallography and the Cambridge Structural Database Workshop – Dr. S. Parsons	1st July 1998	3 hours
Special Topics in Inorganic Synthesis – Various lecturers	17th February 1999	4 hours
Collection of Lectures by Prof. A. Sargeson, Australian National University	3rd - 17th March 1999	5 hours
Chemistry and the Discovery of New Medicines Symposium	22nd March 1999	3 hours
Fourier Transform Mass Spectrometry for the Life Sciences - The Royal Society of Edinburgh	19th November 1999	5 hours
AMES Symposium – Lighting the Way: Recent Developments in Applied Luminesence	25th November 1999	3 hours
An Introduction to Patents - Avecia	13th April 2000	3 hours
Edinburgh Magnetic Resonance Forum	29th March 2000	5 hours

Departmental requirements, also attended:

Meeting	**Description**	**Duration**
PJS Group Meetings	Presentations on current research by postgraduate and postdoctoral group members	1 hour per week
Inorganic Section Meetings	Presentations on current research by postgraduates and postdoctoral workers in the inorganic section	1 hour per week
Inorganic Colloquia Lectures	Presentations by visiting lecturers from other universities	1 hour per month
Firbush Meetings	Final presentations for inorganic PhD. students and poster presentations	Annual 2/3 day meeting

A.4 Published Papers

1 K. Neplechová, J. Kašpárková, O. Vrána, O. Nováková, A Habtemariam, B. Watchman, P. J. Sadler, V. Brabec, *Mol. Pharm.* **1999**, *56*, 20

2 A. Habtemariam, B. Watchman, B. S. Potter, R. Palmer, S. Parsons, A. Parkin, P. J. Sadler, *J. Chem. Soc. Dalton Trans.*, **2001**, 1306

0026-895X/99/010020-11$3.00/0

MOLECULAR PHARMACOLOGY, 56:20–30 (1999).

DNA Interactions of New Antitumor Aminophosphine Platinum(II) Complexes

KAMILA NEPLECHOVÁ, JANA KAŠPÁRKOVÁ, OLDŘICH VRÁNA, OLGA NOVÁKOVÁ, ABRAHA HABTEMARIAM, BETH WATCHMAN, PETER J. SADLER, and VIKTOR BRABEC

Institute of Biophysics, Academy of Sciences of the Czech Republic, Brno, Czech Republic (K.N., J.K., O.V., O.N., V.B.); and Department of Chemistry, University of Edinburgh, Edinburgh, United Kingdom (A.H., B.W., P.J.S.)

Received November 23, 1998; accepted April 5, 1999

This paper is available online at http://www.molpharm.org

ABSTRACT

Mechanistic studies are presented of a novel class of aminophosphine platinum(II) complexes as potential anticancer agents. These new agents, which have demonstrated activity against murine and human tumor cells including those resistant to cisplatin are *cis*-[$PtCl_2(Me_2N(CH_2)_3PPh_2$-*P*)$_2$] (Com1) and *cis*-[$PtCl(C_6H_{11}NH(CH_2)_2PPh_2$-*N,P*)$(C_6H_{11}NH(CH_2)_2PPh_2$-*P*)] (Com2). We studied modifications of natural and synthetic DNAs in cell-free media by Com1 and Com2 by various biomedical and biophysical methods and compared the results with those obtained when DNA was modified by cisplatin. The results indicated that Com1 and Com2 coordinated to DNA faster than cisplatin. Bifunctional Com1 formed DNA adducts coordinating to single adenine or guanine residues or by forming cross-links between these residues. In comparison with cisplatin, Com1 formed the adducts more frequently at adenine residues and also formed fewer bidentate lesions. The monofunctional Com2 only formed DNA monodentate adducts at guanine residues. In addition, Com1 terminated DNA synthesis in vitro more efficiently than cisplatin whereas Com2 blocked DNA synthesis only slightly. DNA unwinding studies, measurements of circular dichroism spectra, immunochemical analysis, and studies of the B-Z transition in DNA revealed conformational alterations induced by the adducts of Com1, which were distinctly different from those induced by cisplatin. Com2 had little influence on DNA conformation. It is suggested that the activity profile of aminophosphine platinum(II) complexes, which is different from that of cisplatin and related analogs, might be associated with the specific DNA binding properties of this new class of platinum(II) compounds.

Current platinum-based drugs are limited in their use by their severe side effects, narrow spectrum of anticancer activity, and problems due to drug resistance. We are investigating the design of novel platinum(II) aminophosphine complexes as potential anticancer agents.

The aminophosphine complexes of platinum(II), *cis*-[$PtCl_2$-$(Me_2N(CH_2)_3PPh_2$-*P*)$_2$] (Com1) and *cis*-[$PtCl(C_6H_{11}NH$-$(CH_2)_2PPh_2$-*N,P*)$(C_6H_{11}NH(CH_2)_2PPh_2$-*P*)] (Com2; Fig. 1) contain the possibility of *cis* amine ligands, which are a feature found in many active platinum anticancer agents (Reedijk, 1996), together with *cis* phosphine ligands. Certain diphosphines have also been shown to exhibit anticancer activity, especially 1,2-diphenylphosphine (dppe) complexes of Cu(I), Ag(I), and Au(I) (Berners-Price and Sadler, 1988). Furthermore, lipophilic cations such as $[Au(dppe)]^+$ can disrupt the mitochondrial membrane potentials (Berners-Price et al., 1997), and thereby act via a different mode of action to platinum am(m)ine antitumor complexes for which DNA is the target (Johnson et al., 1989).

Metal aminophosphine complexes have been shown to be cytotoxic toward cancer cells with a potency approaching that of *cis*-diamminedichloroplatinum(II) [*cis*-$[PtCl_2(NH_3)_2]$] (cisplatin) and, moreover, are active against some cisplatin-resistant cell lines (Habtemariam and Sadler, 1996; Papathanasiou et al., 1997). These complexes can exist in chelate ring-opened and ring-closed forms in aqueous solution (Fig. 2). The equilibrium can be controlled under conditions of

This work was supported by Grants 305/99/0695, 301/98/P231, 307/97/P029, and 204/97/P028 from the Grant Agency of the Czech Republic, Grants A5004702 and A7004805 from the Grant Agency of the Academy of Sciences of the Czech Republic, the Biotechnology and Biological Sciences Research Council, and the Engineering and Physical Sciences Research Council. V.B. is the recipient of an International Research Scholar's award from the Howard Hughes Medical Institute. This research is part of the European Cooperation in the Field of Scientific and Technical Research program (Projects D8/0009/97 and D8/0012/97).

ABBREVIATIONS: Com1, *cis*-[$PtCl_2(Me_2N(CH_2)_3PPh_2$-*P*)$_2$]; Com2, *cis*-[$PtCl(C_6H_{11}NH(CH_2)_2PPh_2$-*N,P*)$(C_6H_{11}NH(CH_2)_2PPh_2$-*P*)]; Ab_{cis}, polyclonal antibodies that bind selectively to adducts formed on linear double-helical DNA by cisplatin at r_b = 0.08; bp, base pair(s); CD, circular dichroism; cisplatin, *cis*-diamminedichloroplatinum(II) {*cis*-$[PtCl_2(NH_3)_2]$}; [PtCl(dien)]Cl, chlorodiethylenetriamineplatinum(II) chloride {$[PtCl(H_2NCH_2CH_2NHCH_2CH_2NH_2)]Cl$}; DPP, differential pulse polarography; EtBr, ethidium bromide; FAAS, flameless atomic absorption spectrophotometry; RP, reversed phase; ICL, interstrand cross-link; r_b, the number of the molecules of the platinum complex fixed per nucleotide residue; r_i, the molar ratio of free platinum complex to nucleotide-phosphates at the onset of incubation with DNA; CT, calf thymus.

biological relevance by variation of pH and chloride concentration (Habtemariam and Sadler, 1996). The ring-closed form (Fig. 2A), being a lipophilic cation, could thus act as an antimitochondrial agent and the ring-opened forms (Fig. 2, B and C), which contain labile chloride ligands, offer potential binding sites to DNA.

Recently we have shown that chelate ring-opening platinum(II) aminophosphine complexes can bind rapidly and reversibly to the DNA bases guanine (Habtemariam and Sadler, 1996) and thymine as well as to the RNA base uracil (Margiotta et al., 1997), under physiologically relevant conditions, in contrast to platinum am(m)ine anticancer complexes (Reedijk, 1996). The binding was observed to the bases contained in monomeric nucleotides or in a short oligonucleotide duplex [8 base pairs (bp)]. In this work the modification of natural DNA and synthetic single- or double-stranded polydeoxyribonucleotides in cell-free media was studied by using various biomedical and biophysical methods. Com1 was chosen for these studies as a representative of the bifunctional aminophosphine complexes with leaving chloride ligands in *cis* position to compare its effects on double-helical DNA with those of cisplatin, whereas Com2, which has one chloride-leaving group, was used as a model.

Experimental Procedures

Materials. Cisplatin and chlorodiethylenetriamineplatinum(II) chloride {[PtCl($H_2NCH_2CH_2NHCH_2CH_2NH_2$)]Cl} ([PtCl(dien)]Cl) were synthesized and characterized in Lachema (Brno, Czech Republic). Com1 and Com2 (Fig. 1) were prepared and characterized as reported elsewhere (A.H., R. Palmer, P. Potter, and P.J.S., submitted). Calf thymus (CT) DNA (42% guanine + cytosine, mean molecular mass ca. 2×10^7) was prepared and characterized as described previously (Brabec and Paleček, 1970). Denatured CT DNA was prepared by heating at 100°C for 10 min and subsequent rapid cooling on an ice bath. Plasmids pSP73 (2464 bp) or pSP73KB (2455 bp) were isolated according to standard procedures and banded twice in CsCl/ethidium bromide (EtBr) equilibrium density gradients. Synthetic single-stranded homopolydeoxyribonucleotides poly(dA), poly(dC), poly(dG), poly(dT), and double-helical alternating polydeoxyribonucleotides poly(dA-dT) and poly(dG-dC) were purchased from Boehringer-Mannheim Biochemica (Mannheim, Germany) [all references in the text to poly(dA-dT) and poly(dG-dC) refer to duplex molecules] (the concentrations of synthetic polynucleotides are related to their phosphorus content). The oligodeoxyribonucleotide duplex containing 40 bp, 5′-CCCGGATTATACGGCTTAAACCAAATTGCTTAAATTGGCC)/5′-GGCCAATTTAAGCAATTTGGTTTAAGCCGTATAATCCGGG was obtained from East Port (Prague, Czech Republic); the single-stranded oligonucleotides constituting this duplex were purified by strong anion exchange chromatography (Pharmacia MonoQ column) on a Pharmacia fast protein liquid chromatography system with 10 mM NaOH, 0.2 to 0.8 M NaCl gradient. The duplex was formed by heating the mixture of the complementary single-stranded oligonucleotides at equal concentrations (related to the mononucleotide content) at 90°C for 5 min followed by incubation at 25°C for 4 h. Restriction endonucleases and Thermal Cycle Dideoxy DNA Sequencing Kit with $Vent_R$(exo$^-$) or $Vent_R$(exo$^+$) DNA polymerases were purchased from New England Biolabs (Beverly, MA). A primer 5′-d(GATTTAGGTGACACTATAG) was obtained from BioVendor (Brno, Czech Republic). T4 polynucleotide kinase and Klenow fragment of DNA polymerase I were also obtained from Boehringer-Mannheim Biochemica (Mannheim, Germany). DNase I from bovine pancreas, nuclease P1 from *Penicillium citrinum*, and alkaline phosphatase from calf intestine were purchased from Sigma-Aldrich (Prague, Czech Republic). EtBr, acrylamide, (bis)acrylamide, urea, and agarose were obtained from Merck KgaA (Darmstadt, Germany). The radioactive products were purchased from Amersham (Arlington Heights, IL).

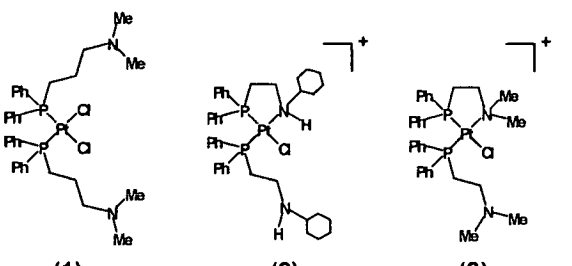

Fig. 1. Structures of bis(aminophosphine) platinum(II) complexes: 1, *cis*-[$PtCl_2(Me_2N(CH_2)_3PPh_2$-*P*)$_2$], 2, *cis*-[PtCl($C_6H_{11}NH(CH_2)_2PPh_2$-*N*, *P*)($C_6H_{11}NH(CH_2)_2PPh_2$-*P*)], 3, *cis*-[PtCl($Me_2N(CH_2)_2PPh_2$-*N*, *P*)($Me_2N$-$(CH_2)_2PPh_2$-*P*)].

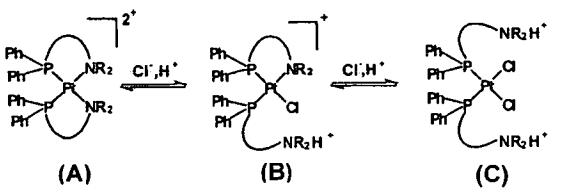

Fig. 2. Schematic representation of chelate ring opening in bis(aminophosphine) platinum(II) complexes.

Platination Reactions. DNAs were modified by platinum complexes in 10 mM $NaClO_4$ (pH 7.0) at 37°C in the dark for 48 h unless stated otherwise. In these samples, the number of the molecules of the platinum complex fixed per nucleotide residue (r_b) was determined by flameless atomic absorption spectrophotometry (FAAS) or by differential pulse polarography (DPP; Kim et al., 1990).

HPLC Analyses. These analyses were performed using a Hitachi Series 4 liquid chromatograph equipped with a LCI-100 computing integrator and a Waters μBondapack C18 column. If not stated otherwise, the products were separated by reversed phase (RP)-HPLC (isocratic elution with 0.1 M ammonium acetate, pH 5.0 in 4% CH_3CN at 1 ml/min flow rate). The following enzymatic digestion protocol was used to characterize the platinated deoxyribooligonucleotides. The samples (50 μg of the oligonucleotide) were incubated with 72 U DNase I at 37°C. After 4 h nuclease P1 (40 μg) was added, and the reaction was allowed to continue at 37°C for 18 h. Finally, alkaline phosphatase (39 U) was added and the incubation continued for additional 4 h at 37°C. The digested samples containing constituent nucleosides were then heated for 2 min at 80°C, centrifuged, and the supernatant was analyzed by RP-HPLC. Each analysis was performed four times and the data varied on average ± 1% from their mean.

Sequence Specificity of DNA Adducts. The (*HpaI*/*NdeI*) restriction fragment of pSP73KB DNA (212 bp) was obtained as described previously (Brabec and Leng, 1993). Ten micrograms of pSP73KB were treated with *NdeI* to obtain linear plasmid followed by treatment with alkaline phosphatase. The linear fragment was then 5′-end labeled by treatment with T4 polynucleotide kinase in the presence of [^{32}P]γ-ATP. The 212-bp fragment was obtained by subsequent treatment with *HpaI* and isolated by electrophoresis through a preparative 1% agarose gel. The modification of this fragment by cisplatin, Com1, or Com2 was carried out in 10 mM $NaClO_4$ (pH 7) for 48 h at 37°C to obtain r_b = 0.01. CircumVent Thermal Cycle Dideoxy DNA Sequencing Kit with $Vent_R$(exo$^-$) or (exo$^+$) DNA polymerases was used with the protocol for thermal cycle DNA

sequencing with 5′ end-labeled primer recommended by the manufacturer with small modifications (Nováková et al., 1995).

EtBr Fluorescence. These measurements were performed with the aid of a Shimadzu RF 40 spectrofluorophotometer using a 1-cm quartz cell. Fluorescence measurements of DNA modified by platinum in the presence of EtBr were performed using the excitation wavelength of 546 nm and the emitted fluorescence was measured at 590 nm. The fluorescence was measured at 25°C in 0.4 M NaCl to avoid the second fixation site of EtBr to DNA (Butour and Macquet, 1977). The concentrations were 0.01 mg/ml for DNA and 0.04 mg/ml for EtBr, which corresponded to the saturation of all intercalation sites of EtBr in DNA (Butour and Macquet, 1977).

Unwinding of Negatively Supercoiled DNA. Unwinding of closed circular supercoiled pSP73 plasmid DNA was assayed by an agarose gel mobility shift assay (Keck and Lippard, 1992). The unwinding angle Φ, induced per platinum-DNA adduct was calculated upon the determination of the r_b value at which the complete transformation of the supercoiled to relaxed form of the plasmid was attained. Samples of pSP73 plasmid were incubated with Com1 or Com2 in 10 mM $NaClO_4$, pH 7.0 at 37°C in the dark for 48 h. All samples were precipitated by ethanol and redissolved in TAE or the TBE buffer (0.04 M Tris-acetate + 1 mM EDTA, pH 7.0 or 0.09 M Tris-borate + 1 mM EDTA, pH 9.0, respectively). An aliquot of the precipitated sample was subjected to electrophoresis on 1% agarose gels running at 25°C in the dark with TAE or TBE buffer with voltage set at 30 V. The gels were then stained with EtBr, followed by photography on Polaroid 667 film with transilluminator. The other aliquot was used for the determination of r_b values by FAAS.

Interstrand Cross-Link (ICL) Assay. If not stated otherwise, Com1 or Com2 at varying concentrations were incubated with 2 μg of pSP73 DNA linearized by *Eco*RI. The platinated samples were precipitated by ethanol and analyzed for DNA ICLs in the same way as described in several recent papers (Farrell et al., 1990; Brabec and Leng, 1993). The linear duplexes were first 3′-end labeled by means of Klenow fragment of DNA polymerase I and [α-^{32}P]dATP. The samples were deproteinized by phenol, precipitated by ethanol, and the pellet was dissolved in 18 μl of a solution containing 30 mM NaOH, 1 mM EDTA, 6.6% sucrose, and 0.04% bromophenol blue. The number of ICLs was analyzed by electrophoresis under denaturing conditions on alkaline agarose gel (1%). After the electrophoresis was completed, the intensities of the bands corresponding to single strands of DNA and ICL duplex were quantified by means of a Molecular Dynamics PhosphorImager (Storm 860 System with ImageQuant software; Sunnyvale, CA). As shown below, some platinated DNA samples were also analyzed for the ICLs using milder conditions, when the DNA samples were treated with formamide or dimethyl sulfoxide at 40 or 55°C and then analyzed in native agarose gel. The details of these milder assays can be found in the papers previously published (Konopa, 1983; Cullinane and Phillips, 1994).

Circular Dichroism (CD). If not stated otherwise, CD spectra of DNA modified by the platinum complexes were recorded at 25°C in 10 mM $NaClO_4$ (pH 7.0) on a JASCO spectropolarimeter, Model J720 (Tokyo, Japan).

Immunochemical Analysis. Polyclonal antibodies that bind selectively to adducts formed on linear double-helical DNA by cisplatin at r_b = 0.08 (Ab_{cis}) were elicited against double-helical calf-thymus DNA modified by cisplatin at r_b = 0.08 in 10 mM $NaClO_4$ for 48 h at 37°C. They were purified and characterized as described in previously published papers (Sundquist et al., 1987; Vrána et al., 1992). The procedures for their immunoenzymatic analysis and enzyme-linked immunosorbent assay have been also described (Sundquist et al., 1987; Vrána et al., 1992).

Results and Discussion

DNA Binding. Solutions of double-helical CT DNA at a concentration of 32 μg/ml were incubated with Com1 or Com2 at the molar ratio of free platinum complex to nucleotide-phosphates at the onset of incubation with DNA (r_i) values of 0.08 in 10 mM $NaClO_4$ (pH 7.0) at 37°C. At various time intervals an aliquot of the reaction mixture was withdrawn and assayed by DPP for the amount of platinum bound to DNA (r_b) (Kim et al., 1990). Figure 3 shows a plot of r_b against the time of DNA incubation with Com1 or Com2. The amount of platinum coordinated to DNA increased with time. After 48 h, approximately 100% or 80% of the complex Com1 or Com2, respectively, present in the reaction mixtures was coordinated to DNA [exhaustive dialysis of the samples of DNA treated with Com1 or Com2 against platinum-free background solution (10 mM $NaClO_4$) did not affect the amount of the platinum bound to DNA]. In these binding reactions, the time at which the binding reached 50% ($T_{50\%}$) was ca. 3 h for both Com1 and Com2. The value of $T_{50\%}$ for the reaction of cisplatin or monofunctional [PtCl(dien)]Cl with DNA under conditions identical with those specified in Fig. 3 were ~4 h, respectively (Bancroft et al., 1990). This comparison indicates that the presence of the aminophosphine groups as nonleaving ligands enhances the rate of the coordination of monofunctional chloro or bifunctional dichloro platinum(II) complexes to natural double-helical DNA. When the same binding experiment was carried out with thermally denatured CT DNA, the binding of Com2 remained unchanged whereas the binding of Com1 was somewhat faster ($T_{50\%}$ was ~2 h; Table 1).

We also studied the binding of Com1 and Com2 to several synthetic single-stranded homopolydeoxyribonucleotides and double-helical synthetic alternating polydeoxyribonucleotide complexes (Table 1). The polynucleotides at a concentration of 1×10^{-4} M (the concentration is the mononucleotide content) were incubated with Com1 or Com2 at r_i = 0.08 in 10 mM $NaClO_4$ (pH 7.0) at 37°C. The binding of the platinum compounds was quantified in the same way as described above for the reaction of Com1 and Com2 with CT DNA. Both complexes bound readily to single-stranded poly(dA), poly(dC), and poly(dG) (the values of $T_{50\%}$ were about 2 h for Com1 and 6–7 h for Com2; Table 1). Importantly, at pH 7 Com1 did not bind to single-stranded poly(dT) whereas Com2

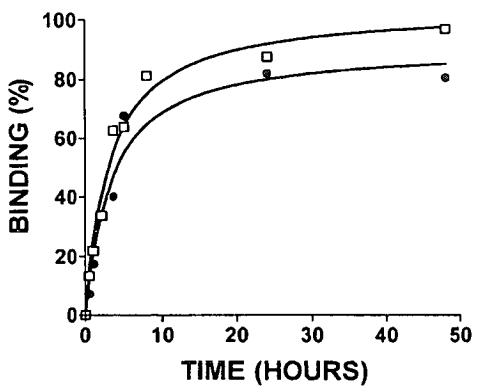

Fig. 3. Formation of DNA adducts by bis(aminophosphine) platinum(II) complexes as a function of incubation time. CT DNA at the concentration of 32 μg/ml was mixed with Com1 (□) or Com2 (●) at r_i = 0.08 in 10 mM $NaClO_4$ and at 37°C in the dark. At various time intervals the aliquots were withdrawn and platinum coordinated to DNA was estimated by DPP assay. Data points measured in triplicate varied on average ± 2% from their mean.

was bound to poly(dT), but considerably more slowly than to other single-stranded polynucleotides (Table 1). Also importantly, both platinum complexes bound to double-stranded poly(dA-dT) or poly(dG-dC) with markedly higher rates than to single-stranded polynucleotides (Table 1). The binding of Com1 and Com2 to double-helical CT DNA and poly(dT) was also quantified in the following way. Aliquots of the reaction withdrawn at various time intervals were quickly cooled on an ice bath and then exhaustively dialyzed against 10 mM $NaClO_4$ at 4°C to remove free (unbound) platinum compound. The content of platinum in these samples was determined by FAAS. Results identical with those obtained using the DPP assay were obtained. Taken together, the results of these binding studies suggest that at pH 7 Com1 binds to adenine, cytosine, and guanine residues in synthetic polynucleotides with approximately the same rate, and it does not bind to thymine residues. On the other hand, the monofunctional complex Com2 seems to bind to all base residues in synthetic polynucleotides including thymine residues. The binding to the latter residues is, however, noticeably slower than to other DNA base residues, and in general the DNA binding of Com2 is slower than that of Com1. Thus, these results suggest that Com1 and Com2 bind to different base residues in DNA and have different base sequence preferences than their simpler analogs cisplatin or [PtCl(dien)]Cl, which both bind preferentially to guanine residues, and cisplatin to a less extent to adenine residues (Johnson et al., 1982, Fichtinger-Schepman et al., 1985; Eastman, 1987).

It has been shown by NMR studies that under physiological conditions the monofunctional complex 3 (Fig. 1) binds to the mononucleotide dTMP or thymine residues at the ends of a short (8-bp) oligodeoxyribonucleotide duplex (Margiotta et al., 1997). It was found that these reactions were fast (completed within several minutes) and that the amount of binding increased with increasing pH. Similar results have been obtained for Com1, with binding to dTMP observed over a large pH range (4–12). For this reason we repeated studies on the binding of Com1 and Com2 to poly(dT) at pH 8 (the pH was adjusted by adding a small amount of 2 M NaOH or 1 mM Tris/HCl buffer, pH 8, to 10 mM $NaClO_4$). The binding of Com2 was affected only negligibly whereas 30% of Com1 was now bound after 48 h (Table 1). However, when the binding of Com1 and Com2 to CT DNA was also investigated at pH 9 (the pH was again adjusted by adding either a small amount of 2 M NaOH or 1 mM Tris/HCl buffer, pH 9, to 10 mM $NaClO_4$) no binding of either complex was observed.

TABLE 1

The binding of the Com1 and Com2 to CT DNA and synthetic polydeoxyribonucleotides determined by DPP[a]

Nucleic Acid	$T_{50\%}$[b]		Binding after 48 h	
	1	2	1	2
	h		%	
ds CT DNA[c]	3.0	3.3	99	78
Denatured CT DNA[d]	1.7	3.3	99	85
Poly(dA)	2.2	5.7	89	89
Poly(dC)	1.9	7.6	79	75
Poly(dG)	2.0	6.2	83	79
Poly(dT), pH 7.0		18.2	0	68
Poly(dT), pH 8.0[e]		17.6	30	70
Poly(dA-dT)	0.3	4.0	90	80
Poly(dG-dC)	0.7	1.5	96	91

[a] CT DNA (double-stranded or denatured) at the concentration of 32 μg/ml or synthetic single- or double-stranded polynucleotides at the concentration of 1×10^{-4} M were mixed with the platinum complexes at $r_i = 0.08$ in 10 mM $NaClO_4$ (pH 7) and at 37°C in the dark. Data measured in triplicate varied on average ±2% from their mean.

[b] The time of the reaction at which the binding reached 50% ($r_b = 0.04$).

[c] Double-helical DNA.

[d] DNA was thermally denatured before the platinum complex was added.

[e] pH was adjusted by NaOH.

The amount of binding of the complexes to poly(dT) is lower than might have been expected from the NMR work on the monomeric nucleotides. The reason for this is unclear but it may imply that N3 atoms in poly(dT) under these conditions are not accessible to platinum.

In addition, it was previously shown by NMR studies (Habtemariam and Sadler, 1996) that the addition of 0.5 M KCl led to the displacement of coordinated 5′ dGMP from *cis*-[PtCl{$Me_2N(CH_2)_2PPh_2$-*N*,*P*}{$Me_2N(CH_2)_2PPh_2$-*P*}(5′-dGMP-N7)]$^{3+}$. Therefore, we prepared a sample of CT DNA modified by Com1 or Com2 at $r_b = 0.08$ (at 37°C in 10 mM $NaClO_4$ for 48 h). The concentration of KCl in these samples was adjusted by 5 M KCl to give a final concentration of 0.5 M. The samples were incubated at 37°C for an additional 48 h, and the content of unbound platinum was determined by DPP. No free platinum compound was found, indicating that the presence of chloride ions did not result in the displacement of Com1 or Com2 from high molecular mass DNA. Therefore, it appears that the duplex structure of DNA increases the kinetic stability of platinum aminophosphine adducts perhaps by shielding platinum from attack by chloride ions. Such a shielding is thought to increase the stability of 5′-G monofunctional adducts with cisplatin (Reeder et al., 1997).

Characterization of DNA Adducts by HPLC Analysis of Enzymatically Digested DNA. To further characterize the coordination mode of the two aminophosphine platinum(II) complexes, a 40-bp deoxyribooligonucleotide duplex (with a random nucleotide sequence, see *Experimental Procedures*) modified by Com1 or Com2 (in 0.1 M $NaClO_4$, pH 7) was enzymatically digested to mononucleosides and analyzed by RP-HPLC. RP-HPLC analysis of enzymatic digests of Com1- or Com2-modified oligonucleotide duplex was performed by recording optical density at 260 nm. The profile in Fig. 4 (curve 1) shows well resolved mononucleoside peaks that reflect the proper proportions of the single mononucleosides in unplatinated duplex when integrated and normalized by their extinction coefficients. Digestion of the platinated samples (Fig. 4, curves 2 and 3) resulted in the decrease of the integrated area of the deoxyriboguanosine peak and, in the case of the digestion of the duplex modified by Com1, also in the decrease of deoxyriboadenosine peak. The peaks of deoxyribocytidine and thymidine were not affected. It was verified by FAAS that no product containing platinum coeluted with the peaks corresponding to unplatinated deoxyribonucleosides. The platinated products were not retained by the column under the conditions used, so they could not be identified and quantified.

The integrated area of the deoxyriboguanosine peak decreased by ~24% as a consequence of the platination of the duplex by the monofunctional compound Com2 at $r_b = 0.05$ (Fig. 4, curve 3). The 40-bp duplex used in these analyses contained 17 guanine residues. Thus, this decrease corresponds to the loss of four guanine residues due to the modification by Com2. The peaks corresponding to other nucleosides were unchanged, which implies that only guanine

residues were platinated by Com2 in a monofunctional manner. Thus, the DNA binding mode of Com2 appears to be similar to that of the other monofunctional platinum(II) complex, [PtCl(dien)]Cl, which also binds preferentially to guanine residues in DNA (Johnson et al., 1982). In other words, the presence of aminophosphine groups in the coordination sphere of platinum in monofunctional triamineplatinum(II) complexes has no effect on the preference of these complexes to bind to guanine residues in double-helical DNA.

The modification of the duplex by bifunctional Com1 at r_b = 0.09 resulted in the decrease of the integrated area of the deoxyriboguanosine and deoxyriboadenosine peaks by ~28% and ~21%, respectively (Fig. 4, curve 2; the duplex contained 17 guanine and 23 adenine residues). This decrease corresponds to the loss of five guanine and five adenine residues. The duplex was, however, modified at r_b = 0.09, which implies that each duplex only contained 7.2 adducts on the average. The loss of ten unmodified bases due to the platination by Com1 suggests that ca. three adducts, i.e., ca. 40% of all platinum adducts, were bifunctional cross-links. The results of RP-HPLC analyses are consistent with the idea that cisplatin analog Com1 preferentially forms DNA adducts by coordinating to both a single purine or to two purine residues.

For comparative purposes, the modification of the 40-bp duplex used in the present study by cisplatin at r_b = 0.09 was also investigated. This modification also resulted in the decrease of the integrated areas of the deoxyriboguanosine and deoxyriboadenosine peaks (not shown). However, in contrast to the modification by Com1, the areas of these peaks decreased by 70% and 5%, respectively. These decreases correspond to the loss of ~12 guanine and ~1 adenine residues, which suggests that ca. 80% of all cisplatin adducts were

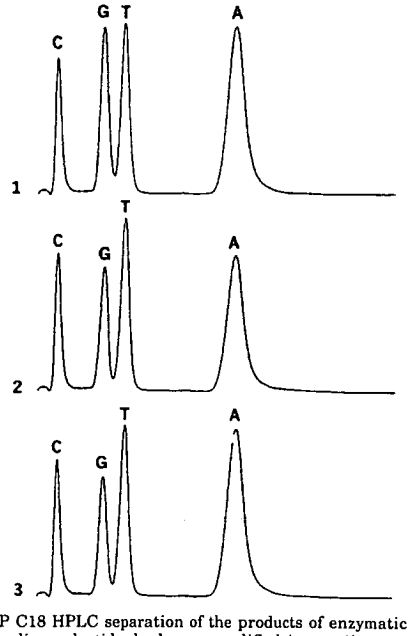

Fig. 4. RP C18 HPLC separation of the products of enzymatic digest of the 40-bp oligonucleotide duplex nonmodified (curve 1) or modified by Com1 at r_b = 0.09 (curve 2) or by Com2 at r_b = 0.05 (curve 3). For other details, see the text.

bifunctional cross-links. This is in good agreement with the previous analyses (Fichtinger-Schepman et al., 1985; Eastman, 1987) indicating that cisplatin forms mainly bifunctional adducts (intrastrand cross-links and ICLs) and that the preferential sites involved in the adducts of cisplatin are guanine residues and, in a considerably smaller extent, also adenine residues. Thus, the results of the present work based on RP-HPLC analysis of enzymatically digested platinated DNA strongly support the view that in comparison with cisplatin, Com1 forms DNA adducts more frequently at adenine residues and also forms fewer bifunctional lesions.

Mapping of DNA Adducts. Recent work has shown that the in vitro DNA synthesis by DNA polymerases on DNA templates containing several types of bidentate adducts of platinum complexes can be prematurely terminated at the level or in the proximity of adducts (Comess et al., 1992; Murray et al., 1992; Vrána et al., 1996). Importantly, the efficiency of monofunctional DNA adducts of several platinum(II) complexes to terminate DNA synthesis is considerably smaller (Comess et al., 1992).

DNA synthesis by $Vent_R$ DNA polymerase using *HpaI*/*NdeI* fragment of pSP73KB modified by Com1 at r_b = 0.01 in 10 mM $NaClO_4$ (pH 7) yielded fragments corresponding to the DNA synthesis that was prematurely terminated at the level of the platinum adducts (Fig. 5A, lane 1). Thus, the adducts formed by Com1 formed on the DNA template were capable of terminating DNA synthesis in vitro. Several termination sites were identical with those yielded by the adducts of cisplatin, but several termination sites were different. Com1 terminated DNA synthesis preferentially at guanine and adenine residues whereas cisplatin terminated DNA synthesis preferentially at guanine residues in d(GG) and 5′-d(AG)-3′ sites (Comess et al., 1992; Murray et al., 1992; Vrána et al., 1996), the termination sites produced by Com1 were mainly at guanine and adenine residues flanked by various base residues [C*G*A, G*G*T, T*G*A, G*G*G, T*A*A, T*A*T, A*A*C, C*A*G (bold and italic letters represent the termination site)] (Fig. 5B). These results are consistent with the results of RP-HPLC analysis of enzymatically digested DNA modified by Com1 (Fig. 4), which suggest that the preferential sites in DNA at which Com1 is coordinated are guanine and adenine residues. In addition, the results of the present replication mapping studies indicate that Com1 binds to DNA with a less regular sequence preference, i.e., with a considerably different nucleotide sequence specificity than cisplatin.

The monofunctional compound Com2 terminated DNA synthesis only slightly. Very faint bands were observed if the DNA template was modified at r_b values as high as 0.05 (Fig. 5A, lane 2). This result indicates that the efficiency of DNA adducts of Com2 to inhibit DNA synthesis in vitro is low, and similar to that of DNA adducts of the monofunctional platinum(II) complexes such as [PtCl(dien)]Cl and $[PtCl(NH_3)_3]Cl$.

Characterization of DNA Adducts by EtBr Fluorescence. EtBr as a fluorescent probe can be used to distinguish between perturbations induced in DNA by monofunctional and bifunctional adducts of platinum(II) compounds (Butour and Macquet, 1977; Žaludová et al., 1997b). Binding of EtBr to DNA by intercalation is blocked in a stoichiometric manner by formation of the bifunctional adducts of a series of platinum complexes including cisplatin and transplatin,

which results in a loss of fluorescence intensity (Butour and Macquet, 1977; Žákovská et al., 1998). On the other hand, modification of DNA by monodentate platinum(II) complexes (having only one leaving ligand) results in only a slight decrease of EtBr fluorescence intensity as compared with nonplatinated DNA-EtBr complex.

Double-helical DNA was modified by Com1 or Com2 and for comparative purposes also by cisplatin or [PtCl(dien)]Cl for 48 h. The levels of the modification corresponded to the values of r_b in the range between 0 and 0.15. Modification of DNA by all platinum complexes resulted in a decrease of EtBr fluorescence (Fig. 6). In accordance with the results published earlier (Butour and Macquet, 1977; Žaludová et al., 1997b; Žákovská et al., 1998), cisplatin considerably decreased the fluorescence. The binding of Com1 to DNA also considerably decreased EtBr fluorescence although less than DNA adducts of cisplatin. On the other hand, the decrease of the fluorescence intensity by the adducts of Com2 was only very small and similar to that induced by the adducts of [PtCl(dien)]Cl. This result suggests that Com2 forms the DNA adducts, which resemble, from the viewpoint of their capability to inhibit EtBr fluorescence, those formed by monofunctional platinum complexes. Taken together, the fluorescence analysis is consistent with the idea and supports the postulation that the major DNA adducts of Com2 are monofunctional lesions even after long incubations of DNA with this platinum complex (48 h). On the other hand, under comparable conditions Com1 forms monofunctional adducts and also bifunctional cross-links on DNA that are capable of inhibiting EtBr fluorescence. The amount of the cross-links is, however, smaller in comparison with DNA modification by cisplatin.

CD. CD spectroscopy has already been used to obtain information about the global changes in DNA conformation induced by platinum complexes. It has been shown (Vrána et al., 1986; Brabec et al., 1990) that the intensity of the positive CD band yielded by B-DNA at ~275 nm is increased as a consequence of DNA modification by the complexes containing the *cis*-[$PtCl_2$(amine)$_2$] unit (Fig. 7, B and C); at higher levels of the modification ($r_b > \sim 0.5$) the intensity of this CD band begins to decrease (Fig. 7, B and C). On the other hand, the modification of DNA by clinically ineffective transplatin or dienPt only slightly decreases this positive band (Vrána et al., 1986; Brabec et al., 1990). It has been suggested (Vrána et al., 1986; Brabec et al., 1990) that the enhancement of the CD band at ~275 nm due to the modification by the complexes containing *cis*-[$PtCl_2$(amine)$_2$] unit reflects distortions in DNA of a nondenaturational nature. The slight reduction of this CD band induced by the binding of platinum complexes is consistent with the occurrence of short segments containing unpaired bases (denatured regions).

The modification of CT DNA by Com2 had only a negligible effect on the CD spectrum (not shown). In this respect, the monofunctional Com2 resembled other platinum(II) complexes that bind to DNA monodentately (e.g., [PtCl(dien)]Cl or [PtCl(NH_3)]Cl). In contrast, the bifunctional compound Com1 (having leaving ligands in *cis* positions) radically affected the CD spectrum of DNA at pH 7 (Fig. 7A), but in a distinctly different way than the binding of cisplatin (Fig. 7B). As a linear function of r_b, there was a marked loss in the intensity of the positive band at around 280 nm already at low r_b values (<0.05; Fig. 7, A and C) accompanied by a loss in the intensity of the negative band at around 245 nm. The changes observed in the positive band are reminiscent of

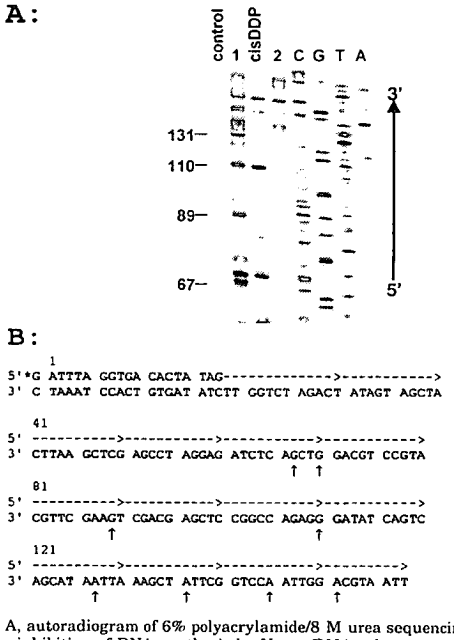

Fig. 5. A, autoradiogram of 6% polyacrylamide/8 M urea sequencing gel showing inhibition of DNA synthesis by $Vent_R$ DNA polymerase on the *HpaII/NdeI* restriction fragment of pSP73KB plasmid DNA modified by platinum complexes. The gel contained the linear amplification products of DNA treated with Com1, Com2, and cisplatin. Lanes: control, unmodified template; cisDDP, DNA modified by cisplatin at r_b = 0.01; 1, DNA modified by Com1 at r_b = 0.01; 2, DNA modified by Com2 at r_b = 0.05; C, G, T, A, chain-terminated marker DNAs (note that these dideoxy-sequencing lanes give the sequence complementary to the template strand). The numbers correspond to the nucleotide sequence numbering of 5B. B, schematic diagram showing a portion of the sequence used to monitor inhibition of DNA synthesis on the template containing adducts of the platinum complexes. * indicates the 5'-end labeling of the primer. The dashed arrow indicates the start site of the DNA polymerase and the direction of the synthesis. ↑, stop signals from A, lane 1. Nucleotides 1 and 18 correspond to 2539 and 1 on the pSP73KB nucleotide sequence map.

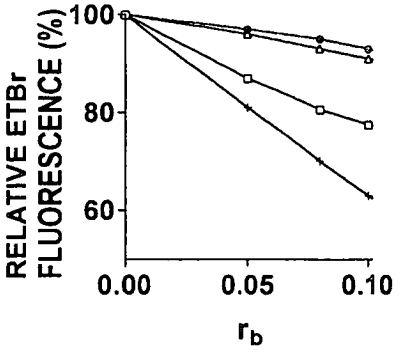

Fig. 6. Dependences of the EtBr fluorescence on r_b for DNA modified by various platinum complexes in 10 mM $NaClO_4$ at 37°C for 48 h. (+), cisplatin; (Δ), [PtCl(dien)]Cl; (□), Com1; and (●), Com2. Data points measured in triplicate varied on average ± 2% from their mean.

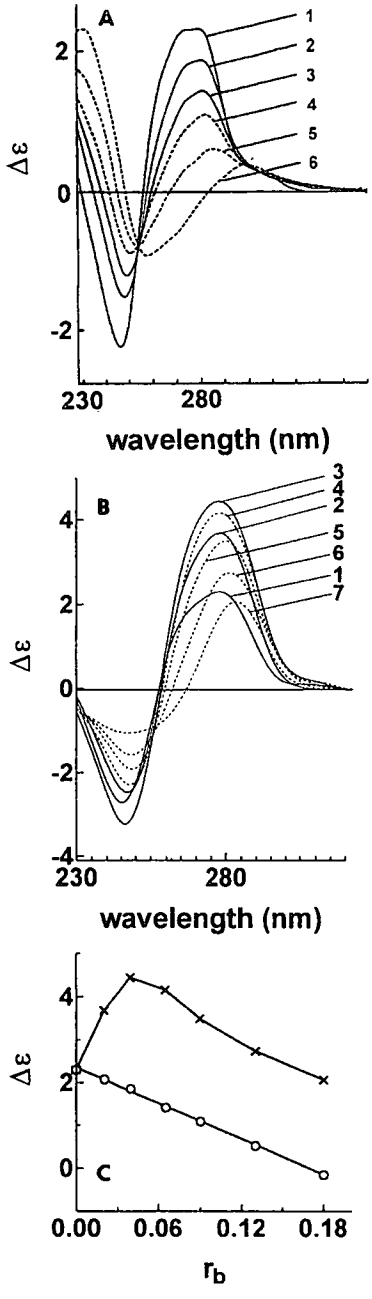

Fig. 7. CD spectroscopy of CT DNA modified by Com1 and cisplatin. The spectra were recorded for DNA in 10 mM $NaClO_4$, pH 7.0. A, CD spectra of DNA modified by Com1. Curves: 1, control (nonmodified) DNA; 2, r_b = 0.04; 3, r_b = 0.065; 4, r_b = 0.09; 5, r_b = 0.13; 6, r_b = 0.18. B, CD spectra of DNA modified by cisplatin. Curves: 1, control (nonmodified) DNA; 2, r_b = 0.02; 3, r_b = 0.04; 4, r_b = 0.065; 5, r_b = 0.09; 6, r_b = 0.13; 7, r_b = 0.18. C, dependence of the maximum ellipticity of the positive CD band at around 280 nm on r_b. (×), cisplatin; (O), Com1. Data points measured in duplicate varied on average ± 1% from their mean.

DNA transformations seen in the presence of high concentrations of electrolyte or by the reaction with a variety of amines. For instance, at the level of DNA binding corresponding to r_b = 0.13, the reduction of the rotational strength of the positive band above 260 nm in the CD spectrum of DNA in 10 mM $NaClO_4$, pH 7.0 (Fig. 7A) was similar to that obtained for underivatized DNA in ca. 6 M LiCl or at ca. 0.1 mol of *n*-butylamine covalently fixed (via CH_2O)/mol of nucleotide (Chen et al., 1981; Gray, 1996). This transformation has been demonstrated to be roughly correlated with the reduction of the electrostatic repulsive interactions in the DNA molecule. These interactions are reduced by high concentrations of electrolytes in the solution or by simple amines (retaining their positive charge) covalently attached to DNA. At pH 7, binding of Com1 to DNA could position two positively charged amino groups in the dangling arms of this complex close to DNA phosphate groups. Such salt bridges could result in an additional stabilization for DNA adducts of Com1 compared to those of Com2 (which contains only one dangling arm with amino group) or cisplatin. This interpretation is also corroborated by the observation that the marked loss in the intensity of the positive band at around 280 nm due to the binding of Com1 became considerably less pronounced if the sample of DNA modified by Com1 at pH 7 for 48 h was transferred into the medium of pH 9 (not shown). The increase of pH could decrease the number of positively charged amino groups of dangling arms due to their deprotonization. It was verified by DPP that due to the increase of pH to 9, no platinum compound dissociated from the DNA modified by Com1 at pH 7.

The changes induced in double-helical DNA by Com1 do not have the character of extensive denaturational distortions. The cooperative character of the melting profile and the hyperchromic increase upon melting are the same as for the unplatinated control, which contains intact Watson-Crick hydrogen bonds (not shown). It has been shown (Chen et al., 1981; Gray, 1996; Johnson, 1996) that the conformation of DNA in concentrated electrolyte solutions or when modified by some amines, which gives rise to a CD spectrum with a markedly decreased rotational strength above 260 nm, is a variant of the B structure. This variant has a higher winding angle than that present in the nonmodified DNA in more modest concentrations of electrolyte. Thus, we suggest that double-helical DNA modified by Com1 adopts some features of the conformation of DNA in concentrated electrolyte solutions or DNA to which positively charged amines are covalently bound. Also importantly, this conformational alteration is apparently unique for bifunctional DNA binding of bifunctional bis(aminophosphine) compounds (no change such as that seen for Com1 was observed for monofunctional Com2).

Unwinding Induced in DNA by Platinum Coordination. The results described above suggest that Com1 forms bifunctional adducts on DNA although to a smaller extent than its bifunctional analog, cisplatin. It has been shown that DNA adducts of cisplatin (and its direct analogs) unwind DNA (e.g., Bellon et al., 1991; Keck and Lippard, 1992; Huang et al., 1995; Gelasco and Lippard, 1998). CD spectra of DNA modified by Com1 (Fig. 7A) suggest that this modification also results in an overall overwinding of the DNA molecule as a whole if the platinated DNA is dissolved in neutral media, whereas no changes in CD spectra indicating over-

winding occur if DNA is modified under identical conditions by cisplatin or if the pH of the sample of DNA modified by Com1 is adjusted to 9.

The unwinding induced by a random modification of DNA by various platinum(II) complexes including cisplatin can be determined by electrophoresis in native agarose gels by monitoring the degree of supercoiling in plasmid DNA (Keck and Lippard, 1992). A compound that unwinds the DNA duplex reduces the number of supercoils in closed circular, negatively supercoiled DNA. This decrease upon binding of unwinding agents causes a decrease in the rate of migration through agarose gels, which makes it possible that the unwinding can be observed and quantified. We used this assay to determine the unwinding induced in pSP73 plasmid by Com1 (Fig. 8). Figure 8A shows an electrophoresis gel run at pH 9 of samples in which an increasing amount of Com1 was bound to a mixture of nicked and supercoiled pSP73 DNA. The unwinding angle is given by $\Phi = 18\,\sigma/r_b(c)$ where σ is the superhelical density and $r_b(c)$ is the value of r_b at which the supercoiled and nicked forms comigrate (Keck and Lippard, 1992). Under the present experimental conditions, σ was calculated to be -0.063 on the basis of the data for cisplatin for which the $r_b(c)$ was determined in this study and $\Phi = 13°$ was assumed (Keck and Lippard, 1992). The $r_b(c)$ for Com1 was determined to be 0.08 (Fig. 8A; this value represents the mean from three measurements and varied on average ±3% from this mean) so that the unwinding angle for Com1 at pH 9 is 14 ± 1°. This value for the average unwinding angle caused by DNA adducts of Com1 is very similar to that found for DNA adducts of cisplatin and its direct analogs using the same experimental approach (13°; Keck and Lippard, 1992). Thus, unwinding of DNA modified by Com1 and transferred into the medium of pH 9 is similar to that of DNA modified by cisplatin and its direct, simple analogs.

CD spectra of DNA modified by Com1 and dissolved in neutral media (Fig. 7A) made it possible to suggest that at pH 7 DNA unwinding induced by the binding of Com1 is more complicated than at pH 9. It is reasonable to suggest that DNA adducts of Com1 unwind DNA similar to cisplatin or Com1 at pH 9 [i.e., that they increase the number of bp per turn of B-DNA by ca. 0.38 or 0.41 (these values correspond to the unwinding angle of 13° found for cisplatin or 14° found for Com1]. In addition, CD spectra of DNA modified by Com1 and dissolved in neutral media (Fig. 7A) suggest that Com1, upon binding to DNA and at pH 7, is also capable of overwinding DNA (i.e., to decrease the number of bp per turn of DNA). It has been shown (Gray, 1996; Johnson, 1996) that the dramatic reduction of the intensity of DNA-positive CD band at around 280 nm (Fig. 7, A and C) corresponds to a decrease in the number of bp per turn in B-DNA by approximately 0.2, which corresponds to the winding angle of ~7°. Thus, the resulting DNA unwinding by Com1 at pH 7 could be the sum of the two antagonistic effects. The $r_b(c)$ value for the sample of plasmid pSP73 determined by means of gel electrophoresis at pH 7 was 0.2 (Fig. 8B) so that the total unwinding angle for Com1 at pH 7 was only 6 ± 1°. A plausible explanation of this observation is that in neutral media DNA unwinding caused by the adducts of Com1 (~14°) is partially compensated by overall overwinding of DNA molecules (~7°) induced by the binding of Com1 and deduced from CD spectra (Fig. 7, A and C).

No comigration of the relaxed and supercoiled forms of pSP73 DNA at pH 7 or 9 was reached even at a value of r_b as high as 0.2 if the sample of the plasmid was modified by monofunctional Com2 (not shown). This result indicates that

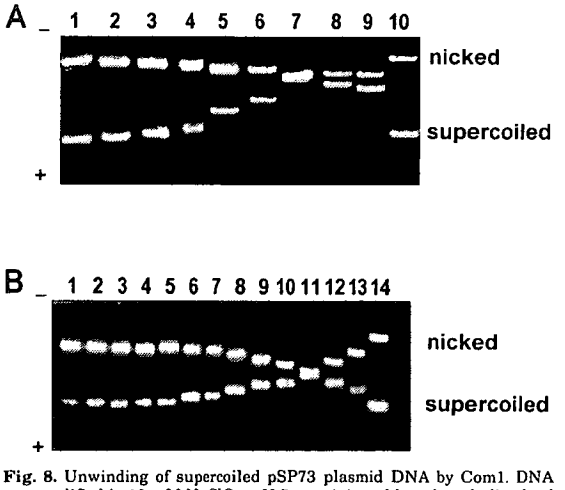

Fig. 8. Unwinding of supercoiled pSP73 plasmid DNA by Com1. DNA was modified in 10 mM $NaClO_4$, pH 7, precipitated by ethanol, dissolved in TBE buffer, pH 9.0 (A) or TAE buffer, pH 7.0 (B), and analyzed by gel electrophoresis using the same buffer in which DNA was dissolved. The top bands correspond to the form of nicked plasmid and the bottom bands to the closed, negatively supercoiled plasmid. A, lanes: 1 and 10, $r_b = 0$; 2, $r_b = 0.008$; 3, $r_b = 0.01$; 4, $r_b = 0.02$; 5, $r_b = 0.04$; 6, $r_b = 0.06$; 7, $r_b = 0.08$; 8, $r_b = 0.09$; 9, $r_b = 0.11$. B, lanes: 1 and 14, $r_b = 0$; 2, $r_b = 0.0008$; 3, $r_b = 0.002$; 4, $r_b = 0.004$; 5, $r_b = 0.0064$; 6, $r_b = 0.008$; 7, $r_b = 0.02$; 8, $r_b = 0.04$; 9, $r_b = 0.064$; 10, $r_b = 0.08$; 11, $r_b = 0.2$; 12, $r_b = 0.4$; 13, $r_b = 0.64$.

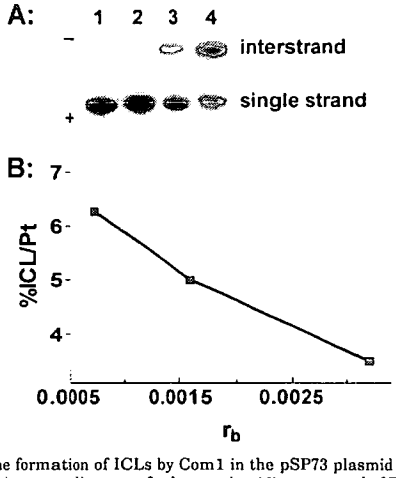

Fig. 9. The formation of ICLs by Com1 in the pSP73 plasmid linearized by *Eco*RI. A, autoradiogram of a denaturing 1% agarose gel of DNA which was 3'-end labeled. The interstrand cross-linked DNA appears as the top bands migrating on the gel more slowly than the single-stranded DNA (contained in the bottom bands). DNA was incubated with Com1 for 48 h at 37°C. r_b values: lane 1, 0; lane 2, 0.0007; lane 3, 0.0016; lane 4, 0.0032. B, dependence on r_b of the number of ICLs per adduct (%ICL/Pt). The ratio of ICLs to total platinum bound was calculated as described previously (Farrell et al., 1990; Brabec and Leng, 1993); %ICL/Pt was then calculated by multiplying this ratio by 100. Data points measured in triplicate varied on average ±3% from their mean.

Com2 induces a very small DNA unwinding ($\ll 6°$), which is consistent with a low DNA unwinding efficiency of monofunctional adducts of several platinum(II) compounds observed earlier (Keck and Lippard, 1992; Žaludová et al., 1997b; Balcarová et al., 1998).

Interstrand Cross-Linking. The amounts of ICLs formed by Com1 or Com2 in linear DNA were measured in pSP73 plasmid (2464 bp) that was first linearized by *Eco*RI (*Eco*RI cuts only once within pSP73 plasmid) and subsequently modified by Com1 or Com2 at various r_b. The samples were analyzed for the ICLs by agarose gel electrophoresis under denaturing conditions.

An electrophoretic method for precise and quantitative determination of interstrand cross-linking by platinum complexes in DNA was described previously (Farrell et al., 1990; Brabec and Leng, 1993). Upon electrophoresis under denaturing conditions, 3′-end labeled strands of linearized pSP73 plasmid containing no ICLs migrated as a 2464-base single strand, whereas the interstrand cross-linked strands migrated more slowly as a higher molecular mass species. The bands corresponding to more slowly migrating interstrand-cross-linked fragments were observed if Com1 was used to modify linearized DNA at r_b as low as 7×10^{-4} (shown in Fig. 9A, lane 2). The intensity of the more slowly migrating band increased with the growing level of the modification. The radioactivity associated with the individual bands in each lane was measured to obtain estimates of the fraction of noncross-linked or cross-linked DNA under each condition. The frequency of ICLs (the amount of ICLs per one molecule of the platinum complex bound to DNA) was calculated using the Poisson distribution from the fraction of noncross-linked DNA in combination with the r_b values and the fragment size (Farrell et al., 1990). Com2 showed no interstrand cross-linking efficiency even at a high r_b such as 0.1 (not shown). On the other hand, Com1 formed in DNA ICLs with a similar efficiency as cisplatin (frequency of ICLs formed in DNA was small, 4–6%; Fig. 9B).

It has been demonstrated that the ICLs formed in DNA by some nonmetal-based anticancer drugs are destroyed at alkaline pH and/or elevated temperatures. It is, therefore, possible that the lability of the ICLs of Com1 or Com2 in alkaline medium used in gel electrophoresis under denaturing conditions (Fig. 9) could account for the negligible frequency of DNA ICLs of Com2 or could result in underestimation of the frequency of ICLs formed in DNA by Com1. Therefore, we have also used a milder procedure that has allowed determination of alkali-unstable DNA ICLs formed by several anthracyclines (Konopa, 1983; Cullinane and Phillips, 1994). These techniques are based on the denaturation of modified DNAs at significantly lower temperatures, in the presence of either formamide or dimethyl sulfoxide and subsequent analysis in native agarose gel. The milder DNA interstrand cross-linking assays gave, however, frequencies of the ICLs of Com1 or Com2 that are similar to those determined by means of the agarose gel electrophoresis in an alkaline medium. Thus, it appears unlikely that Com1 or Com2 form alkali-unstable ICLs in DNA.

Immunochemical Analysis. We prepared Ab_{cis}, which recognizes two neighboring purine residues of the same strand of DNA *cis* coordinated to the platinum atom of *cis*-$[Pt(amine)_2]^{2+}$ (Sundquist et al., 1987; Vrána et al., 1992). They do not recognize monofunctional platinum adducts and the adducts of transplatin and its analogs.

Using competitive enzyme-linked immunosorbent assay, the inhibition of the binding of Ab_{cis} to their immunogens (double-stranded CT DNA modified by cisplatin at $r_b = 0.08$ for 48 h) by double-stranded DNA modified by Com1 or Com2 at various r_b values in the range of 0.005 to 0.1 was mea-

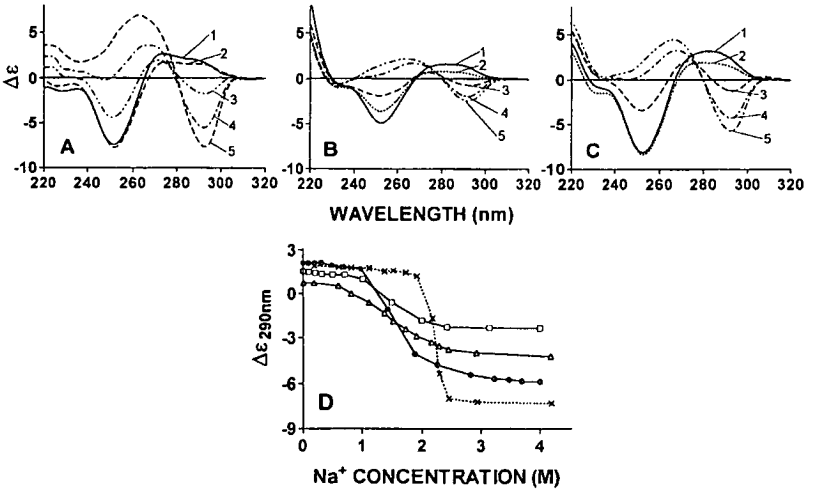

Fig. 10. CD spectroscopy of poly(dG-dC) nonmodified (A) or treated with Com1 (B) or Com2 (C) at $r_b = 0.1$. The polymer was modified when it was in B-form (in 10 mM $NaClO_4$) and was subsequently transferred into the media containing 10 mM $NaClO_4$ with 1 mM phosphate buffer, pH 7.5, plus 10 mM EDTA and various concentrations of NaCl. A, control, nonmodified polymer; curves: 1, 0.19 M NaCl; 2, 1.53 M NaCl; 3, 2.17 M NaCl; 4, 2.29 M NaCl; 5, 4.18 M NaCl. B, polymer modified by Com1; curves: 1, no NaCl added; 2, 1.01 M NaCl; 3, 1.51 M NaCl; 4, 2.00 M NaCl; 5, 3.14 M NaCl. C, polymer modified by Com2; curves: 1, no NaCl added; 2, 0.97 M NaCl; 3, 1.44 M NaCl; 4, 1.89 M NaCl; 5, 2.82 NaCl. D, plot of the molar ellipticity at 290 nm ($\Delta\epsilon_{290\ nm}$) as a function of Na^+ concentration for poly(dG-dC) nonmodified (×) or treated with Com1 (□), Com2 (●), and cisplatin at $r_b = 0.1$ (Δ). Data points measured in duplicate varied on average ±1% from their mean. Other details are described in the text.

sured. It was found (not shown) that double-stranded DNA modified by Com1 or Com2 did not inhibit the binding of the Ab_{cis}.

Ab_{cis} exhibits an equally good specificity for DNA modified by several analogs of cisplatin having varied nonleaving amine groups (Sundquist et al., 1987; Vrána et al., 1992). The observation that Ab_{cis} did not recognize DNA modified by bifunctional Com1 is very likely related to distinct conformational alterations induced in DNA by Com1 in comparison with cisplatin.

B→Z Transition. The effect of various platinum compounds on the salt-induced B→Z transition in poly(dG-dC) has already been described in several papers (for instance, Ushay et al., 1982; Pérez-Martin et al., 1993; Žaludová et al., 1997a). In the present work, DNA modifications by Com1 or Com2 are compared with those by cisplatin or [PtCl(dien)]Cl, respectively. Cisplatin was found to facilitate the B→Z transition, but the resulting Z form was distorted and the transition cooperativity was considerably reduced. [PtCl(dien)]Cl has been shown to stabilize the Z-form of DNA; for [PtCl(dien)]Cl-treated poly(dG-dC), the Z conformation is observed at a considerably lower salt concentration than for the nontreated polymer, and the transition cooperativity is considerably reduced.

The effect of Com1 and Com2 binding on the B→Z transition in DNA was investigated in poly(dG-dC) during salt-induced transition from the right- to left-handed double helix. The transition was monitored by CD spectroscopy at a series of NaCl concentrations between 0 and 4 M added to the medium containing 10 mM $NaClO_4$, 1 mM phosphate buffer, pH 7.5 and 0.1 mM EDTA. All of our experiments were done at r_b of 0 or 0.1. The r_b value of 0.1 was chosen as a compromise between a low value, which would have some relevance to the therapeutic effects of the platinum compounds, and a larger value, which would cause more pronounced changes in the spectra.

The CD spectra of nonplatinated poly(dG-dC) at various concentrations of NaCl are shown in Fig. 10A. The figure shows the characteristic inversion in the CD spectrum on going from the right-handed B form to the left-handed Z form after addition of at least 2.0 M NaCl, and is used as the standard with which to compare the platinum-treated duplexes. The CD spectra at different NaCl concentrations of poly(dG-dC) pretreated with either Com1 or Com2 in 10 mM sodium perchlorate (i.e., the polymer was treated when it was in the B conformation) are shown in Fig. 10, B and C, respectively.

A plot of the molar ellipticity at 290 nm as a function of the concentration of NaCl added to 10 mM $NaClO_4$ with 0.1 mM EDTA plus 1 mM phosphate buffer, pH 7.5 (Fig. 10D) can be used to monitor the B→Z transition in poly(dG-dC) (Žaludová et al., 1997a). From an examination of these plots presented in Fig. 10D it is evident that the maximum variation in the ellipticity at 290 nm for the nonmodified (control) polymer and the polymers treated with Com1 or Com2 occurs over a more or less narrow range in salt concentration. Thus, the transitions appear to be cooperative. The efficiency of platinum complexes to inhibit or facilitate the B→Z transition in DNA can be evaluated by means of the comparison of the midpoints in salt-induced transitions of control and modified polymers. The transition midpoint for control poly(dG-dC) occurs at 2.3 M whereas the transition midpoints of poly(dG-dC) modified by Com1 or Com2 were at ~1.6 M NaCl (Fig. 10D).

The results of the present work indicate that Com1 and Com2 facilitate the B→Z transition in DNA, but the resulting Z forms are distorted. Com1 distorts the Z-DNA more extensively than Com2. Com1 and Com2 affect B→Z transition differently, which implicates a different mode of their binding to DNA. In addition, the different effects of Com1 or Com2 on the B→Z transition in comparison with the effects of cisplatin (Fig. 10D) and [PtCl(dien)]Cl are consistent with unique DNA binding modes of the new aminophosphine platinum(II) complexes, as potent drugs with antitumor efficacy different from that of cisplatin.

Conclusions. In broad terms, we have demonstrated that the DNA binding mode, and very likely also the mechanism of antitumor activity of the new class of platinum(II) aminophosphine complexes, is different from that of cisplatin. This difference reflects the distinct nature of nonleaving ligands. The replacement of amine ligands in *cis*-dichloroplatinum(II) complexes by phosphine groups has been shown to influence considerably the selectivity for the adducts containing adenine and guanine residues and for monodentate and bidentate lesions. In addition, conformational alterations induced in DNA by Com1 are different from those induced by cisplatin. The different conformational changes and the increased bulk of the lesions are consistent with a role of these factors in the processing of DNA platinated by Com1. In particular, Com1 is more efficient than cisplatin in blocking DNA synthesis. A specific role of aminophosphine ligands in the modification of DNA by Com1 is also evident from the observation that DNA platinated by Com1 is not recognized by the antibodies elicited against DNA modified by cisplatin despite an equally good specificity of these antibodies for DNA modified by several analogs of cisplatin having varied nonleaving amine groups. A further processing of platinum(II) adducts by cellular components has been suggested to play an important role in the mechanism underlying antitumor activity of platinum compounds. The different cellular processing of DNA modified by *cis*-dichloroplatinum(II) complexes containing on the one hand nonleaving amine groups and aminophosphine ligands on the other might be relevant to the different biological activity of these two classes of platinum compounds. Structural studies of site-specific DNA adducts with aminophosphine platinum(II) complexes should provide a basis for analyzing and re-evaluating the structure-pharmacological activity relationships of platinum compounds. Studies toward this end are in progress, from which may ultimately arise a rational basis for design of a novel class of platinum antitumor drugs.

References

Balcarová Z, Kašpárková J, Žákovská A, Nováková O, Sivo MF, Natile G and Brabec V (1998) DNA interactions of a novel platinum drug, *cis*-$[PtCl(NH_3)_2(N7\text{-acyclovir})]^+$. *Mol Pharmacol* **53**:846–855.

Bancroft DP, Lepre CA and Lippard SJ (1990) Pt-195 NMR kinetic and mechanistic studies of *cis*-diamminedichloroplatinum and trans-diamminedichloroplatinum(II) binding to DNA. *J Am Chem Soc* **112**:6860–6871.

Bellon SF, Coleman JH and Lippard SJ (1991) DNA unwinding produced by site-specific intrastrand cross-links of the antitumor drug *cis*-diamminedichloroplatinum(ii). *Biochemistry* **30**:8026–8035.

Berners-Price SJ, Bowen J, McKeage MJ, Galettis P, Ding L, Baguley C and Brower W (1997) Selective antitumour activity of metal complexes of bidentate pyridylphosphines. *J Inorg Biochem* **67**:154.

Berners-Price SJ and Sadler PJ (1988) Phosphines and metal phosphine complexes: Relationship of chemistry to anticancer and other biological activity. *Struct Bonding (Berlin)* **70**:27–102.

Brabec V, Kleinwächter V, Butour JL and Johnson NP (1990) Biophysical studies of

the modification of DNA by antitumour platinum coordination complexes. *Biophys Chem* **35**:129–141.

Brabec V and Leng M (1993) DNA interstrand cross-links of *trans*-diamminedichloroplatinum(II) are preferentially formed between guanine and complementary cytosine residues. *Proc Natl Acad Sci USA* **90**:5345–5349.

Brabec V and Paleček E (1970) The influence of salts and pH on polarographic currents produced by denatured DNA. *Biophysik* **6**:290–300.

Butour JL and Macquet JP (1977) Differentiation of DNA-platinum complexes by fluorescence. The use of an intercalating dye as a probe. *Eur J Biochem* **78**:455–463.

Chen C, Kilkuskie R and Hanlon S (1981) Circular dichroism spectral properties of covalent complexes of deoxyribonucleic acid and *n*-butylamine. *Biochemistry* **20**: 4987–4995.

Comess KM, Burstyn JN, Essigmann JM and Lippard SJ (1992) Replication inhibition and translesion synthesis on templates containing site-specifically placed *cis*-diamminedichloroplatinum(II) DNA adducts. *Biochemistry* **31**:3975–3990.

Cullinane C and Phillips DR (1994) Sequence specificity of (cyanomorpholino)adriamycin adducts in human cells. *Biochemistry* **33**:6207–6212.

Eastman A (1987) The formation, isolation and characterization of DNA adducts produced by anticancer platinum complexes. *Pharmacol Ther* **34**:155–166.

Farrell N, Qu Y, Feng L and Van Houten B (1990) Comparison of chemical reactivity, cytotoxicity, interstrand cross-linking and DNA sequence specificity of bis(platinum) complexes containing monodentate or bidentate coordination spheres with their monomeric analogues. *Biochemistry* **29**:9522–9531.

Fichtinger-Schepman AMJ, Van der Veer JL, Den Hartog JHJ, Lohman PHM and Reedijk J (1985) Adducts of the antitumor drug *cis*-diamminedichloroplatinum(II) with DNA: Formation, identification, and quantitation. *Biochemistry* **24**:707–713.

Gelasco A and Lippard SJ (1998) NMR solution structure of a DNA dodecamer duplex containing a *cis*-diammineplatinum(II) d(GpG) intrastrand cross-link, the major adduct of the anticancer drug cisplatin. *Biochemistry* **37**:9230–9239.

Gray DM (1996) Circular dichroism of protein-nucleic acid interactions, in *Circular Dichroism and The Conformational Analysis of Biomolecules* (Fasman GD ed) pp 469–500, Plenum Press, New York.

Habtemariam A and Sadler P (1996) Design of chelate ring-opening platinum anticancer complexes: Reversible binding to guanine. *Chem Commun* 1785–1786.

Huang HF, Zhu LM, Reid BR, Drobny GP and Hopkins PB (1995) Solution structure of a cisplatin-induced DNA interstrand cross-link. *Science (Wash DC)* **270**:1842–1845.

Johnson JW (1996) Determination of the conformation of nucleic acids by electronic CD, in *Circular Dichroism and The Conformational Analysis of Biomolecules* (Fasman GD ed) pp 433–468, Plenum Press, New York.

Johnson NP, Butour J-L, Villani G, Wimmer FL, Defais M, Pierson V and Brabec V (1989) Metal antitumor compounds: The mechanism of action of platinum complexes. *Prog Clin Biochem Med* **10**:1–24.

Johnson NP, Macquet JP, Wiebers JL and Monsarrat B (1982) Structures of adducts formed between [Pt(dien)Cl]Cl and DNA in vitro. *Nucleic Acids Res* **10**:5255–5271.

Keck MV and Lippard SJ (1992) Unwinding of supercoiled DNA by platinum ethidium and related complexes. *J Am Chem Soc* **114**:3386–3390.

Kim SD, Vrána O, Kleinwächter V, Niki K and Brabec V (1990) Polarographic determination of subnanogram quantities of free platinum in reaction mixture with DNA. *Anal Lett* **23**:1505–1518.

Konopa J (1983) Adriamycin and daunomycin induce interstrand DNA cross-links in HeLa S3 cells. *Biochem Biophys Res Commun* **110**:819–826.

Margiotta N, Habtemariam A and Sadler PJ (1997) Strong, rapid binding of a platinum complex to thymine and uracil under physiological conditions. *Angew Chem Int Ed Engl* **36**:1185–1187.

Murray V, Motyka H, England PR, Wickham G, Lee HH, Denny WA and McFadyen WD (1992) The use of Taq DNA polymerase to determine the sequence specificity of DNA damage caused by *cis*-diamminedichloroplatinum(II), acridine-tethered platinum(II) diammine complexes or 2 analogues. *J Biol Chem* **267**:18805–18809.

Nováková O, Kašpárková J, Vrána O, vanVliet PM, Reedijk J and Brabec V (1995) Correlation between cytotoxicity and DNA binding of polypyridyl ruthenium complexes. *Biochemistry* **34**:12369–12378.

Papathanasiou P, Salem G, Waring P and Willis AC (1997) Synthesis of gold(I), silver(I) and cooper(I) complexes containing substituted (2-aminophenyl)phosphines. Molecular structure of [AuI(2-$H_2NC_6H_4PPhe$)], [AuI{(±)-$2H_2NC_6H_4PMePh$}] and (±)-[Cu(2-$H_2NC_6H_4PPh_2)_2$]PF_6. *J Chem Soc Dalton Trans* 3435–3443.

Pérez-Martin JM, Requena JM, Craciunescu D, López MC and Alonso C (1993) The anti Z-DNA reactivity of Z-DNA forming sequences is affected by platinum antitumor drugs. *J Biol Chem* **268**:24774–24779.

Reeder F, Guo ZJ, Murdoch PD, Corazza A, Hambley TW, BernersPrice SJ, Chottard JC and Sadler PJ (1997) Platination of a GG site on single-stranded and double-stranded forms of a 14-base oligonucleotide with diaqua cisplatin followed by NMR and HPLC—Influence of the platinum ligands and base sequence on 5′-G versus 3′-G platination selectivity. *Eur J Biochem* **249**:370–382.

Reedijk J (1996) Improved understanding in platinum antitumour chemistry. *Chem Commun* 801–806.

Sundquist WI, Lippard SJ and Stollar BD (1987) Monoclonal antibodies to DNA modified with *cis*- or *trans*-diamminedichloroplatinum(II). *Proc Natl Acad Sci USA* **84**:8225–8229.

Ushay HM, Santella RM, Caradonna JP, Grunberger D and Lippard SJ (1982) Binding of [(dien)PtCl]Cl to poly(dG-dC).poly(dG-dC) facilitates the B->Z conformational transition. *Nucleic Acids Res* **10**:3573–3588.

Vrána O, Boudný V and Brabec V (1996) Superhelical torsion controls DNA interstrand cross-linking by antitumor *cis*-diamminedichloroplatinum(II). *Nucleic Acids Res* **24**:3918–3925.

Vrána O, Brabec V and Kleinwächter V (1986) Polarographic studies on the conformation of some platinum complexes: Relations to antitumour activity. *Anti-Cancer Drug Des* **1**:95–109.

Vrána O, Kiseleva VI, Poverenny AM and Brabec V (1992) Conversion of DNA adducts of antitumour *cis*-diamminedichloroplatinum(II)-immunochemical analysis. *Eur J Pharmacol* **226**:5–13.

Žákovská A, Nováková O, Balcarová Z, Bierbach U, Farrell N and Brabec V (1998) DNA interactions of antitumor *trans*-[$PtCl_2(NH_3)$(quinoline)]. *Eur J Biochem* **254**: 547–557.

Žaludová R, Natile G and Brabec V (1997a) The effect of antitumor *trans*-[$PtCl_2$(*E*-iminoether)$_2$] on B→Z transition in DNA. *Anticancer Drug Des* **12**:295–309.

Žaludová R, Žákovská A, Kašpárková J, Balcarová Z, Vrána O, Coluccia M, Natile G and Brabec V (1997b) DNA modifications by antitumor *trans*-[$PtCl_2$(*E*-iminoether)$_2$]. *Mol Pharmacol* **52**:354–361.

Send reprint requests to: Dr. Viktor Brabec, Institute of Biophysics, Academy of Sciences of the Czech Republic, Královopolská 135, CZ-61265 Brno, Czech Republic. E-mail: brabec@ibp.cz

DALTON
FULL PAPER

Control of aminophosphine chelate ring-opening in Pt(II) and Pd(II) complexes: potential dual-mode anticancer agents

Abraha Habtemariam,[a] Beth Watchman,[a] Brian S. Potter,[b] Rex Palmer,[b] Simon Parsons,[a] Andrew Parkin[a] and Peter J. Sadler *[a]

[a] *Department of Chemistry, University of Edinburgh, West Mains Road, Edinburgh, UK EH9 3JJ. E-mail: P.J.Sadler@ed.ac.uk*
[b] *Department of Crystallography, Birkbeck College, University of London, Malet Street, London, UK WC1E 7HX*

Received 14th November 2000, Accepted 17th January 2001
First published as an Advance Article on the web 27th March 2001

We show that bis(aminophosphine) complexes of the type $[M(R^1R^2N(CH_2)_nPPh_2)_2]^{2+}$, M = Pt(II) or Pd(II), can exist in chelate ring-closed and ring-opened forms both in the solid state and in aqueous solution. The equilibrium between them in solution can be controlled by the nature of the groups R^1 and R^2 (H, Me, Bz, cyclohexyl), by the bridge length *n*, and by the pH and Cl^- concentration. X-Ray crystal structures are reported for the ring-closed complexes *cis*-$[Pt(H_2N(CH_2)_2PPh_2\text{-}P,N)_2]Cl_2$, *cis*-$[Pt(H_2N(CH_2)_3PPh_2\text{-}P,N)_2]Cl_2$, and *cis*-$[Pt(Me(H)N(CH_2)_2PPh_2\text{-}P,N)_2][HCl_2]_2$, the mono-ring-opened complex *cis*-$[Pd(Me_2N(CH_2)_2PPh_2\text{-}N,P)Cl(Me_2NH(CH_2)_2PPh_2\text{-}P)](NO_3)_2$, the di-ring-opened complex *cis*-$[Pt(Me_2N(CH_2)_3PPh_2\text{-}P)_2Cl_2]$, and, for comparison, the monochelate *cis*-$[Pd(Me_2N(CH_2)_3PPh_2\text{-}N,P)Cl_2]$. These square-planar complexes exhibit varying degrees of distortion and variable M–N bond lengths dependent not only on the *trans* influence of P but also on steric effects within the complex. pH-induced chelate ring-opening of *cis*-$[Pt(Me_2N(CH_2)_2PPh_2\text{-}P,N)_2]Cl_2$ had an associated p*K* value of 6.9. In contrast, complexes with R^1 and R^2 = H, *n* = 2 or 3 or R^1 = H and R^2 = Me, *n* = 2, are more difficult to ring-open. Thus the complexes *cis*-$[Pt(Me(H)N(CH_2)_2\text{-}PPh_2\text{-}P,N)_2]Cl_2$ and *cis*-$[Pt(H_2N(CH_2)_3PPh_2\text{-}P,N)_2]Cl_2$, had associated p*K* values of 2.1 and 2.9, respectively. These aminophosphine complexes may exhibit anticancer activity by two mechanisms: by disrupting mitochondrial membrane potentials as bis-chelated (ring-closed) lipophilic cations, or by direct binding to DNA bases as ring-opened complexes.

Introduction

Aminophosphine complexes contain mixed donor ligands: one soft phosphorus donor and one relatively hard nitrogen donor, and can act as bridging ligands or as chelating agents thereby conferring enhanced stability to the complex. In Pt(II) complexes, the nitrogen atom binds more weakly than phosphorus, especially when N is *trans* to P, which exerts a high *trans* influence.[1] Furthermore, the strength of M–N bonds is affected much more by steric factors than for the corresponding M–P bonds.[2] Thus with the appropriate choice of nucleophiles, and under a given set of conditions such as pH, and chloride concentration, equilibria involving the dissociation of the amino group can be established resulting in ring-opened complexes with a potential binding site on the metal centre. Consequently, P,N chelated Pt(II) complexes are known to display a considerably higher reactivity than the bis(phosphine) complexes.[3] Depending on the steric demands of the substituents on N and the length of the N–P linker in the aminophosphine ligand, bis-chelate, mono-chelate ring-opened, or non-chelate complexes can be formed (Scheme 1).

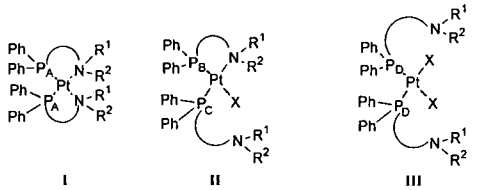

I II III

Scheme 1 Ring-closed (I), mono-ring-opened (II) and di-ring-opened (III) aminophosphine complexes. X = Cl, OH_2.

There are many previous reports relating to the potential use of aminophosphine Pt(II) complexes in catalysis.[4–7] However, very few[8] of these studies have explored the potential biological activities of these complexes, even though they contain *cis* amine ligands, a feature found in many active platinum anticancer agents,[9] together with *cis* phosphine ligands. Certain diphosphines have also previously been shown to exhibit anticancer activity, especially 1,2-diphosphinoethane (dppe) complexes of Cu(I), Ag(I) and Au(I).[10] In addition a range of monophosphine complexes of Au(I) exhibit antiarthritic activity and one of these, the PEt_3 complex auranofin, is now in clinical use as an antiarthitic drug.[10] In addition, they offer potential as anticancer agents *via* disruption of mitochondrial function due to their lipophilic cationic character.[11]

Recently we have established that the chelate ring-opening reactions of Pt(II) aminophosphine complexes can be controlled under conditions of biological relevance, and that they bind reversibly to the DNA base guanine.[12,13] We have also shown that chelate ring-opened Pt(II) aminophosphine complexes can bind rapidly and strongly to the DNA base thymine as well as to the RNA base uracil under physiological conditions, in contrast to platinum(II) am(m)ine anticancer complexes.[14] Some aminophosphine complexes are cytotoxic to cancer cells including cisplatin-resistant cells, but the potency depends on the cell type. Different complexes may act *via* different mechanisms in different kinds of cells.[12] The biological activity may arise from a combination of antimitochondrial activity due to the ring-closed forms and attack on DNA by the chelate ring-opened complexes.

In the present work, we have prepared and characterised both chelate ring-closed and ring-opened aminophosphine complexes of Pt(II) and Pd(II) and investigated the effect of pH and

 DOI: 10.1039/b009117k

chloride on chelate ring-opening in aqueous solution. Our aim is to develop a rational approach towards the design and synthesis of new Pt and Pd drugs with improved therapeutic properties, in particular overcoming factors which limit the use of current Pt anticancer drugs: resistance, toxicity, and narrow spectrum of treatable cancers.

Experimental

Reagents

$H_2N(CH_2)_2Cl{\cdot}HCl$, $H_2N(CH_2)_3Cl{\cdot}HCl$, $Me_2N(CH_2)_2Cl{\cdot}HCl$, $Bz_2N(CH_2)_2Cl{\cdot}HCl$, BzN(H)Me, 5%Pd/C and ethylene oxide were purchased from Aldrich, $C_6H_{11}(H)N(CH_2)_2OH$ and $Bz(H)N(CH_2)_2OH$ from Lancaster Synthesis. $(COD)PtCl_2$ (COD = cycloocta-1,5-diene) and $(COD)PdCl_2$ were purchased from Aldrich or prepared by literature methods.[15,16] Solvents were generally dried and purified by standard methods, and freshly distilled before use.

NMR spectroscopy

Spectra were recorded on JEOL GSX270 (67.80 MHz for ^{13}C, 109.25 MHz for ^{31}P and at 57.94 MHz for ^{195}Pt) and DMX 500 spectrometers (202 MHz for ^{31}P). Chemical shifts (δ) are reported in ppm relative to internal TMS ($CDCl_3$) or TSP (D_2O) for ^1H and ^{13}C, and to external 85% H_3PO_4 for ^{31}P, and 1 M Na_2PtCl_6 for ^{195}Pt. Coupling constants (J) are given in Hz and NMR signals are described as singlets (s), doublets (d), triplets (t), multiplets (m) and quintets (q).

Microanalyses and mass spectrometry

Microanalyses were obtained from the Department of Chemistry, University College, London, and the University of Edinburgh. Fast atom bombardment (FAB) mass spectra were obtained at the School of Pharmacy, University of London on a VG Analytical ZAB-SE instrument.

pH Measurements

These were made using a Corning 145 pH meter equipped with an Aldrich micro combination electrode calibrated with standard buffer solutions at pH 4 and 7. Readings of the pH meter for D_2O solutions were not corrected for deuterium isotope effects and are designated as pH* values.

pK Determinations

The relative concentrations of species were determined from ^{31}P peak integrals and fitted to the Henderson–Hasselbalch equation using the program KALEIDAGRAPH.[17]

Crystallography

Table 1 summarises the crystal data, data collection, structure solutions and refinement parameters for complexes **1**, **2**, **8**, **9**, **14b** and **18**. The X-ray data for complexes **1**, **14b** and **18** were collected on a Nonius CAD4 diffractometer. The structures were solved by heavy atom methods using SHELXS-97[18] and SHELXL-93.[19] Subsequent refinements were made by the full-matrix least-squares technique on $|F^2|$. Anisotropic displacement parameters were used for non-H-atoms, isotropic for H-atoms in geometrically fixed, riding mode.

X-Ray data for **8** were collected on a Bruker SMART APEX CCD diffractometer. The structure was solved by the Patterson method and refined against F^2 (SHELXTL).[20] Hydrogen atoms attached to O1W were placed using the difference map and refined freely. Other H-atoms were placed in calculated positions and treated using a riding model.

X-Ray data for **2** and **9** were collected on a Stoe Stadi-4 diffractometer. The structures were solved by the Patterson method; structure **2** was refined against F^2 (SHELXTL),[20] and structure **9** was refined against F(CRYSTALS).[21] In structure **2**, one of the two phenyl rings exhibited 50/50 rotational disorder about a common pivot atom (C11). The disorder components were restrained to be similar and have a C_2 axis of symmetry running through the ordered atoms. Partial weight C-atoms were refined with common isotopic thermal parameters for C21/C21′, C31/C31′ *etc.* The assignment of the anion as $[Cl{-}H{-}Cl]^-$ was made on the basis of the Cl · · · Cl distance and the suggestion of a hydrogen position in a ΔF map, this H-atom being subsequently refined freely. Other H-atoms were placed in calculated positions and treated using a riding model. H-atoms on partially occupied H_2O molecules were placed to form favourable H-bonds. In **9** the ligands were restrained to be geometrically similar.

CCDC reference numbers 152973–152978.

See http://www.rsc.org/suppdata/dt/b0/b009117k/ for crystallographic data in CIF or other electronic format.

Preparation of ligands

$H_2NCH_2CH_2PPh_2$. The preparation was based on a literature method.[22] To a suspension of Bu^{t}OK (8.5 g, 76 mmol) in dry and freshly distilled THF (100 ml), PPh_2H (5 ml, 5.35 g, 28.76 mmol) was added under Ar, and stirred at ambient temperature for 40 min. Then crystalline $H_2NCH_2CH_2Cl{\cdot}HCl$ (3.24 g, 28.2 mmol) was added and the reaction mixture was heated under reflux for 20 h. During that time the deep-red solution became almost colourless. The solvent was then removed *in vacuo* and 10% HCl solution was added. The solution was then washed with benzene and made alkaline with 10% NaOH solution. The product was then extracted into benzene (3 × 50 ml), washed with brine, and dried over Na_2SO_4. After filtration and rotary evaporation, a colourless viscous liquid was obtained, which was dissolved in ether and purified by passage through a short alumina column. Yield 46%, ^1H NMR ($CDCl_3$): δ 1.51 (2 H, br, s, H_2N), 2.26 (2 H, m, P–CH_2), 2.86 (2 H, m, N–CH_2), 7.1–7.4 (10 H, m, Ph); $^{31}P{-}\{^1H\}$ NMR ($CDCl_3$): δ −21.5. The following compounds were prepared by analogous methods.

$H_2NCH_2CH_2CH_2PPh_2$. Yield 40%, ^1H NMR ($CDCl_3$): δ 1.32 (2 H, br, s, H_2N), 1.43–1.49 (2 H, q, CH_2), 1.91–1.97 (2 H, t, CH_2), 2.62–2.67 (2 H, t, CH_2) 7.17–7.33 (10 H, m, Ph); $^{31}P{-}\{^1H\}$ NMR ($CDCl_3$): δ −21.5.

$Me_2NCH_2CH_2PPh_2$. Yield 40%, ^1H NMR ($CDCl_3$): δ 2.24 (6 H, s, N–CH_2), 2.26–2.28 (2 H, m, P–CH_2), 2.38–2.44 (2 H, m, N–CH_2), 7.31–7.34 (10 H, m, Ph); $^{31}P{-}\{^1H\}$ NMR ($CDCl_3$): δ −19.07.

(c-C_6H_{11})$HNCH_2CH_2PPh_2$. To a cooled solution (0 °C) of (c-C_6H_{11})$HNCH_2CH_2OH$ (14.32 g, 0.1 mol) in $CHCl_3$ (200 ml) thionyl chloride (90.44 g, 60 ml, 0.76 mol) was added dropwise under Ar. The reaction mixture was then heated under reflux for 3 h. The solvent and excess thionyl chloride were removed *in vacuo* to leave a dark-brown oily solid. This was washed with ether and dried over P_2O_5. The product was recrystallised from ethanol–ether to give a shiny whitish crystalline solid of (c-C_6H_{11})$HNCH_2CH_2Cl{\cdot}HCl$. Yield 70%, (Found: C, 48.76; H, 8.64; N, 6.99. Calc. for $C_8H_{16}Cl_2N$: C, 48.48; H, 8.58; N, 7.07%).

The above compound was then used to prepare (c-C_6H_{11})-$HNCH_2CH_2PPh_2$ in a similar way to that described for the above ligand. Yield 50%, ^1H NMR ($CDCl_3$): δ 1.18–1.26, 1.69–1.86 (11 H, br), 2.26–2.29 (4 H, m), 7.36–7.48 (10 H, m, Ph); $^{31}P{-}\{^1H\}$ NMR ($CDCl_3$): δ −19.92.

(Me)$HNCH_2CH_2PPh_2$. In the first instance (Me)$BzNCH_2$-CH_2OH was prepared as described below. THF (200 ml) was added to ethylene oxide (100 ml, 2.38 mol), obtained by condensation of the gas from a lecture bottle into a 500 ml 3-neck round-bottom flask fitted with a dry ice–acetone condenser,

Table 1 Details of X-ray data collection and refinements for compounds **1**, **2**, **8**, **9**, **14b**, and **18**

Compound	**1**	**2**	**8**	**9**	**14b**	**18**
Empirical formula	$C_{28}H_{38}Cl_2N_2O_3P_2Pt$	$C_{30}H_{40}Cl_4N_2OP_2Pt$	$C_{32}H_{44}Cl_2N_4O_5P_2Pt$	$C_{35}H_{46}Cl_4P_2N_2Pt$	$C_{32}H_{45}ClN_4O_8P_2Pd$	$C_{17}H_{22}Cl_2NPPd$
M	778.49	843.47	892.64	893.61	817.54	448.48
Temperature/K	291(2)	220(2)	150(2)	220(2)	291(2)	293(2)
Space group	$P2_1/n$	$P2_1/n$	$P\bar{1}$	$P2_1/c$	$P2_1/n$	$P2_1/n$
Crystal system	Monoclinic	Monoclinic	Triclinic	Monoclinic	Monoclinic	Monoclinic
λ/Å	1.54180	0.71073	0.71073	0.71073	1.54180	1.54180
a/Å	9.1827(4)	8.938(4)	9.4849(8)	10.141(1)	12.120(2)	10.128(4)
b/Å	25.826(5)	12.149(4)	11.3914(9)	18.817(2)	12.4800(10)	11.527(4)
c/Å	13.384(3)	15.7788(5)	17.8243(15)	20.230(2)	24.400(2)	15.795(6)
α/°			95.7700(10)			
β/°	92.25(1)	99.35(3)	96.9850(10)	101.25(1)	91.838(9)	102.42
γ/°			109.0030(10)			
U/Å^3	3171.6(9)	1691.6(11)	1787.1(3)	3786.31	3688.8(7)	1800.8(12)
Z	4	2	2	4	4	4
D_c/g cm^{-3}	1.618	1.656	1.659	1.57	1.380	1.485
μ/mm^{-1}	11.027 (Cu-Kα)	4.584 (Mo-Kα)	4.209 (Mo-Kα)	4.14 (Mo-Kα)	5.904(Cu-Kα)	12.593(Cu-Kα)
F(000)	1520	836	892	1777.39	1576	796
Scan mode	ω–2θ	ω–θ	ψ and ω scans	ω–θ	ω–2θ	ω–2θ
Crystal size/mm	0.42 × 0.25 × 0.18	0.27 × 0.16 × 0.12	0.38 × 0.10 × 0.05	0.16 × 0.16 × 0.04	0.2 × 0.3 × 0.4	0.3 × 0.3 × 0.4
Colour, habit	White, needles	Colourless, block	Colourless, lath	Colourless, tablet	White, needles	Colourless, needles
θ range/°	3.42–71.82	2.61–25.01	1.91–26.38	2.50–25.00	3.62–73.91	4.76–73.89
h, k, l ranges	−11–0, 0–31, −16–16	−10–10, 0–14, 0–18	−11–11, −14–14, −22–22	−12–11, 0–22, 0–24	−15–15, 0–15, 0–30	0–12, −14–0, −19–19
Reflections collected	6631	3783	12153	11044	7648	3873
Independent reflections (R_{int})	6239 (0.0564)	2980 (0.0445)	7160 (0.0261)	6096 (0.05)	7473 (0.0633)	3663 (0.0312)
Data/restraints/parameters	6236/0/308	2970/32/180	7160/0/423	4543/0/398	7424/0/468	3663/0/225
Goodness of fit on F^2	1.089	1.087	0.940	1.0742	0.921	1.010
Final R indices $R1$, $wR2$	0.0535, 0.1546	0.0528, 0.1475	0.0296, 0.0669	0.0530, 0.0547	0.0751, 0.2114	0.0443, 0.1208
Maximum Δ/σ	0.0	0.1	0.001	0.078326	0.001(1)	0.001(1)

and the reaction mixture was kept at 0 °C. To this cold mixture, $PhCH_2NH(Me)$ (15 ml, 0.12 mol) was added dropwise. The reaction was then initiated by the addition of $ZnBr_2$ (1 g) and was left stirring overnight at ambient temperature. The solvent was removed *in vacuo* and the residual oil distilled (100–107 °C, 2 mm Hg) to give $(Me)BzNCH_2CH_2OH$. Yield 55%, ^1H NMR ($CDCl_3$): δ 2.18, (3 H, s, CH_3), 3.43 (2 H, t, O–CH_2), 3.58 (2 H, t, N–CH_2) 7.18–7.25 (5 H, m, Ph); ^{13}C-{^1H} NMR ($CDCl_3$): δ 41.57 (CH_3), 58.49 (N–CH_2), 62.29 (O–CH_2), 127.13 (*para*), 128.6 (*ortho*), 128.93 (*meta*), 138.54.

A solution of $(Me)BzNCH_2CH_2OH$ (10 g, 0.06 mol) in 98% ethanol (20 ml) was placed in a bomb at ambient temperature and 2–3 atm in a standard hydrogenation set-up, in the presence of 2 g of 5% palladium on carbon. The hydrogenolysis was complete in about 2 h. The catalyst was then removed by filtration and the solvent removed on a rotary evaporator to leave a slightly yellowish oil. This was distilled (30–32 °C, 1 mm Hg) to give $(Me)HNCH_2CH_2OH$ as a colourless oil. Yield 67%, ^1H NMR ($CDCl_3$): δ 2.48, (3 H, s, N–CH_3), 2.69 (2 H, t, CH_2), 3.42 (br, NH) 3.61 (2 H, t, CH_2); ^{13}C-{^1H} NMR ($CDCl_3$): δ 35.97, 53.95, 60.44. ν_{max}/cm^{-1} 3641, 1060 (OH), 3294, 1688, 1656 (NH).

It was then chlorinated in the usual manner to give $(Me)HNCH_2CH_2Cl\cdot HCl$ in 95% yield. (Found: C, 27.56; H, 7.01; N, 10.57. Calc. for $C_3H_9Cl_2N$: C, 27.69; H, 6.92; N, 10.77%). The above salt was then used to prepare $(Me)HNCH_2CH_2PPh_2$ using a similar procedure to that described earlier. Yield 30%, ^1H NMR ($CDCl_3$): δ 2.34 (2 H, m, CH_2) 2.81 (6 H, s, N–CH_3), 3.12 (2 H, m, CH_2) 3.6 (2 H, t, CH_2), 7.36–7.48 (10 H, m, Ph); ^{31}P-{^1H} NMR ($CDCl_3$): δ −19.97.

$(Bz)HNCH_2CH_2PPh_2$. The hydrochloride salt $(Bz)HNCH_2CH_2Cl\cdot HCl$ was prepared from $(Bz)HNCH_2CH_2OH$ in the usual manner. Yield 81%, mp 197 °C (dec.) (Found: C, 52.53; H, 6.40; N, 6.79. Calc. for $C_9H_{13}Cl_2N$: C, 52.42; H, 6.31; N, 6.79%). ^1H NMR ($CDCl_3$): δ 3.46 (2 H, m) 3.84 (2 H, m), 4.25 (2 H, s) 7.46 (6 H, s).

The preparation of $(Bz)HNCH_2CH_2PPh_2$ was carried out in the usual fashion, but the work-up was modified as follows. After the THF was removed *in vacuo*, addition of 20% HCl solution gave rise to a whitish solid that was filtered off, redissolved in $CHCl_3$ and filtered to remove the insoluble impurities. The solvent was removed on a rotary evaporator to leave a whitish powder, which was recrystallised from methanol–ether to give shiny white crystals. Yield 84%, (Found: C, 70.41; H, 6.44; N, 4.14. Calc. for $C_{21}H_{23}ClNP$: C 70.88; H, 6.46; N, 3.93%). ^1H NMR ($CDCl_3$): δ 2.59 (m) 2.82 (s, br) 3.8 (s, br) 7.4–7.62 (Ph) 10.09 (NH); ^{31}P-{^1H} NMR ($CDCl_3$): δ −20.33.

The following were also prepared analogously.

$(Bz)MeNCH_2CH_2PPh_2$. $(Bz)MeNCH_2CH_2OH$ was chlorinated to give $(Bz)MeNCH_2CH_2Cl\cdot HCl$ as a whitish solid in 95% yield. mp 144 °C. (Found: C, 54.85; H, 7.04; N, 5.97. Calc. for $C_{10}H_{15}Cl_2N$: C, 54.54; H, 6.81; N, 6.36%). This was then used to prepare $(Bz)MeNCH_2CH_2PPh_2$ with a yield of 45%. ^1H NMR ($CDCl_3$): δ 2.5 (s, br) 3.2–3.50 (m, br) 3.9–4.4 (m, br) 7.1–7.92 (Ph); ^{31}P-{^1H} NMR ($CDCl_3$): δ −19.00.

$(Bz)_2NCH_2CH_2PPh_2$. This was prepared as above in 66% yield. mp 105 °C. (Found: C, 72.25; H, 6.84; N, 3.34. Calc. for $C_{28}H_{28}NP\cdot 3H_2O$: C, 72.41; H, 7.32; N, 3.03%). ^1H NMR ($CDCl_3$): δ 2.59 (m) 2.87 (m) 4.06, 4.27 (m) 7.19–7.77 (Ph); ^{31}P-{^1H} NMR ($CDCl_3$): δ −19.59.

$Me_2NCH_2CH_2CH_2PPh_2$. To a mixture of 37% HCOH (37 g, 0.46 mol) and 98% HCOOH (27 g, 22 ml, 0.57 mol), $H_2NCH_2CH_2CH_2Cl\cdot HCl$ (10 g, 0.076 mol) was added and the reaction mixture heated under reflux for 30 h. The light brown solution was made alkaline with 10% NaOH, extracted with CH_2Cl_2 (3 × 50 ml) and dried over Na_2SO_4. The solvent was then removed *in vacuo* to leave a brownish liquid, to which ethanolic hydrogen chloride (20 ml) was added. The solvent was then removed *in vacuo* to leave a brownish oil which was dissolved in hot propan-2-ol. The precipitate obtained after addition of ether was filtered, and washed with ether to give a whitish highly hygroscopic solid ($Me_2NCH_2CH_2CH_2Cl\cdot HCl$). Yield 30%, ^1H NMR ($CDCl_3$): δ 2.81 (6 H, s, N–CH_2) 3.6 (2 H, t, CH_3), 2.34 (2 H, m, CH_2) 3.12 (2 H, m, CH_2).

$Me_2NCH_2CH_2CH_2Cl\cdot HCl$ was then used to prepare the above ligand as described earlier. Yield 38%, ^1H NMR ($CDCl_3$): δ 1.44–1.53 (2 H, m) 1.93–1.99 (2 H, m, CH_2), 2.05 (6 H, N–CH_3) 2.21–2.26 (2 H, t, CH_2) 7.17–7.21, 7.24–7.35 (10 H, m, Ph); ^{31}P-{^1H} NMR ($CDCl_3$): δ −19.33.

Preparation of platinum complexes

$[Pt(H_2NCH_2CH_2PPh_2)_2]Cl_2\cdot 3H_2O$ 1. A solution of $H_2NCH_2CH_2PPh_2$ (0.2 g, 0.26 mmol) in CH_2Cl_2 (2 ml) was added dropwise to a clear solution of $(COD)PtCl_2$ (0.093 g, 0.26 mmol) in CH_2Cl_2 (25 ml) and the reaction mixture was stirred at ambient temperature for 1 h. The volume was then reduced to *ca.* 7 ml and diethyl ether was added to precipitate a whitish powder which was then filtered off and washed with diethyl ether and recrystallised from acetone–dichloromethane.

Yield 86%, mp 235 °C (dec.) (Found: C, 43.33; H, 4.80; N, 3.44; Cl, 9.62. Calc. for $C_{28}H_{32}Cl_2N_2P_2Pt\cdot 3H_2O$: C, 43.18; H, 4.88; N, 3.59; Cl, 9.12%). *m/z* (FAB MS): 652 (100%, $M^+ - 2Cl$). ^1H NMR ($CDCl_3$) δ 2.71–2.77 (2 H, m, N–CH_2), 3.02–3.07 (2 H, m, P–CH_2), 7.25 (H_2N, br, s, ^2J(PtH) 42 Hz), 7.25–7.53 (10 H, Ph); ^{31}P-{^1H} NMR ($CDCl_3$): δ 33.70 ^1J(PtP) 3300 Hz; ^{195}Pt-{^1H} NMR ($CDCl_3$): δ −4589 ^1J(PtP) 3344 Hz.

The following complexes were also prepared in a similar manner.

$[Pt(H(Me)NCH_2CH_2PPh_2)_2][Cl{-}H{-}Cl]_2\cdot H_2O$ 2. Yield 71% (Found: C, 43.80; H, 4.82; N, 3.30. Calc. for $C_{30}H_{38}Cl_6N_2P_2Pt\cdot H_2O$: C, 42.70; H, 4.74; N, 3.32%). ^1H NMR ($CDCl_3$) δ 2.78 (2H, br), 3.05 (N–Me), 3.35 (2H, br), 6.5 (NH) 7.3–7.6 (10 H, Ph); ^{31}P-{^1H} NMR (D_2O, pH* 3.85): δ 28.9 ^1J(PtP) 3300 Hz, ^{195}Pt-{^1H} NMR ($CDCl_3$): δ −4575 ^1J(PtP) 3330 Hz. Crystals suitable for X-ray structure determination were obtained by recrystallisation from H_2O–EtOH (1 : 1).

$[PtCl((c\text{-}C_6H_{11})HNCH_2CH_2PPh_2)_2]Cl\cdot 4H_2O$ 3. Yield 81% (Found: C, 49.56; H, 6.15; N, 2.87. Calc. for $C_{40}H_{52}Cl_2N_2P_2Pt\cdot 4H_2O$: C, 49.94; H, 6.25; N, 2.91%). ^{31}P-{^1H} NMR ($CDCl_3$): δ 36.45, ^1J(PtP) 3294; ^{195}Pt-{^1H} NMR ($CDCl_3$): δ −4538 (t) ^1J(PtP) 3233 Hz. A $CHCl_3$ solution of the crude product of the above compound was left at 4 °C for about 10 h after which time crystals formed. These were filtered off and dried to give the monochelate complex $[Pt((c\text{-}C_6H_{11})HNCH_2CH_2PPh_2)Cl_2]$ as a minor product (*ca.* 5%). (Found: C, 41.10; H, 4.49; N, 2.22. Calc. for $C_{20}H_{26}Cl_2NPPt$: C, 41.59; H, 4.50; N, 2.42%). ^{31}P-{^1H} NMR ($CDCl_3$): δ 24.81 ^1J(PtP) 4064 Hz.

$[Pt(H(Bz)NCH_2CH_2PPh_2)_2]Cl_2$ 4. Yield 46% (Found: C, 51.74; H, 5.08; N, 2.81. Calc. for $C_{42}H_{44}Cl_2N_2P_2Pt$: C, 51.60; H, 4.74; N, 2.87%). ^1H NMR ($CDCl_3$) δ 2.55, 2.88, 3.1, 3.9, 3.5, 7.0–7.60, (15 H, Ph); 10.09 (NH) ^{31}P-{^1H} NMR ($CDCl_3$): δ 30.3 ^1J(PtP) 3420 Hz, 40.0 ^1J(PtP) 3800 Hz, 5.0 ^1J(PtP) 3348 Hz.

$[PtCl(Me_2NCH_2CH_2PPh_2)_2]Cl\cdot HCl$ 5b. Yield 90%, mp 194 °C (dec.) (Found: C, 47.63; H, 4.99; N, 3.26; Cl, 12.75; P, 8.1. Calc. for $C_{32}H_{40}Cl_2N_2P_2Pt\cdot HCl$: C, 47.03; H, 5.02; N, 3.42; Cl, 13.04; P, 7.59%). *m/z* (FAB MS): 745 (100%, $M^+ - Cl$). ^1H NMR ($CDCl_3$) δ 2.15 (s), 2.17–2.20 (s, br), 2.70–2.79 (s, br), 3.01–3.15 (s, br), 7.16–7.49 (10 H, Ph); ^{31}P-{^1H} NMR ($CDCl_3$): δ 36.52 ^1J(PtP) 3691 Hz, −0.46 ^1J(PtP) 3187 Hz; ^{195}Pt-{^1H} NMR ($CDCl_3$): δ −4505 (dd).

[Pt(Me(Bz)NCH$_2$CH$_2$PPh$_2$)$_2$]Cl$_2$ 6. Yield 83% (Found: C, 56.98; H, 5.13; N, 2.91. Calc. for $C_{44}H_{48}Cl_2N_2P_2Pt$: C, 56.65; H, 5.15; N, 3.00%). ^{1}H NMR ($CDCl_3$) δ 1.8 (s, br), 2.16 (m, br), 2.46 (s, br), 3.44 (s, br) 7.1–7.9 (15 H, Ph); ^{31}P-{^{1}H} NMR ($CDCl_3$): δ 30.69 ^1J(PtP) 3754 Hz, −0.06 ^1J(PtP) 3184 Hz, $^2J(P_BP_C)$ 17 Hz.

[Pt((Bz)$_2$NCH$_2$CH$_2$PPh$_2$)$_2$]Cl$_2$ 7. Yield 81% (Found: C, 61.54; H, 5.15; N, 2.40. Calc. for $C_{56}H_{56}Cl_2N_2P_2Pt$: C, 61.99; H, 5.16; N, 2.58%). ^{1}H NMR ($CDCl_3$) δ 1.18 (s, br), 2.16 (s, br), 2.46 (s, br), 3.44 (s, br) 7.1–7.9 (20 H, Ph); ^{31}P-{^{1}H} NMR ($CDCl_3$): δ 4.5 ^1J(PtP) 3635 Hz.

[Pt(H$_2$NCH$_2$CH$_2$CH$_2$PPh$_2$)$_2$]Cl$_2$ 8. Yield 50%, mp 235 °C (dec.) (Found: C, 43.24; H, 5.52; N, 2.93. Calc. for $C_{30}H_{36}Cl_2N_2P_2Pt\cdot4H_2O$: C, 43.68; H, 5.33; N, 3.39%). *m/z* (FAB MS): 680 (100%, $M^+ - 2Cl$). ^{1}H NMR ($CDCl_3$) δ 1.84–1.99 (2 H, m), 2.60–2.69 (2 H, m), 3.18–3.20 (2H, m), 6.06–6.21 (br, H_2N, ^2J(PtH) = 44.7 Hz), 7.20–7.53 (10 H, Ph); ^{31}P-{^{1}H} NMR ($CDCl_3$): δ −3.77 ^1J(PtP) 3287 Hz. ^{195}Pt-{^{1}H} NMR ($CDCl_3$): δ −4455 (t). Crystals suitable for X-ray structure determination were obtained by recrystallisation from CH_3NO_2 solution as **8**·H_2O·2CH_3NO_2.

[PtCl$_2$(Me$_2$NCH$_2$CH$_2$CH$_2$PPh$_2$-*P*)$_2$] 9. Yield 55%, mp 235 °C (dec.) (Found: C, 49.59; H, 5.27; N, 3.37. Calc. for $C_{34}H_{44}Cl_2N_2P_2Pt$: C, 49.39; H, 5.56; N, 3.38%). *m/z* (FAB MS): 773 (100%, $M^+ - Cl$). ^{1}H NMR ($CDCl_3$) δ 1.71–1.73 (2 H, m), 2.11 (6 H, s), 2.16–2.11 (2 H, m) 2.26–2.32 (2 H, m), 7.25–7.53 (10 H, Ph); ^{31}P-{^{1}H} NMR ($CDCl_3$): δ 8.18 ^1J(PtP) 3640 Hz. ^{195}Pt-{^{1}H} NMR ($CDCl_3$): δ −4408 (t) ^1J(PtP) 3642 Hz. Crystals suitable for X-ray structure determination were obtained by recrystallisation from a CH_2Cl_2–Et_2O mixture as **9**·CH_2Cl_2.

[PtCl(Me$_2$NCH$_2$CH$_2$CH$_2$PPh$_2$)$_2$]Cl 9b. To a solution of [$PtCl_2$(Me$_2$NCH$_2$CH$_2$CH$_2$PPh$_2$)$_2$] (0.1 g, 0.12 mmol) in $CHCl_3$ (20 ml) $AgBF_4$ (0.024 g, 0.12 mmol) was added and the reaction mixture stirred at room temperature for 10 minutes in the dark. The milky suspension was then filtered. To this solution Et_2O was added to initiate recrystallisation. Storage of the solution at 4 °C resulted in the formation of yellowish crystals of [PtCl(Me$_2$NCH$_2$CH$_2$CH$_2$PPh$_2$)$_2$]BF_4 in 95% yield. ^{31}P-{^{1}H} NMR ($CDCl_3$): δ 7.95 ^1J(PtP) 3761 Hz, 4.85 ^1J(PtP) 3199 Hz.

The preparation of palladium complexes

The palladium complexes were prepared in an analogous way to the platinum complexes.

[Pd(H$_2$NCH$_2$CH$_2$PPh$_2$)$_2$]Cl$_2$ 10. Yield 95%. Recrystallised from acetone–dichloromethane (Found: C, 49.05; H, 5.22; N, 4.07. Calc. for $C_{28}H_{32}Cl_2N_2P_2Pd\cdot3H_2O$: C, 48.76; H, 5.51; N, 4.06%). *m/z* (FAB MS): 599 (20% $M^+ - 2Cl$), 563 (100% $M^+ - Cl$). ^{1}H NMR ($CDCl_3$) δ ^{31}P-{^{1}H} NMR ($CDCl_3$): δ 55.80.

[Pd(H(Me)NCH$_2$CH$_2$PPh$_2$)$_2$]Cl$_2$·6H$_2$O 11. Yield 71%. (Found: C, 46.80; H, 5.20; N, 4.00. Calc. for $C_{30}H_{36}Cl_2N_2P_2Pd\cdot6H_2O$: C, 46.69; H, 5.96; N, 3.63%). ^{31}P-{^{1}H} NMR ($CDCl_3$): δ 52.55.

[Pd((c-C$_6$H$_{11}$)HNCH$_2$CH$_2$PPh$_2$)$_2$]Cl$_2$·H$_2$O 12. Yield 78%. Recrystallised from ether–dichloromethane (Found: C, 57.65; H, 6.68; N, 3.35. Calc. For $C_{40}H_{52}Cl_2N_2P_2Pd\cdot H_2O$: C, 57.48; H, 6.46; N, 3.35%). ^{31}P-{^{1}H} NMR ($CDCl_3$): δ 54.4 (br).

[Pd(H(Bz)NCH$_2$CH$_2$PPh$_2$)$_2$]Cl$_2$·HCl·2H$_2$O 13. Yield 46% (Found: C, 56.91; H, 5.62; N, 2.87. Calc. for $C_{42}H_{44}Cl_2N_2P_2Pd\cdot HCl\cdot2H_2O$: C, 56.78; H, 5.52; N, 3.15%). ^{31}P-{^{1}H} NMR ($CDCl_3$): δ 60.5, 22.5, ^2J(PP) 13 Hz.

[Pd(Me$_2$NCH$_2$CH$_2$PPh$_2$)$_2$]Cl$_2$ 14a. Yield 90%. Recrystallised from acetone–dichloromethane (Found: C, 53.76; H, 5.60; N, 4.04. Calc. For $C_{32}H_{40}Cl_2N_2P_2Pd\cdot H_2O$: C, 54.16; H, 5.92; N, 3.94%). ^{1}H NMR ($CDCl_3$) δ 1.71–1.73 (2 H, m), 2.11 (6 H, s), 2.16–2.11 (2 H, m) 2.26–2.32 (2 H, m), 7.25–7.53 (10 H, Ph); ^{31}P-{^{1}H} NMR ($CDCl_3$): δ 50.0 (broad, $\Delta\nu_{\frac{1}{2}}$ 186 Hz).

[PdCl(Me$_2$NCH$_2$CH$_2$PPh$_2$)$_2$]Cl 14b. To a solution of [Pd(Me$_2$NCH$_2$CH$_2$PPh$_2$)$_2$]Cl_2 (30 mmol), was added HNO_3 to lower the pH to *ca.* 2. After a few hours at ambient temperature, crystals of *cis*-[Pd(Me$_2$N(CH$_2$)$_2$PPh$_2$-*N*,*P*)Cl(Me$_2$NH(CH$_2$)$_2$PPh$_2$-*P*)$(NO_3)_2\cdot2H_2O$ formed which were suitable for X-ray structure determination. ^{31}P-{^{1}H} NMR (D_2O, pH* 4.5): δ 58.90, 23.55.

[Pd(Me(Bz)NCH$_2$CH$_2$PPh$_2$)$_2$]Cl$_2$·2HCl 15. Yield 83%. (Found: C, 53.07; H, 5.41; N, 3.00. Calc. for $C_{44}H_{48}Cl_2N_2P_2Pd\cdot2HCl$: C, 53.47; H, 5.06; N, 2.83%).^{31}P-{^{1}H} NMR (D_2O–EtOD-d_6): δ 14.60.

[Pd((Bz)$_2$NCH$_2$CH$_2$PPh$_2$)$_2$]Cl$_2$·2HCl 16. Yield 81% (Found: C, 62.02; H, 5.44; N, 2.44. Calc. for $C_{56}H_{56}Cl_2N_2P_2Pd\cdot2HCl$: C, 62.80; H, 5.42; N, 2.61%). ^{31}P-{^{1}H} NMR ($CDCl_3$): δ 13.5.

[Pd(H$_2$NCH$_2$CH$_2$CH$_2$PPh$_2$)$_2$]Cl$_2$ 17. Yield 70%. Recrystallised from acetone–dichloromethane (Found: C, 50.32; H, 5.77; N, 3.82. Calc. for $C_{30}H_{36}Cl_2N_2P_2Pd\cdot3H_2O$: C, 50.20; H, 5.85; N, 3.90%). *m/z* (FAB MS): 628 (28% $M^+ - Cl$), 591 (62% $M^+ - 2Cl$). ^{1}H NMR ($CDCl_3$) δ 1.7–1.8 (2 H, br, m), 2.5–2.66 (2 H, br, m) 3.14–3.16 (m, br), 5.62 (NH_2, br), 7.20–7.57 (10 H, m, Ph); ^{31}P-{^{1}H} NMR ($CDCl_3$): δ 20.0.

[PdCl$_2$(Me$_2$NCH$_2$CH$_2$CH$_2$PPh$_2$)] 18. Yield 88%. Recrystallised from acetone–dichloromethane (Found: C, 45.62; H, 4.94; N, 3.02. Calc. For $C_{17}H_{22}Cl_2NPPd$: C, 45.63; H, 4.91; N, 3.13%). *m/z* (FAB MS): 450 (10% M^+), 414 (21% $M^+ - Cl$) 376 (30% $M^+ - 2Cl$). ^{1}H NMR (CD_2Cl_2–DMF-d_7) δ 2.08 (2 H, m), 2.53 (2 H, m) 2.98 (2H, s), 3.43 (6 H, s), 7.52–7.63 (10 H, m, Ph); ^{31}P-{^{1}H} NMR (CD_2Cl_2–DMF-d_7): δ 16.76.

Results and discussion

Preparation and properties of ligands

A number of methods have been reported for the preparation of aminophosphine ligands.[4–7,22] In the present work, the most convenient starting materials were aminoalcohols, a large number of which are either available commercially or can be prepared by the reduction of amino acids.[22–28] The aminoalcohol, H(Me)NCH$_2$CH$_2$OH was prepared as shown in Scheme 2a. Chlorination of the aminoalcohol followed by reaction with the diphenylphosphine anion afforded the required ligand (Scheme 2b). The ligands were obtained as viscous oils except for Bz(R)NCH$_2$CH$_2$PPh$_2$ (R = H, Me or Bz), which were obtained as the hydrochloride salts. The oily ligands were readily purified by passing solutions in ether through a short alumina column and the salts were recrystallised from methanol–ether. The ^{1}H NMR spectra of the ligands in $CDCl_3$ showed the expected peaks with the backbone CH_2 appearing as triplets and the NH_2 as broad peaks in the region of 1–2 ppm. The ^{31}P NMR spectra showed single resonances in the region of −19 to −21 ppm.

Synthesis and characterisation of Pt(II) and Pd(II) complexes

The Pt(II) and Pd(II) complexes were characterised by FAB mass spectrometry, ^{1}H, ^{31}P, ^{195}Pt, ^{13}C NMR and IR spectroscopies, and elemental analysis. X-Ray crystal structures were obtained for complexes **1**, **2**, **8**, **9**, **14b** and **18** (see Table 2 for definitions of complexes). The ^{31}P NMR spectra showed coordination shifts ranging from 65 ppm to 18 ppm downfield for

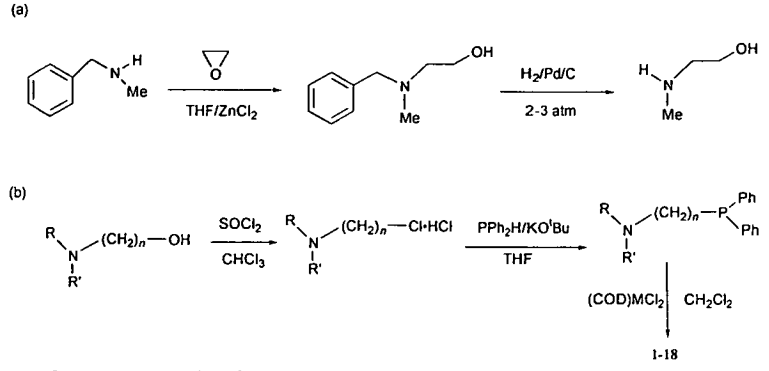

Scheme 2 Preparation of (a) $H(Me)NCH_2CH_2OH$ and (b) aminophosphines and complexes.

Table 2 Complexes prepared in this work. All have a 2:1 ligand-to-metal ratio except **18** (1:1). See Scheme 1 for different coordination modes adopted by the complexes

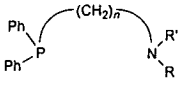

Complex number		Substituents		
M = Pt	M = Pd	R	R′	Linker *n*
1[a]	**10**	H	H	2
2[a]	**11**	H	Me	2
3	**12**	H	c-C_6H_{11}	2
4	**13**	H	Bz	2
5a[b]	**14a**	Me	Me	2
5b	**14b**[a,c]			
6	**15**	Me	Bz	2
7	**16**	Bz	Bz	3
8[a]	**17**	H	H	3
9[a]				
9b[b]	**18**[a]	Me	Me	3

[a] X-Ray structure determined. [b] Prepared by reacting **5b** with $AgNO_3$ or **9** with $AgBF_4$ and subsequent removal of AgCl. [c] Prepared by lowering the pH to <4.

^{31}P in 5- and 6-membered chelate rings, respectively. Such low-field shifts upon chelation are common for complexes of Pt(II) and Pd(II) phosphines.[29] In the FAB MS spectra, the base peaks were usually [molecular ion − Cl] which has also been found to be the case for similar complexes.[30] The expected isotopic patterns for platinum were also found. The ^{13}C NMR spectra were generally very broad and peaks in the aromatic region were difficult to assign. Remarkably, most of the complexes were generally soluble in water as well as in common organic solvents.

Complex **1**, *cis*-$[Pt(H_2N(CH_2)_2PPh_2\text{-}P,N)_2]Cl_2$, is a water-soluble white solid which decomposes upon heating at about 250 °C. The FAB MS spectrum had a base peak of 652 (M^+ − 2Cl) with the expected isotopic pattern for platinum. The ^1H NMR spectrum in $CDCl_3$ indicated that the resonances of the CH_2 groups were broad multiplets and the NH_2 peak was at δ 7.25 with a ^2J(PtH) of 42 Hz. This is a large downfield shift from the free ligand at δ 1.51 indicative of N coordination and the formation of 5-membered chelate rings. The ^{31}P NMR spectrum (Table 3) showed a single peak at δ 33.7 (P_A, for atom labelling see Scheme 3) with a co-ordination shift of 55 ppm, consistent with the formation of a bis-chelated complex.[29] The coupling constant $^1J(PtP_A)$, of 3300 Hz is typical of ^{31}P *trans* to nitrogen.[31-33] The ^{195}Pt NMR spectrum also showed a triplet at δ −4589 confirming the bis-chelated nature of the complex. The

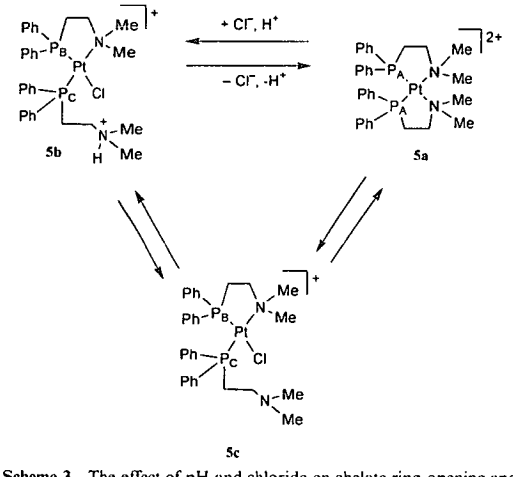

Scheme 3 The effect of pH and chloride on chelate ring-opening and closure in 5.

^1H and ^{31}P NMR spectra in D_2O were similar to those from $CDCl_3$ solutions. The Pd analogue, **10**, *cis*-$[Pd(H_2NCH_2CH_2PPh_2\text{-}P,N)_2]Cl_2$, was also shown by ^{31}P NMR to exist in a ring-closed form in both $CDCl_3$ and D_2O, and, as for the Pt analogue, it remained ring-closed even under highly acidic conditions (pH < 2).

The FAB MS spectrum of **5b** had a base peak at 745 (M^+ − Cl). The elemental analysis showed that the complex was isolated as the hydrochloride salt suggesting that one of the amino groups is protonated and thus the complex exists in a ring-opened form (*cis*-$[Pt(Me_2N(CH_2)_2PPh_2\text{-}N,P)Cl(Me_2NH(CH_2)_2PPh_2\text{-}P)]Cl_2$) in the solid state. The ^{31}P NMR spectrum in $CDCl_3$ (Table 3) showed two resonances: a peak at δ 36.5 assignable to P in a P,N chelate ring (P_B) and at δ −0.46 assignable to P in a P-bound ring-opened ligand (P_C) (for atom labelling see Scheme 1). The respective ^1J(PtP) couplings were 3691 and 3187 Hz, which are values typical of P *trans* to Cl and N, respectively.[31-33] The corresponding co-ordination shifts were 55 ppm for P_B and 19 ppm for P_C. The peaks were relatively broad and did not show any doublet splitting due to $^2J(P_BP_C)$. The ^{31}P NMR data thus show that the ring-opened species is also the preferred form of the complex in solution ($CDCl_3$). The inequivalence of the two phosphorus atoms was also confirmed from the ^{195}Pt NMR spectrum, which showed a doublet of doublets centred at δ −4505. The ^1H NMR spectrum in $CDCl_3$ showed the expected peaks, albeit very broad ones. The broadening may arise from an exchange process involving chelate ring-closing and opening. This was even more

Table 3 ^{31}P NMR data for complexes **1–18** and pK values for ring-opening determined from pH* titrations

Complex	Chemical shifts[a] (^1J(PtP)/Hz) $\delta(P_A)$	$\delta(P_B)$	$\delta(P_C)$	$\delta(P_D)$	pH*	pK
1[c]	33.7(3300)	—	—	—	—	<1
2[c]	28.9(3300)	—	—	—	3.85	2.1
	—	41.1(3770)	1.9(3300)	—	<2	
3[d]	—	38.89(3783)	0.5(3239)	—	4	6.3
3	36.45(3294)	—	—	—	—	—
4	30.3(3420)	40.0(3880)	5.0(3348)	—	—	—
5b	—	36.5(3691)	−0.46(3187)	—	—	—
5b[c]	25.25(3294)	36. 5(3792)	−0.06(3128)	—	8.6	6.9
	—	36.5(3792)	−0.06(3128)	—	5.0	
5a[c]	25.5(3225)	—	—	—	8.6	*ca.* 2
	—	25.3(4008)[b]	−1.96(3298)	—	2.0	
6	—	30.7(3754)	−0.06(3184)	—	—	—
7	—	—	—	4.50(3635)	—	—
8[c]	−1.88(3199)	—	—	—	6.5	2.9
	—	0.55(3625)	4.24(3272)	—	1	
8	−3.77(3287)	—	—	—	—	—
9	—	—	—	8.18(3640)	—	—
9b	—	7.95(3761)	4.85(3199)	—	—	—
10	55.50	—	—	—	—	—
11	52.55	—	—	—	—	—
12	54.44	—	—	—	—	—
13	—	60.5	22.5	—	—	—
14a	50.0	—	—	—	—	—
14b[c]	50.48	—	—	—	8.6	6.0
	—	58.9	23.55	—	4.5	
15[d]	—	—	—	14.6	—	—
16	—	—	—	13.5	—	—
17	20.0	—	—	—	—	—
18[e]	16.76	—	—	—	—	—

[a] See Scheme 1 for atom labelling. (P_A = P in bis chelate, *trans* to N; P_B = P in P,N chelate-ring, *trans* to Cl; P_C = P in P-bound, ring-opened ligand, *trans* to N; P_D = P in P-bound ring-opened ligand, *trans* to Cl). Solvent $CDCl_3$ unless otherwise stated.[b] *trans* to OH_2. [c] D_2O. [d] D_2O–EtOD-d_6. [e] CD_2Cl_2–DMF-d_7.

evident in the ^{13}C NMR spectrum, in which the ethylene carbons were so broad that they were difficult to observe.

The ^{31}P NMR spectrum of **6** in $CDCl_3$ showed that it exists exclusively as a mono-ring-opened species, *cis*-[Pt(Bz(Me)N-$(CH_2)_2PPh_2$-*N*,*P*)Cl(Bz(Me)N$(CH_2)_2PPh_2$-*P*)]Cl. In contrast to **5b**, the peaks were sharp doublets: doublets at δ 30.7 (P_B) and −0.06 (P_C) with the corresponding ^1J(PtP) values of 3754 and 3184 Hz, respectively. The doublet splitting can be assigned to a $^2J(P_BP_C)$ coupling of 17 Hz. The sharpening of the peaks suggest the absence of an exchange process involving chelate ring-closing and -opening under these conditions.

Complex **5b** dissolves readily in water. The ^{31}P NMR spectrum of the solution in D_2O (Fig. 1a, pH* 8.56), in contrast to the spectrum recorded in $CDCl_3$, showed two sets of peaks. There was a broad singlet at δ 25.25 (P_A) with a $^1J(PtP_A)$ value of 3294 Hz, assignable to a bis-chelated (ring-closed) form of the complex, and singlets at δ 36.5 (P_B) and −0.06 (P_C) with ^1J(PtP) couplings of 3792 and 3128 Hz, respectively, assignable to the ring-opened form. The ratio of ring-closed to ring-opened species was 2:1. The ^{195}Pt NMR spectrum showed a doublet of doublets centred at δ −4505 for the ring-opened species, with splitting due to two inequivalent P atoms, and a triplet centred at δ −4653 corresponding to the bis-chelated species. Thus in aqueous solution the two forms of the complex exist in equilibrium. The position of the equilibrium was found to be dependent upon pH and chloride concentration, and is further discussed in the next section.

The ^{31}P NMR spectrum of the palladium analogue, **14a**, *cis*-$[Pd(Me_2N(CH_2)_2Ph_2$-*P*,*N*)$_2]Cl_2$, in $CDCl_3$ showed a single peak at δ 50.0 (P_A) with a co-ordination shift of 70 ppm. The peak was broad with a width at half height ($\Delta\nu_{1/2}$) of 186 Hz. The spectrum of **14a** recorded in D_2O (pH, 8.6), showed a very broad single peak at δ 50.5 ($\Delta\nu_{1/2}$ 1656 Hz). The broadening suggested that exchange between the ring-opened and ring-closed species was occurring. It was, however, possible to isolate

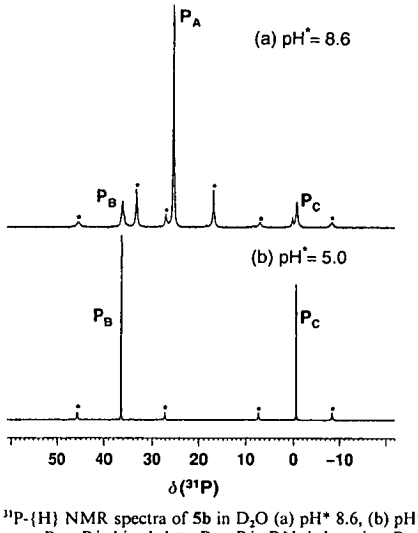

Fig. 1 ^{31}P-{H} NMR spectra of **5b** in D_2O (a) pH* 8.6, (b) pH* 5.0. Assignments: P_A = P in bis-chelate; P_B = P in P,N chelate-ring, P_C = P in P-bound, ring-opened ligand (see Scheme 3). * = ^{195}Pt satellites.

the ring-opened form of the complex (**14b**) at low pH (*ca.* 4). The X-ray crystal structure of the ring-opened species and the pH dependence of the chelate ring-opening and -closing processes are discussed further below.

Complex **2** was prepared as shown in Scheme 1 and was isolated as the hydrogen dichloride salt: *cis*-[Pt(Me(H)N-$(CH_2)_2PPh_2$-*P*,*N*)$_2$]·$[HCl_2]_2$. The ^{31}P NMR spectrum in D_2O (pH* 3.85) showed a peak at δ 28.9 (P_A) with $^1J(PtP_A)$ coup-

lings of 3300 Hz. Complex **2** exists as a ring-closed, bis-chelated complex above pH* 3. The ^{31}P NMR spectrum of **3**, [PtCl-((c-C_6H_{11})$HN(CH_2)_2PPh_2)_2$]Cl, in $CDCl_3$ showed a broad single peak at δ 36.45 (P_A) with the $^1J(PtP_A)$ value of 3294 Hz. The ^{195}Pt NMR spectrum showed a triplet centred at δ −4538. There was also a minor product (*ca.* 5%) which was isolated by fractional recrystallization from chloroform and shown to be the mono-chelate complex, *cis*-[Pt(c-C_6H_{11})$HN(CH_2)_2PPh_2$-*N*,*P*)Cl_2], by elemental analysis. The ^{31}P NMR spectrum showed a peak at δ 24.8 with a $^1J(PtP)$ value of 4064 Hz, consistent with the formation of a monochelate. The ^{31}P NMR spectrum of the palladium analogue, [Pd(c-C_6H_{11})$HN(CH_2)_2$-$PPh_2)_2Cl_2$], **12**, was recorded in different solvents. In D_2O–ethanol the singlet peak was sharp at δ 52.7 (P_A) accompanied by two minor broad peaks at δ 63.0 (P_B) and 22.0 (P_C), whereas in $CDCl_3$ the peak at δ 54.4 (P_A) was very broad, and, in addition, there were two minor peaks at δ 57.6 (P_B) and 33.7(P_C). In both cases the ring-closed form is the major species and the minor peaks correspond to the ring-opened form. Similarly, in CD_2Cl_2, the broad peak at δ 57.9 (P_A) was accompanied by two broad minor peaks centred at δ 63.5 (P_B) and 22.8 (P_C) possibly as a result of traces of HCl in the solvent.

The ^{31}P NMR spectrum of **4** in $CDCl_3$, showed that there were two sets of peaks assignable to the chelate ring-opened complex *cis*-[Pt(BzHN$(CH_2)_2PPh_2$-*N*,*P*)Cl(BzHN$(CH_2)_2$-PPh_2-*P*)]Cl and ring closed complex *cis*-[Pt(BzHN$(CH_2)_2$-PPh_2-*N*,*P*)$_2$]Cl_2. In contrast, the ^{31}P NMR spectrum of **7**, *cis*-[Pt($Bz_2N(CH_2)_2PPh_2)_2$-*P*)$_2Cl_2$], showed a single peak at δ 4.5 (P_D) with $^1J(PtP_D)$ value of 3635 Hz, suggesting that it exists as a di-ring-opened complex co-ordinated through phosphorus only.

The ^1H NMR spectrum of *cis*-[Pt($H_2N(CH_2)_3PPh_2$-*P*,*N*)$_2$]-Cl_2, **8**, in $CDCl_3$ showed that the NH_2 peaks had shifted from δ 1.38 for the free ligand to δ 6.14 ($^2J(PtH) = 44.7$ Hz), a shift of 4.72 ppm downfield upon coordination. The ^{31}P NMR spectrum also showed a single peak at δ −3.77 (P_A), with a $^1J(PtP_A)$ value of 3287 Hz, showing that **8** was isolated as a bis-chelated complex. However the ^{31}P NMR spectrum of a solution in D_2O–ethanol showed the expected peaks at δ −3.8 (P_A) with $^1J(PtP_A)$ value of 3336 Hz, which corresponds to the ring-closed form. The ^{195}Pt NMR spectrum of the same sample showed a triplet centred at δ −4455 (P_A) with $^1J(PtP_A)$ value of 3330 Hz. The FAB MS spectrum for *cis*-[Pt($Me_2N(CH_2)_3PPh_2$-$P)_2Cl_2$], **9**, showed a base peak at 773 for [molecular ion − Cl]. The ^{31}P NMR spectrum in $CDCl_3$ showed a single peak at δ 8.18 (P_D) with $^1J(PtP_D)$ value of 3640 Hz. Thus the above data show that **9** exists as a di-ring-opened complex. When the complex was reacted with two molar equivalents of $AgBF_4$, it was possible to isolate the mono-chelated (ring-opened) species (**9b**). The ^{31}P NMR spectrum in $CDCl_3$ showed a singlet at δ 7.95 (P_B) with a $^1J(PtP_B)$ value of 3761 Hz and a singlet at δ 4.85 (P_C), with a $^1J(PtP_C)$ value of 3199 Hz.

When two molar equivalents of $Me_2N(CH_2)_3PPh_2$ were reacted with one molar equivalent of (COD)$PdCl_2$ in the usual manner, the only product which could be isolated was the mono-chelated dichloro complex [Pd($Me_2N(CH_2)_3PPh_2$-*P*,*N*)Cl_2], **18**, even when a large excess of the ligand was used. The structure of the product was confirmed by X-ray analysis and the FAB MS spectrum showed a base peak at *m*/*z* 450 which corresponds to the molecular ion.

This series of complexes clearly demonstrates how the steric nature of the substituents on nitrogen as well as the length of the methylene backbone (P–N linker) can determine whether the complex exists in ring-opened or closed forms. Complexes **1** and **10**, which contain only hydrogen substituents on N, exist as ring-closed forms in both $CDCl_3$ and D_2O. As the hydrogen is replaced progressively by more sterically demanding substituents for example in **5b**, in which H is replaced by CH_3, the mono-chelate ring-opened species is favoured in chloroform and an equilibrium exists between the ring-closed and -opened forms in aqueous solution (Fig. 2). In complex **2**, where the substituent on N has a steric bulk between that of **1** and **5b**, it was possible to open the chelate ring only under acidic conditions. In complex **7**, where N has two benzyl substituents, the ligand was co-ordinated *via* the phosphorus atoms only. When the number of methylene carbon atoms in the backbone of the ligand is increased from two to three, together with an increase in the steric bulk on nitrogen, as in **9**, the di-ring-opened species is formed preferentially, chelation being achieved only in the absence of chloride. This illustrates the relatively weak nature of the platinum–nitrogen interaction within the 6-membered chelate rings.

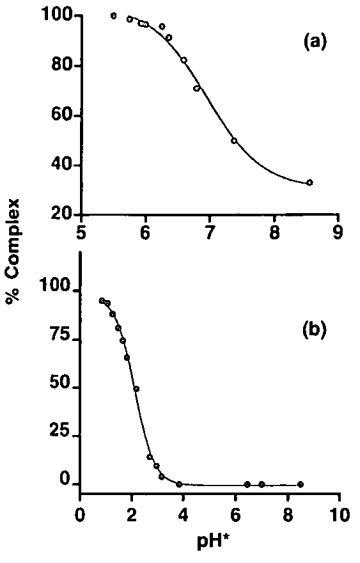

Fig. 2 Plots of the relative amounts of ring-opened complex determined from ^{31}P NMR peak areas *versus* pH*. (a) Complex **5b**. (b) Complex **2**. The curves correspond to computer best fits and p*K* values of 6.9 and 2.1, respectively.

Chelate ring-opening and -closing of complexes in aqueous solution

The equilibrium between the chelate ring-opened and closed forms in aqueous solution as a function of pH and chloride concentration was studied by ^{31}P NMR spectroscopy. The complexes were titrated over a wide pH* range (*ca.* 3–11). For complexes **2**, **3**, **5b**, **8** and **14a**, the p*K* values were determined from computer best fits of plots of the relative amounts of the ring-opened and ring-closed species, as determined by the integration of ^{31}P NMR peaks, *versus* pH* (see Fig. 2). Chelate ring-opening is induced by protonation of amino groups.

The ^{31}P NMR data for complex **5b** in aqueous solution suggest that an equilibrium exists between the ring-opened, **5b**, and ring-closed, **5a**, complexes which is dependent upon pH* and chloride concentrations (Scheme 3). A solution of **5b** (20 mM) in D_2O was titrated over the pH* range 2–11. Under acidic conditions, the amount of ring-opened species, **5b**, increased such that by *ca.* pH* 5.5 it was the only product present. The ^{31}P NMR spectrum at pH* 5 (Fig. 1b) thus shows only one set of doublets, and the peaks were considerably sharper than at higher pH* due to the absence of exchange. The doublet splitting can be assigned to $^2J(P_AP_C)$ coupling of 18 Hz. The reaction was reversible. When the pH* was reversed, a ^{31}P NMR spectrum identical to the original one was obtained. A plot of the relative amounts of the ring-opened and ring-closed species *versus* pH*, is shown in Fig. 2a, and was fitted to a p*K* value of 6.9. Therefore at neutral pH*, the two species exist in

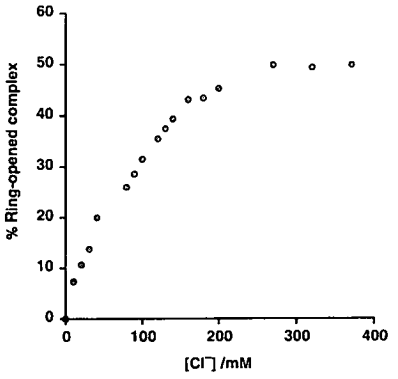

Fig. 3 Dependence of the amount of ring-opened complex **5c** on the concentration of NaCl added to complex **5a**, *cis*-$[Pt(Me_2N(CH_2)_2PPh_2\text{-}P,N)_2](NO_3)_2$ (40 mM, pH* 8.6), as determined from ^{31}P NMR peak areas.

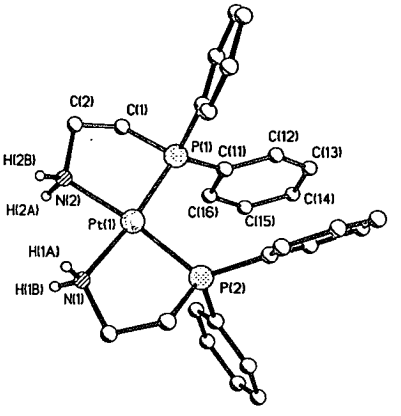

Fig. 4 Crystal structure of the ring-closed complex *cis*-$[Pt(H_2N(CH_2)_2PPh_2\text{-}P,N)_2]^{2+}$, **1**, and numbering scheme.

almost equal amounts. There was no evidence for the opening of the second chelate ring even at very low pH* (1).

When **5b** was reacted with $AgNO_3$, the isolated product was the ring-closed bis-chelate complex, **5a**. In this case, in the absence of chloride, when the pH* was lowered by the addition of DNO_3, it was possible to observe chelate-ring-opening only below pH* 2. The ^{31}P NMR spectrum at pH* 2 showed a singlet at δ 25.5 (P_A) with a $^1J(PtP_A)$ coupling of 3225 Hz, corresponding to the ring-closed species **5a** and a set of peaks assignable to the ring-opened species *cis*-$[Pt(Me_2N(CH_2)_2PPh_2\text{-}N,P)(OH_2)(Me_2N(CH_2)_2PPh_2\text{-}P)]ONO_2$ (singlet δ 25.3 (P_B) and at δ −1.96 (P_C), for atom labelling see Scheme 3). The $^1J(PtP)$ couplings were 4008 and 3298 Hz which are within the range for phosphorus *trans* to O and N, respectively.[31-33]

A titration of **5a** with chloride ions (added as NaCl) was studied at pH* 8.6 (Fig. 3) in order to determine the chloride association constant K_c by measuring the relative intensities of peaks for the ring-opened and ring-closed species in the ^{31}P NMR spectra. A pH* much higher than the p*K* value was chosen so that protonation of the amino group did not influence the position of the equilibrium. The amount of **5c** increased steadily with chloride addition (Fig. 3) and at about 150 mM chloride about 40% of **5c** was present. In a separate experiment, 320 mM chloride was added to a sample containing 20 mM of **5a** which resulted in the formation of a precipitate. The solid and supernatant were separated by centrifugation. The ^{31}P NMR of the supernatant showed that ring-opened and ring-closed species were present in about equal amounts. The ^{31}P NMR spectrum of the precipitate redissolved in D_2O was identical to that of **5a**, (see above) with 80% of the amount present corresponding to the ring-closed form. From the data obtained from a titration of 40 mM **5a** with up to 180 mM chloride an association constant of 4.95 M^{-1} was obtained for chloride binding to **5a**, at pH* 8.6 ($K_c = [\mathbf{5c}]/([\mathbf{5a}][Cl^-]_f$); $[Cl^-]_f$ = free chloride.). Thus chelate ring-opening and -closing can be controlled as a function of both pH* and chloride concentration.

When the pH* of **14a** was measured immediately after dissolving the complex in D_2O, it was found to be alkaline (pH* 8.6). When the pH* was lowered to 5 one of the chelate rings opened to give *cis*-$[Pd(Me_2N(CH_2)_2PPh_2\text{-}N,P)Cl(Me_2NH(CH_2)_2PPh_2\text{-}P)]^{2+}$, **14b**, as seen by the appearance of two sharp peaks at δ 58.9 (P_B) and 23.55 (P_C). A solution of **14a** in D_2O was titrated over the pH* range of 2–9 and afforded a p*K* value of 6.0.

The ^{31}P NMR spectrum of complex **2** at pH* 1.2 showed doublets at δ 41.1 (P_A) and δ 1.9 (P_C) with $^1J(PtP)$ couplings of 3770 and 3300 Hz, respectively. The doublet spitting can be assigned to $^2J(P_AP_C)$ coupling of 18 Hz. A pH* titration of the complex (20 mM) showed that the chelate ring is opened below pH* 3 and afforded a p*K* value of 2.1 (Fig. 2b).

Complex **3** was sparingly soluble in water, however the ^{31}P NMR spectrum in D_2O–ethanol showed the presence of both the ring-opened and closed forms and a pH* titration of a 20 mM solution of **3** afforded a p*K* value of 6.3 uncorrected for the presence of EtOH. As for complex **14**, the switch from ring-opened to ring-closed forms occurred within a narrow pH* range (*ca.* 1), suggesting that protonation of the amino group and chloride binding are co-operative.

When the pH* of the aqueous solution of **12**, $[Pd((c\text{-}C_6H_{11})HN(CH_2)_2PPh_2\text{-}N,P)_2]Cl_2$ was lowered, one of the chelate rings opened as seen by the appearance of two ^{31}P NMR doublets at δ 62.9 (P_B) and 29.9 (P_C). These peaks were relatively sharp with a $^2J(P_BP_C)$ coupling of 12 Hz. A pH* titration of the complex (20 mM) afforded a p*K* value of 6.0. Above pH* 7 only the ring-closed form was observed, whereas below pH* 5 only the ring-opened form was present.

A gradual opening of the chelate ring was observed when the pH* of a solution of **8**, $[Pt(H_2N(CH_2)_3PPh_2\text{-}N,P)_2]Cl_2$ in D_2O was lowered, in contrast to the 5-membered ring analogue, **1**, which remained ring-closed. The ^{31}P NMR resonance for **8** (δ 1.88) began to disappear below pH* 6, and was replaced by doublets with δ 0.55 (P_B) and 4.24 (P_C) and corresponding $^1J(PtP)$ couplings of 3625 and 3272 Hz, respectively, and $^2J(P_BP_C)$ of 17 Hz. A pH* titration of the complex (20 mM) afforded a p*K* value of 2.9.

The above data show that it was not possible to achieve chelate ring-opening for the 5-membered ring complexes **1** and **10** even at very low pH conditions. On the other hand it was possible to ring-open the 6-membered, chelate ring analogue, **8**, at very low pH. The replacement of one of Me substituents on N in **5b** by H as in **2** resulted in a dramatic drop in the p*K* value: from 6.9 for **5b** to 2.12 for **2** (Fig. 2). This highlights the highly acidic conditions required to ring-open complexes with low steric requirements for the substituents on N in these aminophosphine complexes and the greater stability of 5-membered as opposed to a 6-membered chelate rings.

Crystallography

The X-ray crystal structures of **1**, **2**, **8**, **9**, **14b** and **18** were determined and are shown as SHELXTL[20] plots in Figs. 4–9. Data collection and refinement parameters, bond distances and angles are listed in Tables 1 and 4, respectively. The complexes have square-planar co-ordination geometry with varying degrees of distortion. In complexes **1**, **2**, **8**, **9** and **14b**, the two phosphino groups have a *cis* arrangement.

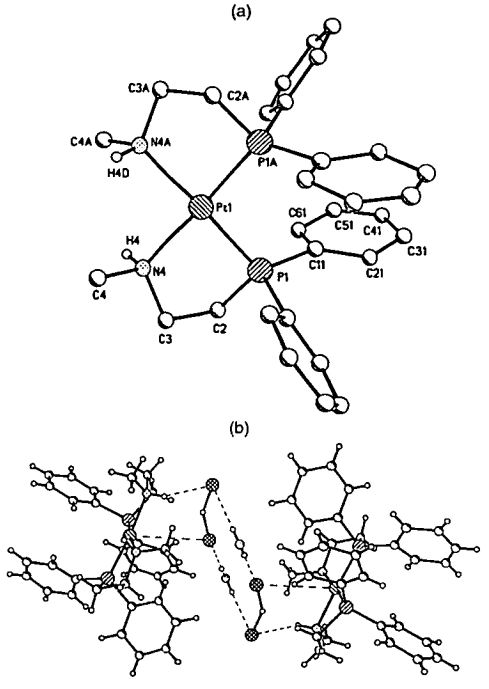

Fig. 5 (a) Crystal structure of the ring-closed complex *cis*-$[Pt(Me(H)N(CH_2)_2PPh_2\text{-}P,N)_2]^{2+}$, **2**, with the numbering scheme. (b) In the unit cell one $[Cl\text{-}H\text{-}Cl]^-$ is associated with each complex ion. The Cl–H and H–Cl distances are 1.631 and 1.610 Å, respectively. The two anions are connected *via* a water molecule with a Cl···H distance of 2.359 Å. One of the *ortho* H atoms of the phenyl rings is also H-bonded (Cl···H = 2.359 Å).

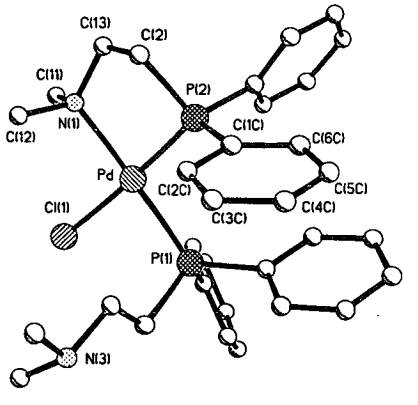

Fig. 6 Crystal structure of the ring-opened complex *cis*-$[Pd(Me_2N(CH_2)_2PPh_2\text{-}N,P)Cl(Me_2NH(CH_2)_2PPh_2\text{-}P)]^{2+}$, **14b**, with the numbering scheme.

In **1**, *cis*-$[Pt(H_2N(CH_2)_2PPh_2\text{-}N,P)_2]Cl_2$, the square-plane formed by N(1), N(2), P(1) and P(2), shows a slight deviation from planarity (Fig. 4). If we consider N(1)–Pt–P(2) be in one plane, then P(1) is out of plane by +0.052 Å and N(2) by −0.054 Å in the opposite direction. The P(1)–Pt–P(2) angle 102.98° is rather large for a square-planar complex. The steric crowding around the phosphorus atoms due to the presence of the phenyl rings, appears to cause the opening up of the angle, which presumably also results in the reduction of the other angles to below 90°, but within the range for five-membered

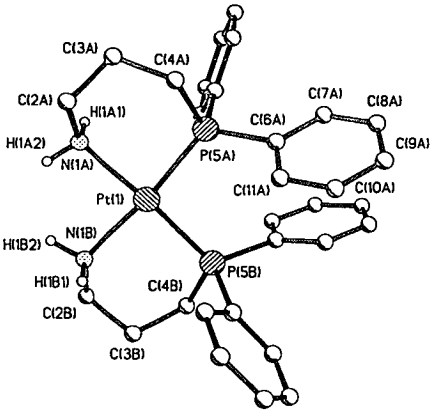

Fig. 7 Crystal structure of the ring-closed complex, *cis*-$[Pt(H_2N(CH_2)_3PPh_2\text{-}N,P)_2]^{2+}$, **8**, with the numbering scheme.

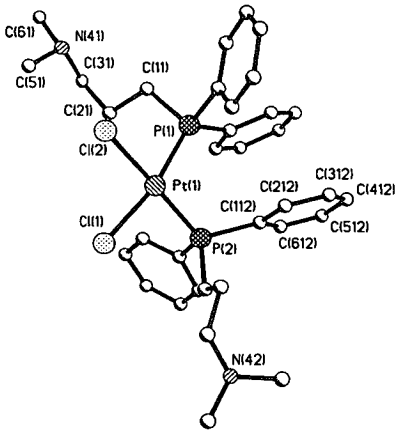

Fig. 8 Crystal structure of the di-ring-opened complex, *cis*-$[Pt(Me_2N(CH_2)_3PPh_2\text{-}P)_2Cl_2]$, **9**, with the numbering scheme.

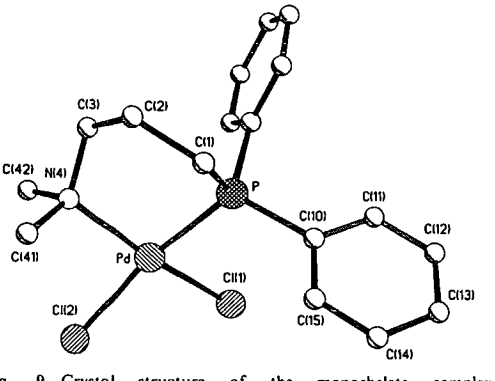

Fig. 9 Crystal structure of the monochelate complex, $[Pd(Me_2N(CH_2)_3PPh_2\text{-}P,N)Cl_2]$, **18**, with the numbering scheme. The bond angles of the alkyl chain deviate from ideality: (N(4)–C(3)–C(2) = 116.6(4), C(2)–C(1)–P(1) = 114.4(3) and C(3)–C(2)–C(1) = 117.2(4)°.

chelate rings.[34] The *trans* angles N(1)–Pt–P(1) and N(2)–Pt–P(2) of 173.1(2) and 172.1(2)°, respectively, also show slight distortions from the ideal value. The Pt–N distances are relatively long (2.090 Å) compared with the literature values,[34]

Table 4 Summary of selected bond lengths [Å] and angles [°] for complexes **1**, **2**, **8**, **9**, **14b** and **18** with estimated standard deviations (e.s.d.s) in parentheses

	1 M = Pt	**2** M = Pt	**8** M = Pt	**9** M = Pt	**14b** M = Pd	**18** M = Pd
Bond lengths						
M–P	2.235(2)	2.34(2)	2.2543(11)	2.247(2)	2.2800(13)[a]	2.224(11)
	2.239(2)	2.34(2)	2.2565(11)	2.251(2)	2.2438(12)[b]	
M–N	2.090(6)	2.148(8)	2.116(3)		2.172(4)	2.1299(3)
	2.111(5)	2.148(8)	2.129(3)			
M–Cl				2.354(3)	2.3721(13)	2.3817(14)[c]
				2.361(2)		2.292(12)[b]
trans angles						
P–M–N	173.1(2)	173.9(2)	171.67(10)			
	172.1(2)	173.9(2)	171.43(10)		176.49(5)	
P–M–Cl				173.61(9)	173.68(5)	167.81(4)
				169.84(9)		
N–M–Cl						170.15(10)
cis angles						
P–M–P	102.98(6)	99.33(13)	98.16(4)	99.76(9)	98.57(11)	
P–M–N	83.8(2)	84.0(2)	89.60(10)		84.63(12)	92.42(10)
	84.8(2)	84.0(2)	86.69(10)			
N–M–N	88.4(2)	93.2(4)	86.04(13)			
P–M–Cl				83.84(9)		87.68(5)
				89.12(9)	85.37(5)	
Cl–M–Cl				87.78(9)		90.66(5)
N–M–Cl					91.32(12)	91.26(10)

[a] *trans* to Cl. [b] *trans* to N. [c] *trans* to P.

Table 5 Comparison of [Cl–H–Cl]$^-$ parameters

Species	Cl···Cl/Å	Cl–H–Cl/°	Method	Ref.
[Cl–H–Cl]$^-$	3.100	180	Calcd.	36
[Cl–H–Cl]$^-$	3.147	180	Exptl.	37
cis-[Pt(Me(H)N(CH$_2$)$_2$PPh$_2$)$_2$][Cl–H–Cl]$_2$·0.5H$_2$O (**2**, Fig. 5)	3.2051	152.4	X-ray	[a]
[K(18-crown-6)][Cl–H–Cl]	3.117(1)		X-ray	38
[Mg(18-crown-6)][Cl–H–Cl]$_2$	3.286(1)	161	X-ray	38
	3.331(1)	173		
[(4-MeOC$_6$H$_4$)(Me)PCl$_2$][Cl–H–Cl]	3.210(3)	172	X-ray	39
[NMe$_4$][Cl–H–Cl]	3.22	180		40
[H$_3$O(18-crown-6)][Cl–H–Cl]	3.11(1)	168	X-ray	41

[a] This work.

but not unprecedented.[3] These distances provide evidence for weakening of the Pt–N bond, due to the strong *trans* influence of the tertiary phosphine. The P–Pt bond distances of 2.235 and 2.239 Å are within the expected range.[34]

The X-ray analysis of **2**, showed that the complex has crystallographic C_2 symmetry and one of the phenyl rings is disordered (Fig. 5a). It was formulated as *cis*-[Pt(Me(H)N(CH$_2$)$_2$PPh$_2$)$_2$][Cl–H–Cl]$_2$·0.5H$_2$O. One [Cl–H–Cl]$^-$ anion is associated with each molecule in the unit cell. The Cl–H and H–Cl distances are 1.630 and 1.610 Å, respectively, with Cl–H–Cl of 152.4°. The [Cl–H–Cl]$^-$ anion appears to be involved in a network of H-bonding with each molecule in the unit cell, and in turn the two anions are connected *via* a water molecule, for which the Cl···H distance is 2.359 Å. The [Cl–H–Cl]$^-$ anion is also H-bonded to one of the *ortho* H atoms of one of the phenyl rings. (Cl···H = 2.359 Å) (Fig. 5b). The anion [Cl–H–Cl]$^-$ was first observed in 1909 in the reaction HNR$_3$Cl + HCl, which resulted in the formation of [HNR$_3$][Cl–H–Cl].[35] The structure of [Cl–H–Cl]$^-$ has been determined using semi-empirical and *ab initio* methods[36] as well as experimentally,[37] and its X-ray structure has been determined in several salts.[38–41] The parameters for [Cl–H–Cl]$^-$ are compared with literature values in Table 5. The platinum atom has a slightly distorted square-planar co-ordination. If we consider the N(4A)–Pt–P(1a) to be in one plane, N(4) is out of plane by +0.202 Å and P(1) by −0.197 Å in the opposite direction. The Pt–N bond distances of 2.148(8) Å are also longer than that observed for **1** which can be attributed to an increase in steric hindrance at N in **2** compared to **1**. The Pt–P distances, both 2.34 Å, are again longer than for the other complexes in this series. The P(1)–Pt–P(2) angles of 99.33° are larger and comparable to **1**. The P–Pt–N angles of 84.0° are also low, presumably related to the large angle of P(1)–Pt–P(2). The *trans* angles N(1)–Pt–P(1) and N(2)–Pt–P(2), both 173.9(2)°, also show distortions from the ideal value.

The X-ray crystal structure for complex **8**, *cis*-[Pt(H$_2$N(CH$_2$)$_3$PPh$_2$-*N*,*P*)$_2$]Cl$_2$·H$_2$O·2CH$_3$NO$_2$ (Fig. 7) shows many similarities to that of complex **1** (Fig. 4). Again the square-planar geometry shows slight deviations from ideal planarity. The P(5A)–Pt–P(5B) angle is increased to 98.16°, due to the steric bulk of the phenyl groups, with corresponding reduction of the other angles around the platinum. The *trans* angles P(5A)–Pt–N(1B) and P(5B)–Pt–N(1A) are 171.43° and 171.67°, respectively, showing slight distortion. The Pt–N bond lengths are further increased to 2.12 and 2.13 Å due to the *trans* influence of the tertiary phosphines. Again the Pt–P bond lengths, 2.25 and 2.26 Å, are within the expected range. The ligands form 6-membered chelate rings and both adopt the chair conformation, although

one ring is oriented above the platinum square-plane and the other below the plane.

Complex **9**, *cis*-[Pt($Me_2N(CH_2)_3PPh_2$-*P*)$_2Cl_2$], crystallised in a fully ring-opened form as a CH_2Cl_2 solvate (Fig. 8). The Pt–P bond lengths, 2.25 Å, show little change from the ring-closed structure despite the presence of chloride and not amine ligands in the *trans* position. The Pt–Cl bond lengths, 2.35 Å are longer than expected due to the high *trans* influence of the phosphine ligands. Despite the removal of strain in the complex due to the lack of chelation, the structure shows a similar distortion from square-planar geometry. The P(1)–Pt–P(2) angle is increased to 99.76° and the *trans* angles, P(1)–Pt–Cl(1) and P(2)–Pt–Cl(2), are reduced to 169.84° and 173.61°, respectively.

Crystals suitable for X-ray analysis of the ring-opened form of the Pd(II) complex **14b** were grown under acidic conditions (pH* *ca.* 4) in D_2O (Fig. 6). Even though the opening of one of the chelate rings must have relieved the severe steric strain along the N–Pd bond, the complex still shows distortion from square-planar geometry, and greater than that observed for **1** and **2**. If N(1)–Pd–Cl atoms are used to define the plane, P(1) is out of plane by 0.072 Å and P(2) by 0.195 Å. The P–Pd–P angle is relatively high at 98.57° due to the steric constraint caused by the presence of the phenyl rings. However the *trans* angles, N(1)–Pd–P(2) and P(2)–Pd Cl(1) of 176.49 and 173.68°, respectively, suggest only minor distortions. The Pd–N bond distance of 2.172 Å is relatively long, and is the longest M–N bond observed in this work, indicative of the weakening of the Pd–N bond. The Pd–Cl distance at 2.37 Å is as expected for Cl *trans* to phosphorus.[42] The two Pd–P distances are relatively short [34] comparable with that *trans* to Cl, 2.28 Å, and somewhat longer than that *trans* to N, 2.243 Å, due to the relatively larger *trans* influence of Cl compared to N.

The X-ray analysis of [Pd($Me_2N(CH_2)_3PPh_2$-*P*,*N*)Cl_2], **18** (Fig. 9), shows that the 6-membered ring is highly sterically strained. This is indicated by the bond angles of the alkyl chain, which show deviations from ideality (116.6(4), 114.4(3) and 117.2(4)°). This type of ring strain has also been observed for the dppp (1,3-bis(diphenylphosphino)propane) ligand which appears to form a significantly strained complex with palladium as opposed to the dppe (1,2-bis(diphenylphosphino)ethane) ligand which has an ideal square-planar geometry with maximum interaction between the phosphorus and palladium atom.[43] In addition the geometry at palladium in **18** is highly distorted from square-planar. The displacement of the P and N from the $PdCl_2$ plane is +0.465 Å and −0.357 Å for P and N, respectively. Similar geometric features have also been observed in [Pd(dppp)(bipy)]PF_6], where the two phosphorus atoms were displaced by −0.33 and +0.50 Å.[44] For [Pd(dppm)Cl_2] the displacements are −0.136 and +0.242 Å[43] and for [Pd(dppp)-Cl_2], are −0.053 and +0.312 Å. In contrast, the displacements observed for 5-membered chelated complexes are relatively small: −0.072 and + 0.195 Å for **14b**, −0.052 and +0.054 Å for **1**, and −0.072 and +0.087 Å for [Pd(dppe)Cl_2][43], confirming the highly sterically strained nature of the 6-membered chelated complex. The two Pd–Cl bond lengths for **18** are different, with that *trans* to P (2.33 Å) being somewhat longer than that *trans* to N (2.22 Å) due to the larger *trans* influence of a tertiary phosphine relative to that of the amine. The Pd–P bond distance is relatively short, at 2.22 Å and the Pd–N bond distance is rather long, at 2.12 Å, a common feature for this type of complex (Table 4). The P–Pd–P angle at 92.42° shows only a minor distortion although, the *trans* angles N(4)–Pd–Cl(1) and P(1)–Pd–Cl(2) of 170.15 and 167.8°, respectively, show a deviation from ideality which can be associated with the steric strain of the 6-membered chelated complex.

The X-ray crystallographic studies show that the metal–nitrogen bond distances for these complexes are relatively long and suggest a weakening of the Pt–N bonds, attributable to the strong *trans* influence of the tertiary phosphine. In addition changing the substituents at nitrogen from hydrogen to the more sterically demanding methyl group, results in the lengthening of the metal nitrogen bond.

Conclusions

The steric bulk of the substituents on nitrogen as well as the length of the $(CH_2)_n$ P–N linker in aminophosphine complexes can determine whether the complexes exist in ring-opened or closed forms. The aminophosphine complex, *cis*-[Pt(Me_2N-$(CH_2)_2PPh_2$-*N*,*P*)Cl($Me_2NH(CH_2)_2PPh_2$-*P*)]Cl, **5b**, has been shown by ^1H and ^{31}P solution studies to undergo reversible chelate ring-opening reactions in aqueous solution. These processes are dependent upon pH and chloride ion concentration. The equilibrium constant for Cl^- binding to *cis*-[Pt-$(Me_2N(CH_2)_2PPh_2$-*P*,*N*)$_2$]$(NO_3)_2$ at pH* 8.6 was determined to be 4.95 M^{-1}, and pH-induced chelate ring-opening of *cis*-[Pt($Me_2N(CH_2)_2PPh_2$-*P*,*N*)$_2$]Cl_2 had an associated p*K* of 6.9. In contrast, the complexes with less steric bulk on nitrogen are more difficult to ring-open, and complexes *cis*-[Pt(Me-(H)$N(CH_2)_2PPh_2$-*P*,*N*)$_2$]Cl_2 and *cis*-[Pt($H_2N(CH_2)_3PPh_2$-*P*,*N*)$_2$]-Cl_2 had associated p*K* values of 2.1 and 2.9, respectively. X-Ray crystallographic studies show that these aminophosphine complexes exhibit square-planar geometries with varying degrees of distortion and relatively long metal–nitrogen bond distances. Some of the complexes are cytotoxic to cancer cells and may be promising new antitumour agents.[12] In chelate-ring-closed form they can act as antimitochondrial agents and destroy membrane potentials, whereas in the ring-opened form they can bind to nucleobases on DNA.

Acknowledgements

We thank the Biotechnology and Biological Sciences Research Council, Engineering and Physical Sciences Research Council, EC COST D8 (Chemistry of Metals in Medicine) and Wolfson Foundation for their support for this work, Johnson Matthey for the loan of some of the metal salts, and ULIRS (Birkbeck College) for the provision of some NMR facilities.

References

1 F. A. Cotton and G. Wilkinson, *Advanced Inorganic Chemistry*, 4th edn., John Wiley & Sons, Chichester, 1980, p. 1200.
2 A. Tongni and L. M. Venanzi, *Angew. Chem., Int. Ed. Engl.*, 1994, **33**, 497.
3 J. Pfeiffer, G. Kickelbick and U. Schubert, *Organometallics*, 2000, **19**, 62.
4 M. Basset, D. L. Davies, J. Neild, L. J. S. Prouse and D. R. Russell, *Polyhedron*, 1991, **10**, 501.
5 V. K. Issleib and A. Kipke, *Z. Anorg. Allg. Chem.*, 1978, **444**, 5; V. K. Issleib and A. Kipke, *Z. Anorg. Allg. Chem.*, 1980, **464**, 176.
6 G. K. Anderson and R. Kumar, *Inorg. Chem.*, 1984, **23**, 4064.
7 M. M. T. Khan and E. R. Rao, *Polyhedron*, 1987, **6**, 1727; M. M. T. Khan, V. V. S. Reddy and H. C. Bajat, *Inorg. Chim. Acta*, 1987, **130**, 163; V. Reddy and S. Vijay, *J. Mol. Catal.*, 1988, 45; V. Reddy and S. Vijay, *J. Mol. Catal.*, 1988, 73.
8 S. Chatterjee, D. C. R. Hockless, G. Salem and P. Waring, *J. Chem. Soc., Dalton Trans.*, 1997, 3889.
9 J. Reedijk, *Chem. Commun.*, 1996, 801.
10 S. J. Berners-Price and P. J. Sadler, *Struct. Bonding (Berlin)*, 1988, **70**, 27.
11 S. J. Berners-Price, R. J. Bowen, M. J. McKeage, P. Galettis and P. C. Healy, *Coord. Chem. Rev.*, 1999, **185**, 823 and references therein; S. J. Berners-Price, R. J. Bowen, M. J. McKeage, P. Galettis, L. Ding, B. C. Baguley and W. J. Brouwer, *J. Inorg. Biochem.*, 1997, **67**, 154.
12 A. Habtemariam and P. J. Sadler, *Chem. Commun.*, 1996, 1785.
13 A. Habtemariam, J. A. Parkinson, N. Margiotta, T. W. Hambley, S. Parsons and P. J. Sadler, *J. Chem. Soc., Dalton Trans.*, 2001, 362.
14 N. Margiotta, A. Habtemariam and P. J. Sadler, *Angew. Chem., Int. Ed. Engl.*, 1997, **36**, 1185.
15 J. McDermott, *J. Am. Chem. Soc.*, 1976, **98**, 6525.
16 D. Drew and J. R. Doyle, *Inorg. Synth.*, 1972, **13**, 47.
17 KALEIDAGRAPH, Synergy Software, Reading, PA, 1994.
18 G. M. Sheldrick, SHELXS-97, Program for the solution of crystal structures, University of Göttingen, 1997.

19 G. M. Sheldrick, SHELXL-93, Program for crystal structure determination, University of Göttingen, 1993.
20 G. M. Sheldrick, SHELXTL, Bruker Analaytical X-Ray Instruments, Madison, Wisconsin, 1995.
21 D. J. Watkin, C. K. Prout, J. R. R. Carruthers and P. W. Betteridge, CRYSTALS, Chemical Crystallography Laboratory, University of Oxford, 1996.
22 T. Hayashi, M. Konishi, M. Fukushima, K. Kanehira, T. Hioki and M. Kumada, *J. Org. Chem.*, 1983, **48**, 2195.
23 D. J. Ager, I. Prakash and D. R. Schaad, *Chem. Rev.*, 1996, **96**, 835.
24 M. J. McKennon, A. J. Meyers, K. Drauz and M. Schwarm, *J. Org. Chem.*, 1993, **58**, 3568.
25 H. C. Brown and T. P. Stocky, *J. Am. Chem. Soc.*, 1977, **99**, 8218.
26 A. Abiko and S. Masamune, *Tetrahedron Lett.*, 1992, **33**, 5517.
27 G. A. Smith and R. E. Gawly, *Org. Synth.*, 1985, **63**, 136.
28 R. Malet, M. Morens-Mañas, T. Parella and R. Pleixats, *J. Org. Chem.*, 1996, **61**, 758.
29 P. E. Garou, *Chem. Rev.*, 1981, **81**, 229.
30 A. Albinati, F. Berger, P. S. Pregosin, H. Ruegger and R. W. Kunz, *Inorg. Chem.*, 1993, **32**, 478.
31 P. S. Pregosin, in *Phosphorus-31 NMR Spectroscopy in Stereochemical Analysis*, eds., J. G. Verkade and L. D. Louis, VCH, New York, 1987, p. 465.
32 A. Handler, P. Peringer and E. P. Müller, *J. Chem. Soc., Dalton Trans.*, 1990, 3725.
33 G. K. Anderson, H. C. Clark and J. A. Davies, *Inorg. Chem.*, 1983, **22**, 434.
34 A. G. Orpen, L. Brammer, F. H. Allen, O. Kennard, D. G. Watson and R. Taylor, *J. Chem. Soc., Dalton Trans.*, 1989, S1.
35 F. Kaufler and E. Kunz, *Chem. Ber.*, 1909, **42**, 385.
36 W. D. Chandler, K. Johnson, B. D. Fahlman and J. L. E. Campbell, *Inorg. Chem.*, 1997, **36**, 776.
37 K. Kawaguchi, *J. Chem. Phys.*, 1988, **88**, 4186.
38 J. L. Atwood, S. G. Bott, M. Means, A. W. Coleman, H. Zhang and M. T. May, *Inorg. Chem.*, 1990, **29**, 467.
39 D. Mootz, W. Poll, H. Wunderlich and H. G. Wussow, *Chem. Ber.*, 1981, **114**, 3499.
40 G. Germain, P. Main and M. M. Woolfson, *Acta Crystallogr., Sect. A*, 1971, **27**, 368.
41 J. L. Atwood, S. G. Bott, A. W. Colman, K. D. Robinson, S. B. Whetstone and M. Means, *J. Am. Chem. Soc.*, 1987, **109**, 8100.
42 G. J. Palenik and T. J. Giordano, *J. Chem. Soc., Dalton Trans.*, 1987, 1175.
43 W. L. Steffen and G. J. Palenik, *Inorg. Chem.*, 1976, **15**, 2432.
44 B. Milani, I. Vicentini, A. Sommazzi, F. Garbassi, E. Chiarparin, E. Zangrano and G. Mestroni, *J. Chem. Soc., Dalton Trans.*, 1996, 3139.